PL–TR–
93–3044

Liquid Stability Mechanisms Program Final Report

E. L. Peterson
G. B. Cox
T. T. Evans

United Technologies Corporation
Pratt & Whitney
Government Engines & Space Propulsion
P. O. Box 109600
West Palm Beach FL 33410–9600

August 1995

Final Report

PHILLIPS LABORATORY
Propulsion Directorate
AIR FORCE MATERIEL COMMAND
EDWARDS AIR FORCE BASE CA 93524–7001

NOTICE

When U.S. Government drawings, specifications, or other data are used for any purpose other than a definitely related Government procurement operation, the fact that the Government may have formulated, furnished, or in any way supplied the said drawings, specifications, or other data, is not to be regarded by implication or otherwise, or in any way licensing the holder or any other person or corporation, or conveying any rights or permission to manufacture, use or sell any patented invention that may be related thereto.

FOREWORD

This report was prepared by United Technologies Corporation, Pratt & Whitney, West Palm Beach FL, under contract F04611-89-C-0088, for Operating Location AC, Phillips Laboratory, Edwards AFB, CA. 93524-7048. Project Manager for Phillips Laboratory was Jay Levine.

This document presents the final report for the Liquid Stability Mechanisms Program. The work included in this document was conducted by Pratt & Whitney/Government Engines and Space Propulsion (P&W/GESP) of United Technologies Corporation in conjunction with the University of California Irvine (UCI) and the United Technologies Research Center (UTRC). Major contributions to this report were provided by T. W. Eastes, G. S. Samuelsen, W. A. Sirignano, and C. H. Chiang of UCI and T. J. Anderson, M. Winter, and L. J. Spadaccini of UTRC.

This report has been reviewed and is approved for release and distribution in accordance with the distribution statement on the cover and on the SF Form 298.

Accesion For	
NTIS CRA&I	☒
DTIC TAB	☐
Unannounced	☐
Justification	
By	
Distribution /	
Availability Codes	
Dist	Avail and / or Special
A-1	

JAY N. LEVINE
Project Manager

STEPHEN L. RODGERS
Director
Propulsion Sciences Division

RANNEY G. ADAMS, III 95-075
Public Affairs Director

REPORT DOCUMENTATION PAGE

Form Approved
OMB No 0704-0188

1. AGENCY USE ONLY (LEAVE BLANK)	2. REPORT DATE	3. REPORT TYPE AND DATES COVERED
	August 1995	Final Dec 89 – May 93

4. TITLE AND SUBTITLE
Liquid Stability Mechanisms

5. FUNDING NUMBERS
C: F04611-89-C-0088
PE: 62302F
PR: 5730
TA: 003Z

6. AUTHOR(S)
E.L. Peterson; G.B. Cox; T.T. Evans

7. PERFORMING ORGANIZATION NAME(S) AND ADDRESS(ES)
United Technologies Corporation
Pratt & Whitney
P.O. Box 109600
West Palm Beach FL 33410-9600

8. PERFORMING ORGANIZATION REPORT NUMBER

9. SPONSORING/MONITORING AGENCY NAME(S) AND ADDRESS(ES)
Phillips Laboratory
OLAC PL/RKFA
9 Antares Road
Edwards AFB CA 93524-7680

10. SPONSORING/MONITORING AGENCY REPORT NUMBER
PL-TR-93-3044

11. SUPPLEMENTARY NOTES
COSATI CODE(S): 2102; 0704; 2005

12a. DISTRIBUTION/AVAILABILITY STATEMENT
APPROVED FOR PUBLIC RELEASE; DISTRIBUTION IS UNLIMITED

12b. DISTRIBUTION CODE
A

13. ABSTRACT (MAXIMUM 200 WORDS)
The processes participating in liquid rocket engine high frequency combustion instability are not well understood. The Liquid Stability Mechanisms (LSM) program investigated the potential, fundamental mechanisms of vaporization and secondary atomization. Using state-of-the-art diagnostic techniques, the vaporization rate of a droplet exposed to an acoustic perturbation was measured; the results indicate that the transient vaporization response is greatly affected by a pressure pulse. A multiphase, continuous injection droplet vaporization model was used to analytically predict droplet vaporization under oscillatory conditions. These results also indicate that the vaporization response is strongly affected by pressure waves and is capable of supplying enough energy to support an ordered oscillation in the combustion chamber. Shadowgraphic cinematography was employed to study the secondary atomization process in a newly built, high-pressure shock tube. Preliminary results were obtained of droplet breakup under Reynolds number and liquid-to-gas density ratio conditions that match those seen under supercritical conditions were also obtained; these data show a process that differs from typical results at low pressure.

14. SUBJECT TERMS	15. NUMBER OF PAGES
combustion instability, supercritical combustion, liquid-propellant rockets, shock tube, droplet vaporization, secondary atomization, laser diagnostics	16. PRICE CODE

17. SECURITY CLASSIFICATION OF REPORT	18. SECURITY CLASSIFICATION OF THIS PAGE	19. SECURITY CLASSIFICATION OF ABSTRACT	20. LIMITATION OF ABSTRACT
Unclassified	Unclassified	Unclassified	SAR

SUMMARY

The objective of the Liquid Stability Mechanisms program was to experimentally and analytically explore the fundamental mechanisms which contribute to high frequency, liquid-propellant rocket combustion instability. Droplet secondary atomization and vaporization were chosen as the primary, potential mechanisms for study. To explore these processes experimentally, unique, non-intrusive diagnostic techniques were developed. A parallel analytical study employed modern computational techniques to investigate the droplet vaporization process under conditions typically seen during combustion instability.

Experimental investigation of the vaporization mechanism explored the effect of a pressure pulse on the vaporization of a droplet. Via creative exploitation of morphology-dependent resonances (MDR's) from fluorescent methanol and water droplets, information regarding the transient nature of the drop diameter was obtained. These precise data were taken at sub-critical conditions using a 1-atm shock tube generating 1.1-1.2 pressure ratio pulses. The transient evaporation of the droplet in the first few microseconds after wave passage was found to be very high, indicating that droplet vaporization is a potential stability mechanism. In addition, a high-pressure pulse tube was used to obtain back-lit images of a LOX droplet in sub- and super-critical environments (P_{crit} = 50 atm.) interacting with a pressure wave. These images show a post-pulse dispersion of the droplet that is drastically different from typical images of droplets at atmospheric pressure.

For the secondary atomization experimental effort, a high-pressure (68-atm test section) shock tube was designed and fabricated to simulate a steep-fronted acoustic disturbance (i.e., N-wave). The non-intrusive diagnostic developed for the secondary atomization investigation involved shadowgraphic cinematography with a 32,000-Hertz copper vapor laser as the light source. A parallel simulant fluid study was conducted to determine the fluids needed to best simulate the acoustic instability of a high-pressure rocket combustion chamber. An ideal test matrix was formulated to cover a range of Reynolds numbers from 100 to 65,000, Weber numbers from 30 to 140,000, and liquid-to-gas density ratios from 56 to 77. Initial tests at atmospheric pressure and at a constant wave strength ($\approx$ 1.5) and initial drop diameter ($\approx$ 120 μm) indicate that droplet breakup time decreases with increasing wave duration. Maximum product drop size also decreases with increasing wave duration and We_{max}.

Efforts in the computational portion of the program concentrated on droplet vaporization. These studies employed an advanced variable-property droplet model which calculates both the gas and liquid phase. Application of the model to a continuous injection, oscillatory environment resulted in a value for the vaporization response factor, or gain, of the system as a function of oscillation amplitude, drop configuration, and oscillation frequency. It was shown that the vaporization response can be sufficiently high to support an ordered oscillation in the combustion chamber, again indicating that

vaporization is a stability mechanism. When applied to the 1-atm vaporization data, the pulse wave was modeled as a step response. The numerical result under-predicts the drop diameter decrease. This is most likely due to boundary layer stripping, the effects of which are not included in the model.

ACKNOWLEDGMENTS

Pratt & Whitney conducted program management of this contract with Mr. George Cox Jr. as the original program manager. Eric Petersen was the principal investigator and later assumed the role as program manager. Tyler Evans was program manager during the final phases of the technical write-up. The Air Force Phillips Laboratory program manager was Jay N. Levine; his helpful guidance and discussions added much to the program. Thanks are also due to Dr. Doug Talley of the Phillips Lab for his input. Most of the technical work was accomplished by the subcontractors, UTRC and UCI. Dr. Lou Spadaccini was the UTRC program manager, and Dr. Mike Winter and Dr. Torger J. Anderson conducted the experiments. Acknowledgment is also given to Mr. Richard J. Daddona of UTRC for his technical assistance and Mr. Martin Haas of UTRC for designing the corporate-funded UTRC shock tube. At UCI, Dr. G. S. Samuelsen served as principal investigator. Researcher Ted Eastes designed and built the UCI shock tube and conducted the experiments; the help of Arash Ateshkadi was also appreciated. Dr. W. A. Sirignano was the principal investigator at UCI and was responsible for the analytical contribution. Dr. C. H. Chiang was the primary researcher in the computational vaporization effort. Appreciation is also due to Mr. David Konopka of Pratt & Whitney for his efforts during the initial phases of the program.

CONTENTS

LIST OF TABLES

LIST OF FIGURES

NOMENCLATURE

Variables

a	acceleration or speed of sound
Bo	Bond number, $\rho_o a R_o^2 / \sigma$
c_p	constant pressure specific heat
c_v	constant volume specific heat
C_D	drop drag coefficient
d	daughter drop diameter
D	drop diameter
g	arbitrary function
G	Rayleigh criterion response factor
La	Laplace number, $1/Oh^2$
Le	Lewis number
MMD	Mass median diameter
Oh	Ohnesorge number, $\mu_o / (\rho_o R_o \sigma)^{1/2}$
Pr	Prandtl number
R	drop radius
Re	Reynolds number, $\rho U_{rel} D_o / \mu$
S	surface area of equivalent mass sphere
Sc	Schmidt number
SMD	Sauter mean diameter
t	time
U_{rel}	relative velocity between convective flow and drop
V	drop volume
We	Weber number, $\rho U_{rel}^2 D_o / \sigma$

x	displacement
Y	species volume fraction
α	empirical function of viscosity
δ	surface deformation distance
ε	gas/liquid density ratio, ρ / ρ_o
γ	ratio of specific heats, c_p/c_v
η	gas/liquid viscosity ratio, μ / μ_o
μ	molecular viscosity
ρ	density
σ	surface tension
τ	dimensionless time
τ_h	droplet heating time
ξ	dimensionless displacement, x/D_O

Subscripts

b	breakup
cr	critical value
fs	freestream value
i	initial condition
l	liquid property
o	drop property
max	maximum value
min	minimum value
N	N-wave property
R	based on drop radius
s	steady state value
v	vibration
-	gas property
1	defined at test section of shock tube
2	defined at location immediately upstream of shock wave
4	defined at shock tube driver section
∞	property far away from droplet

INTRODUCTION

Combustion instability in liquid propellant rocket engines has historically been a major concern in engine development programs. Despite modeling advances, stability rating programs, and injector/combustor designs that avoid instability, unstable operation is still encountered. The effects of operation at supercritical pressures on combustion stability are also of concern since new engines are projected to operate at high chamber pressure. Efforts to understand the mechanisms driving acoustic combustion instability, and to identify remedies when instability is encountered, are still needed. Because of a lack of fundamental understanding of how combustion instabilities arise, current approaches for control of combustion instability rely on damping out pressure oscillations rather than preventing their occurrence.

Organized unsteadiness in the combustion processes and their associated coupling with the feed system dynamics and/or chamber acoustic modes lead to combustion instabilities. Energy supplied by combustion in phase with chamber pressure oscillations causes instability according to the Rayleigh criterion (1). The consequences can be very destructive and include such manifestations as severe vibration (> 1000 g in some cases) due to pressure oscillations (to 1000% of chamber pressure), erosive burning of chamber walls and the injector face due to excessive heat transfer rates, decreased combustion efficiency of well-designed injectors due to oscillation-induced energy losses, enhanced combustion efficiency of poorly performing engines through improved atomization, vaporization, and mixing, and thrust vector variations due to spatial variation of the pressure oscillations.

Combustion instability is generally classified by the frequency of the oscillation, although there are no specific transition points between low (chug), intermediate (buzz), and high frequency (acoustic) combustion instabilities. Frequencies typically range from values less than a hundred Hertz to many thousands of Hertz.

Low frequency combustion instabilities are typically less than a hundred Hertz. These generally result from communication between the combustion chamber and the feed system and are sometimes called a feed-coupled combustion instability. The most important characteristic time appears to be the time from injection until the time propellants are converted to products. Such instabilities are most often eliminated by increasing injector pressure drop, thereby reducing the effect of chamber oscillations on propellant flowrate fluctuations.

Intermediate frequency combustion instabilities are generally greater than a hundred Hertz and less than a thousand Hertz. These also typically result from communication between the combustion chamber and the feed system. Oscillations are generally found in both the feed system and the chamber, although the phase and frequency do not usually correspond to an acoustic mode. Such instabilities are most

often eliminated by increasing injector pressure drop or placing stability aids such as resonators in the feed system.

High frequency acoustic combustion instabilities occur at frequencies related to the acoustic modes of the combustion chamber and are typically greater than several hundred Hertz. These are caused by one or more chamber mechanisms which couples with acoustic modes of the combustion chamber. The characteristic time of these mechanisms is believed to be of most importance. These mechanisms are related to loss of ignition source, physical propellant transport associated with the atomization process and other convective processes, kinetics, vaporization, droplet heating, and mixing. Such instabilities are the most destructive and are most often controlled through injector redesign and/or the use of baffles and acoustic cavities to damp pressure oscillations.

Pressure perturbations on the order of a few percent of the chamber pressure are typically referred to as linear and are most often sinusoidal in shape. Transition to a distorted wave shape usually occurs for perturbations around ten percent of chamber pressure and may appear like spikes or N-waves. However, these effects vary considerably from engine to engine.

While some instabilities are initiated by steady growth in amplitude from a low amplitude noise level initial condition, it is even more common for instabilities to be initiated by naturally occurring "pops" or "spikes" (2). Such a "pop" was recently observed in an SSME oxygen preburner during test (3). These random pressure perturbations have the appearance of local explosions. They have been observed in steady operation (pop) and upon engine startup (spike) and have been known to trigger resonant combustion and ensuing combustion instability and hardware destruction.

A system approach is typically used to model these phenomena. In this approach, a combustion gain function is applied to an initial pressure disturbance to yield the system response. Thus if gain occurs in phase with the disturbance, combustion instability occurs; Figure 1 shows this conceptually.

An understanding of the origins of combustion instability could ultimately permit the design of inherently stable, high performance liquid rocket engines without much of the costly trial-and-error development which is now necessary. Advances in fast-response, non-intrusive instrumentation, measurement, and diagnostic techniques now make possible the investigation of many combustion processes which could cause or participate in liquid rocket combustion instability. Possible measurements include drop sizes and spray patterns, droplet and stream breakup, propellant mixing, chemical reaction rates, chamber flow fields, and fluctuating pressures and velocities. Analysis of the data could assist investigators in determining instability mechanisms and in improving rocket engine design methods and procedures. Thus, current instrumentation and diagnostics capabilities enable a new approach to control acoustic combustion instability:

investigation and eventual control of the basic instability mechanisms. The Liquid Stability Mechanisms program was conducted to investigate these phenomena.

This report summarizes the technical efforts and results of the Liquid Stability Mechanisms program. First, the program setup is described. The rest of the report is divided according to task. Therefore summaries of the mechanism selection procedure (Task 1), the experimental exploration of the stability mechanisms (Task 2), and the analytical verification of the selected mechanisms (Task 3) are included. Plans for future effort are also provided (Task 4). These summaries are supported by the technical papers that were written during the course of the program; each publication is provided as a separate appendix.

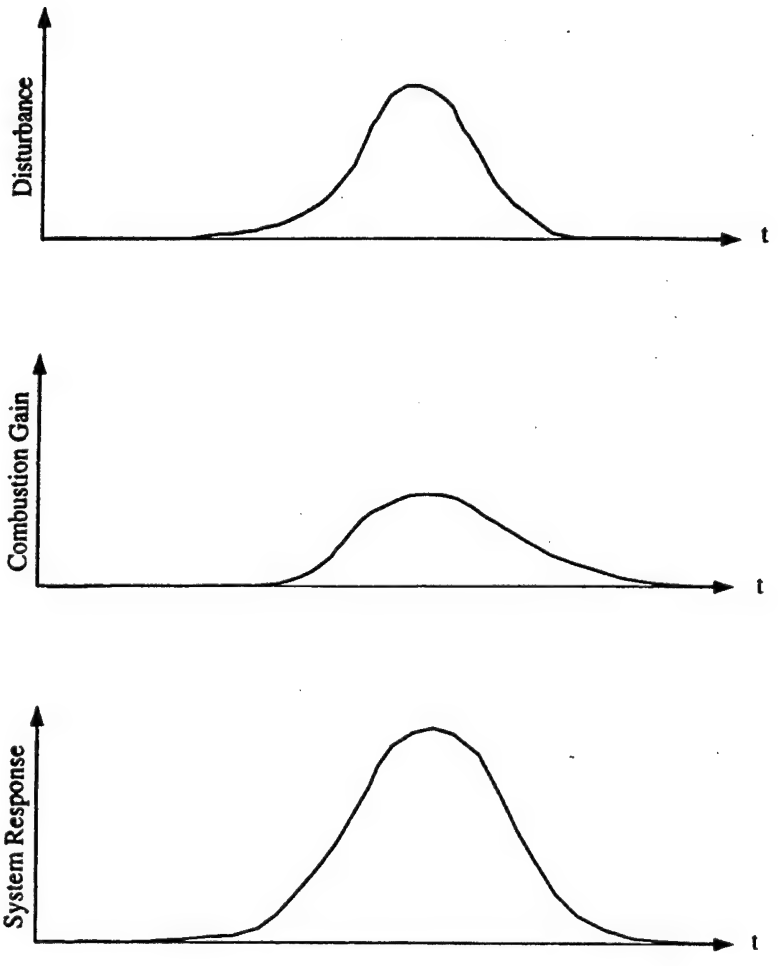

Figure 1
Combustion Instability Conceptualization

PROGRAM DESCRIPTION

The Liquid Stability Mechanisms program consisted of a combined theoretical and experimental effort. Theoretical effort addressed the identification and selection of candidate combustion processes, verification of the applicability of the experimentally studied mechanisms to liquid rocket stability, and development of a program plan for further effort. Experimental effort addressed the investigation of the participation of the selected combustion processes in the instability mechanism. It had the objective of exploring specific processes which participate in acoustic combustion instability via the use of advanced diagnostic techniques.

The program was divided into the following tasks:

Task 1: Selection and verification of combustion processes having the potential for participation in instability mechanisms

Task 2: Development of appropriate test hardware, evolution of novel diagnostic techniques, and performance of experimental investigations of instability mechanisms

Task 3: Verification of the applicability of the mechanisms through comparison with analytical models and the available data base

Task 4: Development of plans for continued effort

Task 5: Program management, coordination, and control

Task 1 was the identification and selection of processes for study. Accomplishment required ten calendar months. Selection of the processes for experimental investigation and generation of the test plan dictated the scope of the succeeding tasks.

Task 2 was test investigation of the selected processes. Accomplishment required thirty-eight calendar months. The UCI and UTRC phases of Task 2 and their respective sub-elements were conducted concurrently. Within this task, high-pressure shock tube techniques and diagnostics were developed.

Task 3 was mechanism verification using appropriate correlations, sub-models, and models. Accomplishment required thirty-two calendar months. Analytical droplet models were revised to account for realistic rocket boundary conditions and acoustic oscillations. These models were applied to existing data and were used to explore the contribution of the selected mechanisms to combustion instability.

Throughout the Liquid Stability Mechanisms program, the following definitions were suggested to distinguish between the events that are occurring as part of combustion and those that are occurring as part of combustion instability.

> Process: The sequence of events, involving one or more propellants, by which a change is produced in some quantity which describes the states or conditions of the propellant(s), such as phase, velocity, temperature, pressure, environment, or chemical composition.
>
> > Example: The vaporization process is the sequence of events which changes a propellant from the liquid phase to a gaseous phase through the addition of heat to the liquid phase.
>
> Mechanism: The sequence of events by which a pressure or velocity perturbation produces a corresponding change in some process that eventually results in a change in the instantaneous energy release rate, and hence may participate in an instability.
>
> > Example: The vaporization mechanism is the sequence of events by which a pressure or velocity perturbation produces a change in the rate at which a propellant changes from a liquid phase to a gaseous phase.

By the above definitions, a combustion process becomes a potential or actual instability mechanism only if it exhibits an appropriate response to the pressure/velocity perturbations seen during combustion instability. Consistent with the program description, the technical effort for the investigation of such mechanisms involved identification of the principle mechanisms, subsequent experimental investigations, and complimentary theoretical modeling to verify the selected mechanisms.

TASK 1 - IDENTIFICATION AND SELECTION OF MECHANISMS FOR STUDY

The effort in Task 1 consisted of: 1) work completed in the form of a candidate mechanism list and a preliminary literature review of the various candidates, and 2) conclusions drawn on mechanism selection. As a result of the literature review and selection from the derived candidate mechanism list, droplet vaporization and secondary atomization were chosen as the principle mechanisms to be investigated. Other processes were also evaluated; although of potential interest, the available program resources did not permit investigation of all the candidates.

Vaporization was selected as a major driving mechanism of combustion instability because analyses show it to be the rate controlling process in rocket combustion. Previous authors demonstrated that vaporization within an oscillating pressure and velocity field could support a combustion instability as measured by the Rayleigh criterion (1). Secondary atomization was chosen as a primary mechanism for its impact on vaporization rates. Greater understanding is needed in the breakup of the larger liquid propellant droplets in both non oscillatory and oscillatory conditions. UTRC investigated the vaporization process, while UCI focused on secondary atomization.

A more detailed explanation of the Task 1 selection process is available in the summary report written by W. A. Sirignano, UCI. This report is included as Appendix A. The results of the literature review are also summarized in the Appendix A report.

As a result of the Task 1 identification and selection procedure, the experimental and theoretical division of effort was formulated. Figure 2 presents the resulting breakdown of the efforts between P&W, UTRC, and UCI.

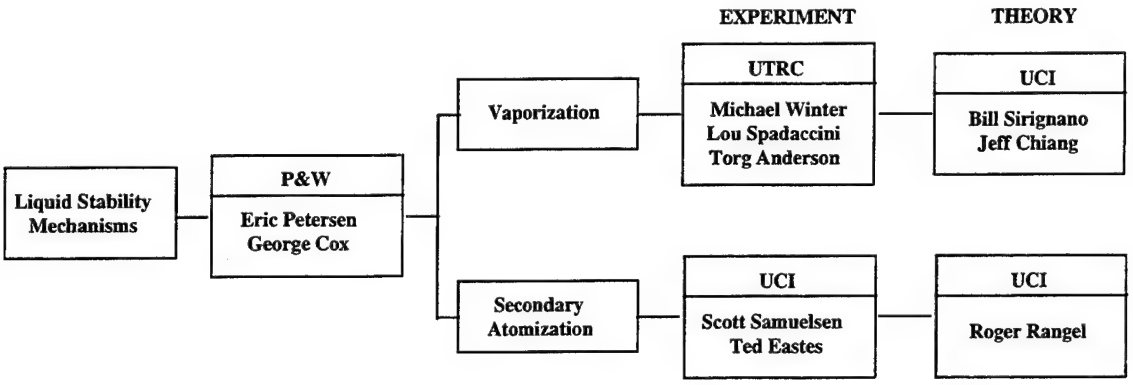

Figure 2
Division of Efforts

TASK 2 - EXPERIMENTAL INVESTIGATION OF MECHANISMS

The experimental investigation of the selected mechanisms was based on the perturbation of drops and the subsequent measurement of the response to the perturbation. In the actual combustion process, the time interval between the perturbation and the burning of the drops measures the phase lag of the process. Through the Rayleigh criterion, the phase lag is related to the appropriate acoustic instability. The perturbation itself is coincident with the passage of a pressure/velocity pulse. The experimental concept was to study the phenomena which occur when a pulse passes transversely through a single droplet.

For these experiments, a shock (or pulse) tube was employed. Droplet streams were injected transversely to the bore of the pulse tube. Figure 3 shows this process conceptually. Details of the design and fabrication of the UCI shock tube are included in later sections of this report. The pulse tube employed by UTRC was built using corporate funds and will not be detailed here; this pulse tube was made available for use on the LSM program.

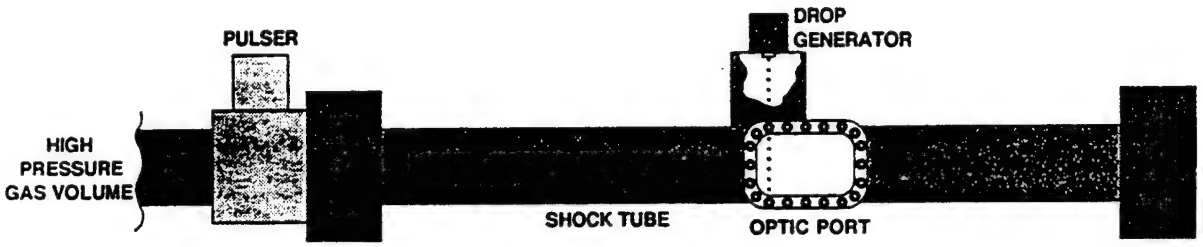

Figure 3
Pulse Tube Concept

Shock tubes in their simplest form are gas-filled tubes divided by a diaphragm into a high-pressure driver gas region and a low-pressure experimental gas region. The sudden bursting of the diaphragm causes a plane shock to propagate into the low-pressure or driven section and a rarefaction to propagate into the high-pressure or driver section. This process is visualized in the Figure 4 x-t diagram. The shock is characterized by a step change in pressure, density, static temperature, and particle velocity and is planar and normal to the shock tube walls. The rarefaction conversely

makes a smooth transition from high to low pressure. The experimental gas and driver gas interface at a contact surface which propagates into the driven section at the gas particle velocity trailing the shock front. Pressure and velocity are preserved across the contact surface ($p_2 = p_3$, $u_2 = u_3 = u_P$), but entropy changes discontinuously. The particle velocity is always less than the velocity of the shock front such that as the distance to the point in the test section increases, the duration of the uniform flow at that point increases. This period of uniform flow is typically known as the test time.

In fact, the particle velocity behind the shock front provides the convective flow required for the secondary atomization and wave-induced droplet vaporization experiments. The magnitude of this convective velocity can be predicted using 1-D gas dynamic relations. The required driver pressure and test section pressure can also be determined *a priori*. A derivation of the applicable gas dynamic equations is provided in Appendix B.

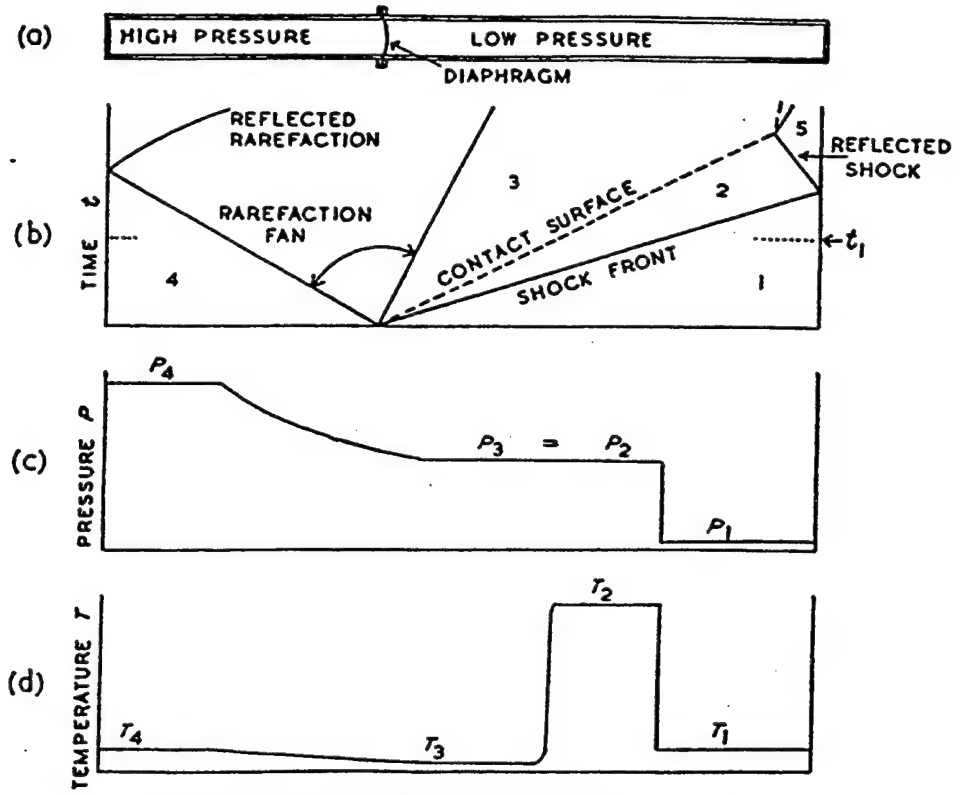

(a) *Conventional shock tube* (b) *An* $(x-t)$ *diagram showing progress of the shock wave, the rarefaction fan and the contact surface separating driver and experimental gases* (c) *The pressure distribution along the tube at time* t_1 (d) *The temperature distribution at time* t_1

Figure 4
Shock Tube Process

Vaporization (UTRC)

The emphasis of the UTRC portion of the program became the experimental study of droplet vaporization. Task 1 indicated that vaporization and atomization were the primary instability mechanisms to be studied, and that the tests should be run under pulsed conditions. Resulting wave strengths and pressures were consistent with expected droplet lifetimes in a rocket combustor with respect to typical instability frequencies. These tests made use of a facility designed and built under corporate funding, described in Appendix D.

Liquid fuel rocket engines typically are operated near or above the critical conditions of the oxidizer. At the outset of the program, however, simulations were only available describing the vaporization behavior of the droplets at or near atmospheric conditions. To satisfy both conditions, UTRC decided to perform measurements at both low-pressure (atmospheric) and high-pressure, sub-critical conditions and at high-pressure, super-critical conditions. While the vaporization process of a droplet in conditions below its critical point are both understood and well defined, the vaporization of a liquid droplet in a supercritical environment is not. In fact, describing the latter process in terms of droplets, vaporization, and gas may be inappropriate. This reexamination of terms also requires careful consideration of how to measure these 'phases' and what actually is being measured. To satisfy these concerns, UTRC settled on a two-pronged approach. The first was to make measurements providing pinpoint accuracy directed to correlating sub-critical droplet vaporization enhancement models. In the second, measurements were directed toward the behavior of droplets exposed to conditions exceeding their critical conditions.

Low-Pressure Experiments. The first set of experiments were performed on droplets of a simulant fluid at or near atmospheric pressures. The purpose of these measurements was to directly address the predictions of Tong and Sirignano (4,5). Their calculations show significant increases in the vaporization after the passage of an acoustic wave with the pressure and velocity field in phase. The technique chosen was the use of Morphology Dependent Resonances (MDRs) (6,7). In this technique, the droplets themselves are transformed into miniature dye lasers whose output mode structure corresponds to droplet size. The application of this technique to droplets undergoing an acoustic perturbation is described in Appendix C. Figure 5 presents a schematic of the experimental setup.

In the present application, changes in droplet diameter were resolved to within 3 nm. Detailed results of the measurements using the MDR technique can be found in Appendices C, D, and E. The conclusions of these experiments directly address both the degree of vaporization enhancement following the droplet/wave interaction as well as the phasing of the enhancement (i.e., response time). A brief summary of the low-pressure vaporization data is given below.

The sub-critical vaporization experiments were conducted using 60-70 μm droplets of water and methanol. Initial evaporation measurements were conducted in quiescent air and are presented by Figure 6. Note that the methanol evaporation rate is approximately 13 times that of water.

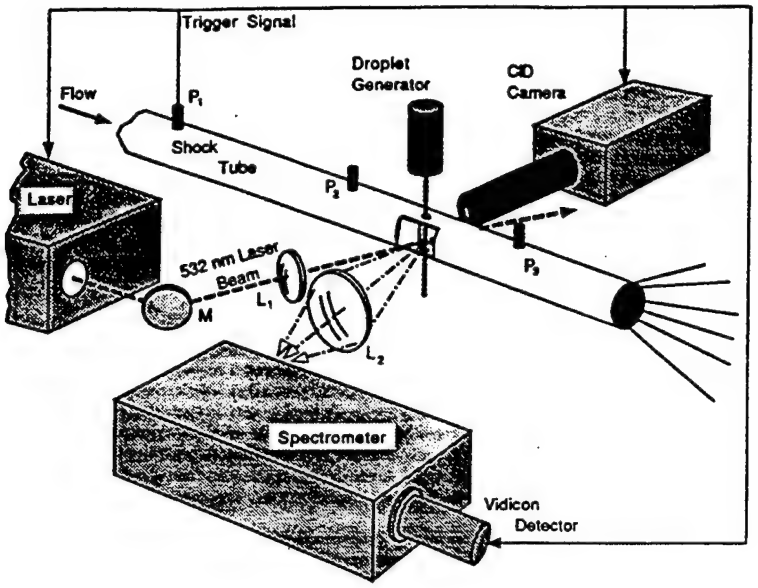

Figure 5
UTRC Experimental Setup for Acquiring MDR Emissions of Drops

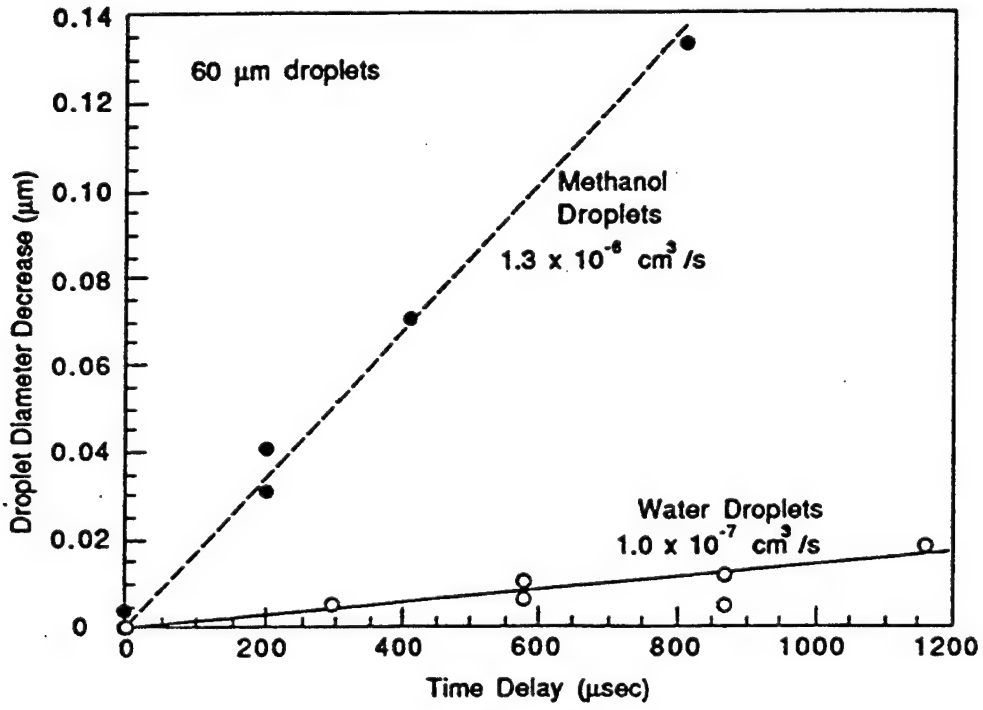

Figure 6
Evaporation Rates for Methanol and Water Droplets

Table 1 shows the range of pulse conditions used for the main vaporization tests. The corresponding Reynolds and Weber numbers for water and methanol are given in Table 2.

Table 1. Pressure Pulse Conditions for UTRC 1-atm Vaporization Measurements

Condition	*PR*	*TR*	*Shock Mach Number*	*Velocity* (m/s)*
Quiescent Air	1.0	1.00	0	7.5 / 5.5
Weaker Shock Wave	1.1	1.03	1.04	24.6 / -
Stronger Shock Wave	1.2	1.05	1.08	46.6/46.3

* velocities shown are for methanol and water, respectively

Table 2. Weber and Reynolds Number Comparisons for UTRC 1-atm Vaporization Measurements

PR	*Droplet Fluid*	*Droplet Dia. (μm)*	*We*	*Re*	*We/Re*
1.1	Methanol	70	1.7	3.3	0.51
1.2	Methanol	70	6.4	6.4	1.00
1.2	Water	70	2.4	3.8	0.62

The results of the three pressure pulse cases are shown in Figure 7 along with the quiescent air data. Although the available data are for short periods after wave passage (less than 10 microseconds), the data clearly indicate that a pulse greatly enhances the transient vaporization process. Therefore a combustion instability-derived acoustic pulse would be expected to have an impact on the vaporization of liquid propellant droplets.

This result supports the assertion that the vaporization process is an instability mechanism.

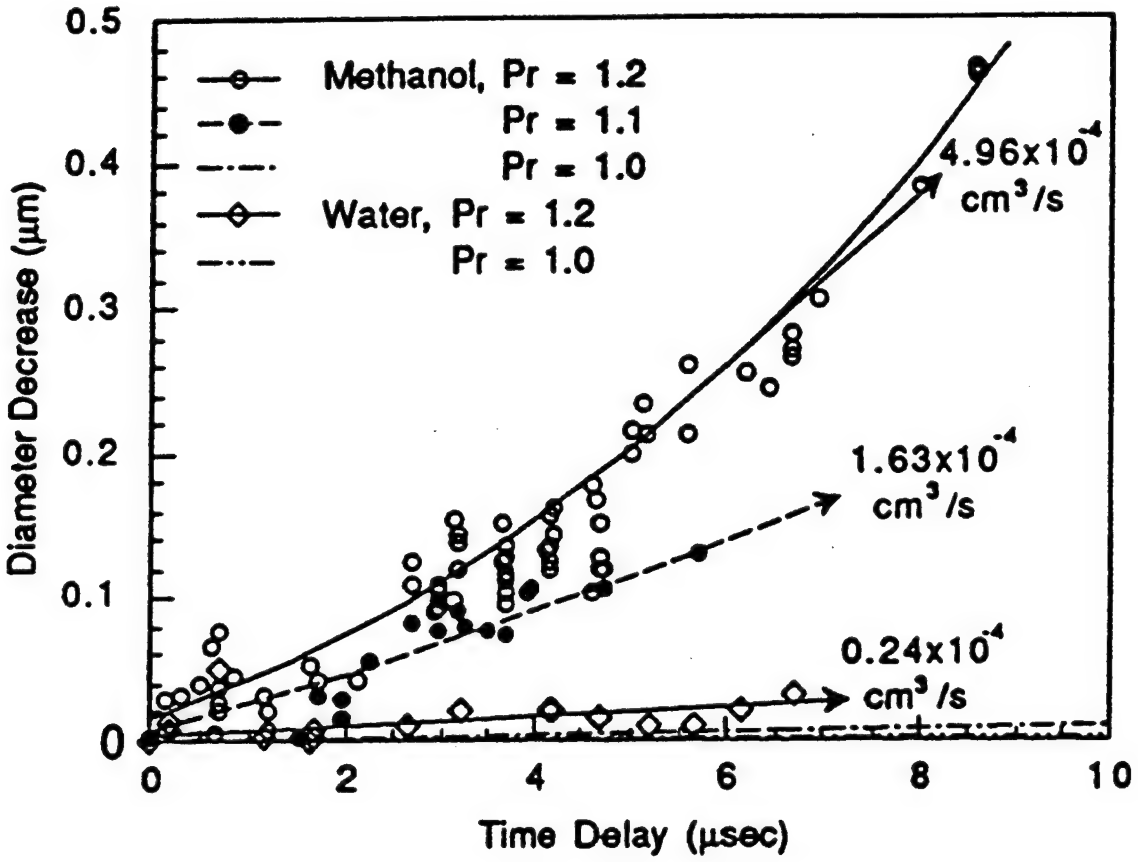

Figure 7
Methanol and Water Droplet Changes Measured Shortly After Pulse Wave Passage

High-Pressure Experiments. Tests were also conducted to study effects which would lead to instabilities in a supercritical environment. Since droplet surface tension and viscosity play a major role in droplet distortion, evaporation, and breakup in sub-critical regimes, there is interest in the processes which occur when these physical parameters are significantly altered in ways consistent with rocket combustor conditions. In the UTRC experiment--as in the environment within a rocket combustor--liquid droplets are injected into pressures above the critical point. The droplet temperature then

increases as heat is absorbed through the outer surface. If the time scales are long enough, the droplet temperature should exceed the critical temperature. With the introduction of a weak pressure pulse, droplet breakup and transition, or 'puffing,' is observed.

The facility used for these experiments is the high-pressure pulse tube described in Appendix D. This shock tube is capable of initial test section pressures of 1000 psi--well above the 734-psi critical pressure of O_2. Line-of-sight optical access to the test section is available through two 2-inch-diameter windows. Ninety-degree access is also available. A driver section, separated from the test section by burst disks, can be pressurized up to 2300 psi for strong shock waves. However, in these experiments, pressure differences between the test section and driver did not exceed 130 psi to produce weak pressure pulses with wave strengths (i.e., pressure ratios) no greater than approximately 1.08.

A liquid oxygen (LOX) droplet generator was designed and built to produce a stream of approximately 100-to-400-micron-diameter O_2 droplets in the high-pressure environment of the test section. Figure 8 presents a drawing of the cryogenic drop generator. LOX was chosen as the droplet simulant for a number of reasons: it is the oxidizer for many liquid-fueled rocket engines of interest; it can easily be produced by condensing gaseous O_2 using liquid nitrogen; and, its critical temperature (155 K) is below room temperature. Liquid oxygen also has additional diagnostic advantages which will be discussed below.

An initial study of potential diagnostic techniques suggested methods of determining the location of droplet fluid as the droplet breaks up after pressure pulse passage. Based on experience in the low-pressure experiments conducted earlier in the program, Schlieren photography appeared to be a simple method for observing the effect of the pressure pulse on the LOX droplets. However, in attempting to implement this technique in the shock tube's high-pressure environment, it was found that large density gradients produced by the cold LOX droplet generator caused the LOX droplet stream to be completely obscured despite attempts to insulate the device.

Raman scattering is a more complex but comprehensive diagnostic which was considered in this program. It has potential for measuring the concentration of O_2 in and around the LOX droplet. Feasibility measurements (conducted as part of a corporate-sponsored program) suggested that at the high pressures of these experiments, Raman signals from O_2, generated from a frequency-doubled Nd:YAG laser, would be strong enough to image the O_2 concentration in the region around a LOX droplet. The possibility of using this Raman technique exists because of the large Raman cross section of O_2; its presence in high concentrations at high pressure; the availability of optical filters to provide high rejection ratios for O_2 Raman against the Nd:YAG laser; and the fact that helium has no Raman cross section, and therefore does not produce a background signal which must be rejected.

Attempts to quickly implement the Raman technique in the high-pressure pulse tube were unsuccessful, however, due to the limited optical access through which the laser beams and Raman signal has to pass. Laser interferences could not be successfully rejected in this configuration. However, it should be noted that this technique holds considerable potential for this application if the laser beam and Raman signal can be directed through separate optical access.

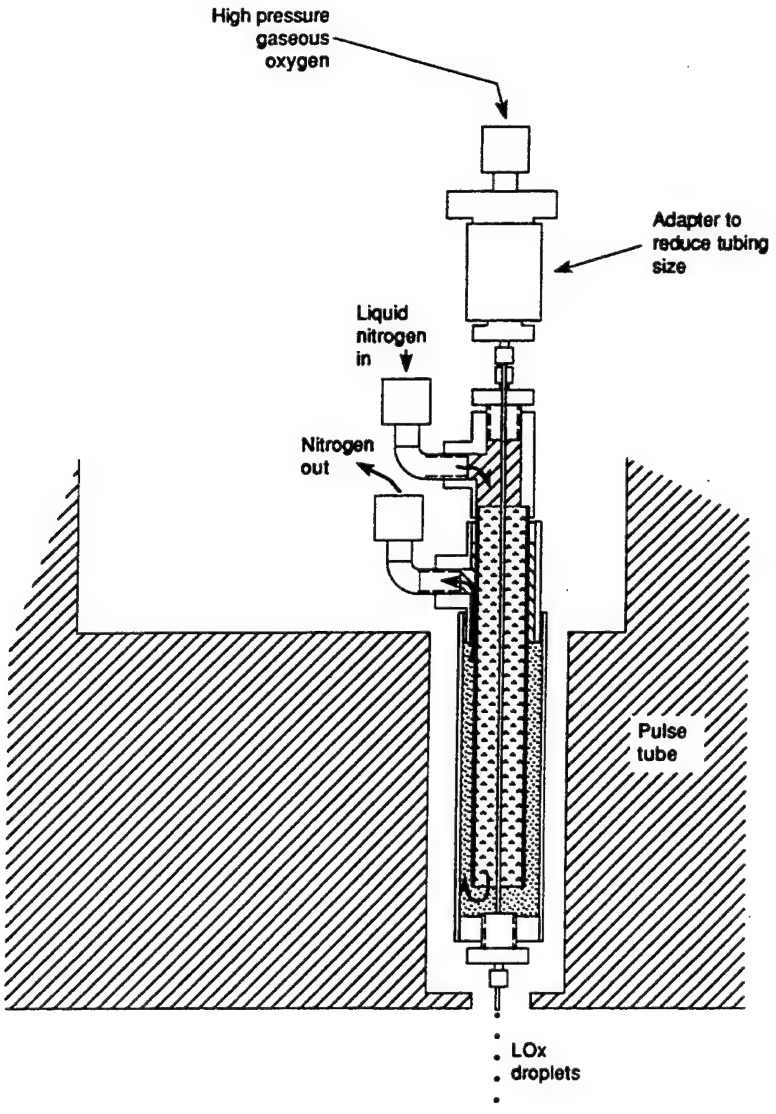

Figure 8
UTRC LOX Droplet Generator Design

Observations of the effect of acoustic pulses on the LOX droplets at supercritical pressures were made using a simple back-lit technique and imaging with a microscope lens and an intensified CID camera. Sets of double exposure images were acquired to view the droplets before and after the pressure pulse passed through the test section. In this way, the initial size and position of the droplets could be compared with the dispersed droplet fluid at some known time delay after pressure pulse passage.

In order to observe the effect of the critical point on droplet breakup, measurements were made at three initial pressures with pressure pulses of approximately the same strength. Data sets were acquired for a 600-psig initial pressure in which the O_2 pressure remained below the critical point throughout the experiment. Images were also acquired for runs with 750-psig and 850-psig initial pressure; note that both conditions are above the critical pressure. Two sets were acquired at an initial pressure of 750 psig: one with a wave strength consistent with the sub-critical condition and one with a stronger pressure pulse. Table 3 provides the test conditions.

Table 3. UTRC High-Pressure LOX Droplet Test Conditions

Initial Pressure (psig)	*ΔP (psid)*	*Pressure Ratio*	*Mach Number*	*Re*	*We*	*Oh*
600	67	1.05	1.021	11,300	501	2.6×10^{-3}
750	67	1.04	1.017	11,700	442	2.6×10^{-3}
750	130	1.08	1.031	21,300	1501	2.6×10^{-3}
850	67	1.04	1.015	11,400	370	2.6×10^{-3}

Image sets were acquired over a range of time delays in order to track the sequence of droplet fluid dispersal. Sample images are shown in Figures 9 through 12. These figures demonstrate that the droplet breakup process appears to be quite similar for droplets above and below the critical pressure, given nearly constant acoustic wave strength. Since one would expect the process to change significantly with a change in the droplet surface tension (which would occur as the surface rises above the critical temperature), these results suggest that the breakup process occurs on time scales much shorter than heat transfer to the droplet surface. Hence, the droplet continues to act as a liquid.

When compared to typical droplet vaporization and breakup results at atmospheric pressure, the high-pressure LOX droplet data herein are markedly different. The back-lit

images shown in Figures 9-12 indicate that a pressure pulse has a drastic effect on LOX droplets in a high-pressure environment. Hence, an acoustic instability-induced pulse should have a similar influence on LOX droplets in a rocket combustion chamber operating at supercritical pressures.

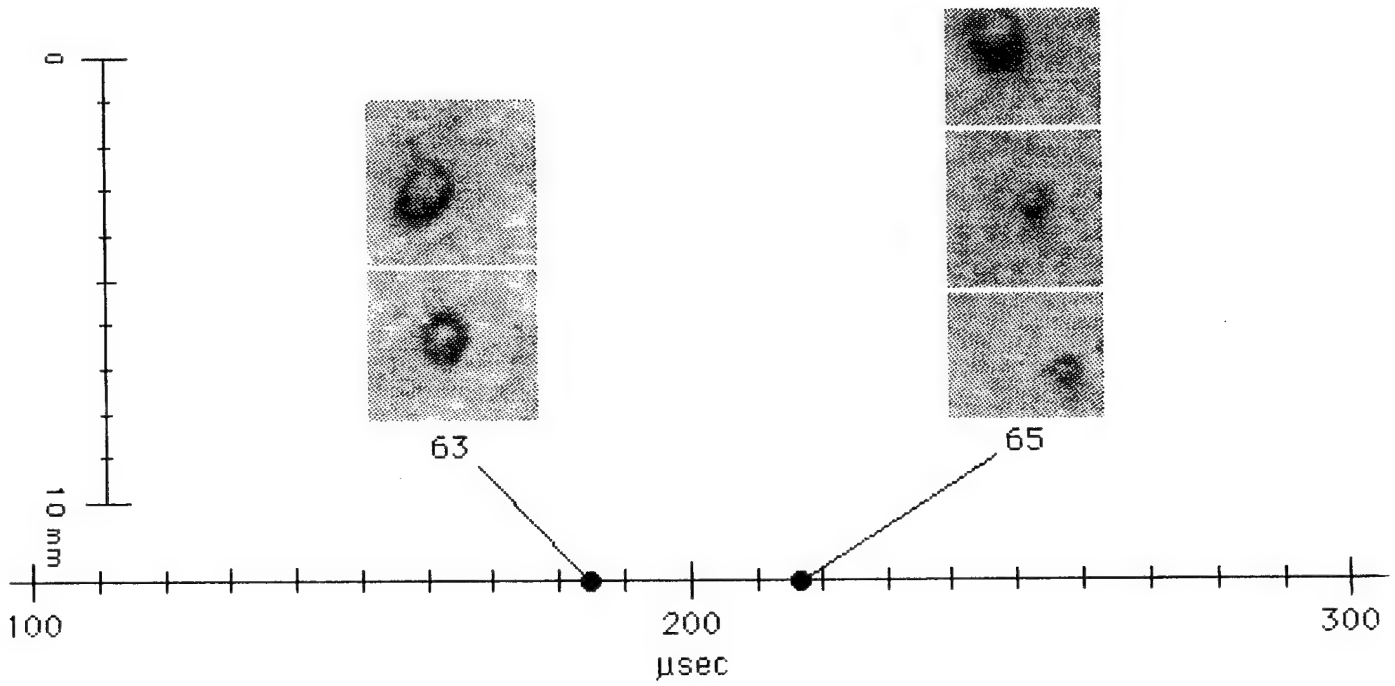

Figure 9a
Images of LOX Droplets Behind a Pressure Pulse-Sub-critical
100-300 µsec after pressure pulse passage; Pc=600 psig; ΔP=67 psid

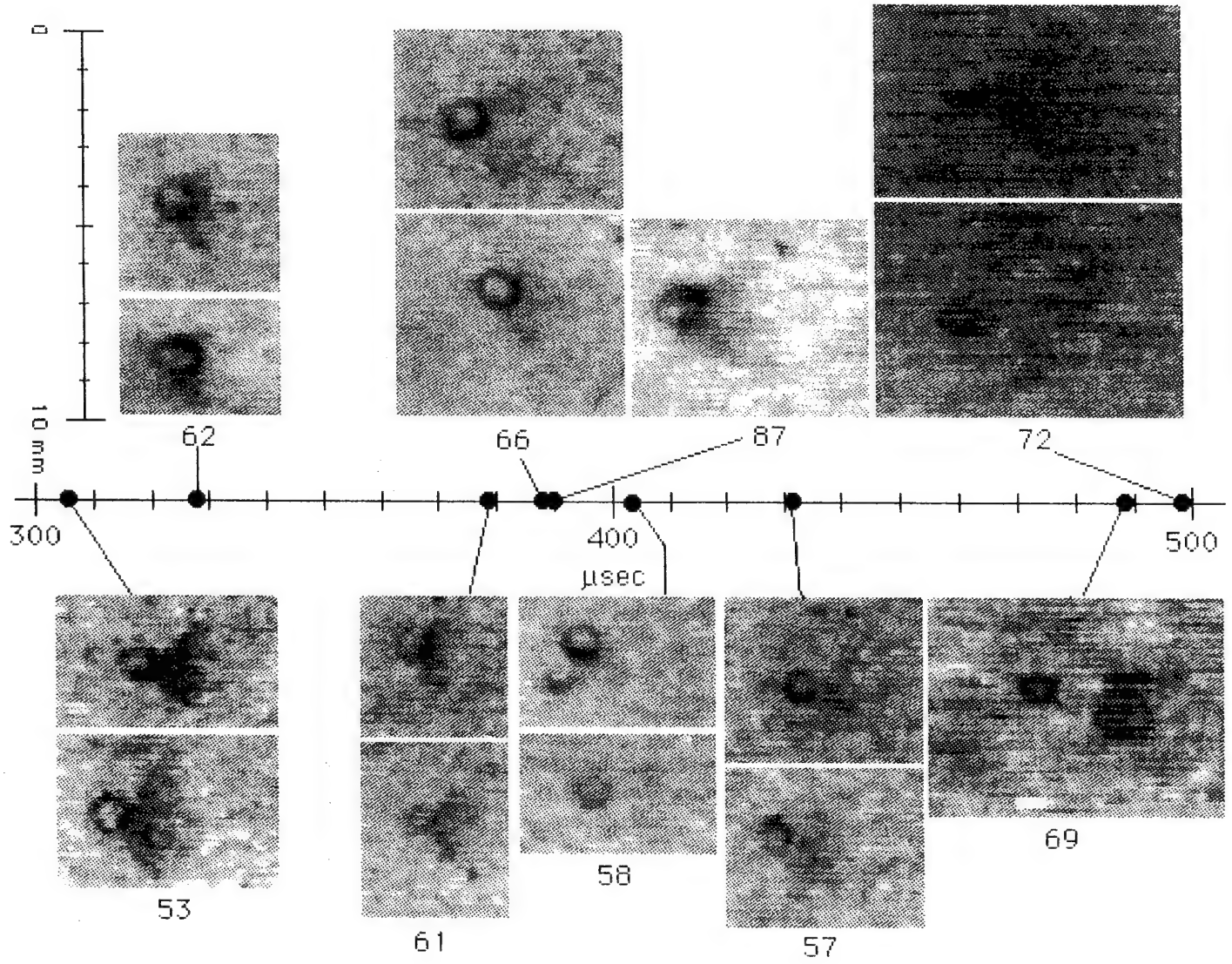

Figure 9b
Images of LOX Droplets Behind a Pressure Pulse-Sub-critical
300-500 µ sec after pressure pulse passage; Pc=600 psig; Δ P=67 psid

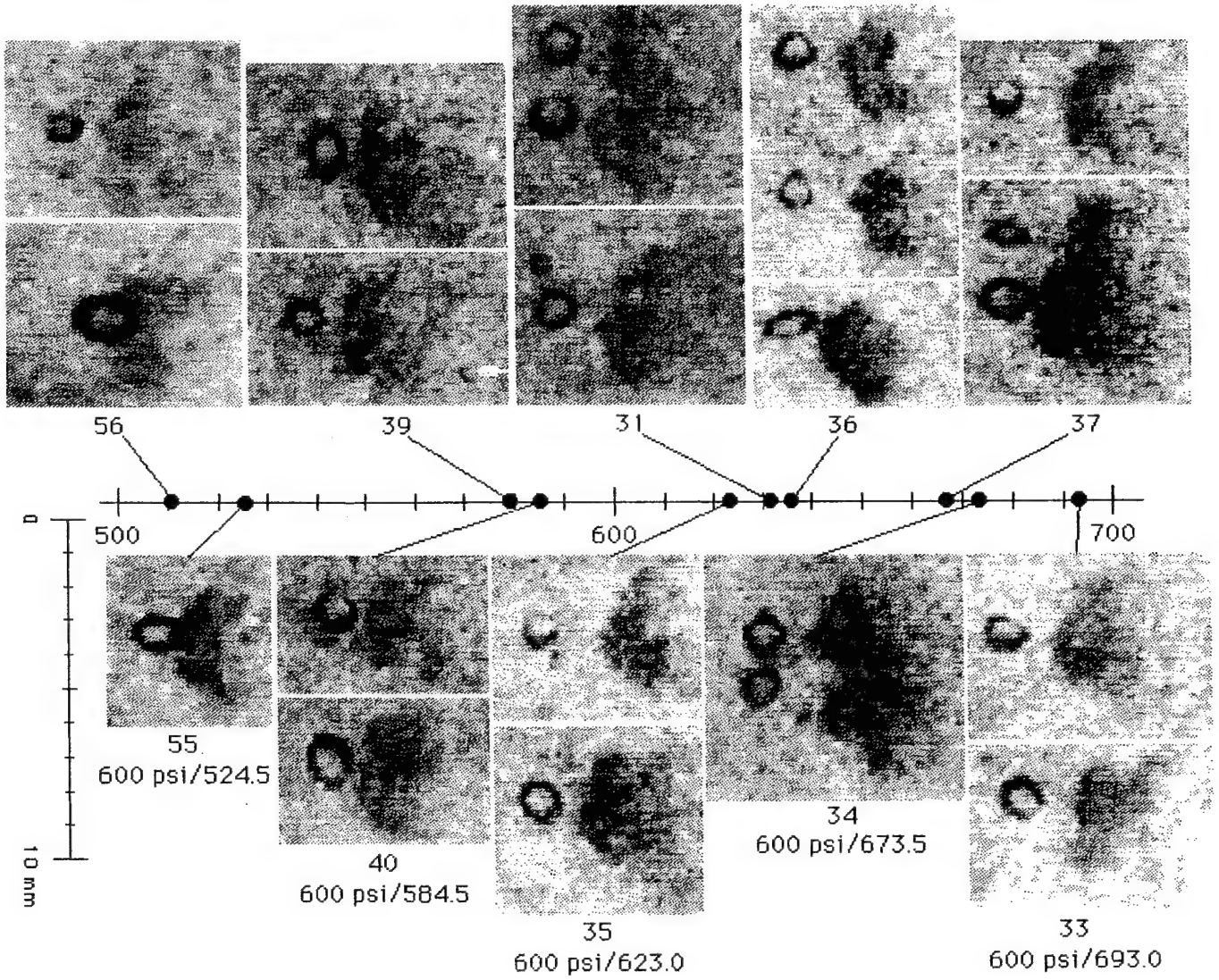

Figure 9c
Images of LOX Droplets Behind a Pressure Pulse-Sub-critical
500-700 μsec after pressure pulse passage; Pc=600 psig; ΔP=67 psid

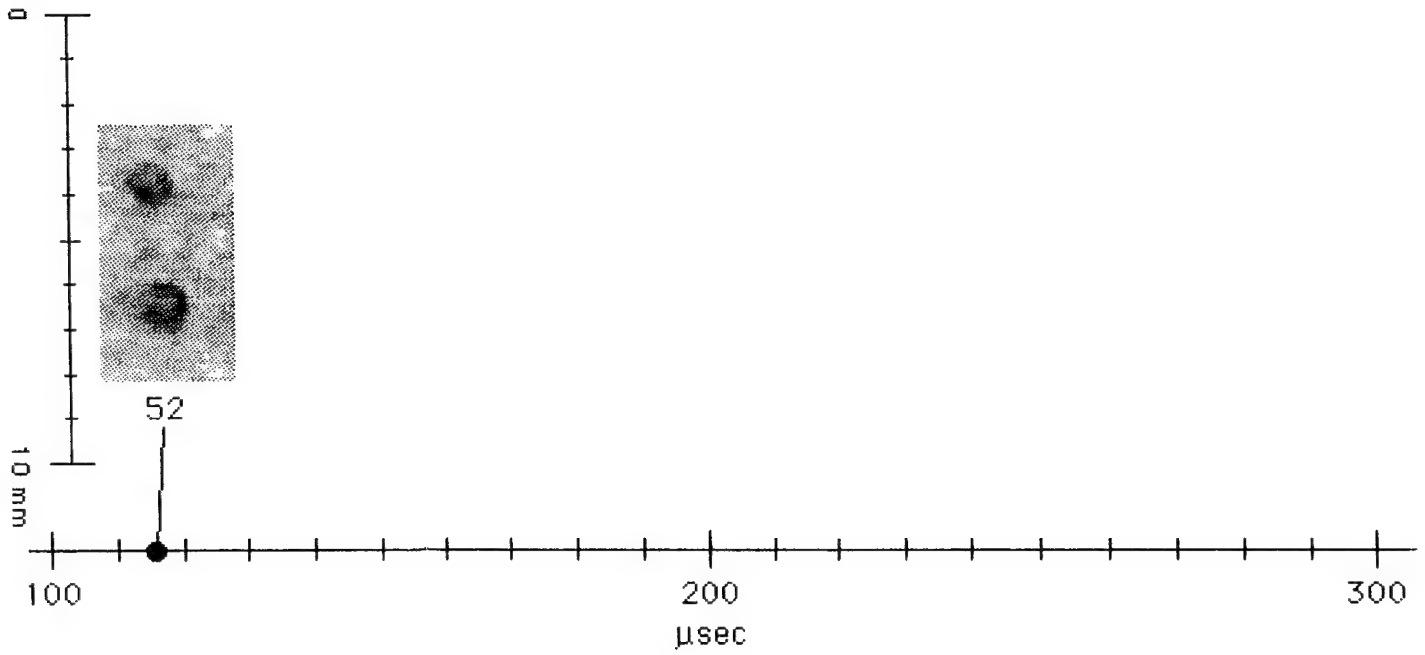

Figure 10a
Images of LOX Droplets Behind a Pressure Pulse-Supercritical
100-300 µsec after pressure pulse passage; Pc=750 psig; ΔP=67 psid

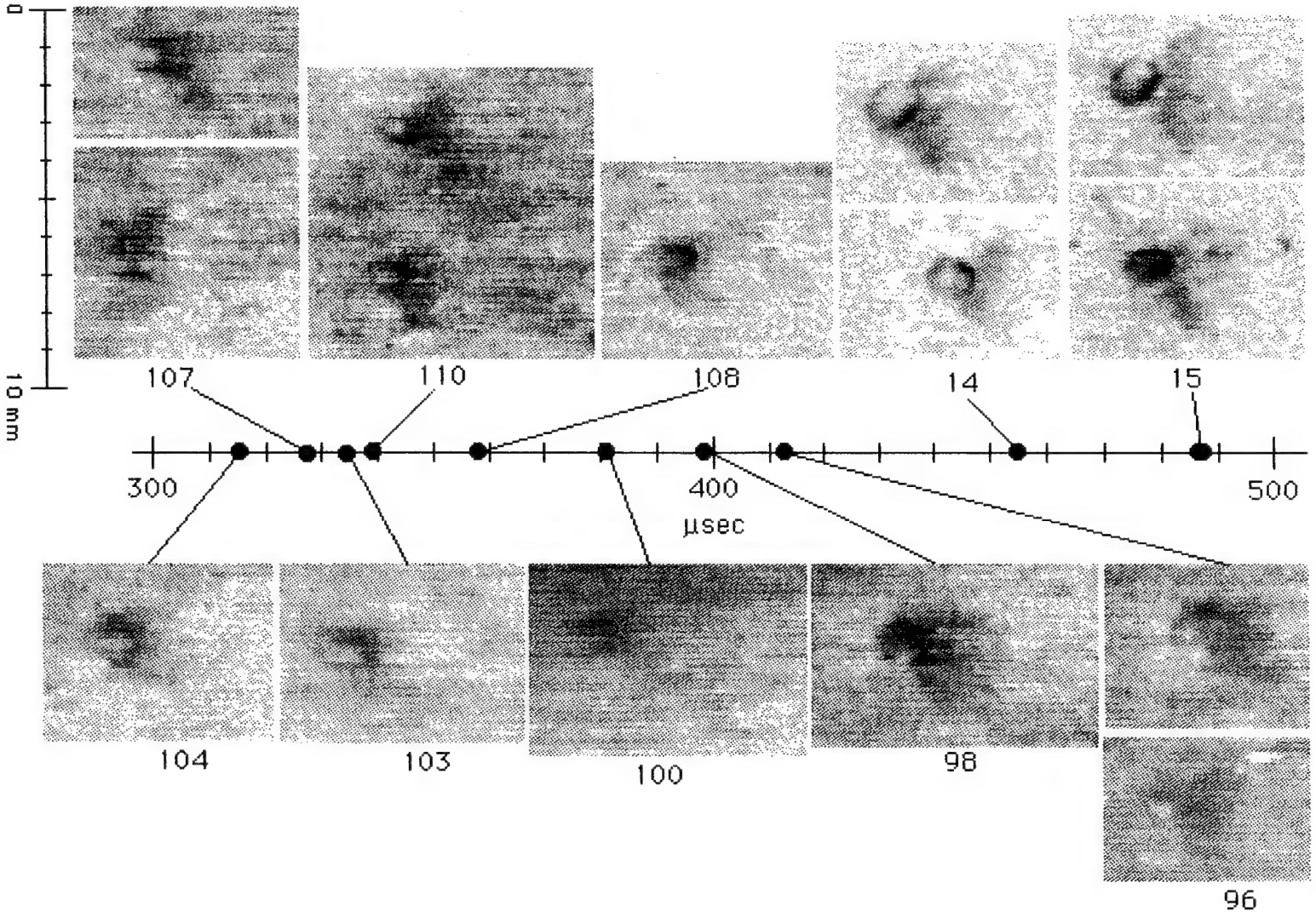

Figure 10b
Images of LOX Droplets Behind a Pressure Pulse-Supercritical
300-500 µsec after pressure pulse passage; Pc=750 psig; ΔP=67 psid

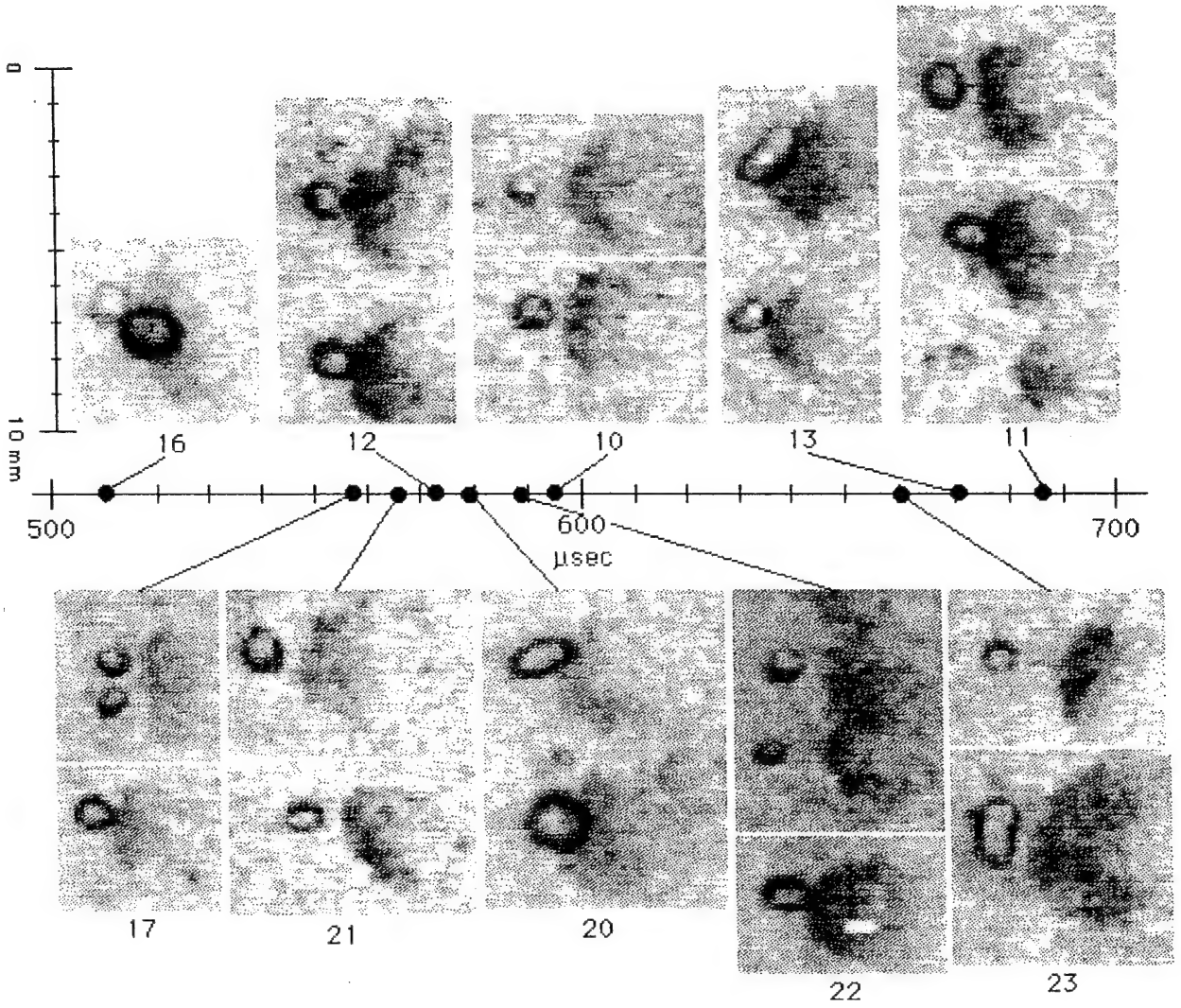

Figure 10c
Images of LOX Droplets Behind a Pressure Pulse-Supercritical
500-700 µsec after pressure pulse passage; Pc=750 psig; ΔP=67 psid

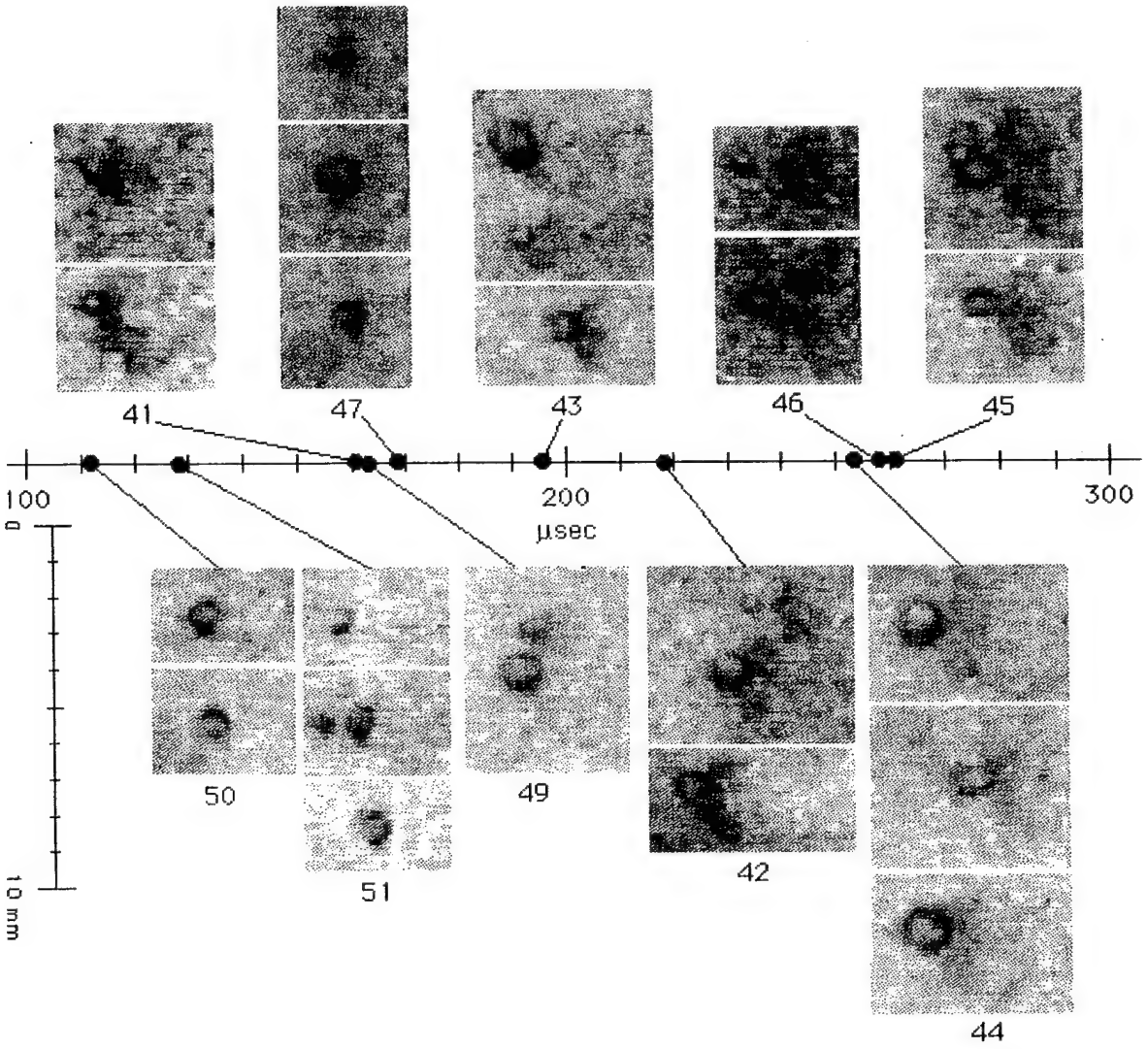

Figure 11
Images of LOX Droplets Behind a Pressure Pulse-Supercritical, Higher Pulse
100-300 µsec after pressure pulse passage; Pc=750 psig; ΔP=130 psid

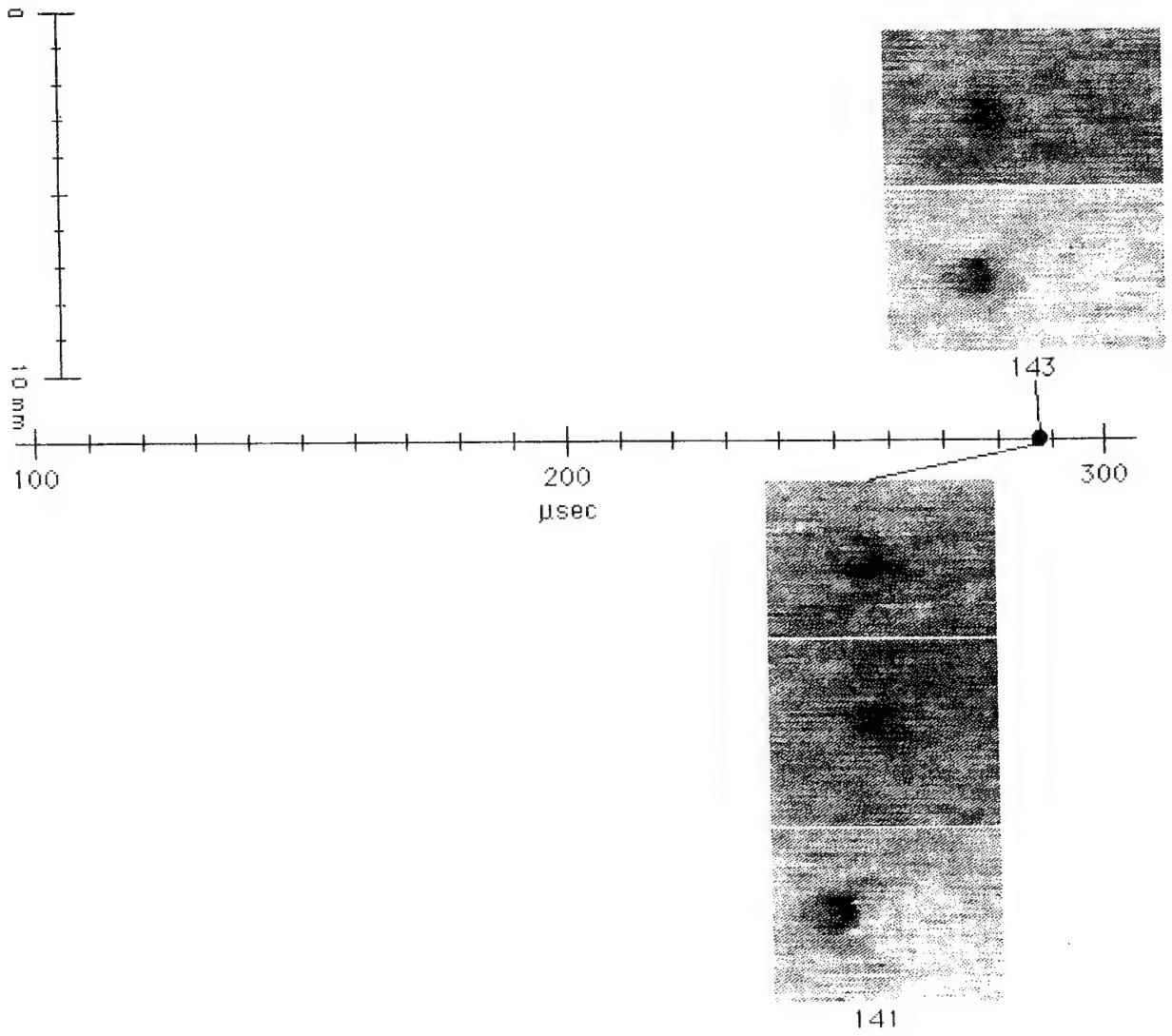

Figure 12a
Images of LOX Droplets Behind a Pressure Pulse-Supercritical, Higher Pressure
100-300 µsec after pressure pulse passage; Pc=850 psig; ΔP=67 psid

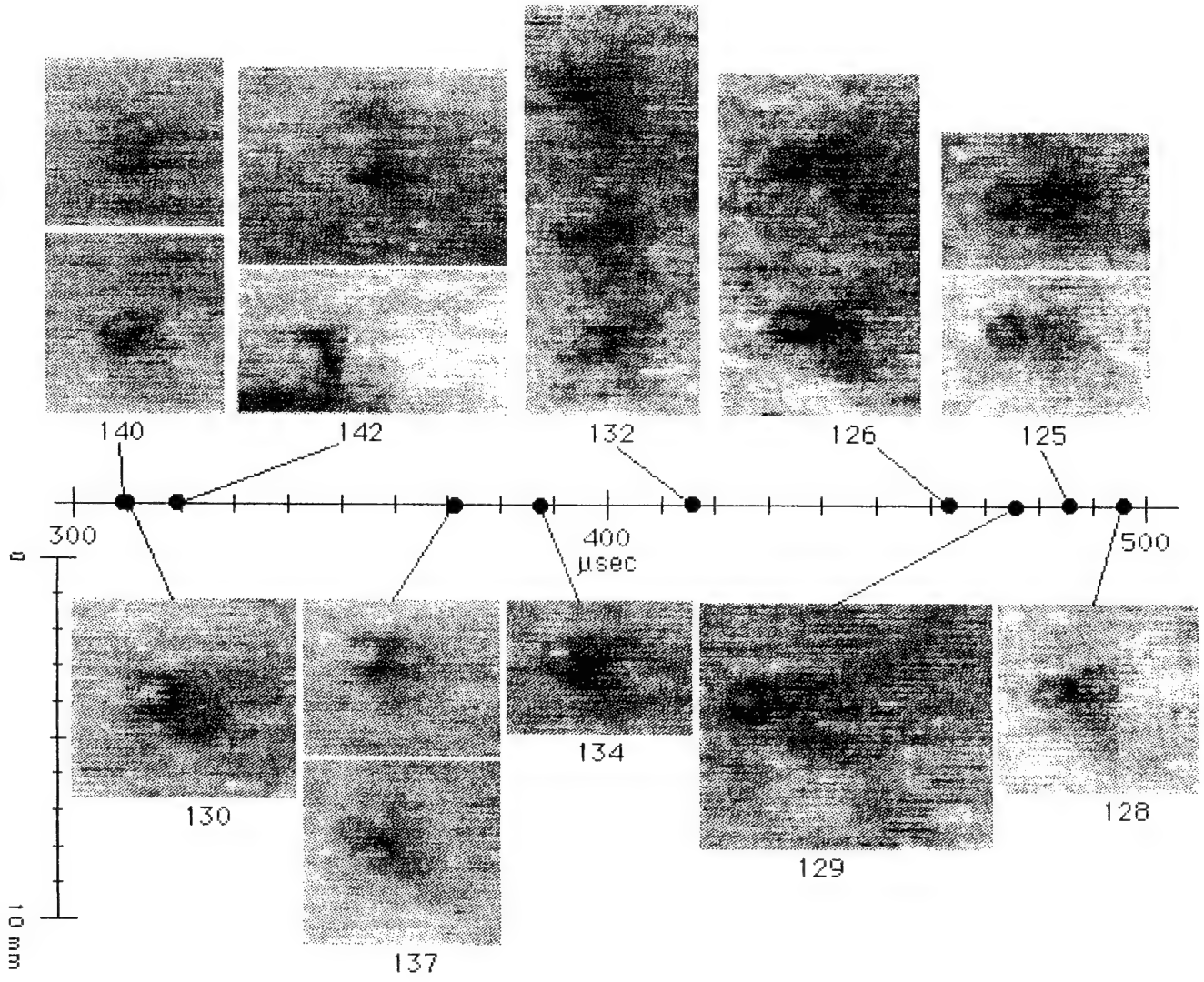

Figure 12b
Images of LOX Droplets Behind a Pressure Pulse-Supercritical, Higher Pressure
300-500 µsec after pressure pulse passage; Pc=850 psig; ΔP=67 psid

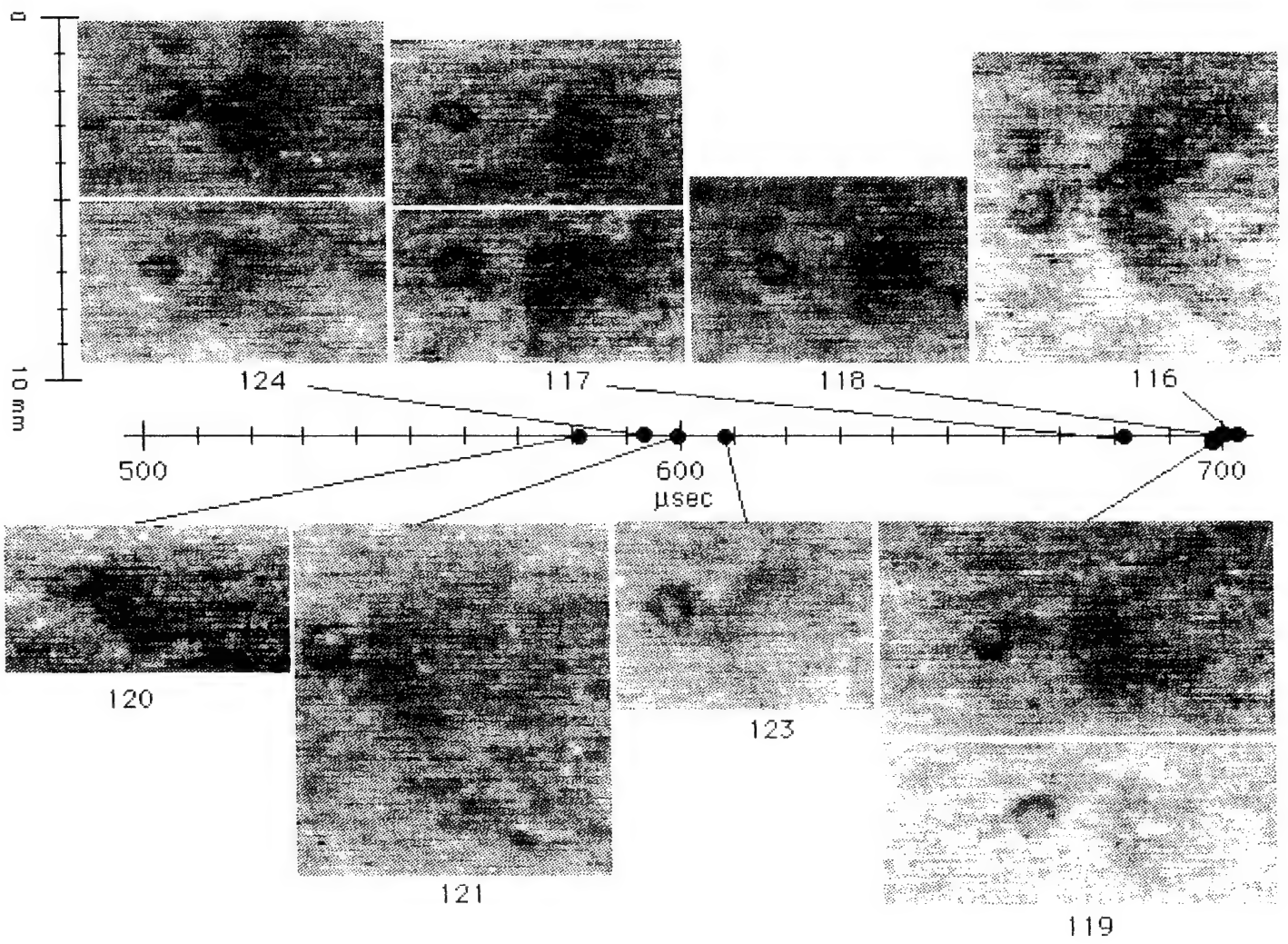

Figure 12c
Images of LOX Droplets Behind a Pressure Pulse-Supercritical, Higher Pressure
500-700 µsec after pressure pulse passage; Pc=850 psig; ΔP=67 psid

Simulant Fluid Study (P&W, UCI)

In support of the experimental investigation, a parallel evaluation of simulant fluid properties was conducted. The emphasis of the study was on the selection of cold-flow fluids and test conditions that closely match actual rocket parameters. A detailed description of the initial effort is provided in Appendix F in the form of a 1991 JANNAF paper. Provided below is a brief summary of the rocket conditions chosen to model, the simulant fluids studied, and the resulting secondary atomization test matrix. Further discussion of the droplet/wave physics is provided in the secondary atomization portion of this report.

Engine Conditions. Experimental modeling of the spray/combustion process inside a high-pressure rocket combustion chamber is difficult due to the extreme temperature and turbulent conditions which exist. Under cold-flow, non-combustion conditions, the best an experiment can do is match certain fluid properties and non-dimensional parameters that occur in the real process. The investigation herein attempts to cover a range of possible engine parameters while matching as closely as possible the expected combinations.

Due to the nature of the liquid rocket engine combustion chamber environment, relatively little is known about the behavior of fluids in the combustion chamber. The properties both of the liquid oxygen droplet as well as in the surrounding flow field are difficult to quantify. No such measurements have ever been made in a rocket engine operating during a combustion instability, and only limited measurements (8) have been made under steady, full-power conditions.

The engine parameters that were selected correspond to the conditions of the proposed Space Transportation Main Engine (STME). This 580k-lb-thrust engine is representative of the next generation of high-pressure, O_2-H_2 rocket engines. The STME has a propellant mixture ratio near 7.0 and a 2300-psia (156.5-atm) chamber pressure.

Properties at the droplet surface strongly affect transport and physical properties typically considered important in the study of vaporization and secondary atomization. While the critical pressure for the hydrogen/oxygen system typically present in rocket engine combustion chambers can be substantially more than the critical pressure of pure oxygen, the instability waves probably act prior to achieving thermodynamic equilibrium; this keeps the critical mixture ratio at the droplet surface almost purely oxygen and the corresponding critical pressure very close to that of pure oxygen (9). On this basis, the properties of liquid oxygen were presumed to be appropriate for the experiments herein.

When exploring stability mechanisms using single droplets, the test fluids must simulate both the LOX droplet and the surrounding gas. The combustion chamber conditions are more difficult to define since conditions near the injector (where combustion instability waves interact with liquid oxygen droplets) are substantially

different from those near the nozzle where combustion is complete. The gas near the injector face consists of hydrogen exiting the injectors and recirculation zones between injector elements. These zones are reasoned to contain a combination of burned products, unburned hydrogen, and vaporized oxygen. Therefore two different assumptions can be made in the definition of the combusting atmosphere of drops near the injection plane.

One assumption is that the ambient species are at the average temperature between the cold propellant and the flame temperature of the mixture. Others have defined the surrounding temperature as such (10). For a 110-K inlet temperature and a 3720-K O_2-H_2 flame temperature, the average temperature would be 1920 K. The second approach is the use of temperature measurements acquired by Boylan and O'Hara (8). Their findings indicate that the average combustion gas temperature near the injector face is approximately 1940 K. This measurement is in agreement with the preceding calculation; therefore the surrounding gas temperature was assumed to be 1940 K.

Table 4 provides the resulting STME droplet and surrounding gas properties. Table 5 presents the expected ranges of droplet Reynolds, Weber, Ohnesorge numbers, and density ratios for the given drop size range and acoustic pulse strengths.

Table 4. Rocket Conditions Chosen to Model

Liquid Properties		*Gas Properties*	
T (K)	94	T (K)	1940
Density (kg/m^3)	1153	γ	1.14
Viscosity ($N\text{-}s/m^2$)	2.2×10^{-4}	Molecular Weight	14.6
Surface Tension (Dyne/cm)	12.1	Viscosity ($N\text{-}s/m^2$)	64×10^{-6}
P_{cr} (atm.)	50		
T_{cr} (K)	154.8		

Table 5. Rocket Parameter Ranges

Drop Diameter (μm)	10 - 500
Pulse Strength	5% - 50%
Re	110 - 65,000
We	30 - 140,000
Oh	9.7×10^{-4} - 0.29
ρ_1 / ρ_2	56 - 77

Simulant Fluids. A number of test liquids were chosen as possible droplet simulants. The physical properties of primary interest included density, surface tension, and viscosity. For modeling supercritical conditions, the critical pressure and temperature were important. Practical considerations such as vapor pressure, ease of handling, and availability also affected the selection procedure.

Two liquid simulant classifications were developed and are referred to as sub-critical and supercritical. The sub-critical liquid choices were intended for secondary atomization and vaporization tests that were exploring the effects of all rocket parameters except the reduced pressure and temperature. The supercritical simulants were chosen to model the response of a droplet to a velocity wave while at conditions above the critical point. Table 6 presents the selected sub-critical liquids, and Table 7 gives the supercritical liquids.

Of the Table 6 sub-critical fluids, water, methanol, and Freon 22 were chosen for the main secondary atomization tests. Methanol and water were used in the UTRC 1-atm vaporization experiments because of their ability to dissolve the MDR dopant. Note that only liquids with sub-atmospheric critical temperatures were selected for Table 7 since the test sections of the UCI and UTRC shock tubes were maintained at room temperature (T_r always > 1). Likewise, the test section pressures were limited to 1000 psia, so liquids with P_{cr} < 1000 were required. As previously mentioned, UTRC employed LOX as the supercritical droplet simulant.

Standard gases were selected as the combustion gas simulant. Air, argon, and helium adequately provided the required wave velocities and densities to match the specified rocket parameters.

Table 6. Sub-critical Simulant Liquids

Liquid	*Density (kg/m^3)*	σ *(Dyne/cm)*	*Viscosity x 10^4 (kg/m-s)*	*Vapor Pressure (atm.)*
Water	1000	73.1	9.67	0.03
Freon 113	1650	17.0	6.84	0.41
n-Pentane	631	16.5	2.26	1.09
Freon 22	1230	9.0	1.98	9.80
N_2O	1225	1.8	0.21	52.4
MIL-C-7024	769	23.0	8.63	< 1.0
Freon 12	1304	9.0	2.07	6.80
Ethanol	791	22.0	11.1	0.01
Methanol	791	22.6	5.62	0.14
n-Decane	730	23.8	9.02	$\cong$ 0
LOX (@ 110 K)	1041	8.2	2.11	6.8

Table 7. Supercritical Simulant Liquids

Liquid	*Pcr (atm.)*	*Tcr (K)*	*Density (kg/m^3)*	σ *Dyne/cm*	μ *$x10^4$ (kg/m-s)*	*Vapor Pressure (atm.)*
LOX (110 K)	50	155	1041	8.2	2.11	6.80
LN_2 (110 K)	33.5	126	624	6.6	0.56	15.6
Ethylene	49.7	282	521	16.5	0.58	-
Freon 23	47.7	299	670	15.0	1.67	9.52
Freon 14	36.9	228	1317	4.0	2.31	14.3
Freon 503	43.0	293	1234	6.0	1.44	11.2

Secondary Atomization (UCI)

Secondary atomization or drop breakup can occur in at least three different manners in liquid rocket engine combustion chambers: 1) in the high velocity shearing flow field in the near injector region of a shear coaxial injector; 2) as gases expand and accelerate in the reaction zone; and, 3) during combustion instability (see Figure 13). In each of these situations, a relative velocity between the gas surrounding the droplet and the droplet exists which tends to aerodynamically deform and potentially break up the droplet.

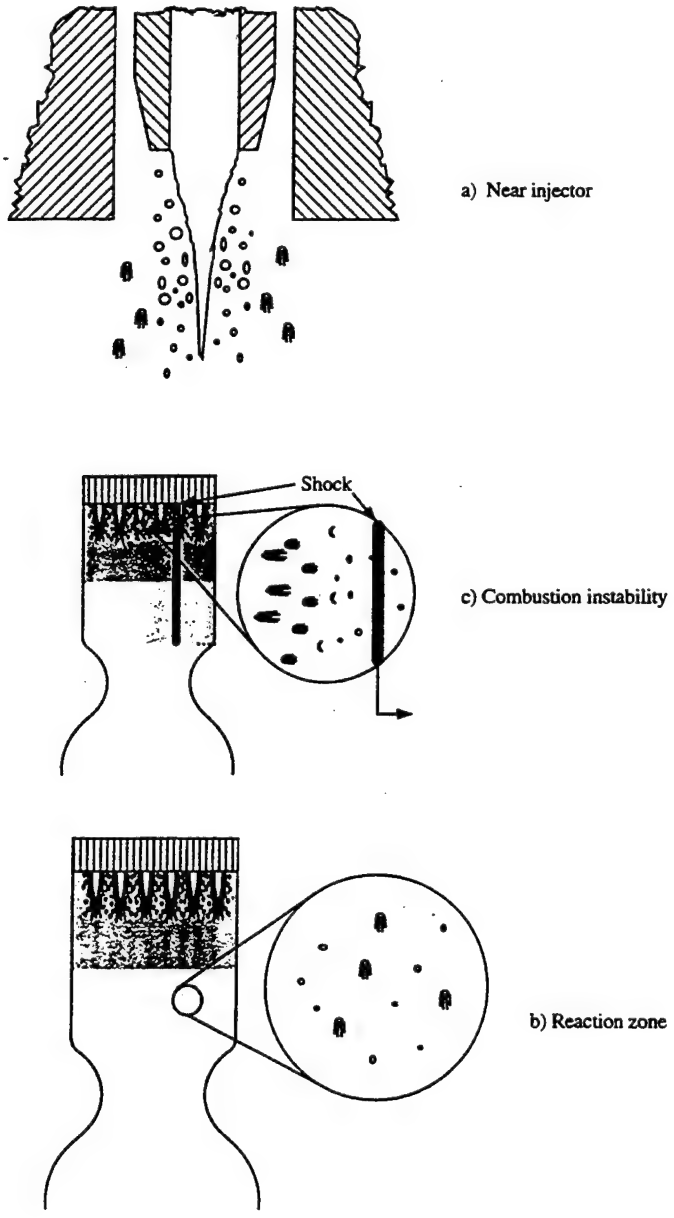

Figure 13
Liquid Rocket Engine Secondary Atomization Processes

In liquid rocket engines, primary and secondary atomization processes prepare the liquid phase for vaporization into and mixing with the gas phase. The degree of secondary atomization determines vaporization and mixing rates of the droplet phase in the surrounding gas. In dilute sprays, vaporization is typically found to control the mixing rate. In some dense sprays, however, secondary atomization can be found to control the mixing rate (11).

Secondary atomization typically occurs in the near injector region where ligaments of liquid break off from a jet or sheet and then further breakup as they are sheared by co-flowing gas. Another source of drop breakup is the reaction induced expansion of the combustion gases which rapidly accelerate relative to any unburned propellant droplets. As a droplet breaks apart, more liquid surface area per unit volume is available for the vaporization process, and the liquid is distributed about a larger volume. Thus in addition to primary atomization, secondary atomization can directly affect the distribution of the liquid phase and therefore the local gas properties such as mixture ratio of the flow field. The resulting drop size and spatial distribution affects how rapidly the mixture can be expected to react, where it will react relative to the injection point, and what combustor length is required to contain the reaction.

During combustion instability, secondary atomization may play a role in initiating, augmenting, and/or sustaining the instability. In high frequency combustion instability for such systems, a spontaneously generated shock wave can cause propellant droplets to shatter, leading to more rapid vaporization and combustion. The passing wave causes step changes in pressure, velocity, temperature, and density. These changes affect either the aerodynamic forces experienced by the droplet, the vaporization environment, or both. Secondary atomization may play an indirect role in providing a vaporized liquid propellant to the gas phase for combustion in phase with the passing wave and directly add to the amplitude of that wave. If the pressure-induced fluctuation of energy release causes a further change of pressure in phase with the initial disturbance, then the result may be an instability (12).

Predominant high amplitude processes are the transient aerodynamic distortion of streams and droplets; the ensuing aerodynamic mass stripping; and the displacement and convection of reactive propellant streams. The drop distortion and breakup mechanisms associated with the passing of a pressure disturbance provide a stepwise change in the liquid surface area available for vaporization and therefore could be indirectly responsible for combustion instability in liquid rocket engines. For an order of magnitude reduction in the size of daughter droplets from the original parent drop, the surface area available for vaporization increases by an order of magnitude. For breakup that might be expected in a typical combustion instability, the daughter droplets might be two orders of magnitude smaller with a resulting hundred-fold increase in vaporizing surface area.

In addition, the smaller droplets tend to follow the pulse-induced flow, thus reducing penetration relative to the original drop and redistributing a reacting component spatially. The displacement and convective mechanisms provide a means to redistribute the gas phase propellants and small, rapidly vaporizing droplets so that they may mix and react with their unreacted counterparts and hot partially reacted streams which serve as ignition sources.

Williams (13) found that for a vaporizing spray, energy release alone would not reinforce an imposed shock and it would eventually dissipate due to large wall losses. However when he considered the same problem accounting for aerodynamic drop shattering to a drop size of less than 10 microns, the spray detonation which developed was found to be essentially the same as a gas detonation. Shear stripping routinely causes drop sizes to be less than this value.

Dabora, Ragland, and Nicholls (14) showed conclusively that aerodynamic shattering and droplet breakup time (which are directly proportional to drop diameter) play major roles in the reaction zone length and thus the characteristic time over which reaction occurs.

The pressure-time histories typically observed in instrumented rocket engine combustion chambers reveal a series of waves similar to N-waves in shape. Figure 14 shows a typical N-wave instability measurement. As such a wave passes, the droplet will initially accelerate and may actually exceed the velocity of the flow field later in the wave at which point it decelerates with respect to the laboratory reference frame. The only known effort to examine this droplet/N-wave interaction to date is that of Temkin and Mehta (15). They examined unsteady droplet drag using single frame stroboscopic photography at an equivalent of 4000 frames per second. The wave strengths were held to less than 0.03 in order to maintain the spherical shape of the 1-atm water droplet (breakup was prevented). The sole motivation for using N-waves appears to lie in their inherent nature to provide both an accelerating and decelerating flow during the same test. Therefore, the results are not applicable to this program. Mehta's dissertation (16) does examine breakup; however, the wave strengths as well as Re and We numbers are relatively low compared to the work proposed here. Therefore, the breakup regime examined is probably not applicable.

A further complication in most liquid rocket engines is that the liquid is injected at pressures above its critical pressure. The critical pressure of pure oxygen is about 730 psia and typical chamber pressures range between 500 and 6000 psia.

The response of a drop subject to the passing of an instability wave can include one or more of the following:

1. Transverse motion with both acceleration and deceleration.
2. Reorientation of the internal Hill's spherical vortex.

3. Aerodynamic deformation.
4. Oscillation.
5. Surface wave formation.
6. Ligament formation and breakup into smaller droplets.
7. Stripping of small drops from the original droplet up to the point of total disintegration.
8. Greatly enhanced evaporation from both the original droplet and smaller drops which are stripped from it.
9. Collision with neighboring droplets with associated motion, dynamics, breakup, and/or coalescence.
10. Redistribution and dispersion of the liquid and gas phases of the propellants.

The approach of this study was to experimentally observe the response of a droplet or droplet stream injected transversely across the bore of a shock tube to the passing of a single N-wave. The diagnostics employed included stroboscopic scattered-light photography, still shadowgraphy, and shadowgraphic cinematography at high magnification. Basic parameters under examination were droplet size, wave strength, and wave duration. Property variations of the droplet liquid and test section gas were also examined. While the basic approach to examination of these phenomena was far from the physical situation, the physics are believed to be similar.

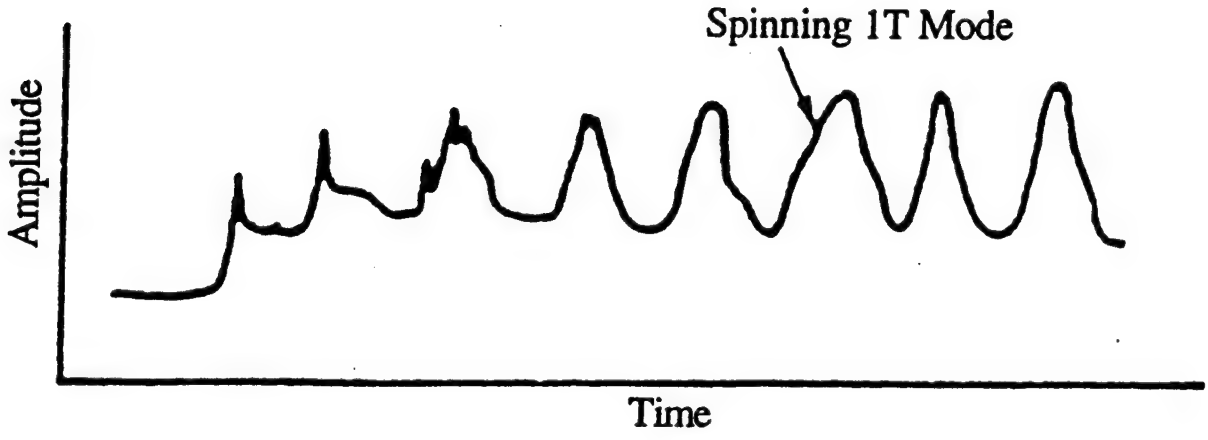

Figure 14
Typical Steep-Fronted Wave, or N-Wave (Harrje and Reardon, 1972)

Approach. Formulation of the secondary atomization experiments was preceded by a literature search. The comprehensive review of the secondary atomization literature was compiled by Ted Eastes and is included as Appendix G. This review details secondary atomization theory and includes applications, diagnostic techniques, characterization parameters, breakup modes, flow-transient effects, drop deformation, drag coefficients, breakup times, and stripping rates. This appendix should be consulted for more in-depth secondary atomization information.

Typical dimensionless numbers are generally employed to characterize secondary atomization. These include, among others, the ratio of convective flow inertial-to-viscous forces, or Reynolds number (Re); the ratio of dynamic pressure forces to droplet surface tension forces, or Weber number (We); and the ratio of liquid surface tension forces to viscous forces, or Ohnesorge number (Oh). Three different types of breakup have been defined, depending on the levels of each of the specified dimensionless numbers. Borisov et al. (17) suggested the following criteria for each breakup mode:

"bag breakup:"	$8 < We < 40$	
"shear breakup:"	$20 < We < 2x10^4$	
"explosive breakup:"	$2x10^3 < We < 2x10^5$	(1)

Breakup time is an important secondary atomization parameter used as the dependent, or measured, experimental variable. The breakup time (τ_b) is defined as a function of the gas-to-liquid density ratio, the convective velocity, and the droplet size. Nonetheless, as described in Appendix G, the definition of breakup time is often not very clear. For the purposes of this study, the breakup time as defined in equation G-8 (K=1) will be used for reporting expeimental results (see later section).

The shock tube experiments proposed for study of secondary atomization were designed to observe how drops of varying sizes break up when subjected to pressure waves of varying amplitudes. In order to extend these observations to what might be typical in an actual liquid propellant rocket engine (see Tables 4 and 5) undergoing high frequency acoustic combustion instability, experimental parameters and conditions were defined as follows:

1. Drop sizes were varied over a range believed to be characteristic of a typical rocket engine (50-500 microns).

2. Pressure wave amplitudes were varied from acoustic levels to strengths representative of those observed in a typical rocket engine combustion instability (10-100%).

3. The wave shape (N-wave) and duration (< 5 msec) were similar to that observed in a typical rocket engine combustion instability.

4. The droplet was exposed to a wave traveling transverse to its original path to simulate the commonly observed spinning transverse wave with a duration corresponding to actual frequencies (> 200 Hz) in a typical rocket engine combustion instability.

Parameters which are believed to influence the secondary atomization process are as follows:

1. Wave amplitude
2. Drop size
3. Drop configuration (single drop, drop stream, drop array, spray)
4. Liquid properties
5. Gas properties
6. Drop velocity/acceleration prior to wave impingement
7. Internal vortical structure progression
8. Convective gas velocity prior to wave impingement
9. Wave character or shape
10. Wave duration
11. Wave frequency

Prudent experimental practice indicates that the relative effects of each of these parameters should be studied independently so that their relative sensitivity to the phenomena can be assessed. Due to the limited nature of the proposed experiments, a number of judgments regarding the relative importance of each of these parameters was required *a priori*. A design of experiments test matrix was thus developed based on these parameter relevance estimates (18). In the initial tests, efforts to simplify the experiment and the flow field were necessary, as de-convolution of these effects is essential to any successful modeling effort undertaken.

Using the chosen simulant fluids (Tables 6 and 7), the test conditions that match the desired rocket conditions (Tables 4 and 5) were calculated. The independent test variables included the test section pressure (P_1), the pressure upstream of the pulse (P_2), the duration of the pulse, and the droplet size (D).

Table 8 gives an ideal 16-test, high-pressure secondary atomization test matrix. Two levels of each independent variable were used. The Table 8 matrix provides a Reynolds number range from 890 to 210,000; a Weber number range from 17 to 34,000; and a density ratio range from 15 to 136. These test parameters bracket the actual rocket ranges seen in Table 5 with the exception of the upper We limit.

Table 8. Ideal Secondary Atomization Test Matrix

Test	*Liquid*	*Gas*	P_2/P_1	D (μm)	P_1 (*psia*)	*Pulse Time*
1	Methanol	Argon	1.1	90	100	short
2	Water	Argon	1.1	90	100	long
3	Freon 22	Air	1.1	90	400	long
4	Water	Air	1.1	90	400	short
5	Freon 22	Air	1.1	360	100	short
6	Water	Air	1.1	360	100	long
7	Methanol	Argon	1.1	360	400	long
8	Water	Argon	1.1	360	400	short
9	Methanol	Air	2	90	100	long
10	Water	Air	2	90	100	short
11	Freon 22	Argon	2	90	400	short
12	Water	Argon	2	90	400	long
13	Freon 22	Argon	2	360	100	long
14	Water	Argon	2	360	100	short
15	Methanol	Air	2	360	400	short
16	Water	Air	2	360	400	long

Shock Tube Facility. The shock tube fabricated for this work is of the double diaphragm variety. Advantages of this type of tube over other varieties include the ability to discharge it on demand and the wave amplitude repeatability obtained. Both qualities are desirable in these experiments. The on-demand capability allows preparation for and sequencing of the photographic diagnostic. The amplitude repeatability capability allows accurate setting of the desired amplitude from test to test. Diaphragm costs are low, and the on-demand characteristic inhibits potential synchronization problems. Other techniques for generation of pulses were reviewed; the results of this examination are included as Appendix H.

The 2" x 2" square cross-section, double diaphragm shock tube used for this effort is capable of holding pressures to 1000 psia in the driven section and 3000 psia in the driver section. This permits, for instance, the observation of wave-induced droplet response for a 675-psia ambient pressure and a 50% wave. Figure 15 shows a system schematic including diagnostics.

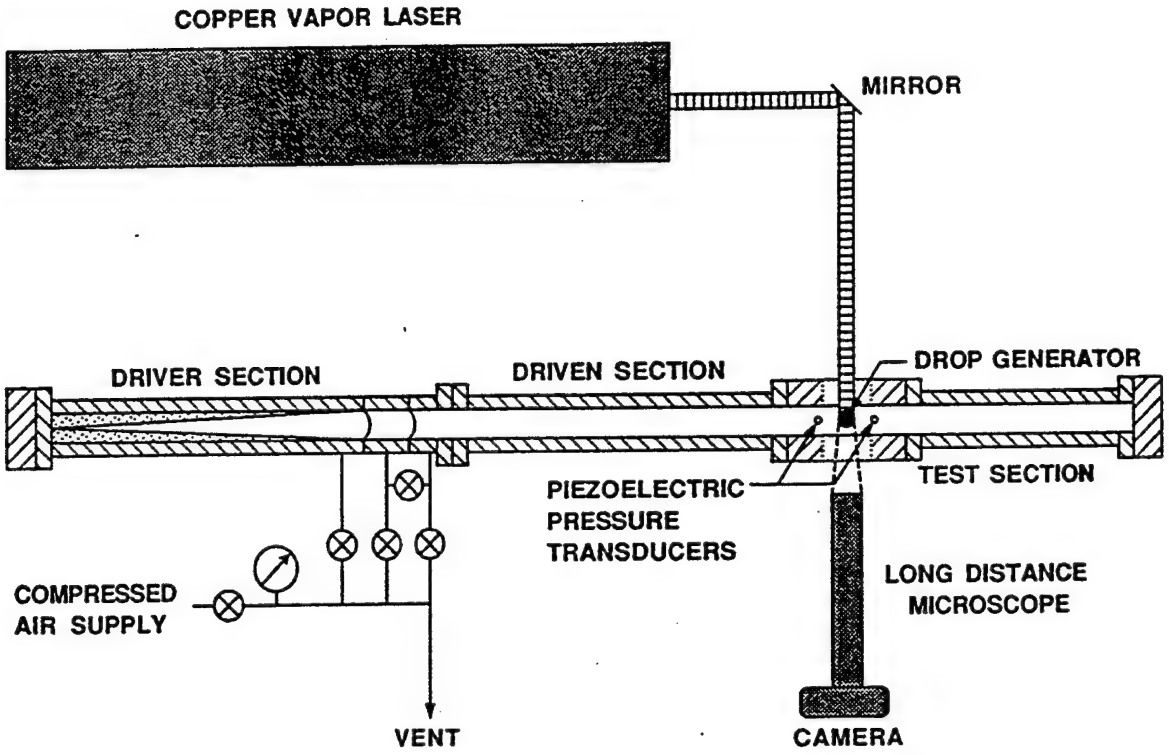

Figure 15
Schematic of Shock Tube Experiment

General design features common to flanged sections of the shock tube include an o-ring seal at one end of each section. The flanges are electron beam welded to tubing (3/4 inches deep) and butt-welded on the inner face. The limiting feature of most hardware is the strength of the bolts (grade 8 alloy used as design reference) used to attach the sections together; higher design pressures are possible with correspondingly stronger bolts.

The driver section is composed of two, 4-inch-diameter, 5/8-inch-wall pieces of 304 stainless steel tube. The longer section is 35.438 inches long and has a blind flange bolted at one end. The shorter, 2-inch section has an o-ring seal at one face which mates to the longer section, contains a 1/8 NPT port for purposes of filling the driver section, and provides a sealing surface for the upstream side of the first diaphragm (see design drawings in Appendix I). This two-piece design provides versatility in the diaphragm holding technique, the driver section overall length, and the fill port design. The 2-inch section provides a manageable piece of hardware for purposes of design changes to both the driver section and the diaphragm holder as well as rework of sealing surfaces which are subject to wear and tear. For room temperature air, this provides a test time of approximately 6 msec in the uniform flow region behind the shock.

In order to obtain an N-wave, a conical volume within the driver section was employed. The conical volume was obtained by forming a soft, clay-like material known as Sculpey using a lance-like mandrill in a rolling pin fashion about the interior of a 2.75" diameter by 1/8" wall aluminum tube (see design drawings in Appendix I). A Plexiglas cap was inserted at the head end with a guide hole though its center so that the mandrill's motion is restricted at one end during the rolling process. This assembly was then placed inside the existing driver section to produce a conical driver section. Mehta and Temkin (15) machined their driver section to a specific length in segments without the versatility of the design used here.

The diaphragm holder is composed of three pieces (fore, mid, and aft sections) of 4-inch-diameter, 5/8-inch-wall, 304 stainless steel tube (see Appendix I for design drawings). Each section is 2 inches long, and the aft section actually makes up the shorter segment of the driver section. Diaphragms composed of sheets of aluminum and brass foils are placed at the interfaces between the fore and mid sections and between the mid and aft sections. The fore section is flanged at one end so that it may be interfaced with driven sections, and all sections have a 1/8-inch NPT port through which gas is introduced. Sealing relies on a crush fit of the diaphragm material at low pressures and 1/16-inch thick Delrin gaskets on either side of the diaphragm at high pressures. The sealing surfaces of the diaphragm holders must periodically be reworked to maintain the seal.

Pressure differentials for different material configurations are shown in Table 9. In theory, the pressure differential between the driver section and the test section varies from slightly more than Δp_{burst} to slightly less than twice Δp_{burst} so that a wide range of shock strengths is available. In practice, imperfections in the diaphragm material, variations of diaphragm material thickness, and the finite volume of the intermediate section (which reduces the pressure of the driver section after the first diaphragm has burst) all reduce this potential range of operation.

Table 9. Diaphragm Material Burst Pressure Differentials

Material Description	Burst Pressure Differential (psi)
Heavy duty Al foil 0.001", 1 sheet	9-10
Heavy duty Al foil 0.001", 2 sheet	18-19
Heavy duty Al foil 0.001", 3 sheet	25-26
Brass foil 0.001"	30-35
Brass foil 0.002"	135-160

The diaphragms divide the shock tube into three sections: 1) the driver section (high pressure); 2) the driven section (low pressure); and, 3) the intermediate section (intermediate pressure) whereby the pressure differential across the diaphragms is insufficient to fail the diaphragm. The filling process is such that all sections are filled to the test section pressure initially; the intermediate and driver sections are then filled to the intermediate section pressure; and then the driver section is filled to its final pressure. To initiate the shock, the gas in the intermediate section is dumped into the driven section. This causes the pressure differential across the first diaphragm to exceed the point at which it fails. The first diaphragm then fails, and because the volume of gas in the driver section is so much greater than the intermediate section volume, the combined volume of the driver section and the intermediate section is still at a pressure in excess of that needed to fail the second diaphragm. The second diaphragm then fails and the wave propagates down the shock tube to the test section.

Six driven section lengths with mating flanges are composed of 3-inch-by-3-inch-square, 1/2-inch-walled aluminum tube to yield a 2-inch-by-2-inch bore encased in a 4-inch-diameter, 1/4-inch-wall, 304 stainless steel tube (see design drawings in Appendix I). The empty volume between the two tubes was filled with epoxy. The square tube bore dimensional variation was found to be approximately .012 inches. However, the mating face variations were reduced to .002 inches by cutting a number of lengths and using only those within a specified tolerance. In this manner, transitions between sections were optimized to provide minimal steps between sections. Transition between the round cross-section of the diaphragm holder and the square cross-section of the driven section was smoothed out with modeling clay.

The test section provides a station where droplets are introduced into the bore of the shock tube, collected liquid is removed, and 3.5-inch-diameter viewports are placed to fully view the drop/shock interaction (see design drawings in Appendix I). The design of the test section also maintains constancy of the 2" by 2" cross-section to minimize reflections from test section internal surfaces which could adversely affect the tractability of the flow field. Provisions for location of piezoelectric pressure transducers before and after the drop injection station were also made. The circular viewports are positioned with a downstream offset from the droplet introduction station so that the viewing region

anticipates the loci of the droplets during the interaction. The windows are composed of quartz (NSG-OZ, which is not optical quality, but is adequate for photography), are 3.5 inches in diameter by 2 inches thick, and have a design pressure is in excess of 1500 psia. The windows are face sealed with a double o-ring technique which has been proofed to over 1100 psia (see design drawings in Appendix I). All metal surfaces in contact with the windows are veneered with either aluminum tape or acrylic tape to avoid excessive point stresses. The modularity of the test section provides for easy modification for any future efforts.

The stand for the shock tube driver section is composed of twin, parallel-mounted I-beams which are bolted together through their central web. Bolted to these I-beams are fore and aft pushes which confine the motion of the fore diaphragm holder on one end and the base of a hydraulic jack at the other end (see Appendix I for design drawings). The hydraulic jack (Norco model 76520G 20 ton bottle jack) is used to compress the diaphragm holder and driver section stack so that the diaphragms seal the pressurized volumes which they bound. The driver section rests on four cam-follower bearings and permits the section to be rolled along its axis for purposes of changing diaphragms. The diaphragm holder rests in a V-shaped gutter which guides the positioning of the pieces relative to each other. This design provides an easy means of changing diaphragms between tests. All test stand sections are bolted to a flat welded to the top of inverted T-shaped stands. These stands are composed of T-bar pieces which are welded together and rest on threaded feet which permit minor adjustments in test stand height.

Gas Flow Facility. The gas flow facility provides regulation and control of gas used to fill the shock tube (see Figure 16). The gas is stored in high-pressure cylinders (typically 3000 psia). Regulators, gages, solenoid control switches and hand-actuated ball valves are mounted on a control panel in the control room. The gas pressure delivered to the shock tube is regulated by a 16-turn Grove model 15LH regulator. Heise, Seegers, and Ashcroft gages are used to monitor static pressure as each of the three sections of the shock tube are filled to their respective pressures. The Heise and Seegers gages are used to accurately determine the pressure in each section and the Ashcroft gages are used for indication purposes. Four Marotta model MV100, normally closed, two-port, two-way solenoid valves mounted on a panel adjacent to the diaphragm holder are used to seal the shock tube volumes as close to the shock tube as possible. Hoke model 2233 10-15-micron filters protect the solenoid valve seating surfaces from dust and debris. One of the solenoid valves is used to initiate the shock by allowing the gas in the intermediate section to flow into the driven section. Additionally, hand operated ball valves (Hoke model 7115) on the flow panel provide a redundant means of controlling the flow of pressurized gas to the shock tube. All lines are 1/4-inch, 304 stainless steel seamless tubing. Connections are made with 37-degree flare fittings (AN) and necessary NPT instrumentation fittings. Flex lines run from the solenoid valve panel to the diaphragm holder fill ports and also from the test cell wall to the shock tube stand.

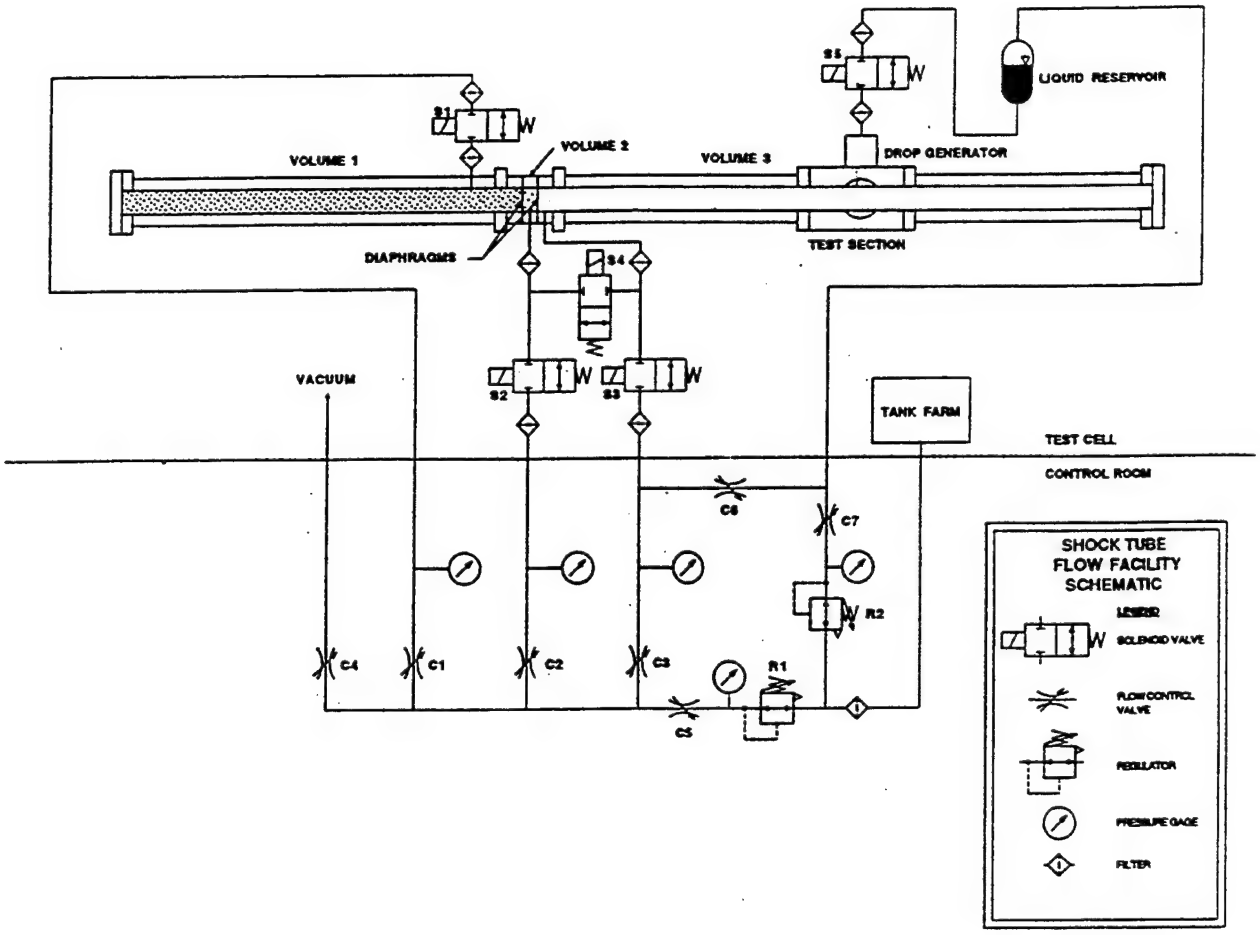

Figure 16
Shock Tube Flow Facility

Drop Generator Facility. The drop generator flow facility operates using a pressure feed system whereby a pressurized ullage in a liquid storage cylinder forces liquid in that cylinder to the drop generator, located in the drop generator housing. Figure 16 also details the drop generator liquid flow circuit.

The gas flow facility provides regulation and control of gas used to pressurize the ullage of the sample cylinder in which the droplet-comprising liquid resides. The gas is stored in high-pressure cylinders (typically 3000 psia) and is the same as that used to fill the shock tube. A regulator, pressure gages, and ball valve (which control the gas flow and pressure) are located on a control panel in the control room. The gas pressure delivered to the shock tube is regulated by a 16-turn Grove model 15LHX regulator. An ITT-Barton differential pressure gage is used to set the pressure in the liquid cylinder

relative to the pressure in the shock tube test section. An Ashcroft gage is used to determine absolute pressure in the ullage. All gas lines are 1/4-inch, 304 stainless steel seamless tubing with 37-degree flare fittings (AN) and necessary NPT instrumentation fittings. A flex line runs from the test cell wall to the shock tube stand as well as from the shock tube stand to the liquid flow facility control panel.

The liquid flow facility provides flow control of the liquid passing through the drop generator and is mounted on a small panel in the test cell adjacent to the pressurized drop generator housing (see Figure 17). The liquid is stored in a Whitey 1-liter sample cylinder which has two Whitey 3-way valves at either end to provide: 1) a means of filling and venting the cylinder during the fill process, and 2) pressurizing and delivering the liquid to the flow control circuit. Also in series along the flow circuit are a Whitey 7-micron filter, a Whitey coarse regulating valve, an Omega #10 flow meter, a Whitey fine metering valve, and two Hoke filters at either port of a Marotta model MV100, normally closed, two-port, two-way solenoid valve. Most liquid side lines are 1/8-inch, 304 stainless steel seamless tubing with Swagelok fittings. Flexible liquid lines are 1/8-inch Tefzel with Swagelok fittings.

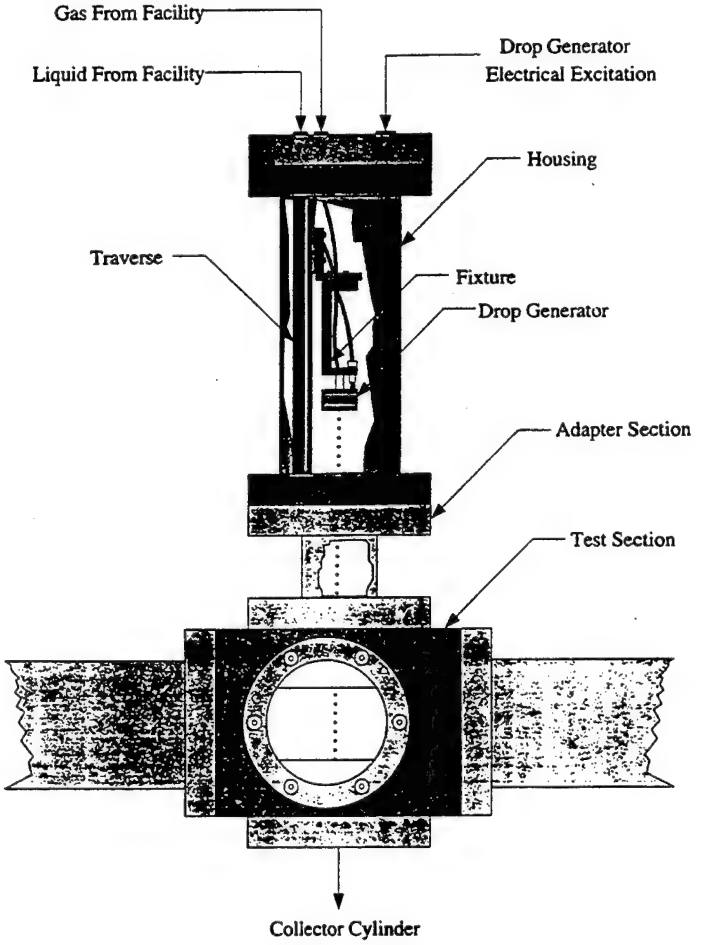

Figure 17
Drop Generator Housing Schematic

The drop generator housing permits injection of droplets into environments at pressures higher or lower than atmospheric pressure or composed of gases other than air (see design drawings in Appendix I). The drop generator housing is composed 304 stainless steel tube 16.5 inches long, 4 inches in diameter with 1/4-inch wall; it is flanged at each end. A transition section between this and the test section is composed of 4.5-inch-long, 2-inch-diameter, 1/4-inch wall, 304 stainless steel tube and has flanges at each end which mate with the test section and the drop generator housing. At the top of the drop generator housing is a blind flange where provisions for introducing droplet liquid, any necessary co-flowing gas, and electrical excitation are made. Electrical access to the drop generator housing is provided by a 3/4-inch NPT electrical feed through manufactured by PAVE with six, 14-gauge wires and two type K thermocouple wires. Fluid access to the drop generator is provided by two 1/8-inch NPT ports. A translation stage manufactured by Velmex and a fixture to which the drop generator is attached inside the housing permit motion of the drop generator exit relative to the test section. The pressurized housing concept permits existing drop generators to be employed without concern for structural integrity or interfacing with the existing test section.

The drop generator used in this work is of the Berglund-Liu variety (19). This device uses an electrically excited piezoelectric wafer to excite Rayleigh instabilities in a liquid stream passing through optical pinholes of varying size (see Figure 18). Further details of this device are found elsewhere. Drop diameters are typically 1.8 times the pinhole diameter although larger droplets are sometimes produced through coalescence of adjacent droplets. Recent work by Connon and Dunn-Rankin (20) has mapped the operating range of this device at pressures to 1000 psia with water injected into helium.

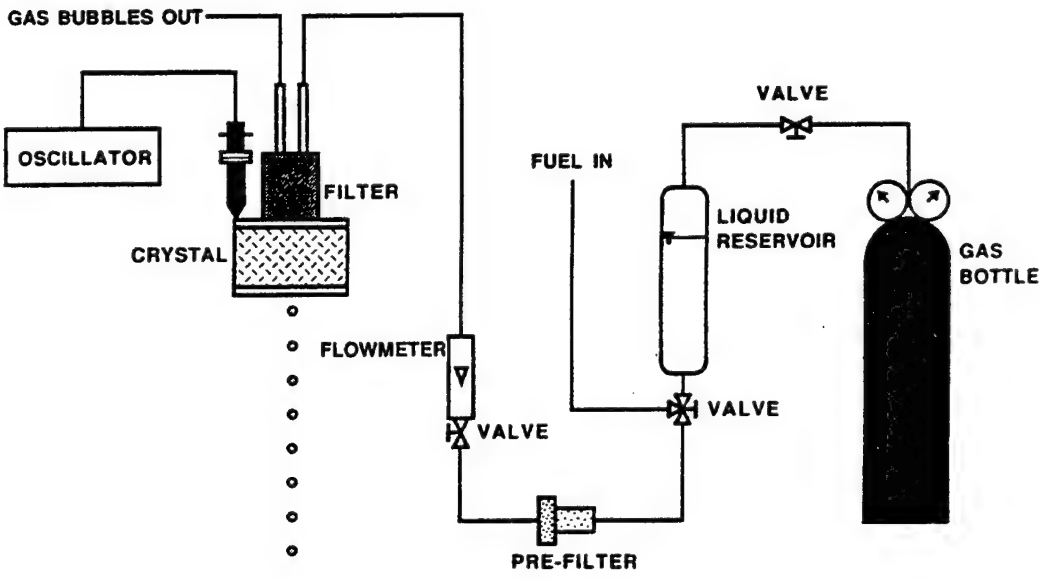

Figure 18
Schematic of Berglund & Liu-Type Drop Generator

The drop generator is mounted on a fixture at the top of the test section. Flexible electrical and fluid lines attach to it from the blind flange at the top of the housing. The translation device is then used to position it relative to the test section bore. The injection point can be placed within 1/8 inch of the shock tube bore and as far away as 6 inches.

Diagnostics. The diagnostic technique employed in this effort was shadowgraphic cinematography of the droplet response to an imposed shock wave using a copper vapor laser as the light source and a high speed streak camera to obtain the images. Pressure gages and piezoelectric pressure transducers measured the pressure history and helped characterize the flow field experienced by a drop during the event.

High speed cinematography, since its advent in the 1940s, has provided a means of recording events too fast for the human eye to resolve. For the present application, resolution at both temporal (due to time scale over which the event occurs) and spatial (due to the small size of the drops observed) levels was necessary to capture and understand the resulting images.

For events which do not produce their own light, lighting is typically done using two basic techniques: 1) continuous exposure of the subject with a shuttered optical path, or 2) shutter sequenced stroboscopic exposure of the subject. The quality of the images produced with high speed cinematography has traditionally been tied to the time stopping ability of the strobe used or the shutter exposure time. In cinematography, the shutter typically controls the exposure duration of the event being photographed. However, because shutters are mechanical in nature, small exposure times are difficult to achieve. The best commercially available strobes have pulse durations on the order of a microsecond and repetition rates up to 6 kHz. For the present application, such time scales are too large to resolve: 1) the droplet motion and response, and 2) the droplets at any given instant due to image blurring of a moving object.

Recently, a commercially available pulse laser has found use as a strobe for high speed cinematography. The copper vapor laser produces pulses 20-30 nsec in duration at repetition rates from single shot to 32 kHz. Because its pulse energy is on the order of 0.1-2 mJ, sufficient light for photographic illumination is available. Most other pulse lasers which produce pulses of sufficient energy for photographic purposes have pulse durations an order of magnitude longer at the top copper vapor laser repetition rate. Most also have similar pulse durations at repetition rates orders of magnitude less than the top rate of the copper vapor laser.

For resolution of the droplet response phenomena to be observed in this effort, Sirignano has suggested temporal resolution on the order of tens of microseconds and spatial resolution on the order of a few microns is necessary.

The Oxford model CU-10A copper vapor laser operating at 32 kHz provides a temporal resolution of 31.25 microseconds and was purchased for this effort. Additionally, the short pulse duration (20-30 nanoseconds) minimizes image smearing.

For example, a 10-micron droplet traveling at 100 m/s moves one-fourth of its diameter during a 25-nanosecond pulse typical of a copper vapor laser, and ten diameters during a one-microsecond pulse typical of the best strobes. The laser produces a 1-inch-diameter, non-polarized beam of green (511-nm) and yellow (578-nm) light which is in a 2:1 intensity ratio. The laser is easily triggered with microsecond order delay and can produce a series of pulses with periods of darkness prior and immediately following the series of pulses. Oxford with technical input from UCI developed a device which controls such sequences called an N-shot controller, and UCI received the first such production device.

Most microscopes are capable of micron level spatial resolution, and long distance microscopes are capable of that order of resolution with the longer working distances necessary to observe phenomena in pressure vessels. An Infinity K-2 long distance microscope has 3-micron resolution at a working distance of 4 inches with the CF-3 objective and was purchased for this effort.

While a video-type digital camera system is ideal for recording most images, no commercially available system has the pixel transfer rate (usually less than 40 Mpixels/s.) to record detailed micron resolution images at 32 kHz. It is estimated that pixel rates on the order of 100 times that of the currently available technology are necessary for this application. Accordingly, a high speed film camera was necessary to provide the resolution for this application. The larger 35-mm format and the laser compatible writing rate of the Cordin model 318 drum streak camera most aptly fit the cinematographic system being developed and was leased for this effort. The non-framing or streak camera can be used because the laser pulse itself acts to frame individual instants of time in the shadowgraphic arrangement for these experiments. If the phenomena recorded produced light, this arrangement could of course not be used.

In the experiments performed, the beam issues from the laser and is diverted by a mirror through the test section, backlighting the droplets relative to the camera. Tests have been done where the beam is diverged with a lens prior to entering the test section and where the collimated beam passes through the test section. Light levels have been found sufficient whether the spot size at the image plane is 1 inch or 3 inches at the highest repetition rates of the laser.

Should digital processing be desirable, a film scanner could be employed to use the full digital resolution of a digital camera to view a distinct region of a film frame of the original film recording at the much lower pixel rate necessary to maintain spatial resolution. Once a digital image is obtained, simple edge detection algorithms in conjunction with symmetry assumptions can be employed to quantify particular quantities of interest.

Two types of pressure measurements were made in conjunction with the optical diagnostics: 1) static pressures of the three volumes which comprise the shock tube and 2) transient pressure histories of the shock as it passes through the test section. The static

pressure of the driver section, P_4, relative to the driven section, P_1, provides a means of projecting the shock strength at the test section after losses are considered. The peak transient pressure summed with the static pressure of the driven section, P_2, relative to the static pressure of the driven section, P_1, determines the shock strength at each of the transducer locations in the test section. From this shock strength--using the one-dimensional equations of Appendix B--the maximum particle velocity and a history of the particle velocity at the two transducer locations can be calculated.

The static pressures were measured using one of three interchangeable gages: 1) 0-100-psia Seegers; 2) 0-1200-psig Heise; or, 3) 0-3000-psig Heise. The transient pressure histories were measured by PCB Piezotronics model 113A20 piezoelectric pressure transducers positioned 2 inches upstream and 2 inches downstream of the geometric center of the test section and on either side of the drop stream injection point.

Due to the transient nature of these experiments, sequencing various events associated with execution of the experiment and recording the images was a primary consideration. Much of the difficulty has been alleviated through the development of the N-shot controller by Oxford Lasers; however, selection of trigger signals and conditioning these signals appropriately is still necessary. The Figure 19 schematic describes the process.

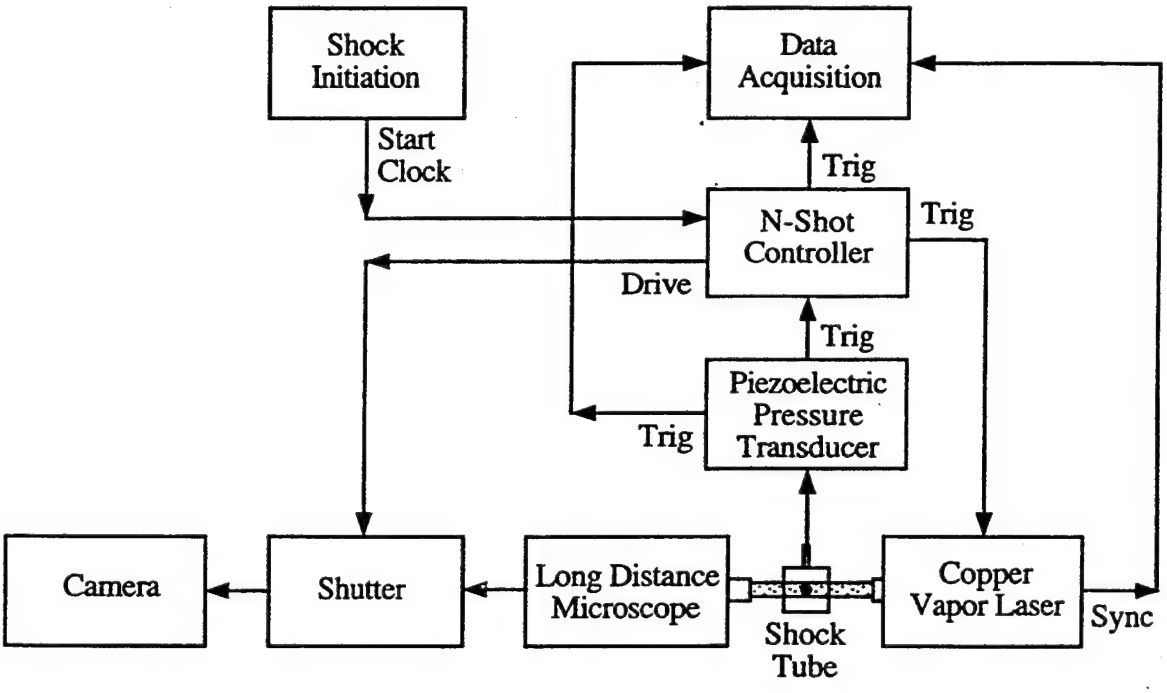

Figure 19
Secondary Atomization Experiment Control Schematic

Once the shock tube has been prepared for firing, the drop generator is operating, and the drum camera is at speed, the experiment is initiated by switching the solenoid which dumps the intermediate section gas into the driven section. The 24-V signal produced by this solenoid switch is voltage divided to a 5-V level which is sent to the N-shot controller to turn the laser off from its free running frequency and initiate opening of the camera shutter. A trigger with user selected delay is also issued by the N-shot controller after which time the laser fire trigger will be accepted. This is a fail-safe mechanism which allows the system to timeout should the shock be inadvertently produced by premature diaphragm failure or not be produced at all. As the shock wave passes the first piezoelectric pressure transducer, the signal produced by this device is used to trigger the data acquisition system, and the delay generator which--after a user selected delay--triggers the N-shot controller to send a series of trigger pulses to the laser at the selected burst frequency. The laser fires the user selected number of pulses, the camera records the images, the N-shot controller initiates closing the shutter, the laser reverts to its free run operating frequency, and the experiment is complete. Figure 20 shows a timeline of this sequence of events.

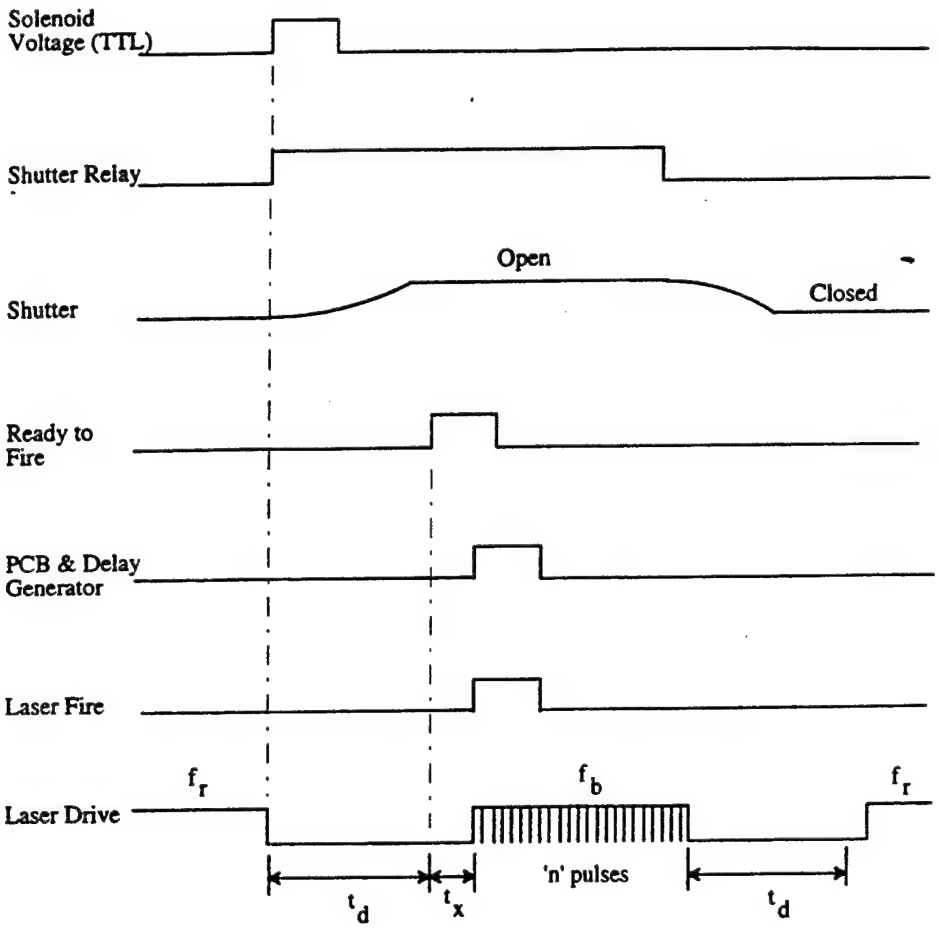

Figure 20
N-Shot Controller Timeline for UCI Shock Tube Experiment

The data acquisition system is a Tektronix TestLab model 2505 with eight, 11-bit channels and four, 2-bit channels at 100 kHz. Because the pressure transducers and laser trigger signals are stored with a common time base, the flow field can be directly related to the images recorded on the film with temporal error on the order of ten microseconds. The delay generator is a Stanford Research Systems model DG535 and is used to set the times the images are recorded. Additional insight into a particular experimental image sequence of droplet response can be obtained by running a similar experiment with the delay set to a value between 0 and the reciprocal of the burst frequency. If, for instance, the delay were changed by an amount equal to half of the reciprocal of the burst frequency, images at time instances halfway between those taken in the previous experiment would be obtained. If conditional sampling can be assumed, the temporal resolution can be decreased significantly in a similar fashion.

A summary of the above shock tube, drop generator, and diagnostic descriptions was originally presented in an AIAA paper. A copy of this paper is provided as Appendix J.

Results. Initial tests were performed at atmospheric pressure. The test conditions and results are shown in Table 10. Two fluids (methanol and water) and three wave durations (1.6 ms., 2.3 ms., and infinite) are presented. All waves have a shock strength of approximately 1.5 and the droplets are initially 117-122 μm in diameter. Measured values of wave duration, original drop diameter, and shock strength as well as corresponding maximum values of previously defined dimensionless parameters (see Appendix G) are also shown in Table 10. The duration of the wave is defined as the time from the pressure peak to the time at which the pressure returns to zero. Square waves are reflective of an N-wave of infinite duration relative to the breakup process and are probably comparable with most other data in the literature.

Table 10. Secondary Atomization Initial Test Parameters

Test No.	*Fluid*	*Wave Duration (ms)*	*D (μm)*	*Shock Strength*	Re_{max}	We_{max}	*Oh*	d_{max} *(μm)*	τ_b
1	Methanol	1.2	122	1.48	1050	84	.0175	40	9.3
2	Methanol	1.8	117	1.50	1060	87	.0179	30	8.8
3	Methanol	∞	117	1.48	1010	81	.0060	30	7.6
4	Water	1.1	122	1.50	1100	28	.0060	90	8.6
5	Water	1.8	122	1.51	1130	29	.0060	65	7.7
6	Water	∞	117	1.50	1060	27	.0061	65	6.7

The sequences of images for each test are shown in Figures 21a and 21b. The interframe spacing is approximately 33 1/3 ms. and the magnification is approximately 4.58. The times are measured from the time at which the shock impinges on the drop stream minus about 10 ms so that a baseline drop size is established in the photographic record. Figures 22a and 22b show the non-dimensional displacement as a function of time normalized by a transformation which accounts for the cumulative dynamic pressure which the parent droplet experiences to time t. Most frames capture at least five droplets so the maximum and minimum displacements are both represented in the figure. The transformation is as follows:

$$\tau = t\sqrt{\frac{\rho}{\rho_0}}\frac{U_{rel}}{D}\left(\frac{X_N}{X}\right) = t\sqrt{\frac{\rho}{\rho_0}}\frac{U_{rel}}{D}\left[\frac{\iint\left(1-\frac{t}{t_N}\right)^2 dt_1 dt_2}{\iint dt_1 dt_2}\right] = t\sqrt{\frac{\rho}{\rho_0}}\frac{U_{rel}}{D}\left[1-\frac{2}{3}\frac{t}{t_N}+\frac{1}{6}\left(\frac{t}{t_N}\right)^2\right] \quad (2)$$

Variation in the methanol curves is probably due to droplet deformation effects on the drag coefficient. Water has a much higher surface tension, and so the parent droplet stays essentially spherical throughout the breakup process. Methanol, however, has roughly a third of the surface tension of water. Therefore, parent methanol droplets distort substantially from their initial spherical shape, which changes the manner in which they are displaced.

Based on these values, water droplets are found to be in the "bag" mode according to equation (2) and the methanol drops are found to be in the "shear" mode, but both are characterized as an intermediate between "bag" and "shear" or "multimode" breakup by Hsiang and Faeth (21).

Detailed analysis of the photos indicates the maximum product drop size is larger for shorter duration waves and smaller for higher We_{max} waves. This could be hypothesized when the longer duration convective field is considered. The longer a convective field has to act on a droplet the more opportunity it has to deform and break up that droplet as previously found by Hinze (22). For an N-wave the relative velocity decreases not only because the convective field associated with the wave is decreasing but also due to the induced motion of the droplet by that flow. For a square wave, the convective field velocity is constant; only the induced motion of the droplet decreases the relative velocity between the flow field and the droplet. Therefore, the relative Weber number between the convective field and the droplet falls off much more quickly for an N-wave than for a square wave and, accordingly, the capacity to break up the droplet is reduced. Qualitative analysis also indicates the average stripped droplet sizes decrease with longer duration waves and higher We_{max} waves, which could be another conclusion drawn from the previous discussion.

As droplet dispersion is also a drag related quantity, the transformation above is believed to apply to dispersion as well. The small droplets sheared-off in the process almost certainly remain spherical and would be expected to track the flow in a fixed relationship to their larger, spherical parent droplets. Because the velocity field of an N-wave drops off as the pressure, the N-wave disperses the product droplets less than a square wave of the same amplitude. This is evident in the photographs even though no quantitative calculation has been completed to date.

Droplet breakup time remains a difficult measurement, if not a very subjective quantity, as completion of breakup is difficult to assess without a more continuous view of the process. In the present work, the rate at which photos were taken dictates that the error in this quantity be +/- 1. There does appear to be an increase in breakup time as wave duration increases, although the error with which the measurement is taken precludes a definitive statement on this trend. If this trend is true, the longer exposure time to the convective gas flow for longer duaration waves would seem to be the reason that the breakup process exceeds that of shorter duration waves. It is difficult to believe that other researchers have been able to obtain values which are more accurate than those presented here due to the high framing rate (30kHz.) afforded by the copper vapor laser. Hsiang and Faeth (21) have taken pictures at a rate less than one third (6-8kHz, 5-14 frames total) of this and thus the error could be expected to be on the order of three to five times that found here for drops with equivalent drop diameter to relative velocity (D/U_{rel}) ratios. The inverse of the number of pictures in a movie of the process is a good way to determine the accuracy of the measurement; therefore, a 5 frame movie could be expected to have an error of 20%, if the movie ended at the completion of breakup and started at the beginning of the shock/drop interaction. This may explain the wide variation in most data presented to date as the previous state-of-art (before copper vapor laser) in the strobe flash rate was about 6 kHz. At best, equivalent drop size distributions for two successive frames are required to assess this quantity. Very little evidence of detailed photographic analysis of this nature has been found in the literature. The suspected subjective nature of this measurement and thus the wide variation (0.5 - 1 order of magnitude) in reported values of breakup time is therefore well founded. The value is very well limited ($2 < \tau_b < 10$) over a substantial range of We, but nonetheless relatively uncorrelated compared to other natural phenomena. At substantially higher We ($>10^5$), where rocket engines operate, the error in measuring breakup time can be expected to increase due to the difficulty in obtaining experimental conditions at relatively low D/U_{rel} with the associated higher framing rates required. Note that at fixed D/U_{rel}, We increases as the cube of U_{rel}. Repeated experiments with conditional sampling at times near the breakup time could be used to improve the accuracy of this quantity, however.

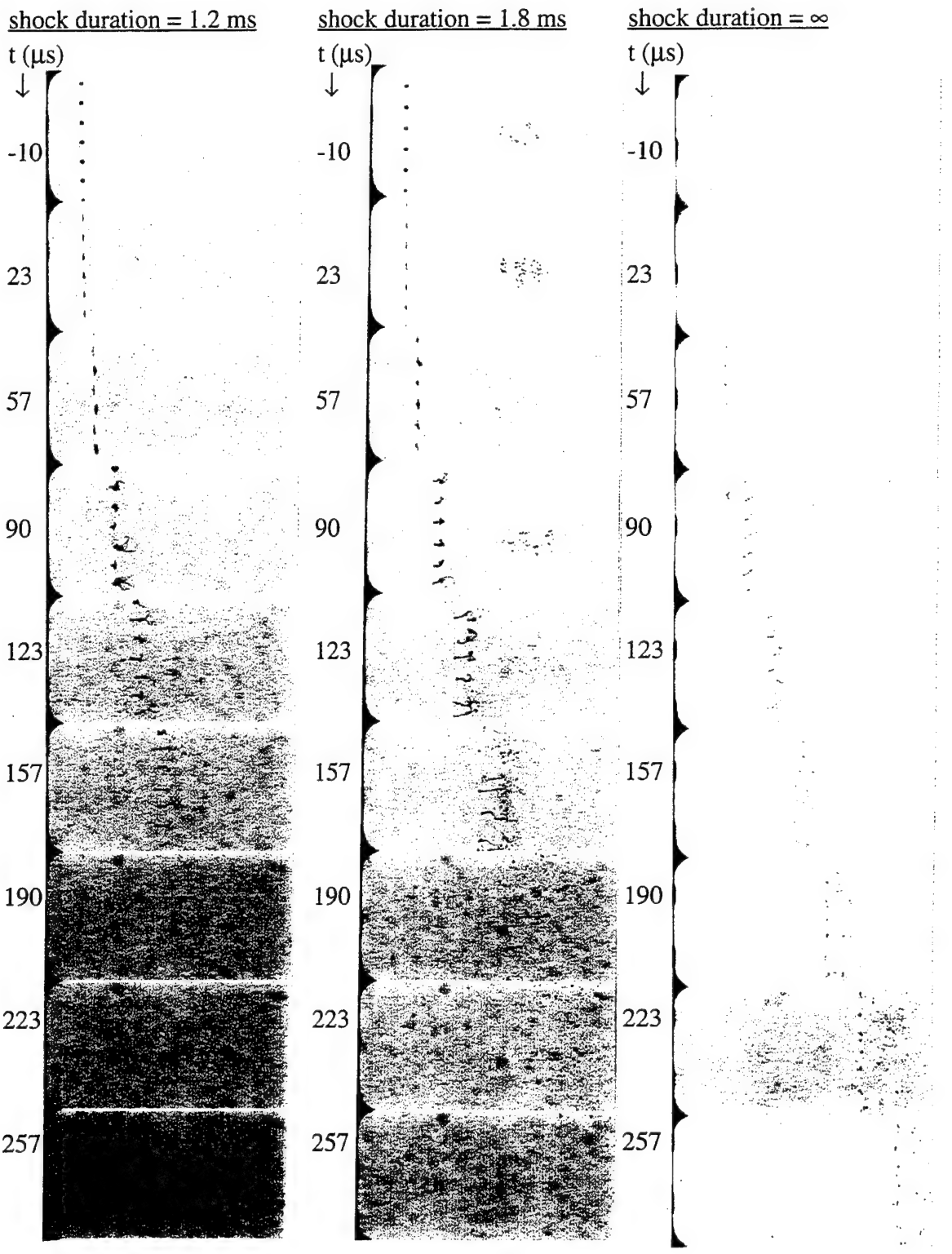

Figure 21a
Shadowgraph Images of Water Drop Stream Interacting with a Shock Wave
D = 145 μm, Shock Strength = 1.5, Shock Direction: Left-to-Right

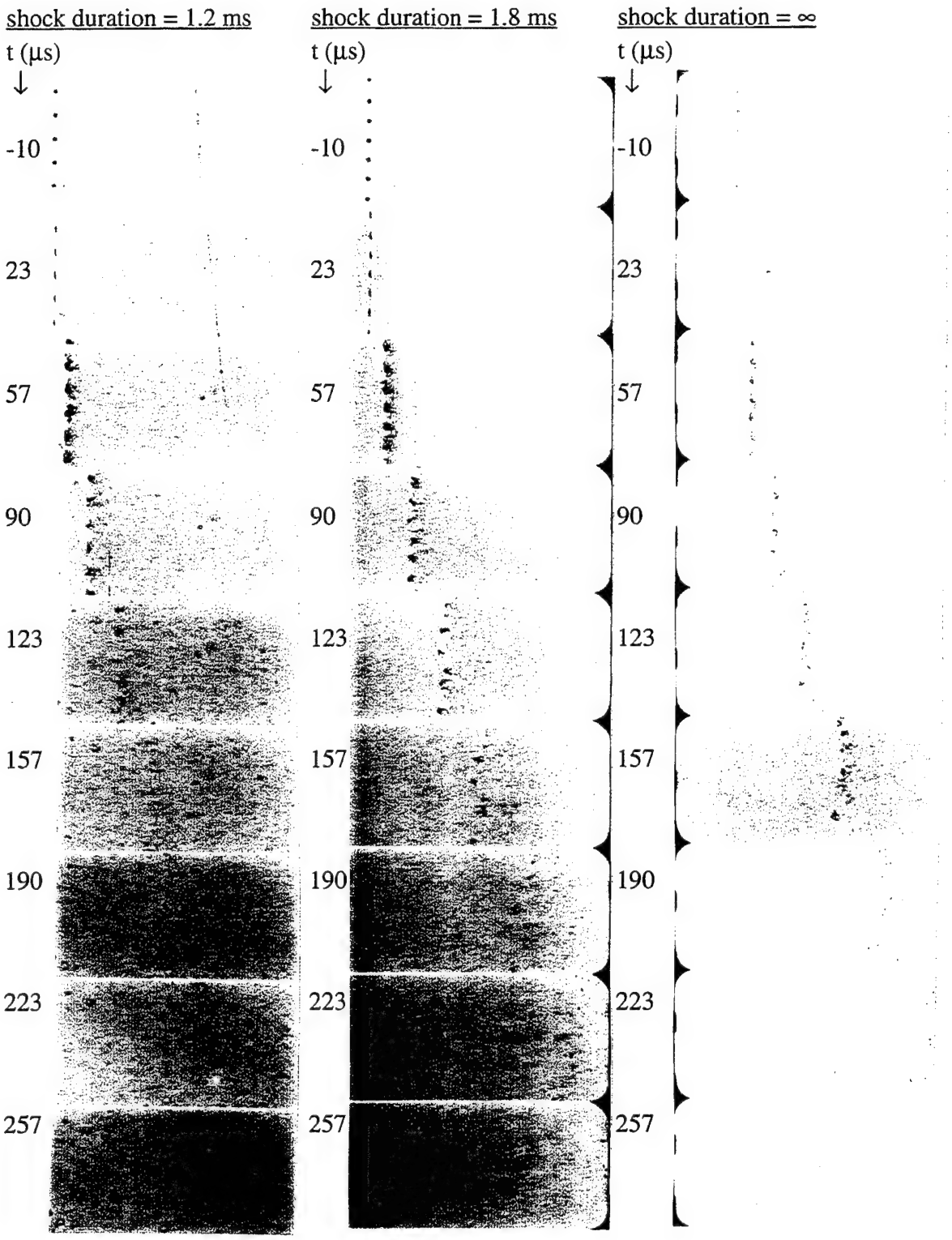

Figure 21b
Shadowgraph Images of Methanol Drop Stream Interacting with a Shock Wave
D = 145 μm, Shock Strength = 1.5, Shock Direction: Left-to-Right

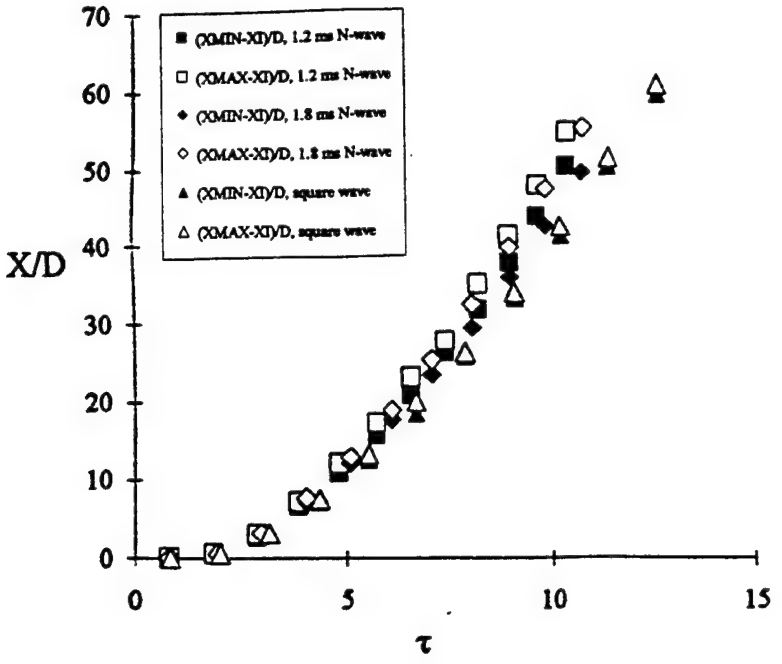

Fig. 22a
Water Droplet Displacement as a Function of Time
D = 145 μm, Shock Strength = 1.5

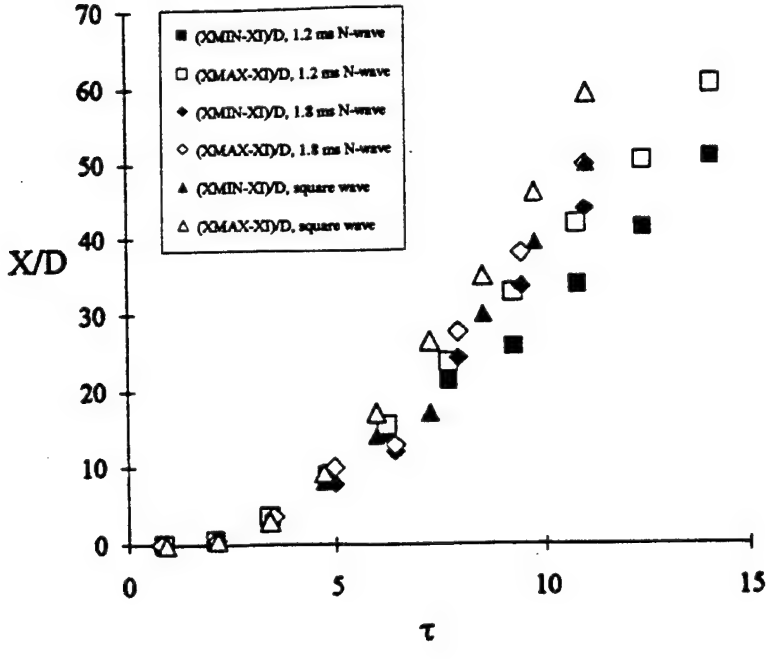

Figure 22b
Methanol Droplet Displacement as a Function of Time
D = 145 μm, Shock Strength = 1.5

TASK 3 - VERIFICATION OF APPLICABILITY OF MECHANISMS

This task was conducted in parallel with the experimental (Task 2) portion of the effort and was performed primarily by the UCI research group under Dr. W. Sirignano's guidance. It involved a theoretical/computational effort to place existing spray combustion theoretical models in a useful form to treat situations where propellant vaporization is the rate-controlling factor. Current models have been developed for hydrocarbon fuel droplets vaporizing under sub-critical conditions. Initial effort concentrated on adjusting these transient droplet heating and vaporization models so that liquid propellant rocket combustion can be studied.

Note that this effort was not a fully independent research project because of the funding constraints of the LSM program. Advantage was taken of other UCI research programs addressing theoretical models of spray combustion. Existing computer codes from these other projects were employed as a base for the new study. Suitable modifications for the rocket combustion process and environment were made to the existing model; however, cryogenic propellants and super-critical pressures were not included.

The object of the Task 3 vaporization work was to compare computational results with experimental results and to make certain inferences about a model for combustion instability in liquid propellant rockets. The model was based upon the assumption that vaporization is the controlling factor in the burning rate of the liquid propellants. Sub-critical pressure conditions for oxidation of liquid hydrocarbon fuels was emphasized. The vaporization of hydrocarbon fuel was considered to be slower than the vaporization of the liquid oxygen and therefore rate controlling.

An axisymmetric, time-dependent computational model for oscillatory and transient gaseous freestream conditions was developed as an advancement on existing models developed by Chiang and Sirignano for steady freestream conditions. The details of the model development are contained in a paper by A. Duvvur, C. H. Chiang, and W. A. Sirignano; a copy is included as Appendix K. This appendix should be consulted for detailed descriptions of the model. (The paper is soon to be published in the AIAA *Journal of Propulsion and Power*). In terms of applications, the model emphasizes oscillatory free streams; it has also been applied to the low-pressure, experimental situation studied by UTRC under Task 2.

Comparison with Experiment

In the low-pressure vaporization experiments, UTRC used a stream of droplets falling through quiescent air with and without transverse shock waves passing by the droplet (see Task 2 description and Appendices C, D, and E). Previously, UCI conducted an axisymmetric droplet calculation (23) where a step function in gas velocity, pressure,

and temperature is experienced by a water droplet. In the current program, the same step-response model was compared to the Task 2 low-pressure vaporization results.

For the numerical calculations, the information provided by Table 1 was used for the property computation. Calculations of an isolated water (or methanol) droplet behind a 1.2-pressure-ratio shock wave were made. At this stage, only a comparison of the droplet diameter decrease in the very early period of its lifetime could be made.

Also, a quasi-steady analysis was conducted by employing Emmons' solutions combined with an empirical correction for a single fuel droplet vaporizing in a convective environment. This simple analysis served as a benchmark test and assumes that Le = Sc = Pr = 1, eventually yielding a "$D^{3/2}$" law:

$$D^{3/2} = D_i - \beta t \tag{3}$$

where

$$\beta = 0.585\sqrt{8}\,\frac{\ln(1+B)}{B^{0.15}}\,\frac{(\rho U \mu)^{1/2}}{\rho_l} \tag{4}$$

$$B = \frac{Y_{f\infty} - Y_{fs}}{Y_{fs} - 1} \tag{5}$$

Table 11 lists the properties used in the quiescent air calculations. For the ambient air (T = 300 K, p = 1 atm.), the viscosity was taken to be 184.6×10^{-7} kg/m-sec, and the density was assumed to be 1.1614 kg/m^3.

For the calculations involving the pulse/droplet interaction, the usual normal shock wave relations were employed:

$$M_2^{\,2} = \frac{1 + \frac{(\gamma-1)M_1^{\,2}}{2}}{\gamma M_1^{\,2} - \frac{\gamma-1}{2}} \tag{6}$$

$$\frac{p_2}{p_1} = 1 + \frac{2\gamma(M_1^{\,2}-1)}{1+\gamma} \tag{7}$$

$$\frac{\rho_2}{\rho_1} = \frac{(1+\gamma)M_1^2}{2+(\gamma-1)M_1^2} \tag{8}$$

$$\frac{T_2}{T_1} = \frac{p_2}{p_1}\frac{\rho_1}{\rho_2} \tag{9}$$

Again, the ambient air temperature, T_1, was assumed to be 300 K, the air viscosity was 192.05×10^{-7} kg/m-sec, and the ambient density (for p_2 = 1.2 atm.) was 1.1060 kg/m^3. Table 12 lists the assumed droplet properties, and Table 13 gives the corresponding shock wave properties.

Table 11. Droplet Conditions for Quiescent Air Calculations

	Water Drop	*Methanol Drop*
Y_{fs}	0.0182	0.1021
B	0.01854	0.11371
ln(1+B)	0.018367657	0.1077
U (m/s)	5.5	7.5
ρ_l (kg/m^3)	996.6	782.5
β	6.02408×10^{-7}	4.00124×10^{-6}

Table 12. Droplet Conditions for Shock Wave Calculations

	Water Drop	*Methanol Drop*
U (m/s)	46.3	46.6
β	1.7136×10^{-6}	8.0709×10^{-6}

Table 13. Parameters for Shock Wave Calculations

γ	1.4
M_1	1.08
M_2	0.9277
p_2/p_1	1.19413
T_2/T_1	1.05217
T_2 (K)	315.65
p_2 (atm.)	1.2
a_1 (m/s)	347.2
u_1 (m/s)	375.0
a_2 (m/s)	356.1
u_2 (m/s)	330.4
U (m/s)	44.6
ρ_∞ (kg/m^3)	1.1667
μ_∞ (N-s/m^2)	1.84×10^{-5}
ρ_l (kg/m^3)	782.5
μ_l (N-s/m^2)	5.09×10^{-4}
σ (N/m)	0.0218
D (microns)	70
Re	207
Re_l	7.48
We	7.46

The axisymmetric results for the quiescent air and convective cases are presented in Figures 23 and 24, respectively. Figure 25 shows the same data in the shock wave case, but at very early droplet lifetime (note that the UTRC data in the case of shock wave conditions are taken very early in the transient). Also presented in these figures are the low-pressure vaporization data originally presented in Figures 6 and 7.

The general observation is that in the quiescent air case, the measurements were smaller than the predicted vaporization rate; in the shock wave case (with highly convective effects), the UTRC results are much higher than the 'theoretical' values. A simple analysis also shows that the experimental results do not follow the trend that vaporization rate increases with the "square root of Reynolds number" as the correlation of Ranz and Marshall suggested.

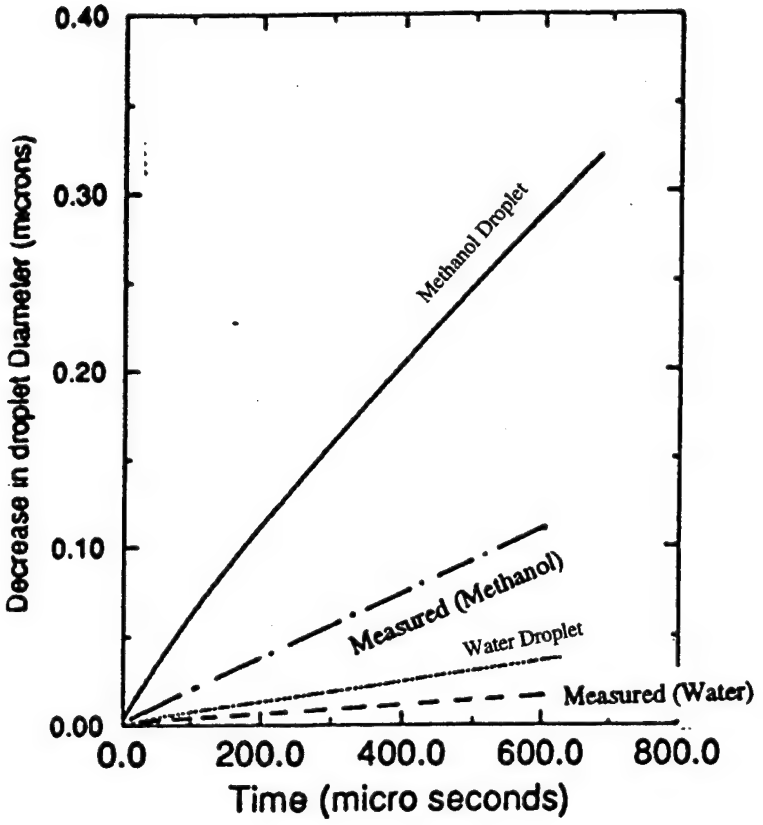

Figure 23
Comparison Between Experimental and Numerical Results for Quiescent Air Case

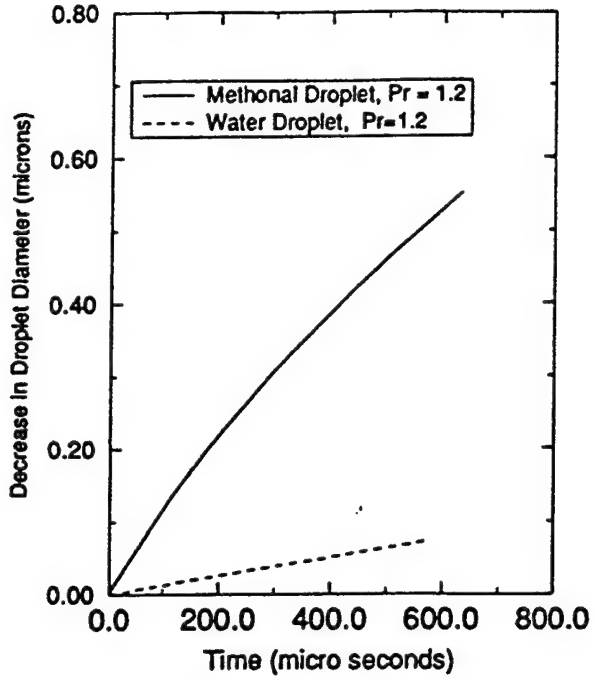

Figure 24
Numerical Results for Shock Wave Case

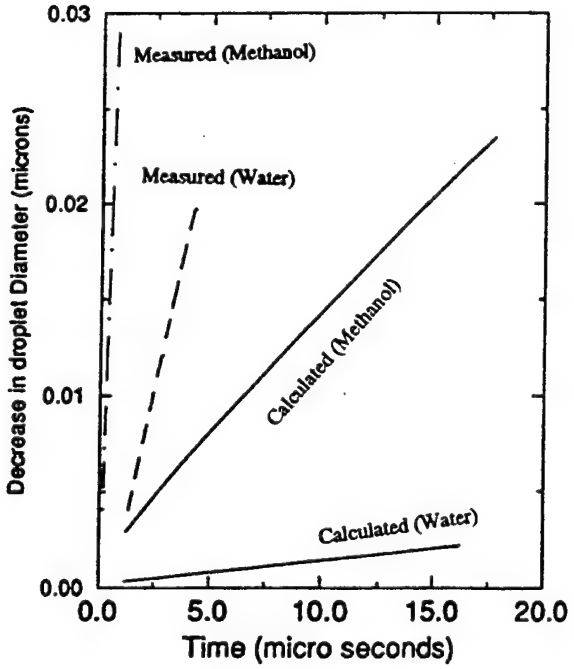

Figure 25
Comparison Between Experimental and Numerical Results for Shock Wave Case

Table 14 compares the droplet diameter decrease (microns) at t = 600 microseconds for the quiescent air conditions (note that the terminal velocity, or free drop speed, of the droplet will yield a droplet Reynolds number around 10). Table 15 compares the droplet diameter decrease (microns) at t = 6 microseconds for the shock wave conditions.

Table 14. Comparison of Droplet Diameter Decrease (Microns) at t = 600 Microseconds for Quiescent Air Case

Droplet	*Theoretical Result*	*Experimental Result*	*$D^{3/2}$ Law*
Water	0.03621	0.01	0.03113
Methanol	0.29	0.1	0.2068

Table 15. Comparison of Droplet Diameter Decrease (Microns) at t = 6 Microseconds for Shock Wave Case

Droplet	*Theoretical Result*	*Experimental Result*	*$D^{3/2}$ Law*
Water	0.001	0.02	0.0009041
Methanol	0.008	0.26	0.004185

Note that the experimental data were taken at the very early period of the droplet lifetime, while the numerical computation is only partially converged. However, the analytical predictions are close to those that the $D^{3/2}$ law predicts. One proposed explanation for the discrepancy between the numerical and experimental data is that boundary-layer stripping may occur with the shock wave, resulting in a significant increase in vaporization. The effects of boundary layer stripping have been discussed by Delplanque and Sirignano (24). The present results indicate that stripping can increase the effective vaporization rate by an order of magnitude. In the case without shock waves, successive droplets are sufficiently close to cause a reduction of the vaporization rate, thus possibly explaining the difference with the experimental results. Although these effects are not discussed in the current work, Chiang and Sirignano (25, 26) have addressed them previously.

Oscillatory Study

There is adequate reason to believe that the liquid phase may prove to be a driving mechanism for combustion instability. For this reason, the transient heating and vaporization of the fuel droplets under oscillating conditions must be examined. This is on the knowledge that transient and liquid thermal inertia are very important under steady operating conditions, and therefore it is expected that they should also be important under unsteady conditions. Previous work by Tong and Sirignano (4) does indeed support this theory, and it has been shown that unsteady droplet vaporization is a likely candidate mechanism for driving instability. Their model assumes constant properties and is a one-dimensional analysis. The Tong and Sirignano model is limited to the liquid phase, and therefore vital information like drag coefficient can not be obtained from their study.

It should be noted that not all droplets injected into the chamber of a liquid rocket combustor--which is under an oscillatory mode of operation--experience the same ambient conditions. As combustion is a continuous process and fuel droplets are injected constantly, droplets injected at different times need not necessarily be going through the same cycle.

This study examined the role of droplet vaporization under oscillating atmospheric conditions and is an extension of previous work by Tong and Sirignano (4). The model used here is an advanced model with fewer assumptions; its emphasis is on studying the effects of an oscillating gas phase on the heat and mass transfer processes in the liquid phase. The present study employs an advanced variable-property droplet model which calculates both the gas and liquid phase. The axisymmetric model has a regressing surface and includes convective effects. Figure 26 shows the axisymmetric droplet model employed. A stream function-vorticity approach is used in the liquid phase. In the numerical model, the effects of decreasing relative velocity, varying thermophysical properties, transient heating, internal circulation of the liquid, boundary layer blowing, and moving interface have been incorporated.

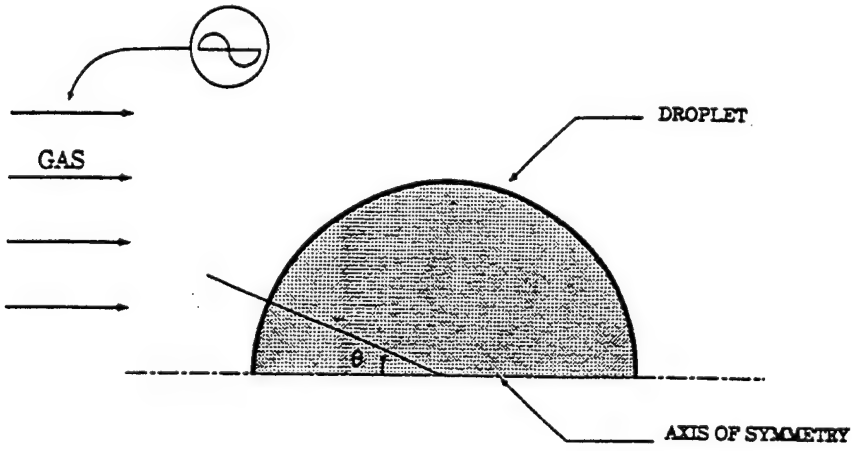

Figure 26
Droplet Model Employed in Oscillatory Study

The oscillations of temperature, pressure, and velocity in the gas phase will show significant changes in the heat and mass transfer rates and also in drag coefficients. Droplets are introduced at various times in order to evaluate the combined effect, and this should provide a comprehensive picture of droplet vaporization under all injection conditions. The response factor of the system is calculated in order to determine if the vaporization process is capable of driving instability.

As mentioned previously, funding limited the model to only hydrocarbon fuels. Therefore, the problem considered in this study was that of a single n-octane droplet injected into the hot gases of a combustor. The steady part of the relative velocity was taken to be 25 m/s, upon introduction of the droplet into the combustor. (Note that the actual value can vary between 15.7 m/s and 34.2 m/s depending on the time of injection and the spatial location.) A mean pressure of 10 atm. was used. The operating pressure varies with time, and the actual value depends not only on the magnitude of the velocity oscillation, but also the initial phase of injection. Gas-phase perturbations are introduced on the velocity, pressure, and temperature. The velocity and pressure oscillations are dictated by the classical standing wave pattern and the corresponding temperature oscillation is calculated by assuming an isentropic flow. Appendix K details the appropriate gas- and liquid-phase oscillatory initial and boundary conditions. For the governing hydrodynamic, energy, and transport equations, one may refer to the work by Chiang (27) and Chiang et al. (23).

In order to determine whether vaporization is capable of driving instability, it is necessary to consider the contributions of every droplet present in the combustor at a particular instant of time. For the vaporization to be able to drive instability, it is necessary to evaluate the component of the vaporization rate that is in phase with the pressure. This is done by evaluating the response factor, G, as suggested by the Rayleigh criterion (4). In order to be able to overcome the losses and drive combustion instability, G should have a minimum, positive value. For the case of distributed combustion, this value corresponds to 3.72 for longitudinal mode instability (28).

Four different parametric studies were conducted. These involved:

1. frequency comparison
2. droplet configuration comparison
3. amplitude comparison
4. variation in the liquid fuel

A variety of frequencies has been known to occur in liquid propellant rockets. For this reason, the frequency of the instability is a key parameter in the study of combustion instability, and it is necessary to identify the frequencies that may be sustained by droplet vaporization. For the purposes of this study, the frequency may be better described by the time period of the oscillation in terms of the droplet heating time. Three different time periods, corresponding to 0.3, 0.6, and 0.9 of the droplet heating time were examined.

In all cases, the spatial phase of injection corresponded to 1/8 of a wavelength, and the amplitude of the pressure oscillation was 2.0% of the steady value (10 atm.). The response factor, G, was calculated for each case. Figure 27 shows the pressure history of droplets exposed to the three frequencies. The imposed 2% pressure oscillation has a significant effect on the variation of the droplet vaporization rate. The distribution of the elementary response factor for the three cases is shown in Figure 28. The elementary response factor distribution varies substantially for the three time periods studied, though it is periodic in nature. Table 16 shows the total response factor for each frequency.

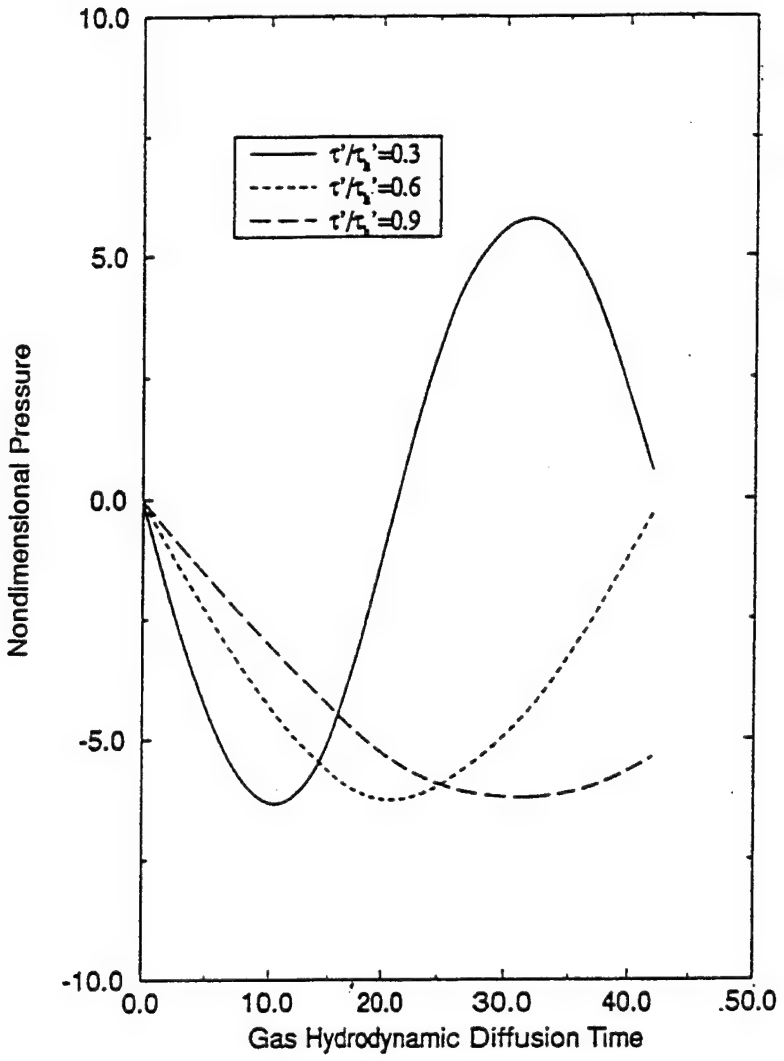

Figure 27
Ambient Pressure History with Varying Frequencies

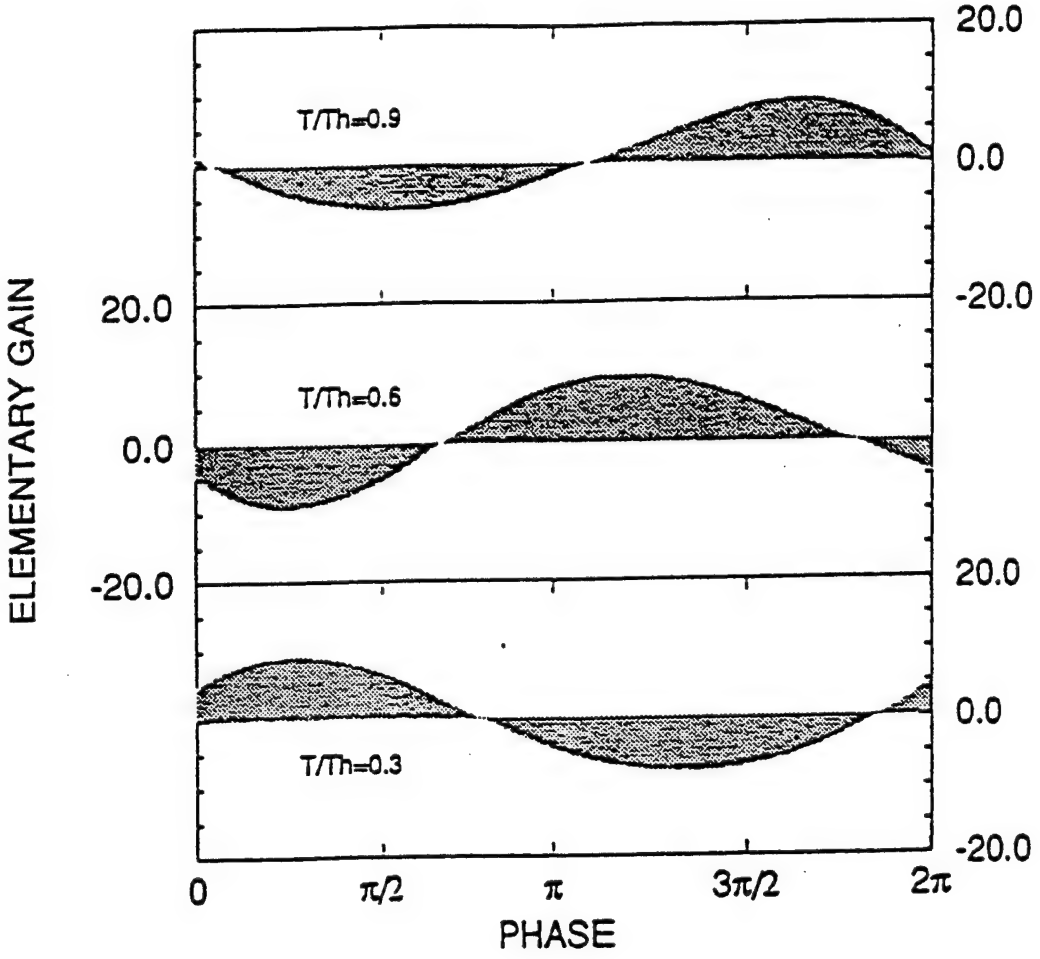

Figure 28
Distribution of Elementary Gain for Varying Time Periods

Table 16. Comparison of Response Factor for Varying Frequencies

τ/τ_h	G
0.3	-0.52
0.6	5.82
0.9	2.98

A response factor greater than 3.72 is required for the vaporization process to be able to drive instability. The oscillation with a time period of 0.3 is not capable of driving instability--a negative G implies that the system damps oscillations. The 0.6 time period case has a high response factor and is therefore capable of driving a longitudinal-mode combustion instability. This means that the component of the vaporization rate in phase with the pressure is large enough to supply enough energy to the system so as to drive it into an unstable operational mode. With a time period of 0.9 droplet heating time, the system is not capable of driving and instability. The 0.6 time period corresponds to the frequency domain found to be most unstable by Bhatia and Sirignano (29).

Figure 29 shows the two different droplet configurations studied. In the first case, the droplet is moving faster than the ambient gas; the droplet wake is therefore behind the droplet. In the second configuration, the droplet is moving slower than the gas; the wake is therefore ahead of the droplet. The velocity fluctuation is in phase with the steady component of the velocity. Thus, a positive velocity fluctuation means an increase in the Lagrangian velocity, augmenting the vaporization rate and other surface properties. In the first case, however, a gas-phase velocity increase means a decrease in the droplet Lagrangian velocity.

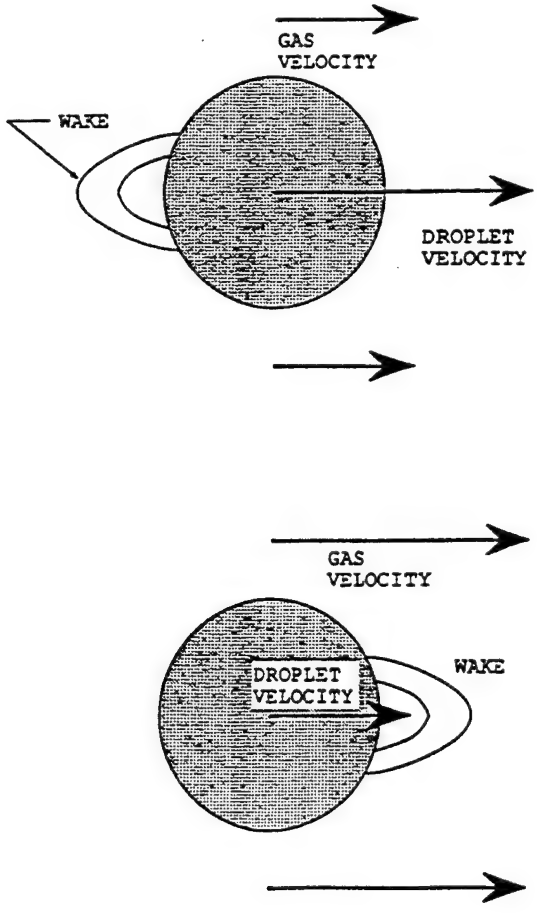

Figure 29
Schematic of Droplet-Faster and Gas-Faster Configurations

Note that, in actual rockets, both Figure 29 configurations exist since the droplet is initially faster than the gas, but as the combustion proceeds, the gases accelerate and eventually move faster than the droplet. Thus the wake is initially behind the droplet but moves ahead of the droplet with the passage of time.

These two droplet geometries were studied with a 2% pressure oscillation. The spatial phase of injection corresponds with a 1/8 wavelength, and the injection time corresponds to a 1/4 time period. The time period of oscillation for each configuration is 0.6 τ_h. Figure 30 presents the resulting distribution of the elementary response factor for the two cases over the entire time period. The elementary response factor for the droplet-faster case is negative over the entire time domain, indicating a heavy damping. The gas-faster case has both negative and positive elementary response factor values. Table 17 lists the integrated response factor values for both situations.

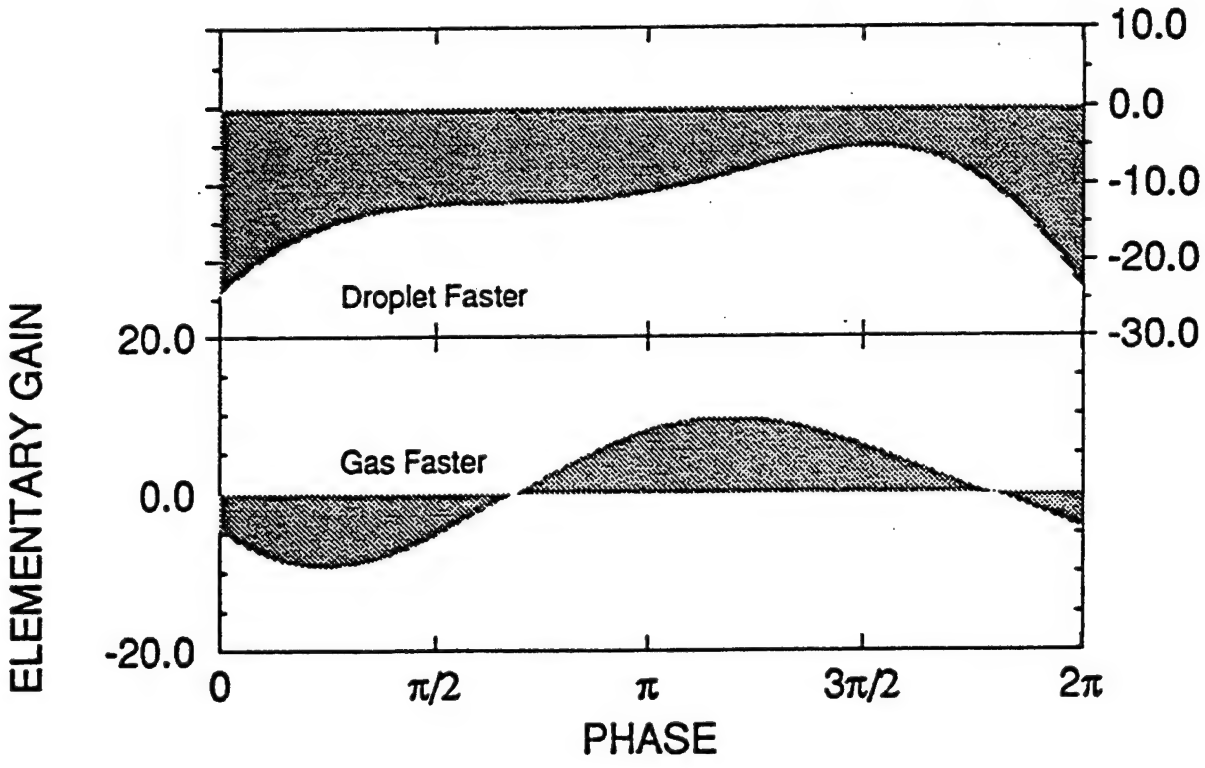

Figure 30
Distribution of Elementary Gain for Varying Configurations

Table 17. Comparison of Response Factor with Droplet-Faster and Gas-Faster Geometries

Configuration	G
Gas Faster	5.81
Droplet Faster	-76.47

For the case with the gas traveling faster than the droplet, Table 17 indicates that the response factor is high and capable of driving instability; but, in the case of the droplet traveling faster than the gas, the response factor is negative and actually damps the oscillations.

Depending on the nature of a particular combustor and operating conditions, the magnitude of the amplitude of the oscillation may vary. In order to get a better understanding of the effects of varying amplitudes, two cases (with pressure oscillations of 1 and 2 percent) were studied. Each case corresponded to a time period of 0.6 droplet heating time, and the time phase of injection corresponded to a quarter time period. The spatial injection phase was again 1/8 of a wavelength. Figure 31 presents the distribution of the elementary response factor. Table 18 lists the integrated response factor values for both pressure-amplitude cases.

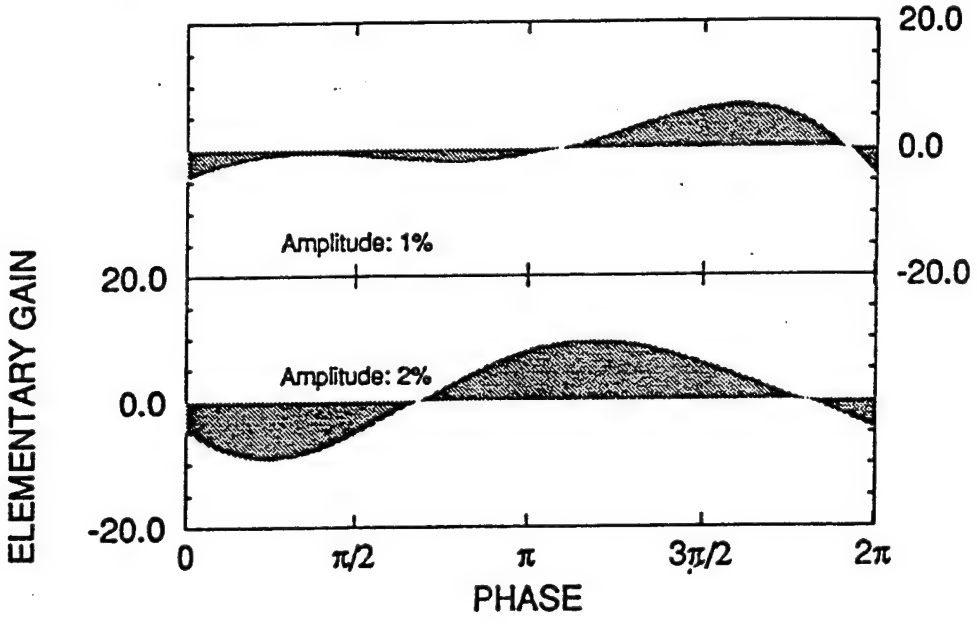

Figure 31
Distribution of Elementary Gain for Varying Amplitudes

Table 18. Comparison of Response Factor with Varying Amplitudes

Pressure Oscillation	G
1%	5.02
2%	5.81

As Table 18 shows, there is a slight decrease in the response factor with a decrease in the amplitude of the oscillation. However, a 50% decrease in the pressure oscillation amplitude only caused a 13% decrease in the response factor; both are still capable of causing an instability. Though the distribution of the response factor is very different for the two cases (Figure 32), its effect on the response factor is not so marked.

The effects of varying the volatility of the fuel were also studied. The base fuel used in the calculations is n-octane. A second fuel has the latent heat of decane but otherwise has the same properties as octane (i.e., "pseudo-decane"). Figure 32 gives the distribution of the elementary response factor, and Table 19 provides the integrated response factors for the two volatility cases. As expected, the more volatile fuel has a slightly larger response factor.

Conclusions

In summary, there is some lack of quantitative agreement between the UTRC low-pressure vaporization measurements and the UCI computations. These differences probably occur because of the absence in the model of the effects of wake interaction between droplets and of secondary atomization via a stripping mechanism. It is possible to include these effects on an oscillatory computation. Some work on these subjects has already been done, especially for the non-oscillatory vaporization of droplets.

The oscillatory study indicates that vaporization as a rate-controlling mechanism can explain combustion instability. In particular, the response of the vaporization rate to an oscillatory ambient pressure and velocity can be sufficiently high to drive an oscillation in a combustion chamber. Preliminary results indicate that the response factor is not highly sensitive to the amplitude of the oscillation. Furthermore, the model is able to handle the situation where the flow relative to the droplet changes direction on account of high amplitudes. When the droplet is faster than the gas, the system has a high damping, whereas when the gas is faster than the droplet, the response factor is high enough to drive the instability. This is primarily due to the effect of the velocity oscillation on the relative velocity. The results were consistent with previous findings that the convective

vaporization mechanism is much more strongly coupled to velocity oscillations than to pressure oscillations.

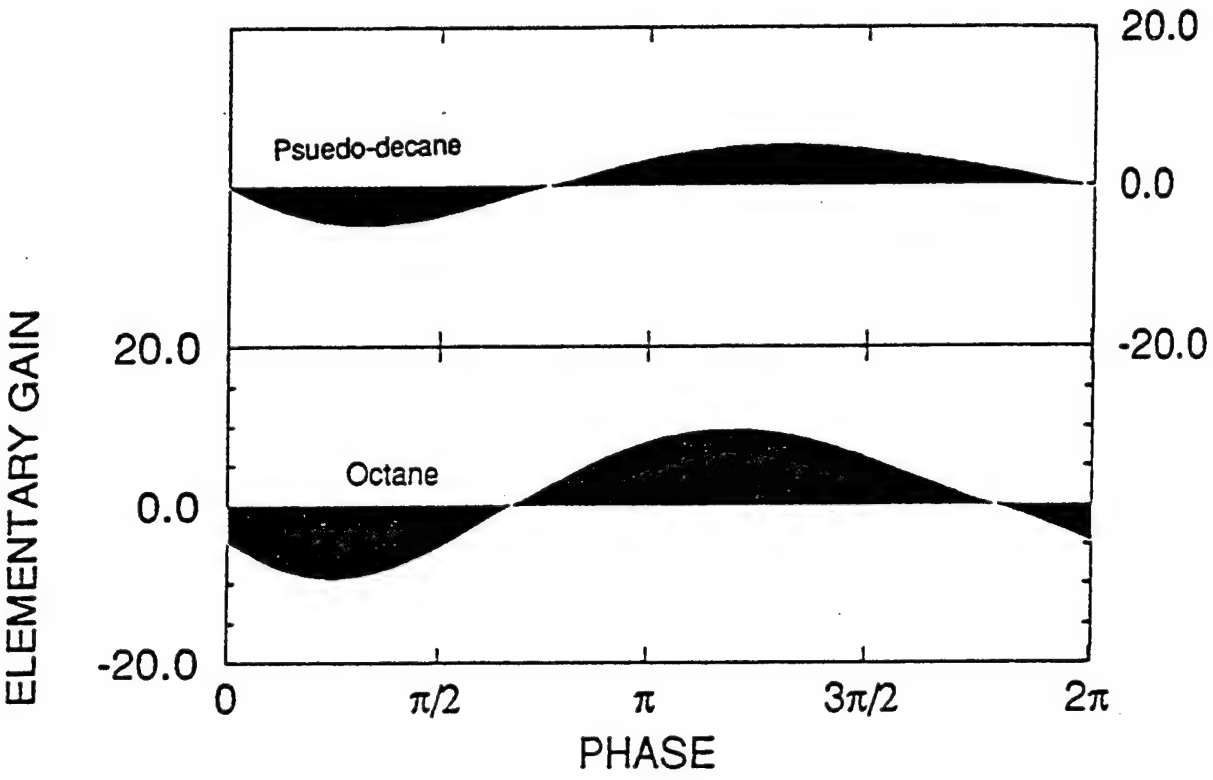

Figure 32
Distribution of Elementary Gain for Varying Fuel Volatility

Table 19. Comparison of Fuels with Varying Volatility

Fuel Configuration	G
Octane	5.81
Pseudo-Decane	4.97

TASK 4 - PRIORITIZED PLAN FOR FUTURE EFFORT

Among the most important benefits of the Liquid Stability Mechanisms Program was the development and application of advanced diagnostic techniques. Such applications are crucial to the detailed investigation of liquid-fueled rocket combustion instability mechanisms as well as other combustion- and spray-related measurements. These developments included the use of the MDR technique by UTRC to obtain accurate changes in droplet diameter and the application of shadowgraphic cinematography by UCI to obtain images of droplet breakup.

Previously, measurements of droplet breakup were predominately done under atmospheric conditions. High-pressure data are important since the corresponding test parameters are closer to those seen in rocket engines (i.e., density ratios, reduced pressures, Reynolds numbers, etc.) This program, however, succeeded in using high-pressure facilities to obtain breakup data at pressures greater than 1 atm. These data include images of liquid oxygen droplet breakup at supercritical conditions. Since most future rocket engines will operate at pressures greater than the critical pressure of LOX, such fundamental data are invaluable for understanding the physical processes. The eventual result is the robust design of stable liquid-propellant rocket engines.

The experimental work accomplished on the LSM program is a good starting point toward the application of new diagnostics and the attainment of fundamental instability mechanism data. Toward the goal of planning for future effort, UTRC has devised a plan for further liquid instability technology diagnostics and measurements. The complete recommendation is included as Appendix L. Provided below is a summary of the proposed effort.

Suggested Tasks

A research program to advance the state-of-the-art in spectroscopic measurement of droplets and sprays undergoing critical point phase transitions and provide data which may include densities, concentrations, temperatures, and critical-surface tracking is proposed. The goal of this program is to produce diagnostic techniques to identify processes relating to liquid stability issues and which can acquire information about phenomena occurring in critical or supercritical conditions. As they develop, these techniques will be evaluated in a high-pressure pulse facility (used in the LSM program) under dynamic conditions corresponding to those of rocket combustors.

Task I. The high-pressure pulse facility will acquire data describing droplet breakup and distribution in critical and supercritical environments as the result of acoustic disturbances. Initial measurements will include back-lit images of droplets following an initial period after the disturbance. Disturbances will be generated as weak (1.1 pressure ratio or lower) shock waves produced from a shock tube. Considerations will also be made to generate continuously varying and repetitive conditions--rather than step change

disturbances--through the use of an acoustic driver. If employed, such a device will provide considerable information describing the effect of the disturbance wave form on the droplet breakup and distribution process.

Task II. Optical diagnostic techniques, such as those listed in Table 20, will be studied with a focus toward employing one or more technique to acquire quantitative data describing droplet breakup in a supercritical environment. Appendix L gives detailed descriptions of each Table 20 diagnostic. Of particular interest is a time-dependent measure of the spatially distributed concentration of droplet fluid following a flow field disturbance. Techniques which provide a means of acquiring an instantaneous image of concentration will be the focus of this investigation.

Task III. Quantitative measurements of the droplet fluid distribution process resulting from the influence of an acoustic pulse on droplets in a supercritical environment will be attempted. This task will be an integration of the use of the facility as in Task I with measurements using the techniques developed in Task II. The measurements will be of limited scope in terms of droplet conditions, but will provide a demonstration of the measurement techniques and a set of results which will describe the droplet breakup process.

Payoff

The completion of this program should provide two basic results. It will define diagnostic techniques applicable to the evaluation of supercritical droplet and spray systems. The intent is to develop techniques applicable to understanding the problems associated with instabilities in liquid-fueled rocket engines. However, these diagnostics will have further applicability for developing an understanding of other droplet and spray processes.

The second result of this program will be the application of techniques for the measurement of fluid mixing properties in sub- and supercritical conditions; an important step for understanding instabilities associated with liquid-fueled rocket engine operation. The measurements should be capable of describing mixing of supercritical droplet injectants or progression of the critical surface within a sub-critical droplet in a supercritical environment. These results should be valuable in understanding the stability processes occurring in combustors at or above the critical conditions.

Table 20. Diagnostic Techniques for Future Effort

Diagnostic Technique	*Measurement Capabilities*
Spontaneous Raman	temperature, density, imaging
Stimulated Raman	temperature, density, phase
Stimulated Brillouin (SBS)	droplet size, liquid-phase concentration
SBS w/degenerate four-wave mixing (DFWM) or DPCFWM	temperature, density, imaging
Morphology-Dependent Resonances (MDR)	droplet size, shape, evaporation rates, critical transition
Second Harmonic Generation	droplet critical phase surface

SUMMARY AND CONCLUSIONS

1. A number of potential liquid-rocket combustion instability mechanisms were initially considered. This preliminary investigation included a comprehensive literature search. Droplet vaporization and secondary atomization were eventually selected as the primary processes for study under the LSM program. A shock tube concept was chosen as the method for experimentally generating the pressure pulses to simulate an instability wave.

2. Morphology-dependent resonances of droplets exposed to 10-to-20-percent pressure waves were used to obtain very accurate measurements of the change in droplet diameter. Both methanol and water droplets (approximately 70 microns) were employed in this 1-atm vaporization investigation. When compared to a droplet in a quiescent environment, the pressure pulse was seen to greatly enhance the vaporization rate. Methanol evaporation in all cases was approximately 13 time greater than water evaporation. Overall, the results indicate that a pressure wave has a significant effect on the transient vaporization response of the droplet. Therefore vaporization is indeed a potential instability mechanism.

3. Application of a two-phase numerical model to the study of fuel droplet vaporization under oscillatory conditions was accomplished. The integrated vaporization response factor was used to determine what effect changes in oscillation amplitude, droplet configuration, oscillation frequency, and fuel volatility have on the stability of the combustor. It was found that the response of the vaporization rate to an oscillatory environment can be sufficiently high to drive an instability. Preliminary results indicate that the response factor is more affected by changes in oscillation frequency and droplet configuration than by oscillation amplitude and droplet volatility.

4. The same computational model was applied to the 1-atm, experimental vaporization results by modeling the pressure pulse as a step disturbance. It was observed that the measurements were smaller than the predicted vaporization rate for the quiescent cases, and the predictions were an order of magnitude smaller than the measurements in the shock wave cases. This discrepancy is partially attributed to the lack of numerical convergence over the short test time and (most likely) due to the model being unable to simulate boundary layer stripping. Nonetheless, the analytical results tend to agree with conventional "$D^{3/2}$" vaporization laws.

5. Images of a LOX droplet exposed to a pressure pulse within a supercritical environment (test section pressure > 50 atm.) were obtained using a simple back-lighting technique. The resulting images show a near-instantaneous breakup of the droplet that is different from usual low-pressure breakup data. These images show that a pressure pulse has a drastic effect on LOX droplets at high pressure, indicating

a mechanism that may be some combination of secondary atomization and vaporization.

6. For the exploration of secondary atomization, a high-pressure (68-atm test section capability) shock tube was designed and fabricated. The driver section was designed to produce steep-fronted, or N-waves. Shadowgraphic cinematography was employed as the imaging diagnostic. Prior to and in conjunction with the experimental effort, reviews of secondary atomization theory and of established pulse techniques were conducted. To better simulate the conditions seen in typical, high-pressure rocket combustors, a simulant fluid study was also undertaken. The resulting ideal test matrix was designed to parametrically investigate a range of test variables; it covers a range of Reynolds numbers from 100 to 65,000, a range of Weber numbers from 30 to 140,000, and a range of liquid-to-gas density ratios from 56 to 77.

7. Initial images of secondary atomization with a constant wave strength (≈ 1.5) and a constant initial droplet diameter (≈ 120 μm) using methanol and water indicate that the maximum product drop size increases with decreasing wave duration and We_{max}. Droplet breakup times also appear to decrease with increasing wave duration, though the accuracy of these measurements is thought to be ±15%. Plotting non-dimensional displacement versus time, water droplets are found to be in the "bag" mode according to equation (2) and the methanol drops are found to be in the "shear" mode, but both are characterized as "multi-mode" breakup by Hsiang and Faeth (21).

8. A plan for future effort was formulated. This plan involves the further development of advanced diagnostics to study the fundamental mechanisms of liquid-rocket combustion instability. In the proposed investigations, further exploration of phenomena related to supercritical combustion are emphasized. The techniques thus developed would also prove invaluable for other combustion-related measurements including spray characterization and liquid-gas mixing.

REFERENCES

1. Lord Rayleigh, *The Theory of Sound*, Dover Publications, New York, 1945.

2. Harrje, D. J. and Reardon, F. H. (Ed.), *Liquid Propellant Rocket Instability*, NASA SP-194, 1972.

3. Dodd, F. E., Private Communication, 1992.

4. Tong, A. Y. and Sirignano, W. A., "Oscillatory Vaporization of Fuel Droplets in an Unstable Combustor," *J. Propulsion and Power*, Vol. 5, pp. 257-261, May-June 1989.

5. Tong, A. Y. and Sirignano, W. A., "Multicomponent Transient Droplet Vaporization with Internal Circulation and Approximate Solution, *Numerical Heat Transfer*, Vol. 10, pp. 253-278, 1986.

6. Tzeng, H.-M., Wall, K. F., Long, M. B., and Chang, R. K., "Evaporation and Condensation Rates of Liquid Droplets Deduced from Structure Resonances in the Fluorescence Spectra, *Optics Letters*, Vol. 9, pp. 273-275, July 1984.

7. Quain, S.-X., Snow, J. B., Tzeng, H.-M., and Chang, R. K., "Lasing Droplets: Highlighting the Liquid-Air Interface by Laser Emission, *Science*, Vol. 231, pp.486-488, Jan. 1986.

8. Boylan, D. M. and O'Hara, J., "Determination of Gas Velocity and Temperature Near a Rocket Injector Face," CPIA 213, 9th JANNAF Combustion Meeting, Vol. II, Sept. 1972.

9. Delplanque, Private Communication, 1992.

10. Sato, J., Tsue, M., Niwa, M., and Kono, M., "Effects of Natural Convection on High-Pressure Droplet Combustion," *Combustion and Flame*, 82, pp. 142-150, 1990.

11. Faeth, G. M., "Structure and Atomization Properties of Dense Turbulent Sprays," 23rd Symposium (International) on Combustion, The Combustion Institute, Pittsburg, PA, pp. 1345-1352, 1990.

12. Culick, F. E. C., "Combustion Instabilities in Liquid-Fueled Propulsion Systems," AGARD Conference Paper No. 450, Neuilly sur Seine, France, Nov. 1989.

13. Williams, F. A., "Structure of Detonations in Dilute Sprays," *Phys. Fluids*, Vol. 4, No. 11, 1961.

14. Dabora, E. K., Ragland, K. W., and Nicholls J. A., "Drop-Size Effects in Spray Detonations," 12th Symposium (International) on Combustion, Pittsburg, PA, pp. 19 - 26, Oct. 1969.

15. Temkin, S. and Mehta, H. K., "Droplet Drag in Accelerating and Decelerating Flow," *JFM*, Vol. 116, pp. 297-313, 1982.

16. Mehta, H. K., "Droplet Drag and Breakup in Shock-Wave Induced Unsteady Flows," Ph.D. Dissertation, Rutgers University, New Brunswick, NJ, 1980.

17. Borisov, A., Gel'fand, B., Natanzon, M., and Kossov, O., "Droplet Breakup Regimes and Criteria for Their Existence," *J. Eng. Phys.*, Vol. 40, No. 1, pp. 44-49, 1981.

18. Ross, Phillip J., *Taguchi Techniques for Quality Engineering*, McGraw-Hill, New York, 1988.

19. Berglund, R. N. and Liu, Y. H., "Generation of Monodisperse Aerosol Standards," *Env. Sci. & Tech.*, vol. 7, no. 2, pp. 147-153, Feb. 1973.

20. Connon, C. H. and Dunn-Rankin, Private Communication, 1993.

21. Hsiang, L. -P. and Faeth, G. M., "Secondary Drop Breakup in the Deformation Regime," AIAA 92-0110, 30th Aerospace Sciences Meeting, Reno, NV, Jan. 1992.

22. Hinze, J. O., "Fundamentals of the Hydrodynamic Mechanism of Splitting in Dispersion Processes," Forced Deformations of Viscous Liquid Globules," *AIChE J.*, vol. 1, no. 3, pp. 289-295, 1955.

23. Chiang, C. H., Raju, M. S., and Sirignano, W. A., "Numerical Analysis of Convecting, Vaporizing Fuel Droplet with Variable Properties," *Int. J. Heat Mass Transfer*, 35, No. 5, pp. 1307-1324, 1992.

24. Delplanque, J.-P. and Sirignano, W. A., "Transcritical Vaporization and Combustion of LOX Droplet Arrays in a Convective Environment," to be presented at the 14th ICDERS, Coimbra, Portugal, August 1993.

25. Chiang, C. H. and Sirignano, W. A., "Interacting, Convecting, Vaporizing Fuel Droplets with Variable Properties," *Int. J. Heat Mass Transfer*, 36, No. 4, pp. 875-886, 1993.

26. Chiang, C. H. and Sirignano, W. A., "Axisymmetric Calculations of Three-Droplet Interactions," *Atomization and Sprays*, 3, No. 1, pp. 91-107, 1993.

27. Chiang, C. H., "Isolated and Interacting, Vaporizing Fuel Droplets: Field Calculation With Variable Properties," Ph.D. Thesis, University of California, Irvine, Department of Mechanical Engineering, 1990.

28. Crocco, L. and Cheng, S. I., *Theory of Combustion Instability in Liquid Propellant Rocket Motors*, Vol. 8, Butterworths Scientific Publications, London, 1956.

29. Bhatia, R. and Sirignano, W. A., "One-Dimensional Analysis of Liquid-Fueled Combustion Instability," *J. Propulsion and Power*, Vol. 7, pp. 953-961, Nov. 1991.

APPENDIX A

"Task One Report"

TASK ONE REPORT

Submitted to

Pratt & Whitney

Prepared by

W. A. Sirignano

Department of Mechanical Engineering

University of California

Irvine, CA 92717

A. PROBLEM DESCRIPTION AND HISTORICAL BACKGROUND

The problem of combustion instability in liquid-propellant rockets is a continuing challenge. Any enclosed or restricted chamber has an infinite number of modes for resonant oscillation. The heat release associated with the combustion processes can potentially provide a driving mechanism for the acoustical oscillation. The acoustical pressure and velocity oscillations tend to cause an oscillation in the local burning rate. If the amplitude of the burning rate oscillation is large enough and if the phase between the burning rate and pressure oscillations is small enough, the instability can be driven. Often the amplitudes are sufficiently large to cause such increased heat transport rates that a structural failure occurs at the injector face or at the nozzle throat.

Combustion instability research was very active during the two decades of the Fifties and Sixties, especially in relation to the Apollo Program. Experience with Lox- kerosene propellants and impinging injectors indicated severe instability problems. A general rule is that the instability is more likely and becomes more severe in terms of damage as the energy release rate per unit volume increases, or in other words, as performance increases. The behavior is more complicated than this simple rule; instability probability depends upon spatial distribution of the energy release rate, combustion time- lag, damping forces, and chamber dimensions (or natural frequencies). The rule, however, is a useful guide.

During the Fifties and Sixties, some limited research was performed on the basic driving mechanism of the instability. Several researchers (1-12) examined fuel droplet vaporization as the rate-controlling phenomenon and as the basic driving mechanism. On account of limitations of their analyses (explained later in the discussion on spray combustion), they could not successfully explain the cause of combustion instability. The most widely used description of the combustion process in analyses was the Crocco time-lag description (1,2,13,14). This was an ad hoc representation of the combustion process through the use of a small number of parameters (usually two). One of these parameters was the sensitive time-lag which was based on the concept that the combustion process had a time-lag so that the

burning rate at some instant depended upon conditions experienced by the reactants for some short time duration prior to that instant. The time duration or time-lag magnitude itself depended upon the conditions prior to the instant of burning. The average time-lag and other ad hoc parameters were considered to be functions of propellant combinations and injector design only, yielding the hope for straightforward scaling of results from small combustors to large combustors. This method had limited success.

The most reliable method for preventing large amplitude oscillations in liquid propellant rocket engines was to damp the oscillations through the use of baffles or acoustic liners. That is, energy was taken from the most unstable modes of oscillation. The science of preventing the addition of energy to the oscillations by modifying or controlling the basic combustion process was never really developed. However, there is reason to believe that this science can now be rapidly developed and that new technology on the control of combustion instability can be advanced. There is still a need for this new technology since the engineering fixes through damping mechanisms lead to increased volume, increased weight, increased cooling requirements, and decreased performance.

The resurgence in interest in space and the renewed interest in liquid-propellant systems creates the need to re-examine the combustion instability problem in an organized and intense manner. There is recent interest in LOX-methane systems whose instability characteristics are not well understood. LOX-kerosene systems are under active consideration again and their instability problems are well-known. The LOX-hydrogen systems have not experienced severe instability problems. However, there is no inherent reason why LOX-hydrogen should be more stable than other systems and our experience with LOX-hydrogen has been with a very narrow range of designs. New designs intended to improve performance could easily lead to serious instability problems.

On account of limitations in the methodologies of those times, theoretical analyses were performed mostly with small perturbation techniques for linearized or weakly nonlinear oscillations. Other nonlinear approaches involved gross simplification and, in some cases, gross mutilation of the basic governing equations. On the experimental side, pressure was the only instantaneous and localized point measurement that could be made; even there pressure was measured only at outer walls. On account of the high-temperature, high-frequency behavior, velocity and scalar point measurements could not be made instantaneously in the field.

B. THE OPPORTUNITY OF MODERN TIMES

Now in the Nineties, we can benefit from the methodologies of computational fluid dynamics and of non-intrusive laser diagnostics. Fully nonlinear coupled systems can be analyzed. Measurements of velocity, temperature, and concentration can be made locally in

high-temperature, oscillatory conditions. Clearly, the potential exists to learn much more about the driving mechanisms and other characteristics of combustion instability.

Since the Sixties, there has been substantial advancement in the understanding of basic combustion phenomena. Understanding of spray combustion, including transient droplet heating and vaporization, has advanced tremendously. Mixing of co-flowing streams of fluids is now much better understood. Our knowledge of atomization processes and chemical kinetics has also advanced substantially. The research that led to these advancements addressed automotive combustion, gas turbine combustion, ramjet combustion and industrial combustion problems rather than liquid rocket combustion. Nevertheless, liquid-propellant combustion research can build upon the recently established foundations.

C. CANDIDATE DRIVING MECHANISMS FOR COMBUSTION INSTABILITY

Many potential mechanisms for combustion instability in liquid-propellant rockets have been identified. They include injection coupling, primary atomization, secondary atomization, vaporization, mixing, and chemical kinetics. Tables I, II and III from Reference (2) present the candidate mechanisms identified by the three major liquid rocket manufacturers in the United States.

One may crudely view combustion in a liquid propellant rocket motor as consisting of a sequence of processes. This sequence would be followed by an infinitesimally small element of propellant. In sequence, injection, primary atomization, secondary atomization, liquid heating, vaporization, gas-phase mixing and heating, gas-phase chemical reaction, and loss of some heat to fresh propellants are the processes. There are some caveats that should be added. The combustion is continuous, so that propellant elements injected at different times would not necessarily be in the same process at a given time. There is also a spatial distribution so that different elements injected at the same time can be in different processes at a given time. The details of any process for a given element can depend upon both the preceding processes for that element and all of the processes for other elements. Fox example, the vaporization rate for an element depends on the atomization process for that element which determines the droplet size. Vaporization rate also depends upon the heat transferred from other propellant elements that have already burned.

Each of the processes has a duration or characteristic time associated with it. The time can vary substantially. If one of the times for the sequential processes is much longer than any of the rest and, in fact, much longer than the sum of the rest, the time for burning of that propellant element is essentially the characteristic time for the longest process. We refer to that particular process as rate-controlling because the burning rate approximately equals the rate for that process.

Variation of pressure, temperature, and velocity in the chamber will affect these processes and, in particular, can affect the characteristic times and rates associated with these processes. Dynamic or frequency-dependent phenomena are expected.

Any driving mechanism must pass certain tests. In particular, the chemical conversion rate (or burning rate) associated with the mechanism must respond adequately to fluctuations of pressure, velocity, and temperature. That is, for a given amplitude of pressure oscillation, the conversion rate must oscillate with a sufficiently large amplitude and a sufficiently small phase relative to the pressure oscillation. Even if the conversion rate responds to some other quantity, such as temperature or velocity, it is the amplitude and phase relative to the pressure amplitude and phase that is important since the feedback of energy to the oscillation depends upon the relationship to pressure. Since maximum amplitudes of pressure and velocity can occur at different positions in the chamber, this results in a complex relationship for feedback of energy to the combustor oscillation. A change in a parameter generally not only affects the amplitude and phase of the burning rate oscillation but also modifies the spatial distribution of the burning. The most important basic parameters are those related to the injector design or the propellant choice.

Three types of mechanisms can be important in combustion instability. The first type is associated with a combustion process that is rate-controlling and has a characteristic time of the same order as the period of oscillation. This process can respond strongly to oscillations of the pressure and velocity in the chamber. The question still remains whether the amplitude is sufficient and the phase is proper to overcome the damping mechanisms and to drive the oscillation.

If the process is not rate-controlling, oscillations in its rate cannot significantly affect the burning rate and the feedback to the combustor oscillation. If the process has a characteristic time much longer than the period of oscillation, it generally cannot respond to the oscillation. That is, the frequency of the oscillation is too high for process; there is insufficient time for the particular process to adjust to the oscillations of pressure and velocity. When the characteristic time of the process is very short compared to the oscillation, it can respond. However, processes with short characteristic times are generally not rate-controlling. If they still are rate-controlling, there is the additional difficulty that the process would only respond in a quasi-steady manner. The dynamic response could result in larger amplitudes of burning rate than the quasi-steady response.

The second type of process is one that affects the characteristic time of some other rate-controlling process. An example of this type would be atomization which has a characteristic time much shorter than the typical period of oscillation; however, pressure and velocity variations produce variations in the initial droplet size distribution which, in turn, affects the

characteristic time of rate-controlling processes. This type of process can have a dramatic indirect affect on the oscillatory process. A third type of mechanism also has an indirect influence. This type of mechanism affects the spatial distribution of the combustion. Therefore, it produces variation in the local response that affects the coupling with a particular mode of oscillation. The second and third types of mechanisms are actually concurrent actions of the same mechanism since a change in characteristic time of a combustion process as viewed from a Lagrangian frame has the impact of a change in combustion distribution as viewed from an Eulerian frame. Let us discuss each of the major processes related to combustion in liquid propellant rocket engines.

Liquid Injection

The liquid feed system involves storage tasks, pumps, feed lines, and injection parts into the combustion chamber. The lengths and volumes (or components) of the feed system tend to be large so that characteristic response times tend to be much longer than a millisecond.

Injection coupling is defined to mean that oscillations in the combustion chamber and oscillations in the feed system are coupled and reinforcement occurs. If there is no significant coupling, the combustion chamber will oscillate with essentially constant mass flow through the injector ports.

Injector coupling tends to be most significant for low frequency chamber oscillations on account of the large characteristic time for the feed system. That is, the feed system time matches better with the residence time in the combustion chamber than with the period of oscillation for any of the acoustical oscillatory modes. In the low frequency modes, the chamber pressure is approximately spatially uniform but time-varying. These low frequency modes have been well understood for decades. Summerfield (1,14) analyzed these modes using a constant time lag concept. Injector coupling is relatively easy to eliminate by isolation of the feed system. Increasing the pressure drop across the injection port is a standard process that isolates the feed system since, for large pressure drops, a given pressure fluctuation in the chamber produces a small variation in pressure drop and therefore in the mass flow.

The fluctuation in the feed system could result in modifications of other processes involved in combustion of the propellants. For example, the jet velocity at the port would fluctuate modifying the primary atomization process of one or both propellants. Initial droplet size and droplet velocity fluctuations would vary. This would produce variations in the characteristic times of other processes. Also, it would affect the spatial distribution of combustion in the chamber. However, since the characteristic times for these other processes are much shorter than the period of oscillation in the low frequency cases, and since little sensitivity to spatial distribution of combustion occurs in those low frequency cases, these

effects are generally not significant in terms of instability. Of course, some exceptions might exist. Nevertheless, injection coupling is not a strong candidate for detailed study in a situation with limited resources.

Primary Atomization

Various atomization schemes are employed in liquid propellant systems. In one scheme called impinging jets, injection ports are designed to work as pairs or triplets with the jets colliding in order to enhance break-up into droplets. Upon impingement, sheets of liquid in a conical fan-like shape emerge. Here, the conical cross-sections are not circular but rather more like ellipses with a very large ratio of semi-major to semi-minor axes. Usually, the impinging streams consist of like (the same) propellants so that liquid-phase mixing does not occur. This scheme is commonly used with LOX/RP1 propellants. In another scheme involving coaxial jets, fuel and oxidizer are injected in parallel streams. This is commonly used for LOX/hydrogen and LOX/methane propellant combinations. LOX is always placed inside in practice with the fuel on the outside. At the high injection velocities employed, the Rayleigh break-up mechanism is not of interest. Rather, the Kelvin-Helmholtz instability is the interesting mechanism. Surface and interface waves form and grow causing distortion and ultimate break-up of the surface in this mechanism. Very little fundamental experimental and theoretical work (15,16) has been done on this mechanism. The characteristic wavelengths and periods of oscillation for these surface waves on the propellant streams are very small. An estimated frequency for these waves is 105 cycles per second. This characteristic time is more than one order of magnitude lower than typical periods of oscillation for chamber instabilities. Variations in chamber conditions due to acoustic oscillations can be treated as quasi-steady as far as primary atomization is concerned. The atomization process will not respond in a resonant fashion to chamber oscillations.

Strahle and Crocco 17) have shown by a linearized analysis that, in the absence of a resonant behavior and at low mean flow, Mach numbers, we should not expect fluctuations in droplet size and droplet number density to drive the instability. The droplets move through the chamber at velocities much less than the speed of sound and carry the effect of initial size and number density. The kinematic wave resulting from the droplet initial conditions undulates more rapidly through the chamber than the pressure wave which travels with an acoustic speed. This results in a rapid undulation of the amplitude of the fluctuating source of burned gases that drives the instability. Due to the rapid undulations of the kinematic wave, three are many regions of both positive and negative reinforcement of the pressure wave. As a result, without a resonance effect, this phenomenon cannot produce a significant global effect since the positive contributions roughly equal the negative contributions.

Primary atomization is not projected to have a major direct effect on the driving mechanism of the instability. If the processes following it in the sequence do not respond significantly to oscillations of pressure and velocity, there would not be any sustained oscillation according to linear theory. It is possible that a nonlinear perturbation could modify the conclusion. However, since the issue relates more to the phase relationship between the source term and the pressure term rather than an amplitude effect, it is not clear how nonlinearities would change the conclusion.

Note that atomization processes are quasi-steady and thus do not respond differently to different frequencies in the range below 104 cycles per second; therefore, this mechanism would not explain observed phenomena even if other factors, discussed above, were not present.

Secondary Atomization

Droplets that are formed by the primary atomization process can undergo further distortion and break-up. When smaller droplets result from a larger droplet, the process is named secondary atomization.

The surface tension tends to keep a droplet intact with a spherical shape. Aerodynamic pressure drag resulting from relative droplet-gas velocity tends to strain the droplet so that it assumes an oval shape with a decrease in the length parallel to the main flow direction and an increase in the transverse lengths. This can result in the "pinching- off" of droplets.

Another mechanism involves a Kelvin-Helmholtz instability along the droplet surface. This results in the stripping of smaller droplets from the surface of the larger droplet.

Droplet distortion can significantly affect droplet drag and trajectory since the drag coefficient is modified. The likelihood for distortion, Kelvin-Helmholtz instability, and the "pinching-off" mechanism increases as the droplet Weber number increases. Secondary atomization tends to occur downstream away from the dense spray regime.

The characteristic times associated with secondary atomization are much smaller than droplet vaporization and heating times. Also, they are much smaller than the typical periods of oscillation. Therefore, the same general conclusions can be made for secondary atomization as were made for primary atomization. It does not emerge as a strong candidate for direct feedback to the oscillation as a mechanism for combustion instability. There are, however, the very important indirect ways in the instability that can be affected by secondary atomization.

Vaporization and Liquid Heating

Droplet vaporization and droplet heating should be considered as an integrated process.

Heat from the high-temperature gaseous environment is transferred to the droplet largely by convective heating. The heat to the surface partially passes to the liquid interior raising the droplet temperature in the interior as well as at the surface. The remainder of the transferred heat sustains the phase change at the surface and increases the temperature of the vapors flowing away from the surface.

In practice, there is generally a relative velocity between the (LOX or fuel) droplet and the surrounding gas. Due to convection, the droplet heating rate and vaporization rate will depend upon the Reynolds number based on this relative velocity. There will be a laminar boundary layer over the surface of the droplet. The shear stress at the surface will cause an internal circulation in the liquid droplet. This affects the transient heating of the liquid and the vaporization note. Below the critical pressure, a clear distinction can be made between the liquid droplet and the surrounding gas. The surface tension tends to keep the droplet spherical. The characteristic time for the liquid heating tends to be higher than the time for boundary layer heating. For kerosene-type fuel droplets, the heating time and droplet lifetime are of the same order while for LOX droplets, the heating time would be longer than the lifetime. In liquid-propellant rocket motors, periods of acoustic oscillation tend to be of the order of the droplet heating time suggesting a potential for coupling. The situation is more complicated at near-critical or supercritical pressures. The reduced surface tension allows deviation from spherical shapes. The increased gas density decreases or removes the distinction between the phases and increases the gas-phase heating time. A coupling with the acoustic oscillations can still be expected, although less is known about the details.

Several investigators (1,3-11,18) have pursued the vaporization process as the driving mechanism for combustion instability in liquid propellant rocket engines. Vaporization is the slowest of the processes, generally, and thus is the rate-controlling process. A quasi- steady response of the vaporization to combustion oscillations cannot provide sufficient feedback to drive the instability. Therefore, a dynamic or resonant response must occur if vaporization were to drive the instability. Strahle (7-11) has examined the gas-phase film and boundary layer surrounding a droplet to determine its oscillatory response. At the frequencies of interest, the heat and mass transport through the gas layer tend to oscillate in a quasi-steady manner, without a resonance effect. Priem and co-workers (3-6,12)have examined transient heating of the liquid interior. There was a dynamic response with their model in the frequency range of interest; however, the amplitude of the vaporization rate was not sufficient to drive the instability. It is noteworthy that their model assumed that liquid temperature was uniform spatially through the interior, albeit time-varying. The model effectively employed an infinite conductivity so that the heat transferred through the liquid surface immediately was distributed throughout the liquid interior. This kept the surface

temperature unrealistically low; the amplitude of surface temperature and consequently the amplitude of vaporization are kept at reduced levels on account of this assumption.

In recent years, transient droplet heating and vaporization has been studied (18-33) with a better modelling of heat and mass diffusion in the liquid phase. In particular, spatial gradients of temperature and concentration through the liquid are taken into account. In these more accurate situations, it is found that amplitudes of surface temperature and vaporization rate can be large enough to drive an oscillation (18,34). The characteristic time for droplet heating is commensurate with the practical periods of oscillation resulting in a strong dynamic response. Droplet heating time is, of course, dependent upon initial droplet size. Some recent results (34) for liquid-fueled ramjets indicate that, along a stability limit, initial droplet diameter increases with the combustion chamber length (or the period of the natural oscillation).

The vaporization rate responds to fluctuations of both the ambient pressure and the relative gas-droplet velocity. It tends to be more sensitive to the latter. For transverse oscillations, the pressure and velocity tend to be in phase so that the pressure sensitivity and the velocity sensitivity can be reinforcing.

The theory for oscillatory droplet vaporization can explain the driving of combustion instabilities in situations where hydrocarbon fuels are employed and chamber operating pressures are subcritical. The theory must be extended to understand more fully situations where the pressure is supercritical or the vaporization of the liquid oxygen is rate-controlling (hydrogen or methane fuel, for example).

In the supercritical pressure case, the temperature will vary significantly from the ambient supercritical value to a subcritical value in the droplet. The latent heat of vaporization is zero in the supercritical pressure domain. Properties will vary substantially over the droplet and its surrounding gas film because of the wide variation in temperature; characteristic diffusion times can therefore be very different in different zones. This means that the supercritical pressure case shares certain generic characteristics with the subcritical pressure case with regard to the response to ambient oscillations. That is, transport processes within certain regions of the field could potentially resonate at some frequency. Again, the theory here is not fully developed.

In the case of oxygen droplets at subcritical pressures, the latent heat of vaporization is very low and the transfer number is high so that the droplet vaporization is very fast. The magnitude of the temperature gradients in the liquid phase remain to be determined. Potentially, they can be large. The sensitivity to fluctuations also remains to be determined.

In summary, we can model an oscillatory vaporizing spray flow reasonably well for standard hydrocarbon type fuels at subcritical conditions. For supercritical conditions or for

oxygen vaporization, the models have greater uncertainties. The vaporization rate is typically rate-controlling and responds in a resonant fashion for frequencies of practical interest. Therefore, vaporization is a most prominent candidate as a driving mechanism for instability.

Mixing

After the two propellants vaporize, they must mix with each other before reaction can occur. The mixing process will be turbulent since Reynolds numbers based upon distance between injector elements and propellant velocities will be in the range of 104 to 106. This distance is relevant for impinging like-on-like injectors. For like-on-unlike impingement or co-axial injectors, the diameter of the injection orifice or port is more relevant. In that case, we see a one order of magnitude reduction in the Reynolds number.

A characteristic time for turbulent mixing can be estimated to be less that 1 millisecond at its upper limit and as small as ten microseconds. Some very small fraction of the propellant requires a time to mix that is substantially longer. That small fraction accounts for only a very small amount of released energy. Mixing, then, is generally faster than vaporization so that it cannot be rate-controlling. It has minor impact on the distribution of the energy release through the chamber.

In this discussion, only mixing and transport on a scale larger than the droplet size or than the size of the boundary layer around the droplet is considered. The mixing and transport in the boundary layer and near wake of the droplet has been considered as part of the vaporization process. Mixing, as defined here, includes both the process of change of local composition and the transfer of heat from burned propellants to the fresh propellants.

On account of the short characteristic time, the mixing process would tend to resonate at higher frequencies than are of practical interest. Mixing is not a promising candidate for a combustion instability driving mechanism.

Chemical Kinetics

After the propellants are well mixed and heated, they can react. At the high pressures and high temperatures associated with rocket combustion chambers, the chemical reaction rate will be large. The characteristic time for the chemical reaction will be very short compared to the vaporization time.

Variations in the chemical reaction time due to fluctuations in pressure and temperature will not be significant compared to variations in the vaporization time. Oscillations in the chemical rate will not, therefore, produce significant oscillations in the overall burning rate. Furthermore, there is no potential for a resonant response of the chemical kinetics in the frequency range of interest.

For these reasons, chemical kinetics is not viewed as an interesting driving mechanism for combustion instability in liquid propellant rocket motors.

Note that, for certain experimental configurations where propellants are introduced as pre-mixed gases, we can see importance to the chemical reaction as a driving mechanism. However, the chemistry would respond in a quasi-steady manner over a wide range of frequencies. No resonant phenomenon has been observed; for example, an increase in the chamber length does not modify the stability of the combustion process.

D. CHOSEN AREAS FOR EMPHASIS

The analysis presented in the previous section leads to the clear conclusion that vaporization and atomization are the primary candidates for emphasis in this study. Several recent workshops have also concluded that atomization and vaporization are the two processes most likely to have major impact on combustion instability in liquid-propellant systems.

The atomization study should address both primary and secondary atomization mechanisms. Effects upon atomization due to transverse waves would be especially interesting. The vaporization study should examine the relationships between the vaporization rate and the fluctuating ambient pressure and velocity. Again, transverse waves are of special interest. Since vaporization rate is very sensitive to initial size, the coupling between atomization and vaporization must be studied.

The designed experiments for this study should lead to improved understandings of individual droplet behavior and of the interactions amongst droplets in a spray both in oscillatory and non-oscillatory conditions.

E. SUGGESTED EXPERIMENTS AND MEASUREMENTS

A sequence of experiments, of increasing complexity and practicality, are suggested. Four levels of experimental sophistication are proposed: (1) a single isolated droplet study, (2) a stream of interacting droplets, (3) a few parallel streams of interacting droplets, and (4) a spray generated by a single injector element. Each experiment could provide information about both atomization and vaporization. Also, the experiments can be used to examine vaporization and atomization phenomena both with steady operation and with wave disturbances. Various pressure levels should be studied.

The isolated droplet experiment should include a number of capabilities. Instantaneous droplet shape, size, and position should be determined. Relative droplet-gas velocity and ambient gas velocity are needed. Internal circulation patterns should be examined. In principle, droplet vaporization rate can be determined by taking the derivative of the droplet diameter as a function of time. This can lead to significant errors, especially under oscillatory

conditions. An alternative approach is to measure surface temperature, the normal temperature gradient at the surface, relative velocity, and the ambient velocity, temperature, and pressure simultaneously. Then, a formula can be employed to infer vaporization rate. Still another possibility involves the simultaneous measurements of the relative velocity, ambient velocity, ambient pressure and temperature, and the mass fractions of the droplet vapors at the surface and in the ambient flow. Then, the vaporization rate can be inferred. The formulas that are used in the last two alternatives become approximate when the Reynolds number based upon relative velocity and droplet diameter is not zero. Also, they only apply in subcritical states.

This experiment should allow for the possibility of secondary atomization. The mode of break-up and the number and sizes of the resulting fragments should be determined. Correlation with the instantaneous Weber number and a characteristic time for break-up should be measured.

Initial droplet diameters will be of the order of one hundred microns. When ninety percent of the droplet has vaporized, the diameter has decreased by a factor only slightly greater than two. For high droplet Reynolds numbers (compared to unity), the thickness of the gas boundary on the droplet is of the order of the droplet radius divided by the square root of the droplet Reynolds number. This layer could easily be of the order of ten mirrors in practice. It is desirable therefore to resolve down to a few microns in space. The characteristic time for vaporization in a high temperature environment is a few milliseconds. The characteristic time for liquid-phase heating is of the same order as the droplet lifetime. Typical periods of oscillation in an unstable combustor vary between a fraction of a millisecond and several milliseconds. Time resolution is required one to two orders of magnitude below this number; a few tens of microseconds is desirable while a few hundreds of microseconds is desirable for transient behavior. Resolution of the secondary atomization process should also require this small a time-scale.

Transverse wave disturbances are the most interesting to study. The velocity amplitudes for the transverse mode are much larger near the injector than the velocity amplitudes for the longitudinal modes. Both atomization and vaporization modification due to transverse waves should be more significant than modifications due to longitudinal waves.

In the practical problem, chamber pressures can range from tens of atmospheres to hundreds of atmospheres and temperatures can reach 3000 K. Flow velocities can reach a few hundred meters per second with the speed of sound at about one thousand meters per second. An interesting wave disturbance should involve a pressure amplitude of mean-to- peak value at least about ten percent of the mean pressure and a velocity amplitude at least about ten percent of the speed of sound.

The deflection of a droplet from its approximately longitudinal direction by a strong transverse wave will be a challenge for the experimentalist who is attempting measurements with high resolution. Compromises can be made by studying situations with lower mean values of pressure, temperature, and speed of sound. However, care must be exercised in extrapolating these results to more practical conditions.

The second type of experiment involves a single stream of droplets. The initial spacing between tandem droplets is an interesting parameter that should vary between a few droplet diameters and about twenty droplet diameters. The interesting measurements and challenges include all of those identified for the isolated droplet. In addition, the temporal variation of the distance between droplet centers should be monitored. The dependencies upon this spacing is very interesting. The characteristic times and lengths, the quantities to be measured, and the desired resolutions remain similar to those for the isolated droplet.

The third type of experiments involves several parallel streams of droplets. The spacing between parallel streams here as well as the spacing between tandem droplets should be monitored. Initial spacing between parallel streams should vary between about one droplet diameter and a few diameters. Tandem spacing should be similar to the single stream study. Otherwise, characteristic times and lengths, quantities to be measured, and desired resolutions are similar to those discussed above. Each droplet in a stream for the second and third types of experiments should have the same initial droplet size and the same initial spacing between droplets.

The final experiment involves the spray resulting from an actual coaxial injector element. In this experiment primary, atomization will occur, making it different from the first three experiments. This presents an opportunity to determine droplet size distributions and droplet velocity distributions resulting from the initial atomization process. Joint diameter-velocity distributions or at least some correlation of size and velocity is required. Observations of the mechanism of primary atomization should be made for the cases with and without wave disturbances. Resolution to below one hundred microns in length and below one hundred microseconds is probably required for this task.

The same quantities are desirable for measurement with the same resolution as discussed for the other experiments. The obvious additional difficulty here is that initial conditions for the droplets are not known a priori as they are in the previous, highly- ordered experimental configurations. It might be impossible to explore in detail the processes of vaporization and secondary atomization in this experiment.

Each of the experiments can be conducted with a gas flow employed to simulate the more volatile propellant. The gas flow surrounding the droplet(s) can have certain temperatures and composition. A cold gas flow can be useful to study atomization but not vaporization

and combustion. A hot, inert gaseous flow is useful for studying both atomization and vaporization but not combustion. A hot, oxidizing (reducing) gas surrounding the fuel (oxygen) droplet is useful for studying atomization, vaporization, and combustion. All three types of experiments can yield important information.

The proposed experiments, measurements, and resolutions have been made here solely on theoretical grounds. It is fully appreciated that compromises will be required based upon practical experimental considerations.

References

[1] D. T. Harrje and F. H. Reardon, eds., *Liquid Propellant Rocket Combustion Instability.* Washington, D. C.: NASA SP-194, 1972.

[2] R. J. Jensen, "A summary of the JANNAF workshop on liquid rocket engine combustion driven instability mechanisms," in *Proceedings of the 26th JANNAF Combustion Meeting*, (Pasadena, California), October 1989.

[3] R. J. Priem and D. C. Guentert, "Combustion instability limits determined by a nonlinear theory and a one-dimensional model," Report TN D-1409, NASA, 1962.

[4] R. J. Priem, "Theoretical and experimental models of unstable rocket combustors," in *Proceedings of the Ninth Symposium (International) on Combustion, The Combustion Institute*, (Pittsburgh, PA), pp. 982–992, 1963.

[5] M. F. Heidmann and P. R. Wieber, "Analysis of n-heptane vaporization in unstable combustor with travelling transverse oscillations," Technical report TN D-3424, NASA, 1965.

[6] M. F. Heidmann and P. R. Wieber, "Analysis of frequency response characteristics of propellant vaporization," Technical memorandum TM X-52195, NASA, 1966.

[7] W. C. Strahle, *A Theoretical Study of Unsteady Droplet Burning: Transients and Periodic Solutions.* PhD dissertation, Princeton University, 1960.

[8] W. C. Strahle, "Periodic solutions to a convective droplet burning problem: the stagnation point," in *Proceedings of the Tenth Symposium (International) on Combustion*, pp. 1315–1325, 1964.

[9] W. C. Strahle, "High frequency behavior of the laminar jet flame subjected to transverse sound waves," in *Proceedings of the Eleventh Symposium (International) on Combustion*, p. 747, 1966.

[10] W. C. Strahle, "Unsteady laminar jet flames at large frequencies of oscillation," *AIAA J.*, vol. 3, no. 5, p. 957, 1965.

[11] W. C. Strahle, "Unsteady reacting boundary layer on a vaporizing flat plate," *AIAA J.*, vol. 3, no. 6, p. 1195, 1965.

[12] R. J. Priem and M. F. Heidmann, "Propellant vaporization as a design criterion for rocket engine combustion chambers," Report TR-R67, NASA, 1960.

[13] F. E. C. Culick, "Combustion instabilities in propulsion systems," in *Combustion instabilities in liquid-fuelled propulsion systems*, (Neuilly-sur-Seine, France), NATO, AGARD, 6–7 October 1988. presented at the Propulsion and Energetics Panel 72nd B specialists' meeting, held in Bath, United Kingdom.

[14] L. Crocco and S. I. Cheng, *Theory of Combustion Instability in Liquid Propellant Rocket Motors*, vol. 8. London, England: Butterworths Scientific Publications, 1956.

[15] R. H. Rangel and W. A. Sirignano, "Nonlinear growth of Kelvin-Helmholtz instability: effect of surface tension and density ratio," *The Physics of Fluids*, vol. 31, pp. 1845–1855, 1988.

[16] R. H. Rangel and W. A. Sirignano, "The linear and nonlinear shear-instability of a fluid sheet," *The Physics of Fluids A*, no. 3, pp. 2392–2400, 1991.

[17] W. C. Strahle and L. Crocco, "Analytical investigation of several mechanisms of combustion instability." presented at the 5th Propulsion Meeting, Tampa, FLA, Nov 1963.

[18] A. Y. Tong and W. A. Sirignano, "Oscillatory vaporization of fuel droplets in an unstable combustor," *J. of Propulsion and Power*, vol. 5, no. 3, pp. 257–261, 1989.

[19] W. A. Sirignano, "Fuel droplet vaporization and spray combustion theory," *Prog. Energy. Combust. Sci.*, vol. 9, pp. 291–322, 1983.

[20] A. Y. Tong and W. A. Sirignano, "Analysis of a vaporizing droplet with slip, internal circulation, and unsteady liquid-phase and quasi-steady gas-phase heat transfer," in *Proceedings of ASME-JSME Thermal Engineering Joint Conference*, vol. 2, (New York, N.Y.), pp. 481–487, ASME, 1983.

[21] K. C. Hsieh, J. S. Shuen, and V. Yang, "Droplet vaporization in high-pressure environments .1. near critical conditions," *Combustion Science and Technology*, vol. 76, no. 1–3, pp. 111–132, 1991.

[22] V. Yang, C. C. Hsiao, and J. S. Shuen, "Pressure-coupled vaporization and combustion responses of liquid fuel droplets in high-pressure environments." AIAA-91-2310, presented at the 27th AIAA/SAE/ASME/ASEE Joint Propulsion Conference, Sacramento, CA, June 24–26 1991.

[23] V. Yang, N. N. Lin, and J. S. Shuen, "Vaporization of liquid oxygen (LOX) droplets at supercritical conditions." AIAA-91-0078, presented at the 30th AIAA Aerospace Sciences Meeting and Exhibit, Reno, NV, January 6–9 1992.

[24] J.-P. Delplanque and W. A. Sirignano, "Numerical study of the transient vaporization of an oxygen droplet at sub- and supercritical conditions," *International Journal of Heat and Mass Transfer*, 1992. in press.

[25] A. Y. Tong and W. A. Sirignano, "Analytical solution for diffusion and circulation in a vaporizing droplet," in *Nineteenth Symposium (International) on Combustion*, pp. 1001–1020, The Combustion Institute, Pittsburgh, PA, 1982.

[26] B. Abramzon and W. A. Sirignano, "Droplet vaporization model for spray combustion calculations," *International Journal of Heat and Mass Transfer*, vol. 32, pp. 1605–1618, November 1989.

[27] G. Patnaik, *A Numerical Solution of Droplet Vaporization with Convection.* PhD dissertation, Carnegie-Mellon University, Department of Mechanical Engineering, 1986.

[28] G. Patnaik, W. A. Sirignano, H. A. Dwyer, and B. R. Sanders, "A numerical technique for the solution of a vaporizing fuel droplet," pp. 253–266, AIAA, 1986. Volume 105 of *Progress in Astronautics and Aeronautics.*

[29] C. H. Chiang, M. S. Raju, and W. A. Sirignano, "Numerical analysis of convecting, vaporizing fuel droplet with variable properties," in *27th Aerospace Sciences Meeting*, (Reno, Nevada), 1989.

[30] C. H. Chiang, M. S. Raju, , and W. A. Sirignano, "Numerical analysis of convecting, vaporizing fuel droplets with variable properties," *International Journal of Heat and Mass Transfer*, vol. 35, pp. 1307–1324, May 1992.

[31] C. H. Chiang, *Isolated and Interacting, Vaporizing Fuel Droplets: Field Calculation With Variable Properties.* PhD dissertation, University of California, Irvine, Department of Mechanical Engineering, 1990.

[32] C. H. Chiang and W. A. Sirignano, "Axisymmetric vaporizing oxygen droplet computations." AIAA-91-0281, presented at the 29th AIAA Aerospace Sciences Meeting and Exhibit, Reno, NV, 1991.

[33] C. H. Chiang and W. A. Sirignano, "Interacting, convecting, vaporizing fuel droplets with variable properties," *International Journal of Heat and Mass Transfer*, vol. 36, pp. 875–886, March 1993.

[34] R. Bhatia and W. A. Sirignano, "One-dimensional analysis of liquid-fueled combustion instability," *J. of Propulsion and Power*, vol. 7, pp. 953–961, November 1991.

APPENDIX B - SHOCK TUBE EQUATIONS

Two texts by Gaydon and Hurle (1963) and Bradley (1962) detail the history, applications, and theory of shock tubes and only background material necessary for definition of the flow field associated with a shock tube will be treated here.

The development of equations for a shock tube in this section will be limited to those necessary to define the flow in the uniform region of flow behind the shock front for a step function wave and those necessary to define the flow field behind the shock front in the expansion behind the shock front for an N-wave. Assumptions consistent with the following analysis include those of ideal gas have a constant specific heat ratio, γ. The speed of sound, a, is defined according to

$$a = \sqrt{\frac{\gamma p}{\rho}} = \sqrt{\frac{\gamma R_u T}{M}} = \sqrt{\gamma R T} \tag{B-1}$$

Development of the basic equations is benefited by defining a coordinate system which is fixed relative to the shock front with the shock tube fixed coordinate system the alternative. Considering the shock front as a control surface and writing the conservation equations for mass, momentum, and energy

$$\rho_1 u_1 = \rho_2 u_2 \tag{B-2}$$

$$p_1 + \rho_1 u_1^2 = p_2 + \rho_2 u_2^2 \tag{B-3}$$

$$h_1 + \frac{1}{2} u_1^2 = h_2 + \frac{1}{2} u_2^2 \tag{B-4}$$

where the enthalpies per unit mass h_1 and h_2 are defined by

$$h = e + \frac{p}{\rho} \tag{B-5}$$

and no heat loss in the shock wave is assumed. These equations are true for any shock wave in gas.

In the shock tube fixed coordinate system, the velocity of the gas upstream of the shock front which moves at W, is $v_1 = 0$, while the velocity of the gas behind the shock is $v_2 = W - u_p$, where u_p is the particle velocity. For the shock fixed coordinate system, gas enters the shock front with relative velocity, u_1, and leaving

the shock with relative velocity, u_2, as shown in Figure B-1. Thus the two coordinate systems can be related by

$$u_1 = W \tag{B-6}$$

$$u_2 = W - u_P \tag{B-7}$$

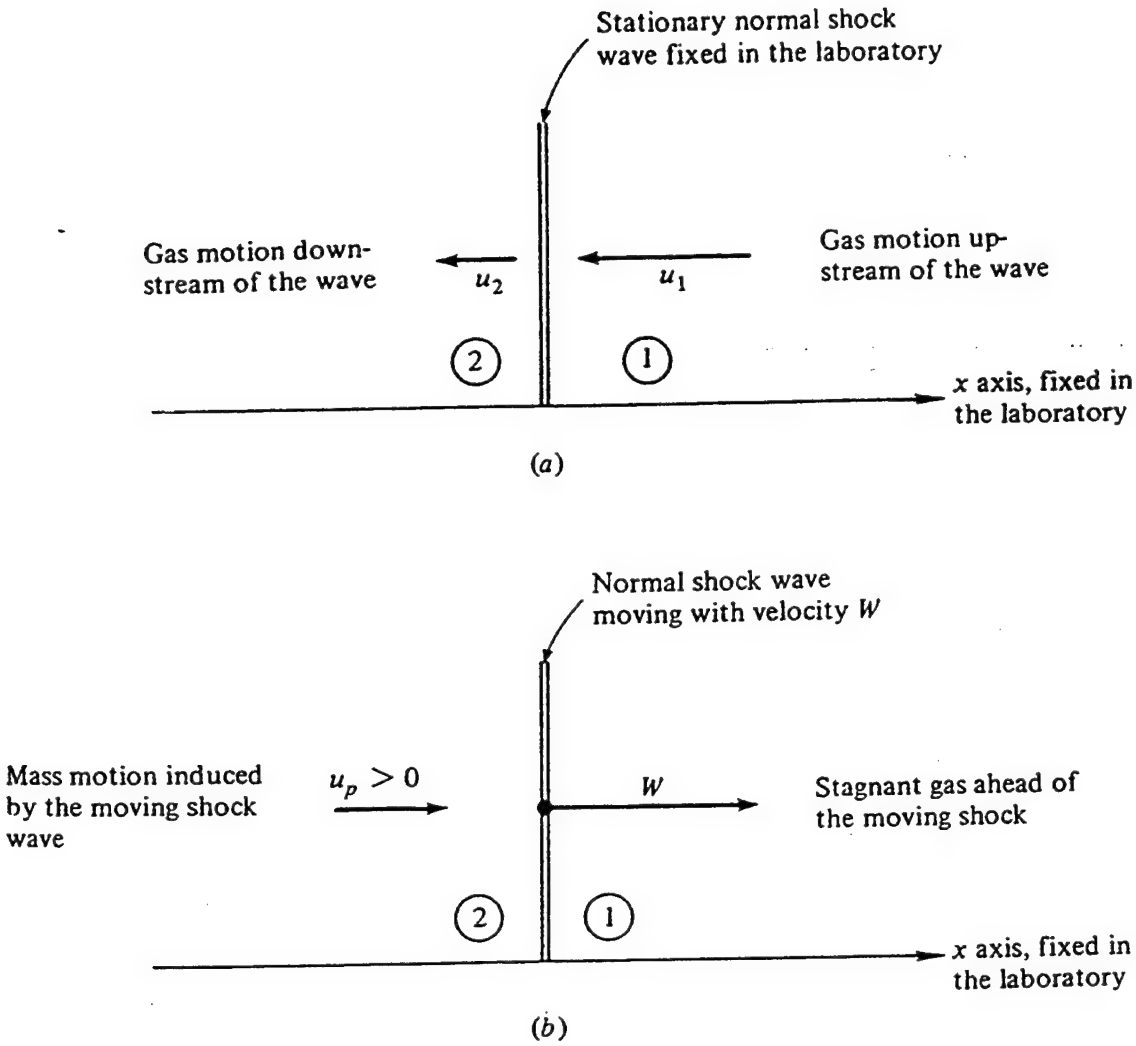

Figure B-1
Schematic of Stationary and Moving Shock Waves

Substituting expressions B-6 and B-7 into equations B-3, B-4 and B-5 yields

$$\rho_1 W = \rho_2 (W - u_p) \tag{B-8}$$

$$P_1 + \rho_1 W^2 = P_2 + \rho_2 (W - u_p)^2 \tag{B-9}$$

$$h_1 + \frac{1}{2} W^2 = h_2 + \frac{1}{2} (W - u_p)^2 \tag{B-10}$$

For a calorically perfect gas with $\gamma = c_p/c_v$,

$$h = \frac{\gamma}{(\gamma - 1)} RT = \frac{\gamma}{(\gamma - 1)} \frac{p}{\rho} \tag{B-11}$$

and

$$p = \rho RT \tag{B-12}$$

From equation B-11, equation B-10 may be rewritten,

$$\frac{\gamma}{(\gamma - 1)} \frac{p_1}{\rho_1} + \frac{1}{2} W^2 = \frac{\gamma}{(\gamma - 1)} \frac{p_2}{\rho_2} + (W - u_p)^2 \tag{B-13}$$

Eliminating velocities from equations B-8, B-9 and B-13 yields, after rearranging

$$\frac{p_2}{p_1} = \frac{1 - \frac{(\gamma - 1)}{(\gamma + 1)} \frac{\rho_1}{\rho_2}}{\frac{\rho_1}{\rho_2} - \frac{\gamma - 1}{\gamma + 1}} \tag{B-14}$$

and solving for ρ_2 / ρ_1 and using equation B-8 yields

$$\frac{\rho_2}{\rho_1} = \frac{\dfrac{\gamma-1}{\gamma+1} + \dfrac{p_2}{p_1}}{\dfrac{(\gamma-1)}{(\gamma+1)}\dfrac{p_2}{p_1} + 1} = \frac{W}{W - u_P} \tag{B-15}$$

Solving for T_2 / T_1 using the ideal gas relation B-12 and equation B-15 yields

$$\frac{T_2}{T_1} = \frac{p_2}{p_1}\frac{\dfrac{(\gamma-1)}{(\gamma+1)}\dfrac{p_2}{p_1} + 1}{\dfrac{\gamma-1}{\gamma+1} + \dfrac{p_2}{p_1}} \tag{B-16}$$

Eliminating W - up from equation B-9 using equation B-8 gives

$$\frac{p_2}{p_1} = 1 + \frac{\rho_1 W^2}{p_1}(1 - \rho_1 / \rho_2) \tag{B-17}$$

Introducing the Mach number defined as the ratio of the speed of a disturbance in gas or the gas velocity itself to the local speed of sound

$$M_S = \frac{u_1}{a_1} = \frac{W}{a_1} \tag{B-18}$$

Substituting equation B-1 into B-17 and using the definition B-18 yields

$$\frac{p_2}{p_1} = 1 + \gamma M_S^2 (1 - \rho_1 / \rho_2) \tag{B-19}$$

Eliminating ρ_2 / ρ_1 from equations B-15 and B-19 gives

$$\frac{p_2}{p_1} = \frac{2\gamma M_S^2 - (\gamma-1)}{\gamma+1} \tag{B-20}$$

and eliminating p_2/p_1 from equations B-19 and B-20 gives

$$\frac{\rho_2}{\rho_1} = \frac{(\gamma+1)M_S^{\,2}}{(\gamma-1)M_S^{\,2}+2} \tag{B-21}$$

and using the ideal gas relationship B-12 and equations B-20 and B-21 gives

$$\frac{T_2}{T_1} = \frac{(\gamma M_s^{\,2} - (\gamma-1)/2)((\gamma-1)M_s^{\,2}/2+1)}{(\gamma+1)^2 M_S^{\,2}/4} \tag{B-22}$$

Solving equation B-19 for M_S gives

$$M_S = \sqrt{\frac{\gamma+1}{2\gamma}(p_2/p_1-1)+1} \tag{B-23}$$

and combining with definition B-18 yields

$$W = a_1\sqrt{\frac{\gamma+1}{2\gamma}(p_2/p_1-1)+1} \tag{B-24}$$

which relates the velocity of the moving shock wave to the pressure ratio across the wave. The particle velocity may be related to this same pressure ratio by combining equations B-8, B-15, and B-24 so that

$$u_p = u_2 = \frac{a_1}{\gamma}(p_2/p_1-1)\sqrt{\frac{2\gamma/(\gamma+1)}{\frac{p_2}{p_1}+\frac{\gamma-1}{\gamma+1}}} \tag{B-25}$$

For a right-running simple wave of rarefraction we have the invariant quantity

$$u - \frac{2a}{\gamma-1} = \text{constant} \tag{B-26}$$

and isentropic flow where

$$\frac{p_x}{p} = (\rho_x/\rho)^{\gamma} = (T_x/T)^{\frac{\gamma}{\gamma-1}} = (a_x/a)^{\frac{2\gamma}{\gamma-1}} \tag{B-27}$$

For the driver section, $u_4 = 0$, $\gamma = \gamma_4$, and $M = M_4$, so that B-26 can be written for a general location as

$$\frac{a_x}{a_4} = 1 - \frac{\gamma_4 - 1}{2}\frac{u_x}{a_4} \tag{B-28}$$

and using the isentropic relation gives

$$\frac{p_x}{p_4} = (1 - (\gamma_4 - 1)(u_x / a_4)/2)^{\frac{2\gamma_4}{\gamma_4 - 1}} \tag{B-29}$$

Applying Equation B-29 between the head (region 4, Figure 5)) and the tail (region 3, Figure 5) of the rarefraction, solving for u_3, and recalling preservation of pressure across the contact surface ($p_2 = p_3$) yields

$$u_3 = \frac{2a_4}{\gamma_4 - 1}(1 - (p_2 / p_4)^{\frac{\gamma_4 - 1}{2\gamma_4}}) \tag{B-30}$$

Now, recalling preservation of velocity across the contact surface ($u_2 = u_3 = u_p$) and equating Equations B-25 and B-30 yields, after rearrangement:

$$\frac{p_4}{p_1} = \frac{p_2}{p_1}\left\{1 - \frac{(\gamma_4 - 1)\frac{c_1}{c_4}\left(\frac{p_2}{p_1} - 1\right)}{\sqrt{2\gamma_1\left[2\gamma_1 + (\gamma_1 + 1)\left(\frac{p_2}{p_1} - 1\right)\right]}}\right\}^{\frac{-2\gamma_4}{\gamma_4 - 1}} \tag{B-31}$$

This expression can be used to determine the driver section pressure required to produce a wave of strength p_2/p_1, although no damping effects are taken into account here, and the actual driver section pressure may be substantially higher for high amplitude waves.

As N-waves are employed in the present effort characterization of the simple wave flow region following the shock front is also necessary. Thus the local velocity, u_{2i} following the shock front can be defined by the local pressure, p_{2i} at that point as

$$u_2(t) = u_{2,max} + \frac{2a_1}{\gamma - 1}(p_2(t) / p_{2,max})^{\frac{\gamma - 1}{2\gamma}} - \frac{2a_1}{\gamma - 1} \tag{B-32}$$

where the local sound speed is given as

$$a_2(t) = a_{2,\max} + \frac{1}{2}(\gamma - 1)(u_2(t) - u_{2,\max}) \tag{B-33}$$

and the local static temperature is given by

$$\sqrt{T_2(t)} = \frac{a_2(t)}{a_{2,\max}}\sqrt{T_{2,\max}} \tag{B-34}$$

and the maximum values are those found in the uniform flow region after the normal shock.

The test time, Δt_{test}, can be found by calculating the difference in arrival times of the shock front and the contact surface at the test section distance, x_{test}, as

$$\Delta t_{test} = \frac{x_{test}}{(W - u_p)} = \frac{x_{test}}{a_1}\frac{\sqrt{\frac{\gamma+1}{2\gamma}(p_2/p_1 - 1) + 1}}{\frac{\gamma-1}{2\gamma}(p_2/p_1 - 1) + 1} \tag{B-35}$$

This is a lower limit estimate of test time for a step wave. Test times for N-waves will be longer due to the continuous reduction in u_p after the passing of the shock front.

Appendix B Bibliography

Bradley, J. N. (1962) *Shock Waves in Chemistry and Physics*, John Wiley and Sons, New York, NY, 1962.

Gaydon, A. G. and Hurle, I. R. (1963) *The Shock Tube in High-Temperature Chemical Physics*, Reinhold Publishing Corporation, New York, NY, 1963.

APPENDIX C

"Measurements of the Effects of Acoustic Disturbances on Droplet Vaporization Rates"

Measurements of the Effect of Acoustic Disturbances on Droplet Vaporization Rates

M. Winter and T. J. Anderson
United Technologies Research Center
East Hartford, Connecticut 06108

Presented at
28th JANNAF Combustion Meeting
October 28-November 1, 1991

Measurements of the Effect of Acoustic Disturbances on Droplet Vaporization Rates

M. Winter and T. J. Anderson
United Technologies Research Center
East Hartford, Connecticut 06108

ABSTRACT

Advanced laser diagnostic measurements are being applied to quantify droplet vaporization enhancement in the presence of acoustic fields which can lead to instability in liquid-fueled rockets. Fluctuating droplet vaporization rates and subsequent reaction rate fluctuations resulting from acoustic disturbances within the combustion chamber may potentially be the cause of these instabilities. Models have been developed to describe the interactions between droplet vaporization and acoustic fields in the surrounding gases, but have not been verified experimentally. One of the difficulties in this experimental verification is identifying techniques with sufficient resolution to measure small changes in droplet diameter which result in significant vapor generation. Extremely accurate vaporization rate measurements are being performed by using individual droplets as miniature lasers, producing morphology-dependant resonances, whose spectral mode-structure contains information about the laser cavity dimensions. These can be related to droplet size. The measurements are being applied to determine droplet vaporization rates in quiescent conditions and after the passage of a weak pressure pulse.

INTRODUCTION

Acoustic instabilities within the combustor have been a concern ever since the development of liquid-

---

This work was performed under Contract No. F04611-89-C-088 with the Air Force Phillips Laboratory.

fueled rocket engines. The mechanisms leading to these instabilities are not well understood but are important since engine performance is sacrificed in order to avoid conditions in which the instabilities occur. The cause is believed to be a reaction rate enhancement produced by and in phase with acoustic waves within the combustor. The enhancement may result from atomization of the fuel and oxidizer droplets or increased evaporation[1] caused by the surrounding gas flow which amplifies pressure waves leading to the instability.

Spherically symmetric droplet models have been developed to describe the effect of acoustic perturbations on evaporation.[2] A program is being conducted to measure the evaporation rate enhancement resulting from the surrounding flow conditions. This is accomplished by generating a strong acoustic perturbation similar in intensity to the acoustic waves within a rocket engine and measuring the effect on droplet vaporization rates. In order to measure the droplet vaporization enhancement, an extremely accurate advanced laser diagnostic technique is combined with a monodispersed droplet stream introduced into a rocket combustor-like flow field.

EXPERIMENTAL

PULSE TUBE SYSTEM

Two pulse tubes are being used for these investigations; an atmospheric pressure pulse tube and a high pressure pulse tube system. Measurements to date have been performed in the atmospheric pressure system which is shown in Fig.1 and described below. A high pressure pulse tube has been designed and fabricated under corporate sponsorship which is capable of test section pressures of 1000 psi and driver section pressures up to 2300 psi resulting in a 50% pressure ratio. The high pressure system will be described below in the Future/Conclusions section

A small pulse tube was made from common materials for the initial experiments in this program. The driven section is a 25 mm diameter copper tube, 2.2 m long, attached to a 1.4 m driver section with a bolted flange. Aluminum foil, inserted in the flange is used as a burst disk when the driver is pressurized with air. Foil thicknesses of 30 μm provide a fairly repeatable pressure pulse with a pressure rise of 1.1. Repeatability was obtained by chemically etching a line nto the foils by dipping them into a solution of NaOH held at 70 C for 5 seconds. The measurement location is 1.1 m from the beginning of the driven section, located so that the steady state test time after wave passage is approximately 5 ms. 2 mm diameter holes are located in the top and bottom of the test section and a droplet generator is positioned so that a stream of droplets falls through the test section.

Flat windows on either side provide optical access to illuminate the droplets with the laser beam, so that they can be observed with an intensified CID camera and imaged on the input slit of a spectrometer to acquire MDR's.

A frequency-doubled pulsed Nd:YAG laser beam is condensed to illuminate the droplets and timed with the camera and spectrometer to acquire a signal at a specified time delay after the pressure pulse has passed the droplets. Timing is determined from pressure transducers located upstream of and surrounding the test section. In addition to providing the timing signal, these provide a means of measuring the actual timing and the wave strength (pressure ratio) and velocity.

The droplet generator is a piezoelectric device that supplies a monodisperse stream of droplets. The droplet size is selected with the installation of an orifice with a specified diameter. Currently droplets of roughly 60 or 120 μm can be produced and the stream velocity is approximately 7 m/s.

DIAGNOSTIC TECHNIQUE

In order to achieve the required measurement accuracy[1], evaporation was measured using morphology-dependent resonances (MDR's).[3] A microscope and video system can provide only rough measurements and typically is able to resolve droplet diameters to within only approximately 10 μm. With the MDR technique, a dye dissolved in the droplet fluid is pumped to an upper electronic state by an external light source. Small droplets (on the order of or less than 100 μm in diameter) of a solvent and dissolved laser dye are illuminated with a high power pulsed laser. Stimulated emissions from dye molecules just inside the circumference of the droplet are constrained to the inner surface by total internal reflection, effectively producing a spherical ring dye laser as shown in Fig. 2. Within the spectral envelope of the dye, frequency modes for which the circumference is an integral number of wavelengths are resonantly enhanced. The spectral location of these modes can be described by

$$\nu = n/(\pi d), \qquad \text{(eqn. 1)}$$

where ν is the spectral location in cm^{-1}, d is the droplet diameter and n is the mode number. A spectrum of such MDR's for a 67 μ droplet is shown in Fig 3. The droplet diameter is calculated from the spacing between modes,

$$\Delta\nu_n = (\Delta n)/(\pi d), \qquad \text{(eqn. 2)}$$

where $\Delta\nu_n$ is the spectral spacing between modes in cm^{-1}. It should be noted that the mode number, n, within the droplet should be an integral value and therefore, Δn for adjacent modes would be 1μm. However, the refractive index changes as the light leaves the droplets and produces an apparent Δn of

$$\Delta n = \tan^{-1}[(m^2-1)^{0.5}]/(m^2-1)^{0.5} \qquad \text{(eqn. 3)}$$

for adjacent modes, where m is the ratio of the droplet refractive index to that of air.

A change in droplet diameter can be determined by simply using MDR's to measure the droplet diameter twice over a given time period and subtracting one from the other to obtain the change in size. However, this technique may not be able to resolve small changes in droplet size. Our detector system limits the resolution with this technique to no better than 1 μ. A more accurate method is to measure the change directly by observing the change in spectral location of a given mode between two spectra. From the spectral position of a mode in the first spectrum and eqn. 1, the mode number, n, can be determined. With this, the derivative of the eqn. 1 and an assumption that $\Delta d \ll d$, the change in diameter is

$$\Delta d = \Delta\nu_t(\pi d^2/n), \qquad \text{(eqn. 4)}$$

where $\Delta\nu_t$ is the change in spectral location of a specific mode between two spectra acquired over a time period, t. The resolution using this technique is greatly enhanced over measurements using mode spacing as shown in Fig. 4.

LASER SYSTEM

Laser energy to pump the dye is provided by the second harmonic of a double-pulsed Nd:YAG laser. Pulses were approximately 10 ns in length provided virtually instantaneous measurements with respect to the droplet and gas flows. The laser system was modified to allow multiple pulsing at high frequencies with temporal spacing around 100 μs to determine evaporation rates. The laser beam was focussed to illuminate a single droplet at a time and timing of the laser pulse was triggered from pressure pulse passage. Using this system, a series of measurements could be acquired using differing delay times on successive pressure pulse runs to describe the evaporation enhancement.

RESULTS

DROPLET BREAKUP SHADOWGRAPHS

Initial shadowgraph measurements were made on water droplets with a diameter on the order of 150μm. A droplet generator produced a droplet stream in which the droplets were separated by approximately two diameters, flowing at a rate of about 7 m/s vertically through small holes in the top and bottom of a horizontally oriented pulse tube and a weak pressure pulse with a pressure rise of 10 to 50% and flow velocities of 24 to 100 m/s was generated in the tube. Droplet shadowgraph images acquired at varying time delays after wave front passage indicated that, at the higher flow conditions, the droplets lose their symmetry and eventually breakup (Fig. 5). At the lower flow conditions (Fig. 6), the droplets lost their spherical shape during acceleration but retained their symmetry and eventually returned to spheres once they had accelerated. Measurements were to be made at both conditions since evaporation could play a part in the instabilities, even in the delay period before droplet breakup at the high flow conditions.

SIZE MEASUREMENT ACCURACY

Our measurements were made on droplets produced by a piezoelectric droplet generator. This system produces a stream of uniform-sized droplets, the size of which can be adjusted over a small range by changing the frequency of operation of the piezoelectric device. The MDR's were acquired with a spectrometer with a large dispersion and recorded using a 2-D Vidicon detector. The detector channel spacing represents 0.275 cm^{-1} /channel and is centered at 593 nm. MDR measurements have been made over this range to determine the resolution of the technique and are shown in Fig. 7. A video system and microscope provided a rough confirmation of the measurements, although that system is limited by its modulation transfer function to resolve droplet diameters to within only approximately 10 μm. These measurements agreed with the MDR's within the resolution of the camera. The spectrometer resolution makes it possible to resolve diameters to approximately 1 μm using MDR spacing and diameter changes to within approximately 3 nm using the mode shift based on detector pixel spacing.

VAPORIZATION RATE MEASUREMENTS

Initial evaporation rate measurements have been made on methanol droplets in a gas flow at atmospheric temperature and pressure in the facility described above and in Fig. 8. Evaporation rates were determined by recording MDR's from droplets at several heights in the droplet stream and observing the spectral shift of a given

mode caused by a change in diameter resulting from evaporation as the droplet proceeded down the stream. The droplets were on the order of 70 μm in diameter and are falling at approximately 7 m/s. MDR's were acquired in 10 shot averages at each of four heights in the droplet stream. Several of the averages were taken at each location to determine the repeatability of the measurements. A sample set of MDR's is shown in Fig. 9 and the mode in the center of the spectrum was used to calculate the change in droplet diameter. The MDR's at the highest location were used as the reference; i.e., the mode spacing at this spatial location was used to determine the absolute droplet diameter, d, and the frequency mode number, n, for the diameter difference calculations (eqn. 4). The change in diameter, with respect to the reference location is plotted in Fig. 10. The linear plot represents a constant evaporation rate of 1.21×10^{-6} cm^3/s.

Evaporation rates after the passage of a pressure pulse will be higher than that observed in the droplet stream in quiescent air because gas velocities will be an order of magnitude higher under simulated rocket conditions. Resolution time scales between MDR measurements may be roughly an order of magnitude smaller, however, and it is anticipated that this technique will be more than capable of providing the resolution necessary for the desired evaporation rate measurements.

FUTURE / CONCLUSIONS

The design of a facility to experimentally investigate vaporization as a mechanism for inducing combustion instability under more realistic combustor conditions is shown schematically in Fig 11. A high pressure pulse tube has been designed and fabricated under corporate sponsorship. In its initial configuration it is being made available for use in this program. It is capable of test section pressures of 1000 psi and driver section pressures up to 2300 psi producing 50% pressure rises across the pulses. The pulse tube, consisting of a high pressure driver section and a lower pressure driven section separated by a double diaphragm burst disk assembly, has been fabricated and is secured to an I-beam platform. The driver section is made of 76 mm, schedule 80 stainless steel pipe which rides on a rail to allow for quick changes of the burst disks. During operation a hydraulic piston retains the driver section and burst disk assembly in position.

The test section is an integral part of the driven section and has a 51 mm square-cross-section. It has been constructed from a stainless steel forging. The test section houses the droplet generator or coaxial injector and the droplet catcher or spray exhaust and contains two 1.90 inch-diameter high-pressure optical windows on either side and a 0.75 inch-diamter window on top. A window purge has been integrated into the test section to help keep the side windows clear of liquid during tests with the coaxial injector. It has a 51 mm-long slot nozzle with an exit height of 0.5 mm and was designed to run choked at the maximum test section steady-state pressure condition (1000 psi) with a mass flow of 1.5 lbm/sec for each window.

The remainder of the driven side of the pulse tube will be composed of a number of spool pieces which provide the flexibility needed to operate the system with either helium or nitrogen as the driver gas and nitrogen as the driven gas. These sections are constructed from a 51 mm-square aluminum extruded tube encased in a 4 inch schedule 80 stainless steel pipe with a concrete filler. An additional optical window is located in the downstream end-cap to allow for 90 degree optical access to the test section windows. In order to reduce the loads on this window, a baffle plate can be positioned just upstream.

In order to operate the pulse tube it is charged from high-pressure gas cylinders through one-half-inch stainless steel tubing. Four independent systems supply the driver section, the cavity between the burst disks, the driven section, and the window purge. Each system has a fill and exhaust line. The fill line contains a pressure gauge, toggle valve, and needle valve.

These facilities and techniques will be used to perform measurements of droplet vaporization over a range of pressures, and pressure ratios to quantify the effects of vaporization enhancement and relate these data to liquid instability mechanisms.

ACKNOWLEDGEMENTS

We would like to thank Mr. Richard J. Daddona for his expert technical assistance, Mr. Martin Haas for designing the high pressure pulse tube, and Dr. Joseph Winter for suggesting the chemical etching technique for the diaphragms.

REFERENCES

1. A. Y. Tong and W. A. Sirignano, "Vaporization Response of Fuel Droplet in Oscillatory Field," presented at the ASME National Heat Transfer Conference, Pittsburgh, PA., Aug. 9-12, 1987.

2. A. Y. Tong and W. A. Sirignano, "Oscillatory Vaporization of Fuel Droplets in an Unstable Combustor," Journal of Propulsion, Vol. 3, pp.257-261, May, 1989.

3. Tzeng, H.-M., K. F. Wall, M. B. Long and R. K. Chang, "Evaporation and Condensation Rates of Liquid Droplets Deduced from Structure Resonancesm in the Fluorescence Spectra," Optics Letters, Vol. 9, pp. 273-275, July, 1984.

4. Quian, S.-X., J. B. Snow, H.-M. Tzeng and R. K. Chang, "Laser Droplets: Highlighting the Liquid-Air Interface by Laser Emission," Science, Vol. 231, pp. 486-488, Jan. 1986.

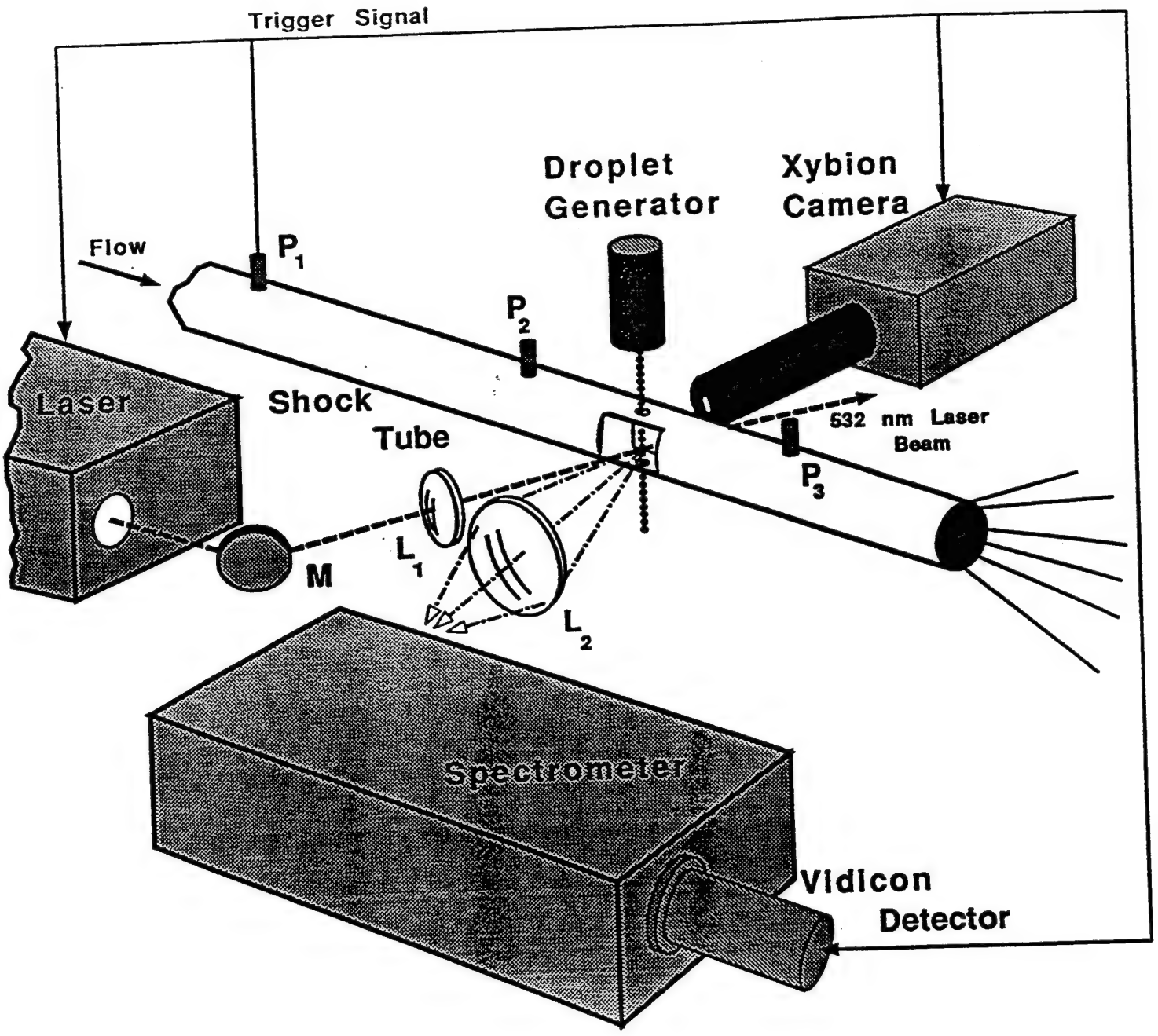

Fig. 1. Optical configuration for generating MDR's in a droplet stream behind a shock wave. The laser is timed to pump fluorescent dye in the droplets at a preset time delay after shock wave passage. Light from the droplets is imaged in the Xybion CID camera and on the slit of a spectrometer.

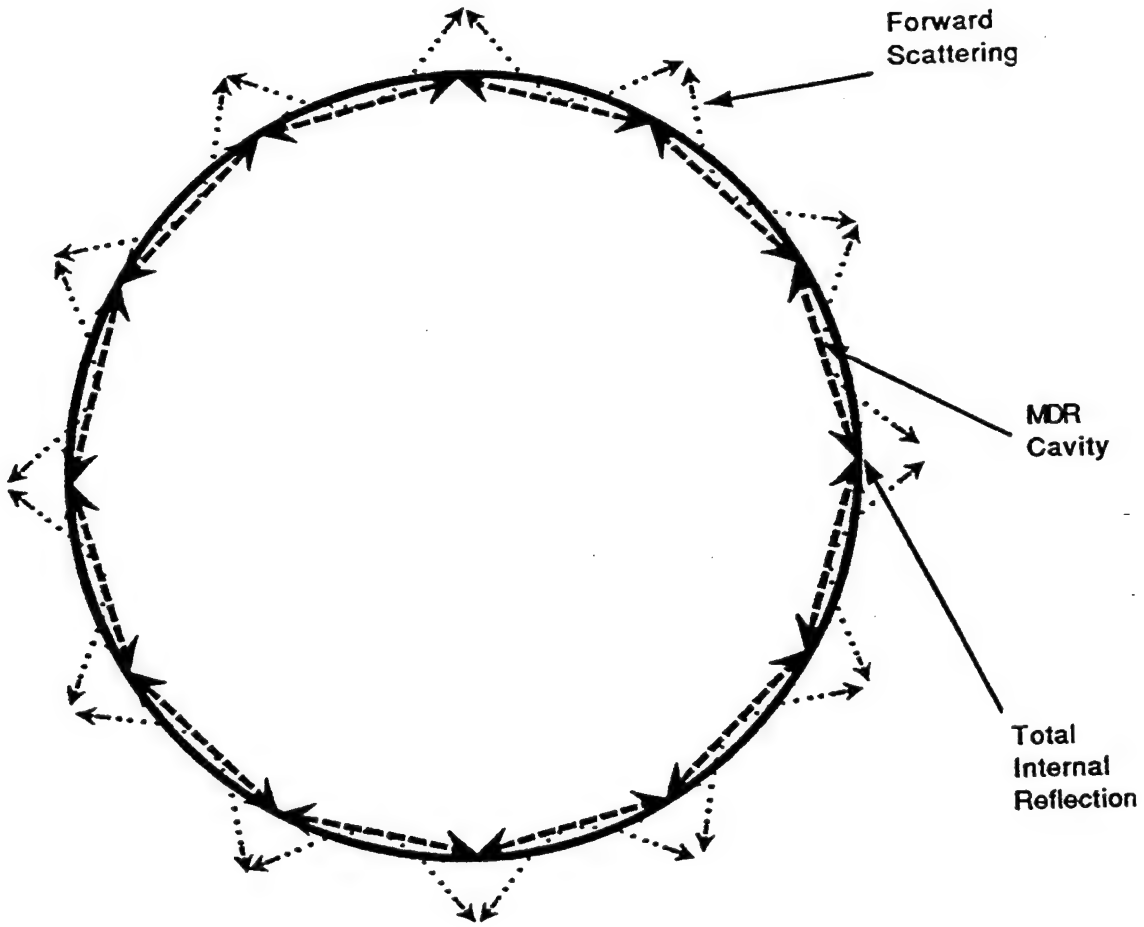

Fig. 2. MDR optical paths in a spherical cavity. Total internal reflection of light emitted near the surface of the droplet forms the cavity. Scattering of this light from within the droplet is observed as MDR emissions.

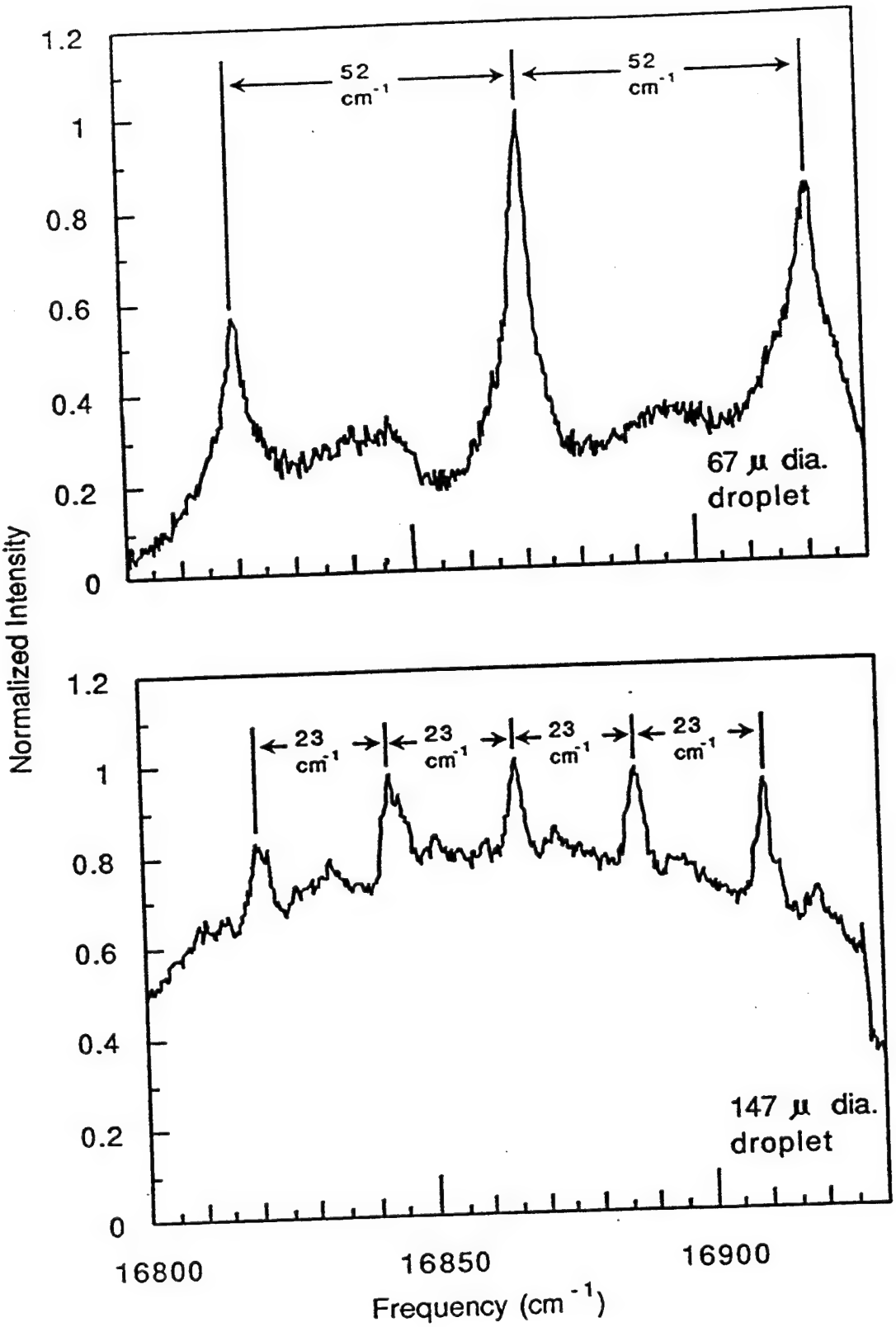

Fig. 3. MDR's from droplets of two different diameters. Note the large fluorescence background in the droplet of larger diameter. Diameters were calculated using the modal spacing.

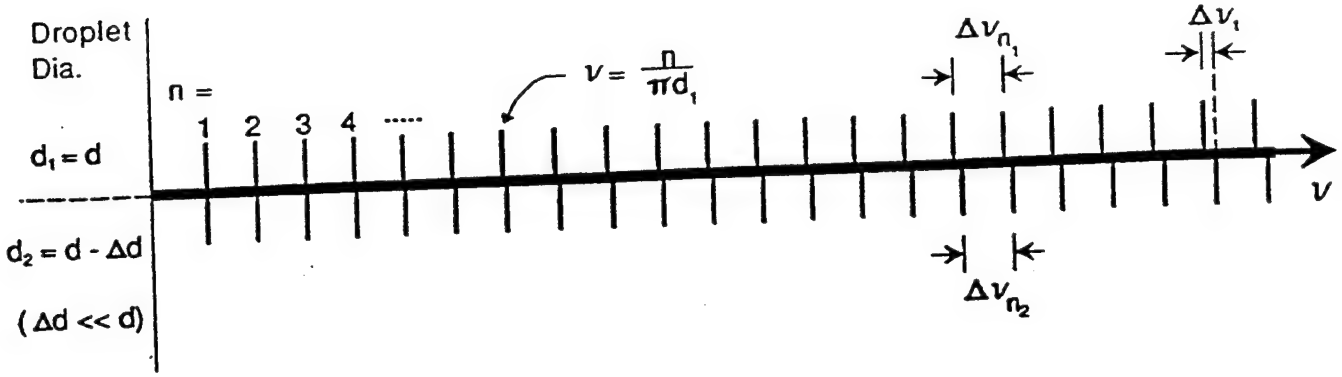

Droplet diameter change from

$$d_1 = \frac{\Delta n}{\pi \Delta \nu_{n_1}} \quad \& \quad d_2 = \frac{\Delta n}{\pi \Delta \nu_{n_2}} \longrightarrow \Delta d = d_2 - d_1 = \frac{\Delta n}{\pi}\left(\frac{1}{\Delta \nu_{n_2}} - \frac{1}{\Delta \nu_{n_1}}\right) \qquad (I)$$

Or

$$\Delta d = -\frac{\pi d^2}{n} \Delta \nu_t \qquad (II)$$

Subscripts

1	Initial MDR spectrum
2	Final MDR spectrum
t	Change in spectral location for a given mode number
n_i	Difference in spectral location for adjacent modes

d = droplet diameter
Δd = change in diameter
n = MDR mode number
Δn = mode no. difference
ν = frequency (cm^{-1})
$\Delta\nu$ = change in frequency

Fig. 4. A change in droplet diameter can be calculated from MDR's in two ways. Both use two MDR spectra with differing mode spacings resulting from the changing droplet size. The first method (I) uses the mode spacings to determine the droplet size at each time. The difference provides the change in diameter but this technique is not capable of measuring small changes which must be determined for the Liquid Stabilities Mechanisms program. An alternative method (II) is to measure the shift in a known mode between the two spectra. With this technique, diameter changes of a few nm can be measured, providing the necessary sensitivity.

EFFECT OF SHOCK ON DROPLET

Pressure Rise: 1.7 **Droplet Diameter: 90μ**

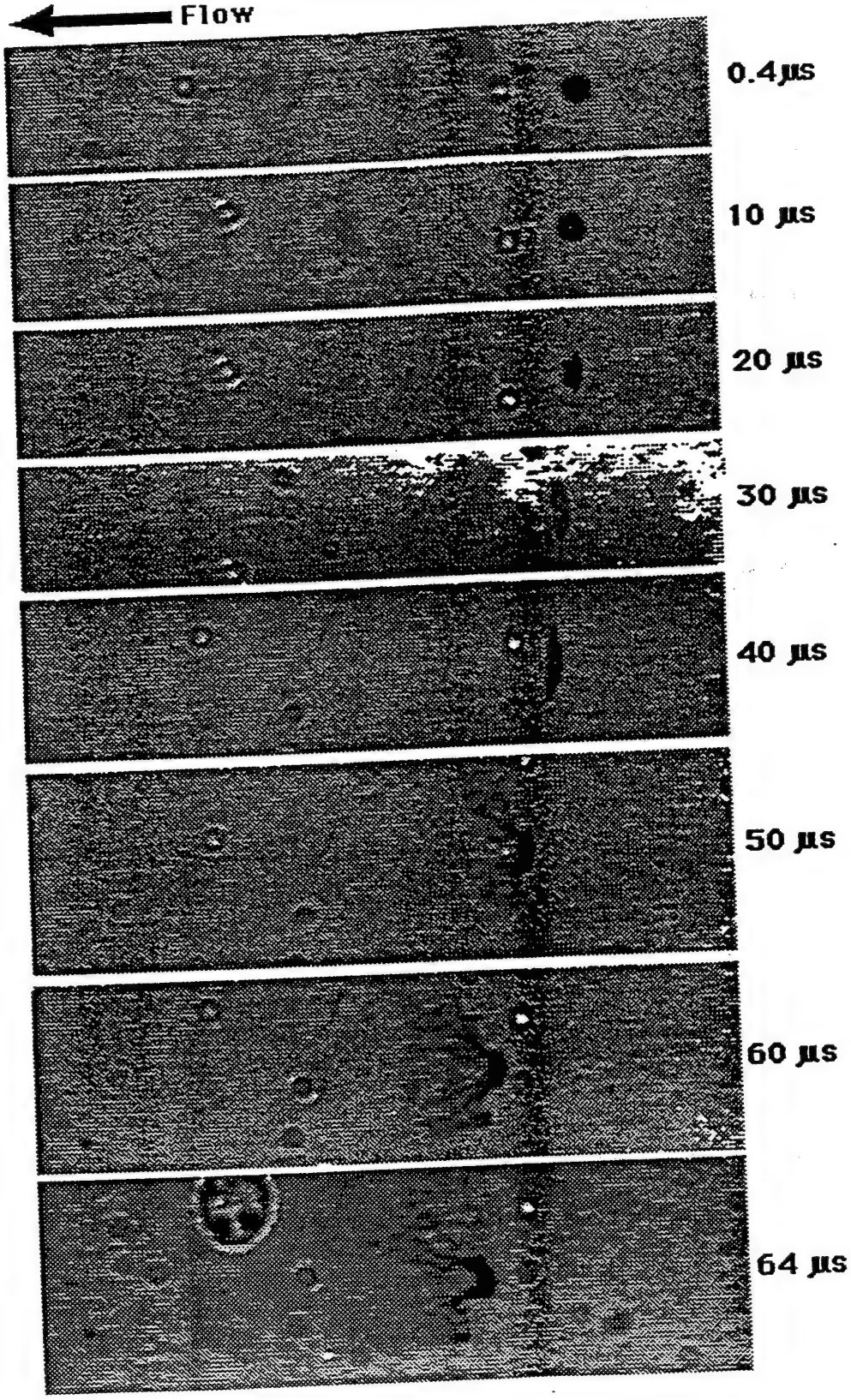

Fig. 5

EFFECT OF SHOCK ON DROPLET

Pressure Rise: 1.2 **Droplet Diameter: 90μ**

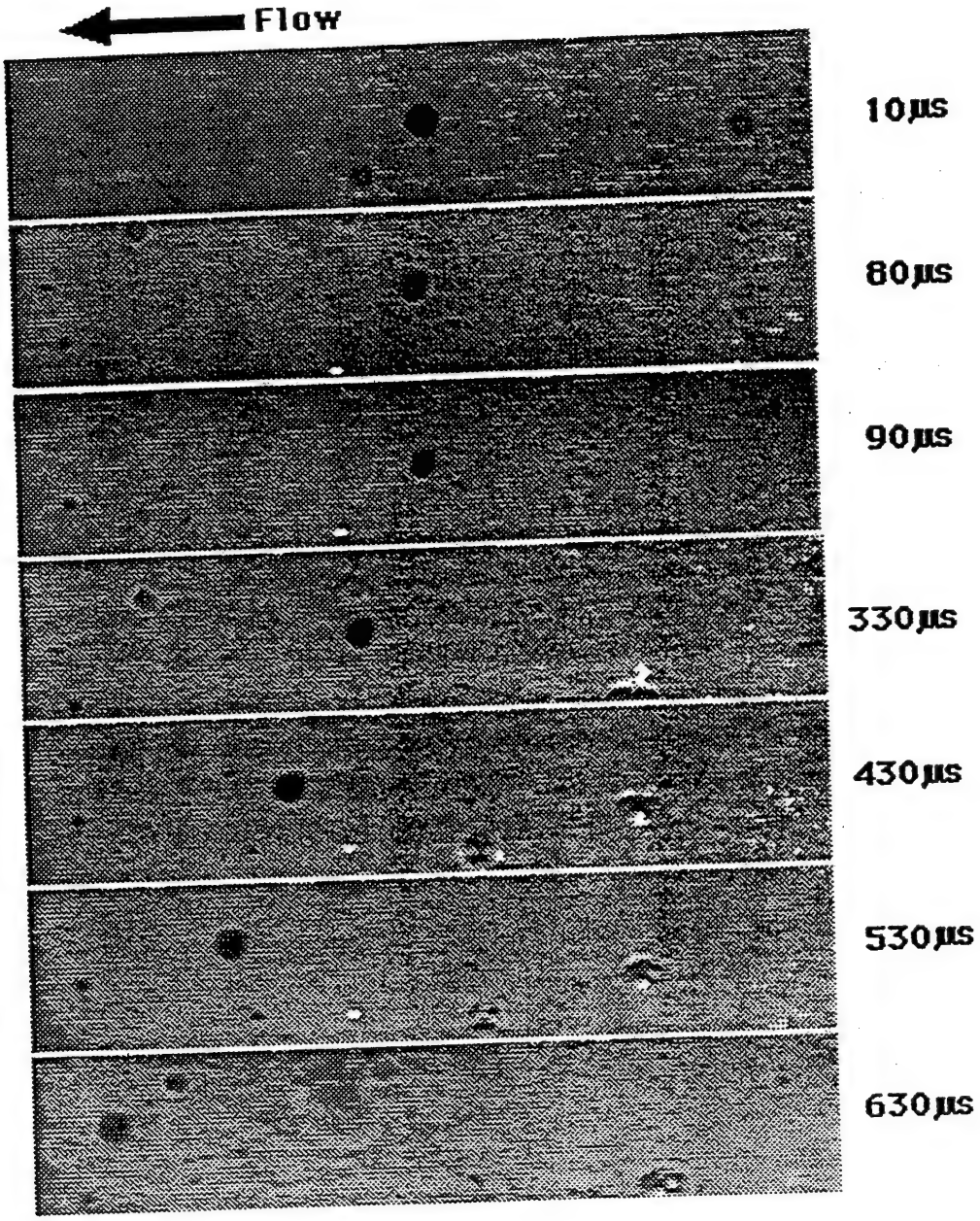

Fig. 6

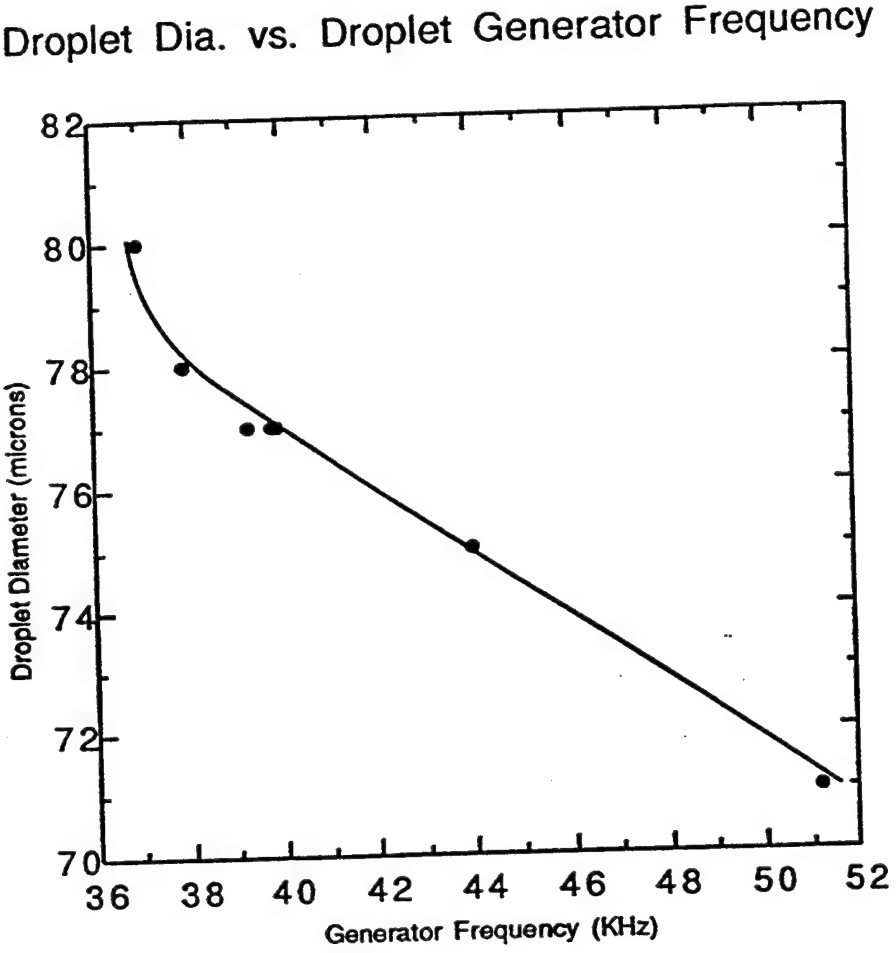

Fig. 7. Droplet diameters as measured with MDR's vs. droplet generator frequency. Diameter variations of this size cannot be measured with our camera system.

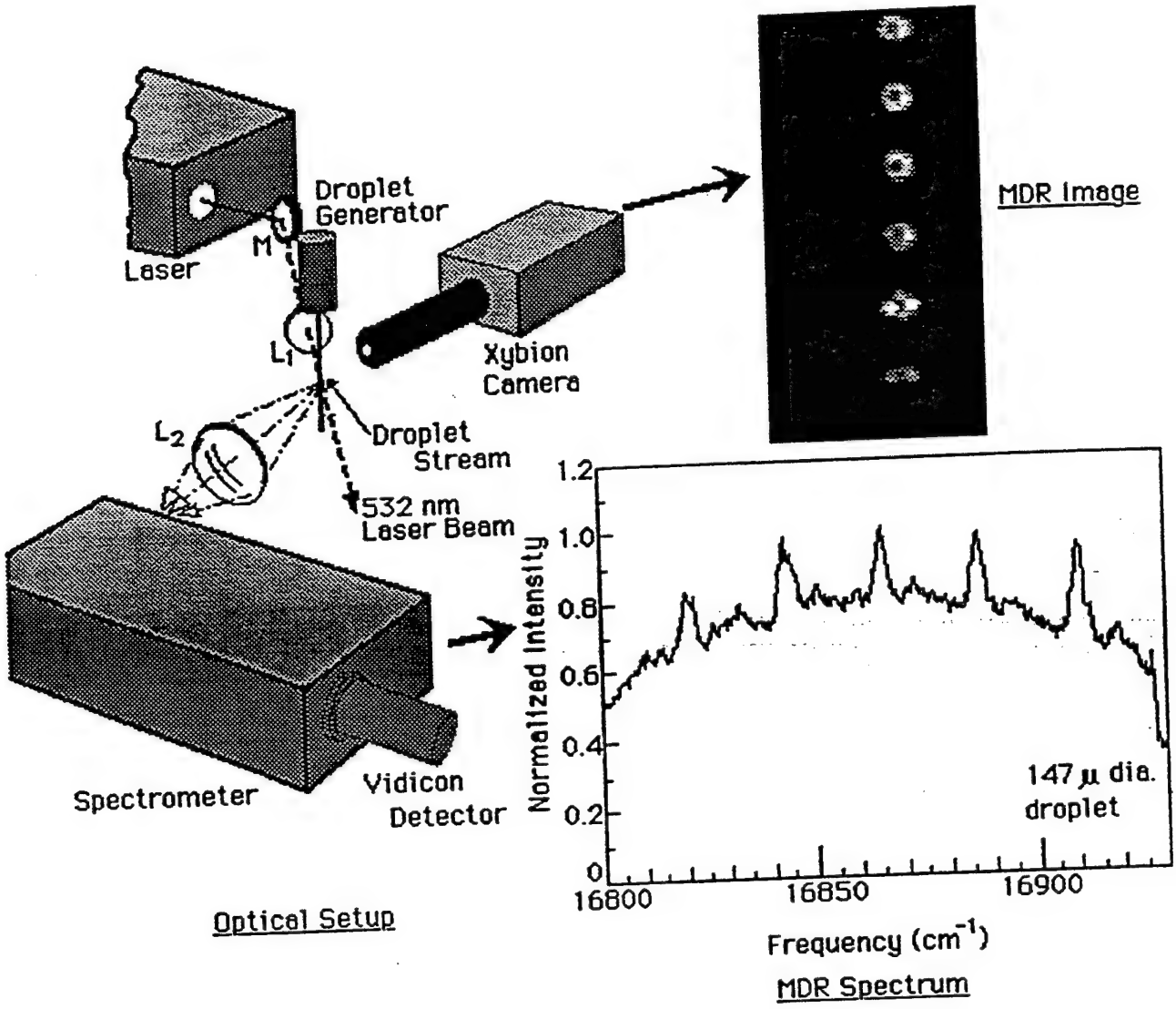

Fig. 8. Setup for generating and observing MDR's in a droplet stream.

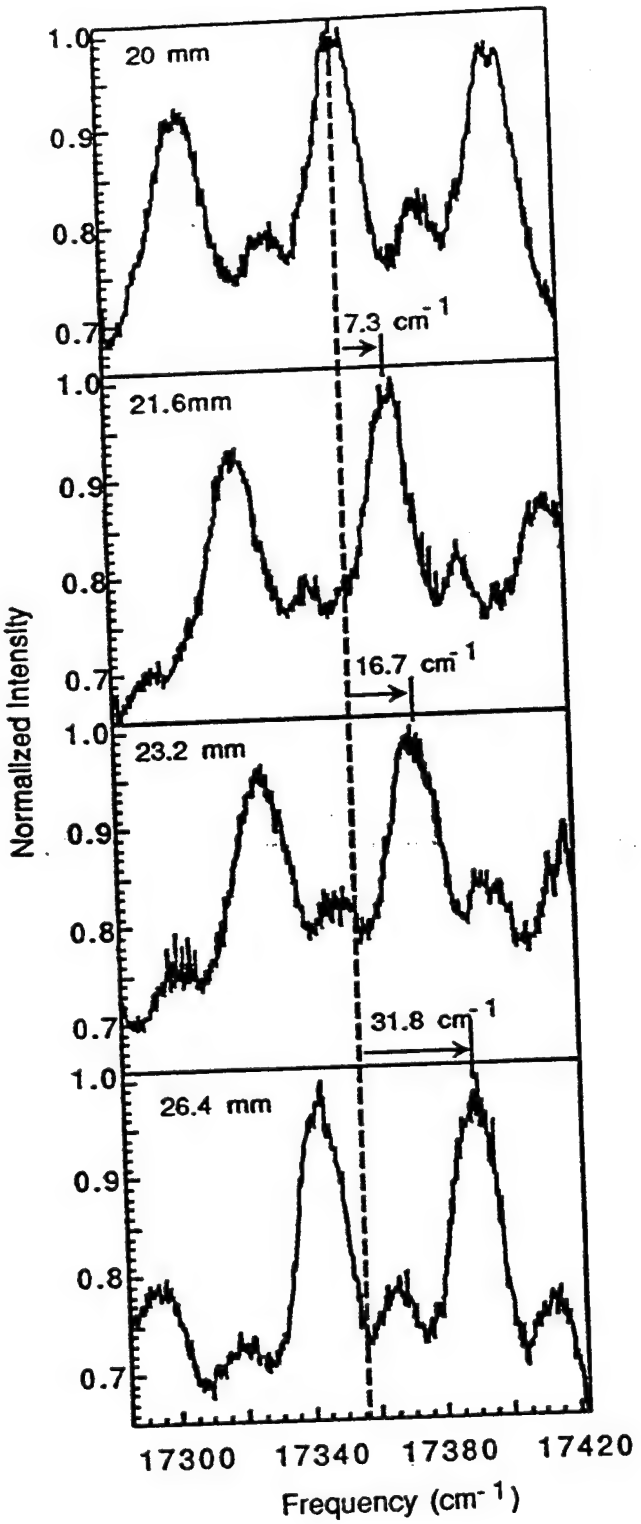

Fig. 9. MDR spectra acquired at varying distances from the bottom of the droplet generator. Each spectrum is an average of 10 shots at each height location. As the droplets get further from the generator, evaporation decreases the diameter, blue-shifting the MDR peaks (to the right). MDR mode spacing (separation between adjacent peaks) also increases, but this method of measuring change in diameter is not sensitive enough to detect the small changes which are occurring due to evaporation.

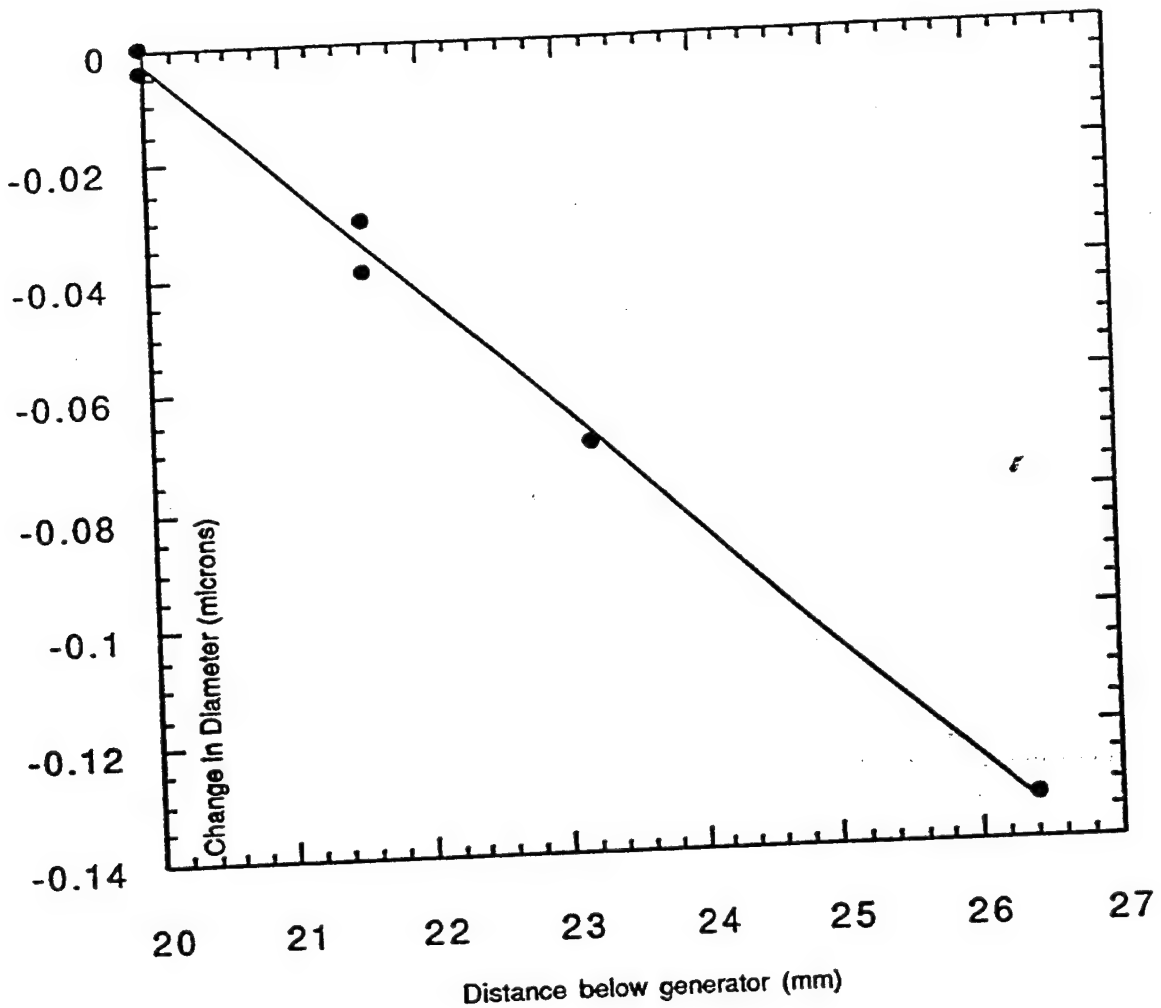

Fig. 10. Change in droplet diameter due to evaporation along the height of a droplet stream below the generator. Initial diameter is approximately 70 μ.

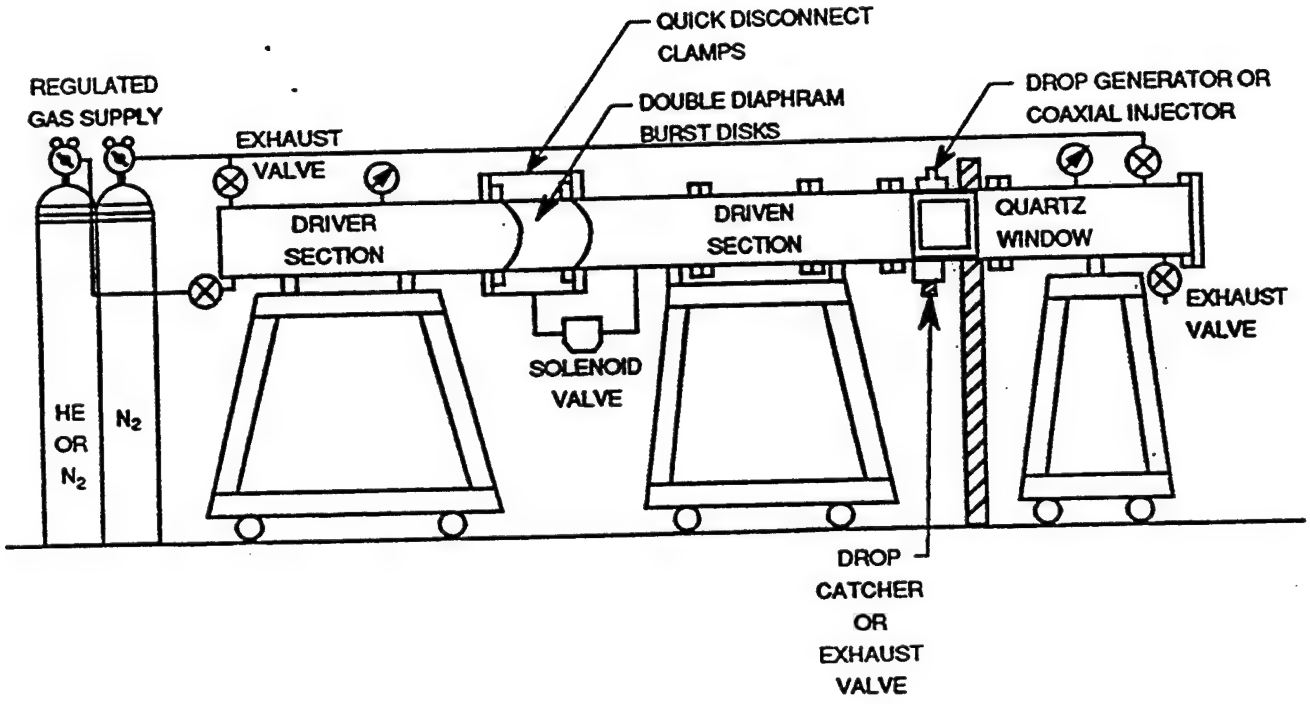

Fig. 11. Pulse tube for liquid stability tests.

APPENDIX D

"Measurements of the Effects of Acoustic Disturbances on Droplet Vaporization Rates"**

** Republished with AIAA permission (Bonnie Midnica).

AIAA-92-0108

Measurements of the Effect of Acoustic Disturbances on Droplet Vaporization Rates

Torger J. Anderson and Michael Winter

United Technologies Research Center
East Hartford, CT 06108

30th Aerospace Sciences
Meeting & Exhibit
January 6-9, 1992 / Reno, NV

MEASUREMENTS OF THE EFFECT OF ACOUSTIC DISTURBANCES ON DROPLET VAPORIZATION RATES

Torger J. Anderson and Michael Winter**
United Technologies Research Center
East Hartford, Connecticut 06108

Abstract

Advanced laser diagnostic measurements are being applied to quantify droplet vaporization enhancement in the presence of acoustic fields which can lead to instability in liquid-fueled rockets. Fluctuating droplet vaporization rates and subsequent reaction rate fluctuations resulting from acoustic disturbances within the combustion chamber may potentially be the cause of these instabilities. Models have been developed to describe the interactions between droplet vaporization and acoustic fields in the surrounding gases, but have not been verified experimentally. One of the challenges in experimental verification is to identify techniques with sufficient resolution to measure small changes in droplet diameter which result in significant vapor generation. Extremely accurate vaporization rate measurements are being performed by using individual droplets as miniature lasers, producing morphology-dependant resonances, whose spectral mode-structure contains information about the laser cavity dimensions. These can be related to droplet size. The measurements are being applied to determine droplet vaporization rates in quiescent conditions and after the passage of a weak pressure pulse.

Introduction

Acoustic instabilities within the combustor have been a concern ever since development of liquid-fueled rocket engines began. Since the mechanisms leading to these instabilities are not well understood, engine performance is sacrificed in order to avoid conditions in which the instabilities occur. The cause is believed to be a reaction rate enhancement produced by and in phase with acoustic waves within the combustor. The enhancement may result from atomization of the fuel and oxidizer droplets or increased evaporation[1] caused by the surrounding gas flow which amplifies pressure waves leading to the instability.

Spherically-symmetric droplet models, have been developed[1-2] to describe the effect of acoustic perturbations on evaporation and show that vaporization enhancement could lead to liquid instabilities in rocket engines. Experimental verification of these models is required and is being accomplished in a pulse tube system using a laser-based diagnostic technique.

Experiment

Pulse Tube System

An experiment was designed to observe the effect of pressure fluctuations and the resulting velocity field on evaporation rates in small droplets. A system which subjects the droplet to a single pressure pulse was chosen as opposed to an oscillating pressure field due to time scale considerations. While droplet lifetimes in a rocket combustor environment are on the order of several milliseconds, instabilities in liquid-fueled rocket engines occur with frequencies on the order of hundreds of Hertz. Thus, a typical droplet sees only one pressure cycle and the effect of Subjecting droplets to an instantaneous pressure rise followed by a steady pressure and velocity field allow the physics of the

---

* Research Scientist, Member AIAA.

evaporation enhancement process to be better understood and comparison to analytical models can be more readily made.

Measurements of the effects of acoustic waves on droplet evaporation rate were accomplished by passing a weak shock wave or pressure pulse over a stream of small droplets (approximately 70 μm) and measuring the rate of change of droplet diameter. A simple pulse tube system was made using a 2.2 m section of 25 mm diameter copper tube as the driven section. Flanges were used to attach a 1.4 m driver section of similar material and the two sections are separated by an aluminum foil diaphram, typically 30 μm thick, at the flange joint. The driver section is pressurized with compressed air until the diaphram breaks, sending a pressure pulse through the driven section. The pressure ratio across this pulse is 1.2 and is repeatable to within about 5%. The air velocity established behind the wave front is approximately 46 m/s. A weaker wave with a pressure ratio of 1.1 can be produced by chemically etching a line in the foil diaphram but this was not used for the tests which will be described.

Measurements are made in a test section located 1.1 meter from the diaphram in the driven section. Here, the steady state test time after wave passage is approximately 5 ms. Flat windows are glued into both sides of the tube to provide optical access and pressure transducers are located on the up and downstream sides to provide a means of measuring pressure rise, wave velocity and timing with respect to a diagnostic laser pulse. 2 mm diameter holes were drilled into the top and bottom of the test section and a droplet generator was positioned to direct a stream of precisely-controlled monodispersed droplets vertically through the holes. This device, produced by Fluid Jet Assoc., directs a stream of fluid under pressure from a reservoir through a 16 μm orifice. A piezoelectric transducer in the reservoir is oscillated at a specific frequency to drive the Rayleigh instability in the fluid stream, causing it to break up into droplets of quite uniform diameter. These droplets are in the region of 70 μm; size dependent on the exact pressure and frequency, but maintained within a range of a few nm.

Diagnostic Technique

In order to achieve the required measurement accuracy, evaporation was measured using morphology-dependent resonances[3] (MDR's). A microscope and video system can provide only rough measurements and typically are able to resolve droplet diameters to within only approximately 10 μm. With the MDR technique, a dye dissolved in the droplet fluid is pumped to an upper electronic state by an external light source. Small droplets (on the order of or less than 100 μm in diameter) of a solvent and dissolved laser dye are illuminated with a high power pulsed laser. Stimulated emissions from dye molecules just inside the circumference of the droplet are constrained to the inner surface by total internal reflection, effectively producing a spherical ring dye laser. Within the spectral envelope of the dye, frequency modes for which the circumference is an integral number of wavelengths are resonantly enhanced. The spectral location of these modes can be expressed by the frequency,

$$\nu = x / (\pi d) \qquad (1).$$

Observed light scattered from the droplet is shifted slightly due to the refractive index change and the result is that x is not an integral quantity. Δx between adjacent modes is no longer 1, but is expressed by[4]

$$\Delta x = \tan^{-1}(m^2-1)^{0.5} / (m^2-1)^{0.5} \qquad (2)$$

where m is the ratio of the droplet refractive index to that of air. The mode spacing is illustrated in Fig. 1 where the MDR modes are

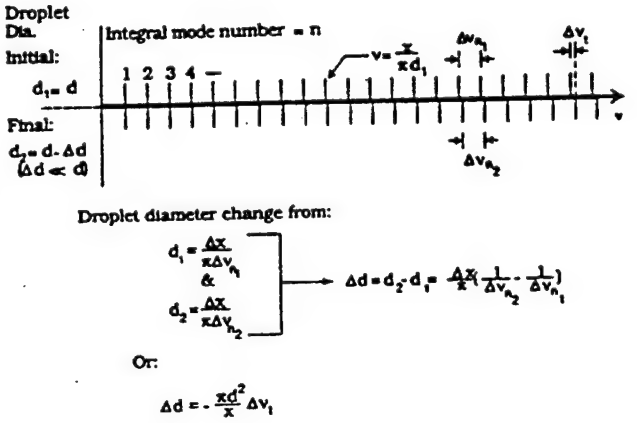

Fig. 1. Illustration of methods for measuring droplet diameter change from MDR mode spacing changes.

represented as vertical lines equally separated in frequency. The upper set of lines represents the modes in an original droplet and the lower lines represent the modes with increased spacing after a slight decrease in diameter. The droplet diameter can be calculated from the measured frequency spacing between modes.

$$\Delta\nu_n = \Delta x / (\pi d) \qquad (3),$$

A change in droplet diameter can be determined by simply using MDR's to measure the droplet diameter twice over a given time period and subtracting one from the other to obtain the change in size. However, this technique may not be able to resolve small changes in droplet size. Our detector system limits the resolution with this technique to no better than 1 μm, based on pixel size and spectrometer dispersion. A more accurate method is to measure the change directly by observing the change in spectral location of a given mode between two spectra. From the spectral position of a mode in the first spectrum and eqn. 1, x can be determined. With this, the derivative of the eqn. 1 and an assumption that $\Delta d \ll d$, the change in diameter is

$$\Delta d = - \pi d^2 \Delta\nu_t / x \qquad (4)$$

where $\Delta\nu_t$ is the time-dependent change in spectral location of any given mode. The resolution using this technique is enhanced by over two orders of magnitude over measurements using mode spacing.

Optical System

In this experiment, Rhodamine 590 laser dye was dissolved in methanol droplets. Laser energy to pump the dye was provided by the second harmonic of a double-pulsed Nd:YAG laser (532 nm). Pulses were approximately 10 ns in length, providing virtually instantaneous measurements with respect to the droplet and gas flows. The laser beam was focused to illuminate individual droplets at the center of the pulse tube as shown in Fig. 2. Timing of the laser pulse with respect to pressure wave passage of the droplet stream was established using a preset time delay after wave passage of an upstream pressure transducer. The MDR's were acquired using a 0.9 m spectrometer with a large dispersion and recorded using a 2-D Vidicon detector. The detector channel spacing represented 0.275

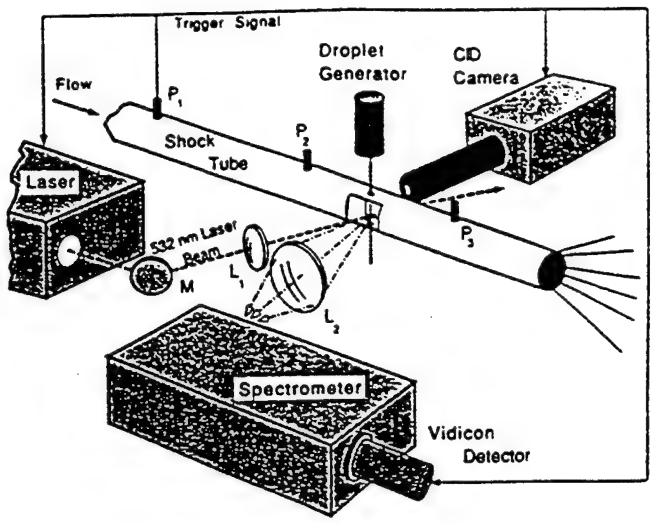

Fig. 2. Optical configuration for generating MDR's in a droplet stream behind a shock wave. The laser is timed to pump fluorescent dye in the droplets at a preset time delay after shock wave passage. Light from the droplets is imaged in the Xybion CID camera and on the slit of a spectrometer.

cm^{-1}/channel and was centered at 593 nm. An intensified CID camera with a microscope lens simultaneously recorded droplet fluorescence to confirm the droplets were in the proper location and not distorted. Based on spectrometer dispersion, it is possible to resolve diameters to approximately 1 μm using MDR spacing and diameter changes to within approximately 3 nm using the mode shift. Actual diameter measurement resolution is reduced because of spectrometer resolution, spectral noise in the dye profile and detector noise.

Evaporation measurements were obtained by determining the diameter difference between MDR's from the droplet stream acquired just before a run in quiescent gas and the MDR measurement at a specific time after shock wave passage. The shift in MDR location provided the diameter change and, combined with the diameter measured from the MDR mode spacing, the volume of evaporated liquid was determined.

Results

Initial evaporation measurements were made in a droplet stream in unperturbed air. This was accomplished by moving the droplet

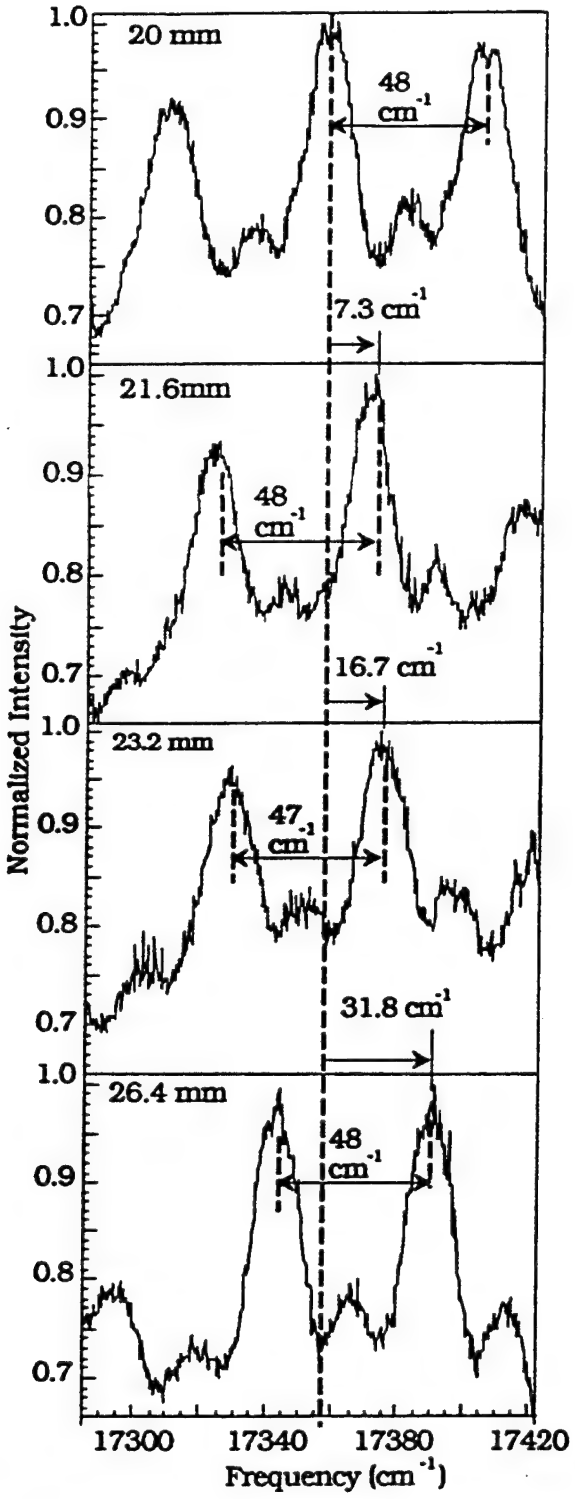

Fig. 3. Ten shot averaged MDR spectra acquired at four locations in a droplet stream. Mode spacing indicates a diameter of 68 μm and the change with position is unresolvable. However, mode shift due to evaporation downstream shows a 125 nm diameter reduction over the 6.4 mm.

generator vertically upward, effectively viewing droplets further along the stream. As the generator was moved, the MDR shift due to the slight evaporation was quite evident. MDR's were acquired in 10 shot averages at each of four heights in the droplet stream. Several of the averages were taken at each location to determine the repeatability of the measurements. A sample set of MDR's is shown in Fig. 3 and the measured droplet diameter change resulting from the shift is plotted in Fig. 4. Based on the measured droplet velocity of 7 m/s, the evaporation rate for these 70 μm droplets was 2.36×10^{-6} cm³/s.

Measurements of change in droplet diameter behind a pressure pulse proved more difficult and several considerations had to be made. Distortion of the droplets occurred only about 8 μs after shock wave passage and the droplets did not recover their spherical shape until approximately 400 μs. While this limited the time period in which measurements could be made, the MDR's clearly identified that shape distortion was occurring and that diameter measurements were inaccurate. When the droplets were distorted, the MDR signal was significantly reduced and multiple irregular modes were observed.

Measurements thus far have concentrated on the initial 8 μs period and they can also be made after the 400 μs delay. However, after long time delays, alignment of the system must include considerations for the droplet trajectory downstream and small fluctuations in pulse strength could complicate the measurements. Measurements of droplet size should be possible during the 8-400 μs period, as well, by observing the MDR structure to determine when oscillating droplets are passing through a near-spherical shape. Analysis of the MDR's at this condition will yield an accurate droplet diameter.

A large number of MDR measurements have been acquired over the initial 8 μs period in order to follow the mode shift. This is necessary to account for shifts greater than the mode spacing and avoid attributing an observed peak to the wrong mode number, i.e., an incorrect amount of shift. The plot which resulted is shown in Fig. 5, indicating the change in diameter with time. The variation in the data is believed to be due, primarily, to the fluctuation in wave strength from run to run.

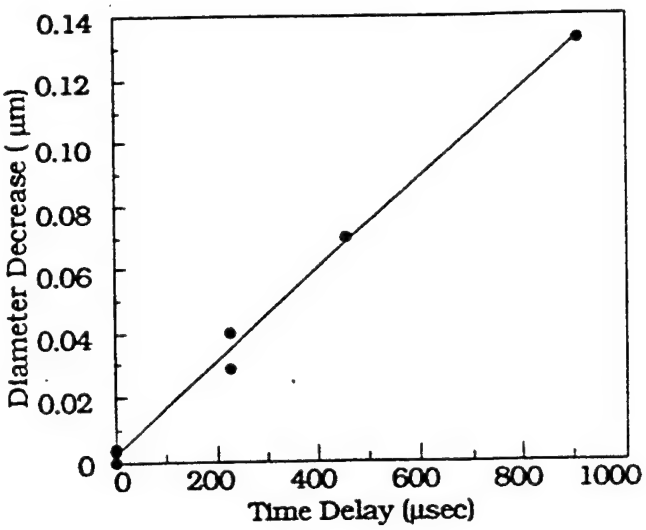

Fig. 4. Decrease in diameter verses distance along a droplet stream. Combined with a measured velocity of 7 m/s and an initial diameter of 73 μm, this indicates an evaporation rate of 2.36×10^{-6} cm³/s.

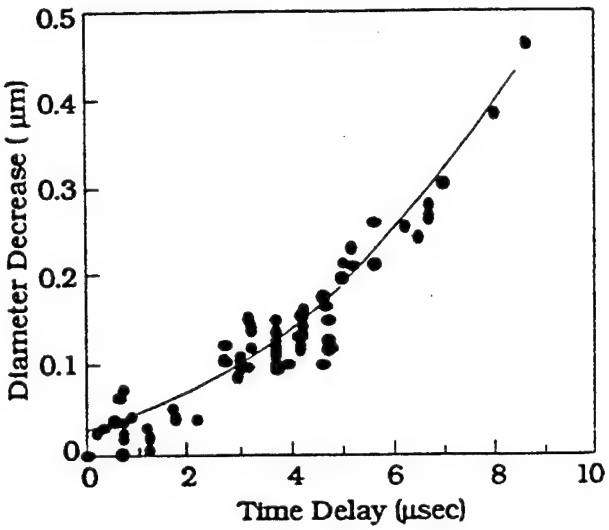

Fig. 5. Droplet size change as a function of time delay after pressure pulse passage with a pressure ratio of 1.2. The line is a quadratic curve fit. Corresponding volumetric evaporation rate at 8 μs is 1.37×10^{-3} cm³/s.

The increasing slope of the curve with time is an indication of a phase lag in evaporation enhancement due to the acceleration of the flow as the pulse passes and to the removal of a methanol vapor-laden region surrounding the droplet stream and inhibiting evaporation in the quiescent gas. The evaporation rate reaches a nearly steady state value 6-8 μs after wave passage, indicating the end of the delay period. This time is significant since the phase lag for enhanced evaporation with respect to the pressure pulse is an important parameter, controlling the combustion instability which occurs in rocket combustors. The volumetric evaporation rate in the 6-8 μs time span, based on the slope of the curve and the droplet diameter, is 1.37×10^{-3} cm³/s. This represents an increase in evaporation rate over that in the stream of quiescent gas by a factor of 584. While this value seems high (the droplet would be entirely evaporated by 130 μs), it will decrease significantly as the droplet accelerates downstream and the relative flow velocity is reduced.

Conclusions/ Future Work

The capability for measuring droplet diameter changes through spectral shift has been demonstrated and successfully used to determine the evaporation rate of droplets behind a weak pressure pulse. It is extremely sensitive to changes in diameter, allowing accurate measurements to be made in extremely short time spans. Further evaporation measurements will be made over larger time periods to confirm this value and determine if the vaporization rate remains constant.

While this information is valuable in validating models of the phenomenon, evaporation rates of droplets in an environment more comparable to that in a rocket combustor is the desired goal of this program. To accomplish this, a high pressure pulse tube has been constructed and will be used to make measurements at pressures up to approximately 68 atm at room temperatures. Ultimately, droplets in super critical conditions will be studied and appropriate fluids and diagnostics will have to be chosen for those measurements.

While a vaporization enhancement by a factor of 584, caused by the pressure pulse, has been shown and a phase lag relationship is apparent, combustor response in a reacting system may influence the overall role of vaporization in liquid instabilities.

Nomenclature

d = droplet diameter
Δd = change in diameter
m = refractive index ratio (droplet liquid to air)
n = MDR integral mode number
x = MDR mode number
Δx = mode number difference between adjacent modes
ν = spectral frequency (cm^{-1})
$\Delta\nu_n$ = frequency difference between adjacent modes
$\Delta\nu_t$ = change in frequency with time

Acknowledgements

We would like to thank Mr. Richard J. Daddona for his expert technical assistance in making the measurements described. This program is funded by the Air Force Phillips Laboratory under contract number F04611-89C-088 through Pratt & Whitney, GESP.

References

1. A. Y. Tong and W. A. Sirignano: AIAA J. Propulsion 5, 257 (1989).

2. A. Y. Tong and W. A. Sirignano: Num. Ht. Trans. 10, 253 (1986).

3. Tzeng, H.-M., K. F. Wall, M. B. Long and R. K. Chang: Opt. Ltrs. 9, 273 (1984).

4. Quian, S.-X., J. B. Snow, H.-M. Tzeng and R. K. Chang: Science 231, 486 (1986).

APPENDIX E

"Measurement of Droplet Vaporization Rate Enhancement Caused by Acoustic Disturbances"

MEASUREMENT OF DROPLET VAPORIZATION RATE ENHANCEMENT CAUSED BY ACOUSTIC DISTURBANCES

T. J. Anderson and M. Winter
United Technologies Research Center
East Hartford, Connecticut 06108

Abstract

Advanced laser diagnostics are being applied to quantify droplet vaporization enhancement in the presence of acoustic fields which can lead to instability in liquid-fueled rockets. While models have been developed to describe the interactions between subcritical droplet vaporization and acoustic fields in the surrounding gases, they have not been verified experimentally. In the supercritical environment of a rocket engine combustor, little is understood about how the injected fluid is distributed. Experiments in these areas have been limited because of the lack of diagnostic techniques capable of providing quantitative results.

Recently, however, extremely accurate vaporization rate measurements have been performed on droplets in a subcritical environment using morphology-dependent resonances (MDR's) in which fluorescence from an individual droplet provides information about its diameter. Initial measurements on methanol droplets behind a pressure pulse with a pressure ratio of 1.2 indicated that the evaporation rate in the first few μsec after wave passage was extremely high. Subsequent measurements have been made to validate these results using MDR's acquired from similarly-sized droplets using a pulses with a 1.1 pressure ratio. A baseline measurement was also made using a non-evaporative fluid under similar Weber and Reynolds number conditions.

The MDR technique employed for these measurements is explained and the facilities are described. The evaporation measurement results are shown and the rates observed from different droplet materials and different wave strengths are compared.

Introduction

Acoustic instabilities within the combustor have been a concern ever since the development of liquid-fueled rocket engines. The mechanisms leading to these instabilities are not well understood but are important since engine performance is sacrificed in order to avoid conditions in which the instabilities occur. The cause is believed to be a reaction rate enhancement produced by and in phase with acoustic waves within the combustor. The enhancement may result from atomization of the fuel and oxidizer droplets or increased evaporation[1] from the surrounding gas flow. This amplifies pressure waves leading to the instability.

Theoretical models have been generated to describe the evaporation processes for spherically-symmetric droplets in a flow field.[1-2] Even for these simple processes, however, experimental validation has been limited because of the inability to make well-resolved measurements on such small length and short time scales using existing diagnostic techniques. Recent experiments have demonstrated the use of a laser-based technique called morphology-dependent resonances (MDR's) to

accurately and instantly measure droplet sizes. Results were acquired in a phased time sequence to determine evaporation rate in a repeatable flow field.[3]

Measurements have now been made at additional conditions in order to validate the original MDR measurement results. This was done to alleviate concerns that the original results reflected effects other than evaporation; for example, droplet distortion. The results include measurements in a weaker flow field and measurements using a relatively non-evaporative fluid. They tend to support the initial measurement results.

Experiment

The experiment was designed to make measurements of droplet evaporation behind a weak shock wave, where a nearly uniform velocity field was instantaneously introduced and the resulting affect on evaporation of droplets in a stream could be measured. MDR's, or morphology-dependent resonances, provides a means of making very accurate droplet diameter measurements and, as a result, can be used for measuring evaporation rate. The technique, described in more detail in ref. 4 and 5, can be implemented using a high-power short-pulsed Nd:YAG laser, frequency-doubled to 532

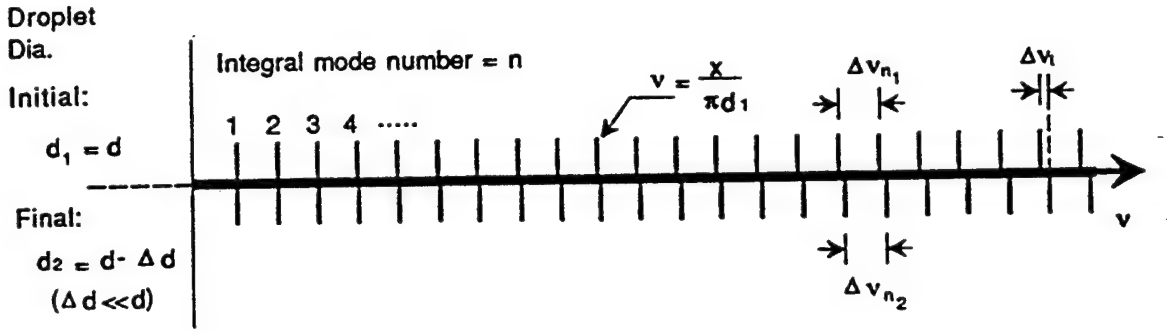

Droplet diameter change from:

$$d_1 = \frac{\Delta x}{\pi \Delta \nu_{n_1}} \quad \& \quad d_2 = \frac{\Delta x}{\pi \Delta \nu_{n_2}} \longrightarrow \Delta d = d_2 - d_1 = \frac{\Delta x}{\pi}\left(\frac{1}{\Delta \nu_{n_2}} - \frac{1}{\Delta \nu_{n_1}}\right) \quad \text{(a)}$$

Or:

$$\Delta d = -\frac{\pi d^2}{x}\Delta \nu_t \quad \text{(b)}$$

Fig. 1. Diagram of MDR frequency modes before and after a droplet diameter change. The vertical lines above the frequency (ν) axis represent the locations of MDR peaks for a droplet of initial diameter, d_1. The vertical lines below the axis show the mode spacing increase and resulting mode shift caused by a slight decrease in droplet diameter. Droplet diameter can be determined from mode spacing ($\Delta\nu_n$) before and after evaporation and diameter change can be determined using eqn. (a). A more accurate measurement of change in droplet diameter can be made by observing the shift of a high order mode ($\Delta\nu_t$) and using eqn. (b).

nm, to generate fluorescence from a laser dye dissolved in the droplet medium. Fluorescence emitted near the droplet surface and at low incidence angles is constrained to the inside of the droplet circumference by total internal reflection and is amplified through stimulated emission. Peaks in the resulting spectral mode structure identify wavelengths which are integer fractions of the droplet circumference.

It is possible to determine the droplet diameter from the peak spacing in the dispersed MDR spectrum, as shown in Fig. 1. This figure shows the MDR mode spectral locations in frequency space (ν) for a droplet of initial size, d_1, and for a droplet of slightly smaller diameter, d_2. The evaporation rate can then be determined from the change in mode spacing ($\Delta\nu_n$) occurring from the decrease in droplet diameter. However, this method is limited by the resolution of the spectrometer system and small diameter changes cannot be detected. An alternative and more sensitive method is to measure the shift occurring in the higher order modes ($\Delta\nu_t$) as a result of a diameter change. This can be used to measure the evaporation which occurs on short time scales, in phase with instability mechanisms.

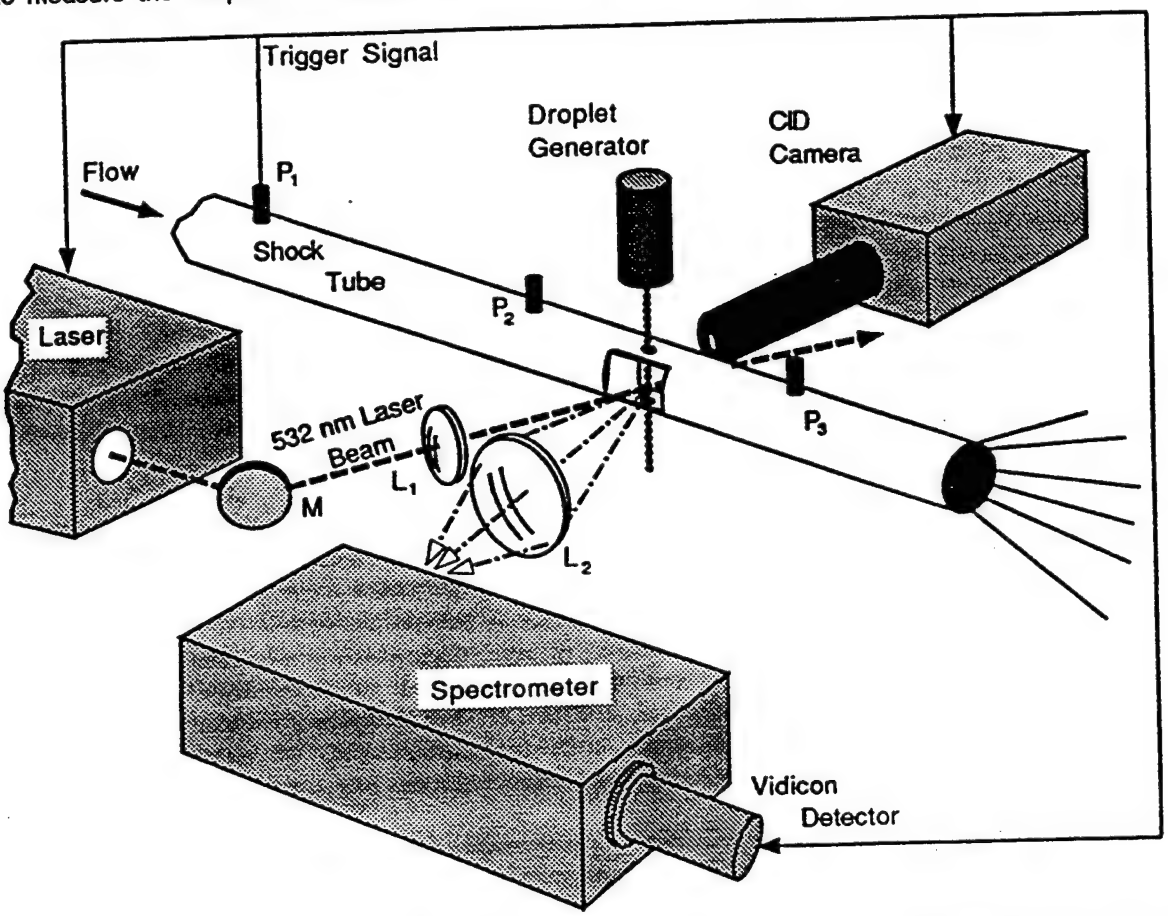

Fig. 2. Experimental setup. The droplet stream is projected through holes in a shock tube and illuminated with the laser, timed with the passage of a shock wave. The MDR emissions are acquired with an intensified camera and dispersed in a spectrometer.

The facility for these experiments is set up as shown in Fig. 2. It was centered around a Fluid Jet Assoc. piezo-electric droplet generator which produced a vertically descending stream of monodisperse droplets, approximately 60-70 μm in diameter and separated by about 2 droplet diameters. Most liquids can be used as the droplet medium but requirements for dye solubility led to the use of methanol or water. Rhodamine 590 dye was used in the methanol because of its high efficiency when pumped by a frequency-doubled Nd:YAG laser. With water droplets, Rhodamine 610 was used because of the low solubility of 590 dye in that medium. The Nd:YAG laser pulses were 10

nsec in duration providing measurements that were virtually instantaneous with respect to any fluid processes being observed. The laser beam was focused to illuminate only one droplet in the stream, providing a measurement from that droplet alone.

Fluorescence from the droplets was imaged on the slit of a spectrometer with a 2-D Vidicon detector. The spectrometer had a dispersion of .275 cm^{-1}/channel and was tuned to the fluorescence envelope of the dye in use. Using an estimated resolution of 2 cm^{-1}/channel based on observed spectra, and considering the spectral locations of the dyes employed, mode spacing measurements were capable of resolving droplet diameters to within approximately 3 μm. The mode shift technique was capable of resolving diameter changes down to 0.008 μm and up to 0.2 μm where the mode shift equals the mode spacing. Beyond this point, the order of the mode being observed becomes ambiguous. In order to make diameter change measurements, one must acquire MDR's at intervals sufficiently small that mode shifts are considerably less than the mode spacing. In this way one can track the mode number as the shift extends over the mode spacing. One should note that the resolution limits described above are based purely on the spectrometer resolution. In reality, this is degraded by the width of the MDR peaks and noise in the laser dye spectrum and in the detector system.

Results

Initial measurements were made on 60-70 μm droplets in the generator stream in quiescent room air. MDR's observed at one location in the droplet stream indicated that the droplets were quite repeatable, remaining constant to within approximately 0.01 μm. Evaporation of the descending droplets was observed by acquiring MDR's at various heights in the stream. Measurements of both methanol and water droplets showed mode shifts to shorter wavelengths lower in the stream as fewer modes could be accommodated in the droplets of decreasing circumference. Fig. 3 shows MDR's acquired for droplets of both fluids and demonstrates the relatively low volatility of water when compared to methanol.

Fig. 4 plots the rate of droplet diameter change determined from these MDR measurements. The measured evaporation rate for methanol is about 13 times that of water and this result seems reasonably close to the ratio of vapor pressures of 18 under room air conditions.[6] The constant rates observed for both fluids is a consequence of the small percentage change in diameter. It should be noted that the observed evaporation rates do not represent the rates for single droplets moving through dry air. Since the droplets are in a stream, the air flow around each droplet is reduced by the wake velocity. In addition, the stream was enclosed in a windowed section of a shock tube in order to reduce disturbances to the surrounding air mass. This increased the partial pressure of the surrounding evaporated vapor and, thus, reduced the evaporation rate that was measured.

Three series of measurements behind weak shock waves were run for the two droplet fluids and two flow conditions. The flow conditions are described in Table I and were determined from normal shock relations based on pressure ratios selected for these measurements. These include the conditions observed in the quiescent gas measurements described above. Evaporation was observed for methanol droplets under each of these conditions and for water droplets under all but the weaker wave condition. Methanol droplets in the strong wave flow were the first measurements to be conducted[3] and measurements in the weak wave flow and the water droplet measurements provided a means of validating these early measurements. The measurements acquired in the weaker shock condition provided a case in which the velocity is significantly lower than the strong wave conditions and reduced evaporation was expected. Measurements in water droplets were expected to provide a near-non-evaporative condition due to the significant difference in volatilities and provided a baseline measurement for comparison.

To provide a valid comparison for methanol measurements and the water baseline, it was necessary to generate conditions with nearly equivalent conditions of Weber number, Reynolds number

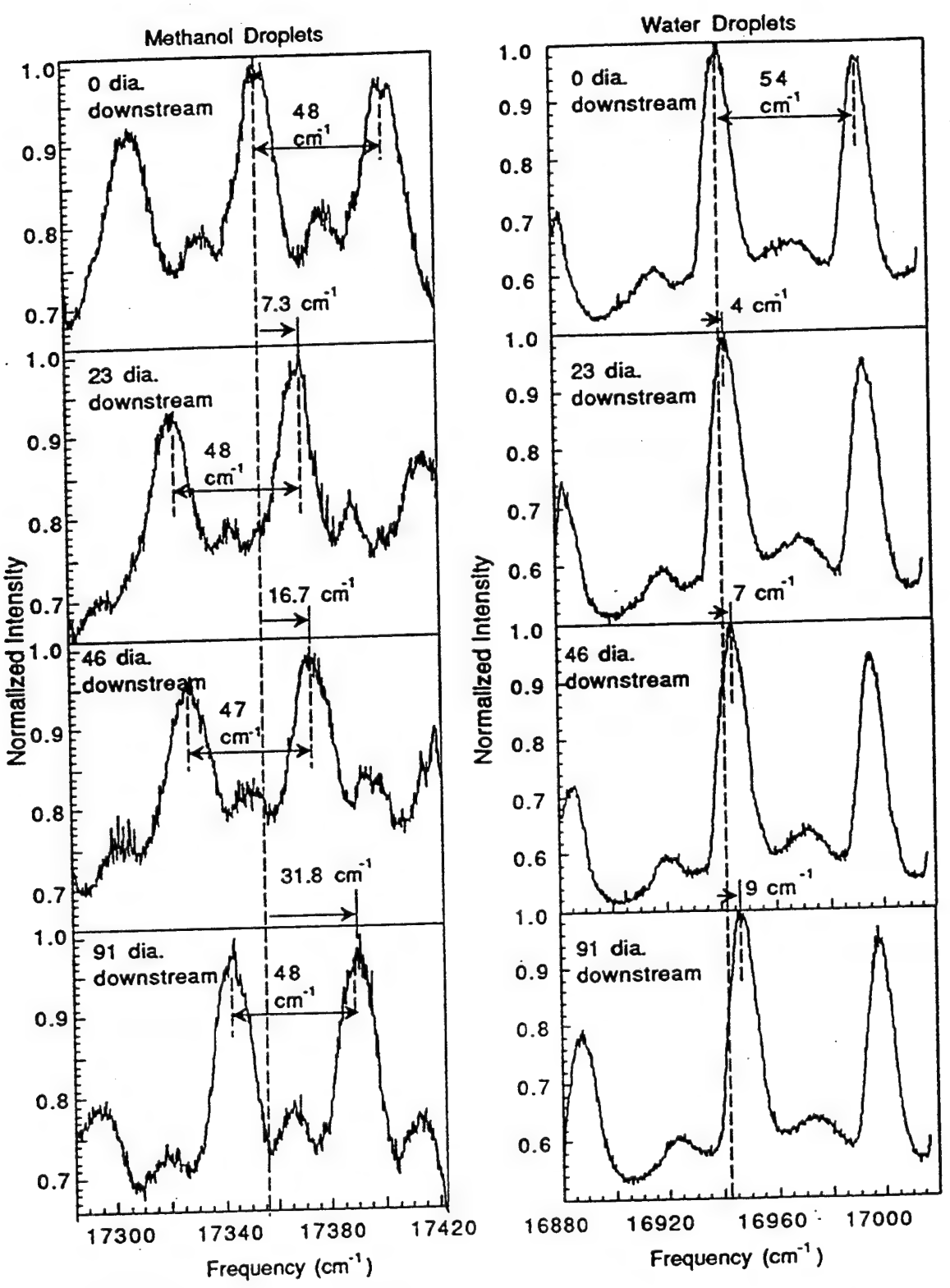

Fig. 3. MDR shifts in droplets in a stream. Height in the stream is shown in droplet diameters from an arbitrary location below the droplet generator. The shift indicates the change in diameter as the droplet evaporates. MDR's from methanol droplets are on the left and water droplets on the right.

and their ratio. It was found that the conditions for methanol in a 1.1 pressure ratio shock wave very nearly matched those for water droplets in the 1.2 pressure ratio case, with respect to these variables, as shown in Table II. While equating these variables establishes similar conditions of relative shear, surface tension and dynamic forces, it does not normalize for the effect that the different velocities has on the evaporation rate. One might expect the relative evaporation rates to be nearly the same for different droplets in the same velocity field, both in the quiescent case and behind a shock wave.

Condition	P_r	T_r	Shock Mach No.	Velocity m/s
Quiescent air	1.0	1.00	0	7.5 / 5.5
Weaker shock wave	1.1	1.03	1.04	24.6 / -
Stronger shock wave	1.2	1.05	1.08	46.6 / 46.3

Table I. Comparison of pressure pulse conditions at which evaporation measurements were made. Velocities include the vertical component (perpendicular to the shock wave) resulting from the droplet motion in the stream. "Quiescent" air refers to the condition of the bulk gas surrounding the droplet stream. The velocities shown are for methanol and water droplets, respectively.

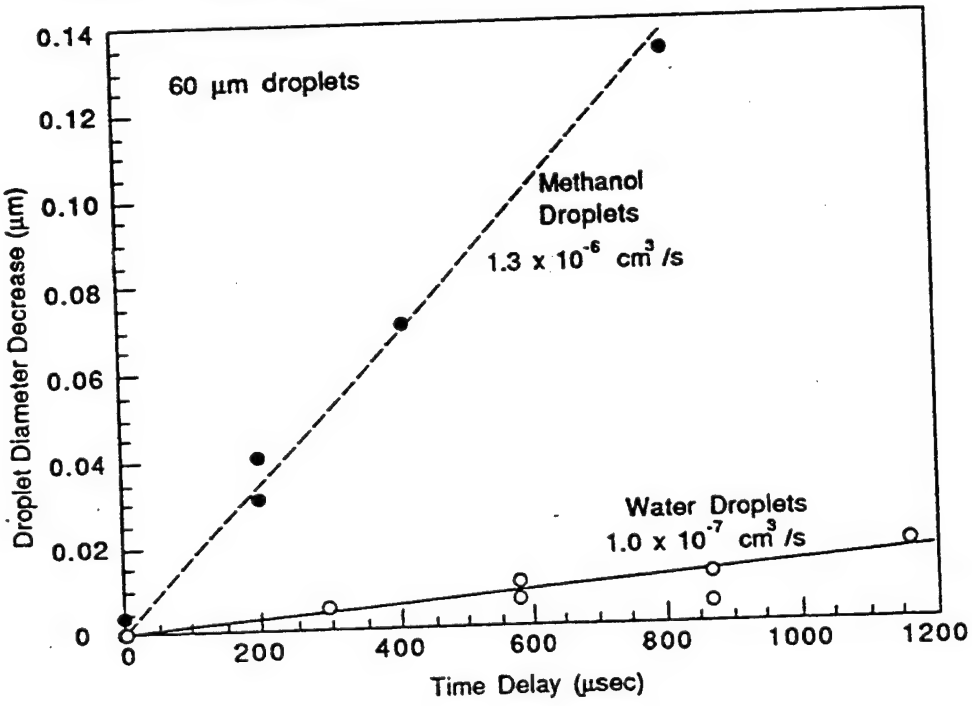

Fig. 4. Evaporation rates observed for droplets of methanol and water in a stream.

The measurements were made in a shock tube as shown in Fig. 2. The wave strength was controlled by the thickness and diameter of a diaphragm separating the 25 mm diameter shock tube from a driver section pressurized with air. Measurements were acquired from droplets traveling through a windowed test section in the shock tube by pulsing the Nd:YAG laser at a preset time delay after shock wave passage. Prior to the rupture of the diaphragm, an MDR spectrum was acquired to identify the location of the peaks for droplet diameter calculation before wave passage. This was

compared with the spectrum acquired after wave passage so that the shift in MDR peaks and, thus, the change in diameter due to evaporation could be determined.

P_r	Droplet Fluid	Droplet Dia. (μm)	We	Re	We/Re
1.1	Methanol	70	1.7	3.3	.51
1.2	Methanol	70	6.4	6.4	1.00
1.2	Water	70	2.4	3.8	.62

Table II. Weber and Reynolds number comparisons for the three test conditions using weak shock waves.

The results for the three different cases are plotted in Fig. 5 along with the evaporation rates observed from the droplet streams in quiescent gas. A second order curve fit is provided to describe the general trend for evaporation. In each of the methanol droplet cases, the rates are plotted over shifts greater than the mode spacing (approximately .12 μm diameter decrease). A number of characteristics are apparent from these plots. The measurement distribution is quite spread in all cases and this is believed to be the result of the inability to reproduce the shock waves at exactly the right wave strength, repeatably. Also, measurements could not be acquired beyond the short initial period after wave passage, extending to about 8 μsec. Video images of the droplets acquired simultaneously with the MDR's at these extended time delays indicated that, while the low Weber number conditions prevented droplet breakup, considerable distortion of the droplets began near 8 μsec. This distortion alters the optical cavity, reducing the homogeneity of the MDR spectra throughout the droplet. As a result, in spectra acquired under these conditions, the MDR peaks were quite weak, limiting the accuracy of the measurement. Contributing to the problems of measurements in this aspherical regime is the fact that the theory is not yet mature enough to describe the relationship between the MDR spectrum and droplet volume.

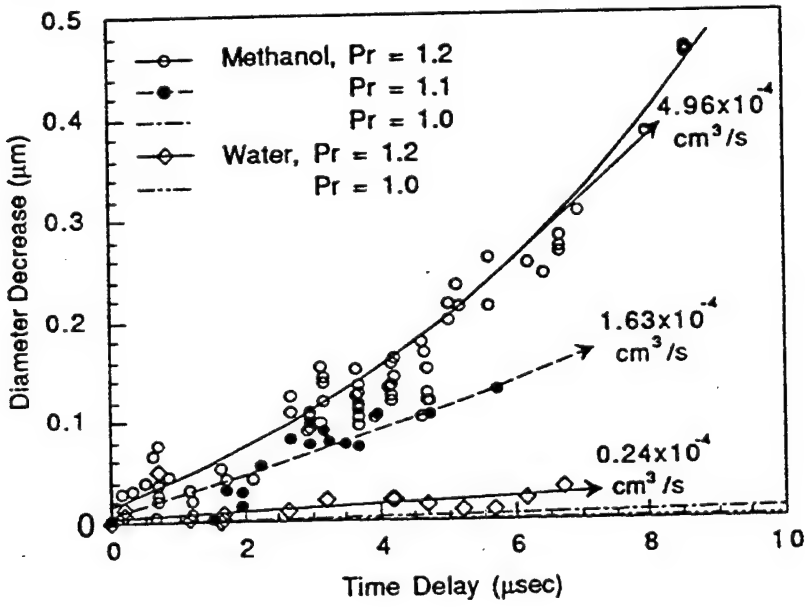

Fig. 5. Methanol and water droplet diameter changes measured shortly after shock wave passage using MDR's. Pr = 1.0 identifies measurements taken in the droplet stream in quiescent gas. Arrows indicate mean slope for each case in the region of 6 μsec after shock wave passage. Values for these slopes are given to the right.

Conclusions

Despite the short period during which measurements could be made, quantitative evaporation rates were acquired and compared by evaluating the curve fits at a single time delay of 6 μsec. The volumetric rates are shown in Fig. 5. For the 1.2 pressure ratio wave, evaporation was enhanced by a factor of 380 and 240 for methanol and water droplets, respectively. While methanol evaporation was 13 times that of water droplets in the quiescent condition, it is approximately 21 times higher behind the 1.2 pressure ratio wave. While the evaporation does not scale equally for the two fluids as conditions change, this is to be expected since heat transfer variables such as thermal conductivity, heat capacity and heat of vaporization have not been considered at this point. The results indicate, however, that the MDR technique is providing a measure of droplet evaporation behind the shock wave for these measurement conditions. The MDR's are providing a true measure of droplet diameter and the evaporation rates are being determined.

These measurements provide a description of the initial interaction between a droplet and an acoustic wave. The short-time behavior shows significant enhancement of vaporization rates. Beyond these initial times, the droplet begins to accelerate in the surrounding flow field and the velocity field driving the vaporization enhancement is relaxed. Therefore, the initial time frame is most important for vaporization enhancement. Furthermore, from a rocket stability standpoint, the phasing of vaporization enhancement is also important. These data can serve as a guide to modeling droplet / acoustic wave interactions and the associated coupling of vaporization as a mechanism in liquid-fueled rocket instabilities.

Nomenclature

d	=	droplet diameter
Δd	=	change in diameter
m	=	refractive index ratio (droplet liquid to air)
n	=	MDR integral mode number
x	=	MDR mode number
Δx	=	mode number difference between adjacent modes
n	=	spectral frequency (cm^{-1})
Δn_n	=	frequency difference between adjacent modes
Δn_t	=	change in frequency with time
P_r	=	pressure ratio across the shock
T_r	=	temperature ratio across the shock
Re	=	Reynolds number
We	=	Weber number

Acknowledgments

We would like to thank Mr. Richard J. Daddona for his expert technical assistance in making the measurements described. This program is funded by the Air Force Phillips Laboratory under contract number R91-254608 through Pratt & Whitney, GESP.

References

1. A. Y. Tong and W. A. Sirignano: AIAA J. Propulsion 5, 257 (1989).

2. A. Y. Tong and W. A. Sirignano: Num. Ht. Trans. 10, 253 (1986).

3. T. J. Anderson and M. Winter, paper number AIAA-92-0108 presented at the AIAA Aerospace Sciences Meeting, Reno, NV, Jan. 6 - 9, 1992.

4. Tzeng, H.-M., K. F. Wall, M. B. Long and R. K. Chang: Opt. Ltrs. 9, 273 (1984).

5. Quian, S.-X., J. B. Snow, H.-M. Tzeng and R. K. Chang: Science 231, 486 (1986).

6. *Handbook of Chemistry and Physics*, 61st edition, p. D-220, CRC Press, Boca Raton, FL, 1981.

APPENDIX F

"Liquid Stability Mechanisms Program Summary"

Presented at
28th JANNAF Combustion Meeting
San Antonio, TX , Oct. 28 - Nov. 1, 1991

LIQUID STABILITY MECHANISMS PROGRAM SUMMARY*

G. B. Cox, Jr. and E. L. Petersen
Pratt & Whitney/Government Engines & Space Propulsion
West Palm Beach, Florida 33410-9600

ABSTRACT

An experimental and analytical program to investigate the fundamental mechanisms of liquid rocket engine high-frequency (acoustic) instability is described. Investigations of the responses of secondary atomization and vaporization to imposed perturbations are being conducted. Test fluids simulate gas-liquid propellants at subcritical and eventually supercritical conditions. Program organization and experimental results to date are summarized. Identification and selection of simulant fluids for the experimental effort are described in detail.

INTRODUCTION

Combustion instability in liquid propellant rocket engines has historically been a major concern in engine development programs. Despite advances in understanding and modeling combustion instability processes, conducting stability rating programs, and designing injectors and combustion systems to avoid instability, unstable operation is still encountered. Acoustic combustion instability thus continues to be an issue, particularly now that a new round of liquid rocket engine development is imminent. The effects of operation at supercritical pressures on combustion stability must also be considered since new engines will operate at high chamber pressure. Efforts to understand the mechanisms driving acoustic combustion instability, and to identify remedies when instability is encountered, are still needed. Because of a lack of fundamental understanding of how combustion instabilities arise, current approaches for control of combustion instability rely on damping out pressure oscillations rather than preventing their occurrence.

An understanding of the origins of combustion instability could ultimately permit the design of inherently stable, high performance liquid rocket engines without much of the costly trial-and-error development which is now necessary. Advances in fast-response, nonintrusive instrumentation, measurement, and diagnostic techniques now make possible the investigation of many combustion processes which could cause or participate in liquid rocket engine combustion instability. Possible measurements include droplet sizes and spray patterns, droplet and stream breakup, propellant mixing, chemical reaction rates, chamber flow fields, and fluctuating pressures and velocities. Analysis of the data could assist investigators in determining instability mechanisms and in improving rocket engine design methods and procedures. Thus, current instrumentation and diagnostics capabilities enable a new approach to the control of acoustic combustion instability: investigation and eventual control of the basic acoustic combustion instability mechanisms. The Liquid Stability Mechanisms program is being conducted to investigate these phenomena.

This paper summarizes the progress of the Liquid Stability Mechanisms (LSM) program between October 1990 and the present. An overall description of the program and summaries of the technical progress are included. The majority of the paper focuses on the experimental investigation of mechanisms (Task 2), which includes the work done by the University of California, Irvine (UCI) on the secondary atomization mechanism, United Technologies Research Center (UTRC) on the investigation of the vaporization mechanism, and Pratt & Whitney (P&W) on simulant fluids.

PROGRAM DESCRIPTION

The Liquid Stability Mechanisms program consists of a combined theoretical and experimental effort. Theoretical effort addresses the identification and selection of candidate combustion processes, verification of the applicability of the experimentally-studied mechanisms to liquid rocket stability, and development of a program plan for further effort. Experimental effort addresses the investigation of the participation of the selected combustion processes in the instability mechanism. It has the objective of isolating specific processes which participate in acoustic combustion instability within liquid propellant rocket engines.

The program includes the following technical efforts:

1. Selection and verification of combustion processes having the potential for participation in instability mechanisms.
2. Development of appropriate test hardware and performance of experimental investigation of instability mechanisms.
3. Verification of the applicability of the mechanisms via comparison with analytical models and the available data base.
4. Development of plans for continued effort to incorporate test results into stability models, continued testing of additional mechanisms, and resolving any remaining issues.

The program schedule, Fig. 1, shows the activity planned for each portion of the effort.

The first effort was the identification and selection of processes for study, and has been completed. Secondary atomization and vaporization are the processes selected for experimental investigation. The second is test investigation of the selected processes. Accomplishment will take thirty months, of which approximately fourteen remain. The division of efforts is shown by Fig. 2. Details of the test plan concepts are described elsewhere (Ref. 1,2). Should early tests reveal unexpected technical difficulties, alternate design and fabrication approaches can still be pursued with little adverse impact on the overall program schedule. So far, there have been no unresolvable difficulties.

* This program is funded under Phillips Laboratory contract F04611-89-C-0088; Dr. J. N. Levine is the contract manager.

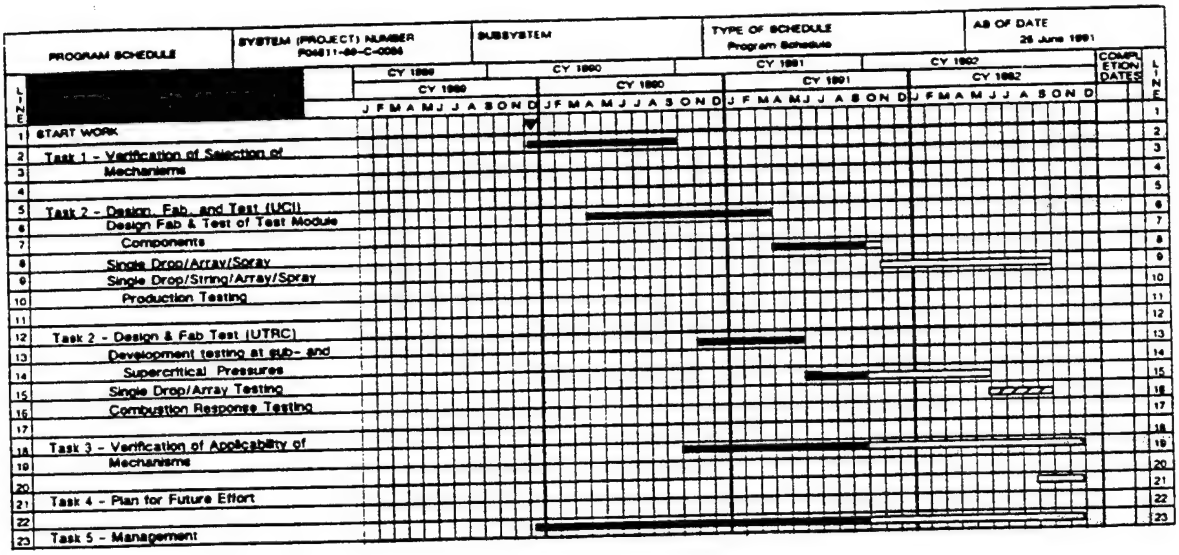

Fig. 1. Liquid Stability Mechanisms Program Schedule

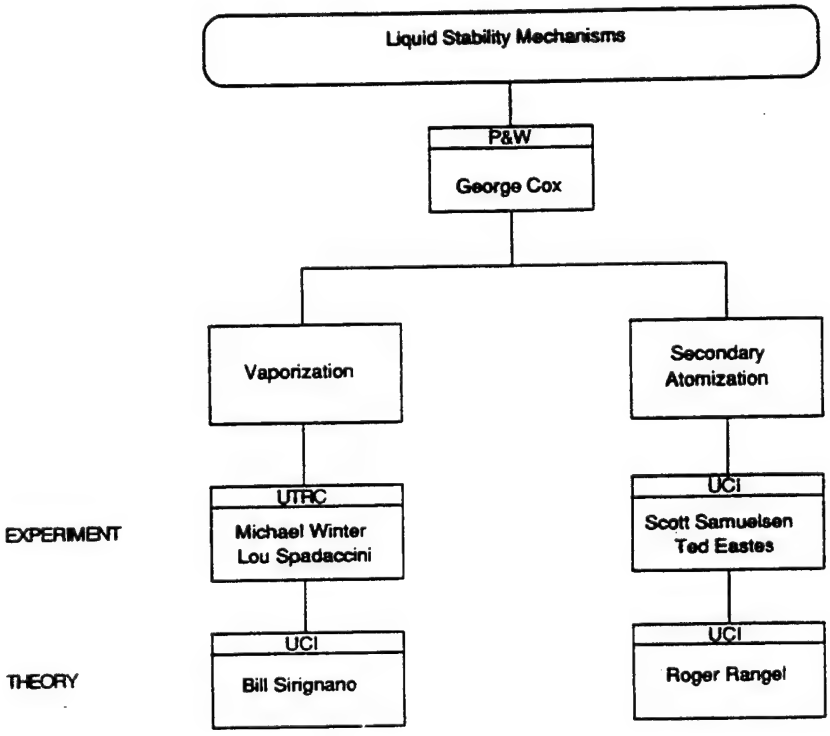

Fig. 2. Division of Efforts

The third effort is data verification using appropriate correlations, sub-models, and models. Accomplishment will take twenty-six calendar months, of which about sixteen remain. This task overlaps the experimental effort, since experimental data will become available well before the end of that effort. Also, analytical models may need revision for relevance to liquid rocket engine conditions. The last is formulation of the plan for future effort in the area of liquid stability mechanisms. Accomplishment will take three months. Completion of this task signifies completion of the Liquid Stability Mechanisms program.

TECHNICAL EFFORT

To distinguish between the events that are occurring as part of combustion, and those that are occurring as part of combustion instability, the following definitions are suggested:

> Process: The sequence of events, involving one or more propellants, by which a change is produced in some quantity which describes the states or conditions of the propellant(s), such as phase, velocity, temperature, pressure, environment, or chemical composition.
>
> > Example: The vaporization process is the sequence of events which changes a propellant from the liquid phase to a gaseous phase through the addition of heat to the liquid phase.
>
> Mechanism: The sequence of events by which a pressure or velocity perturbation produces a corresponding change in some process that eventually results in a change in the instantaneous energy release rate, and hence may participate in an instability.
>
> > Example: The vaporization mechanism is the sequence of events by which a pressure or velocity perturbation produces a change in the rate at which a propellant changes from a liquid phase to a gaseous phase.

By the above definitions, a combustion process becomes a potential or actual instability mechanism only if it has an appropriate response to the pressure/velocity perturbations seen during combustion instability. Consistent with the program description, the technical effort for the investigation of such mechanisms involves identification of the principle mechanisms, subsequent experimental investigations, and use of the acquired data to verify the selected mechanisms via theoretical modelling.

IDENTIFICATION AND SELECTION OF MECHANISMS FOR STUDY (TASK 1)

As seen in Fig. 1, this effort was completed in September 1990 (Ref. 3). The effort consisted of: 1) work completed in the form of a candidate mechanism list and a preliminary literature review of the various candidates, and 2) conclusions drawn on mechanism selection. As a result of the literature review and selection from the derived candidate mechanism list, droplet vaporization and secondary atomization were chosen as the principle mechanisms to be investigated. Other processes were also evaluated; although of potential interest, the available program resources do not permit investigation of all the candidates.

Secondary atomization was chosen as a primary mechanism for its impact on vaporization rates. Secondary atomization probably is not a rate controlling process in terms of its duration; however, through the droplet size distribution yielded by the atomization process, there is substantial impact on vaporization times. Greater understanding is needed in the breakup of the larger liquid propellant droplets in both non-oscillatory and oscillatory conditions. For example, strong pressure/velocity disturbances can affect the atomization process by accelerating the rate of droplet breakup, thereby changing the droplet size distribution and injector spray pattern. The altered propellant spray may vaporize at a different rate than the undisturbed spray. In addition, the wave may be of sufficient strength to displace the spray thereby distorting the fuel and oxidizer mixture distribution. Changes in droplet size, vaporization rates and propellant mixture distributions can lead to changes in spatial energy release patterns. The literature supports a study of atomization. Heidmann and Groeneweg (Ref. 4,5) and Ingebo (Ref. 6) studied atomization and its effects on the stability of rocket engine combustors. They found the highly nonlinear atomization process to be extremely sensitive to velocity and pressure oscillations.

Vaporization was selected as a major driving mechanism of combustion instability because analyses show it to be the rate controlling process in rocket combustion. The current literature supports the selection of the vaporization study. In recent works by Tong and Sirignano (Ref. 7) and Sirignano et al. (Ref. 8), combustion instability in liquid rocket and ramjet engines was studied with current developments in droplet vaporization. The authors demonstrated that vaporization within an oscillating pressure and velocity field could support a combustion instability as measured by the Rayleigh criterion.

Greater understanding is needed of the vaporization of droplets under non-oscillatory and oscillatory conditions. In these cases, special consideration for high density sprays and the high temperature, high pressure environments is needed.

EXPERIMENTAL INVESTIGATION OF MECHANISMS (TASK 2)

The experimental investigation of the selected mechanisms is based on perturbing drops and the subsequent measurement of the response to the perturbation. In the actual combustion process, the time interval between the perturbation and the burning of the drops measures the phase lag of the process. Through the Rayleigh criterion, the phase lag is related to the appropriate acoustic instability. The perturbation itself is coincident with the passage of a pressure/velocity pulse. The experimental concept is to study the phenomena which occur when a pulse passes transversely through either a single drop, a stream of droplets, or a spray.

For conducting the experiments, pulse tubes will be used by both investigating organizations. A number of possible pulse techniques were considered. It has been concluded that a burst diaphragm technique has the least development risk. A double diaphragm technique will be used as the pulse method in the current program. In the double diaphragm technique, the driver gas pressure and the pressure of the gas between the diaphragms is brought up to pressures such that they do not exceed the pressure drop required to fail each of the diaphragms. At a specified time the volume between the diaphragms is exhausted, failing the first and then the second diaphragm as the maximum pressure drop is exceeded for each. The pulse is produced and propagates down the tube to the test section. This method has been widely applied and does not require precision rupture discs or a plunger.

Details of the design and fabrication of the UCI and UTRC pulse tubes are given elsewhere (Ref. 1,3). Although turnaround time may be substantially more than that associated with other techniques, other inter-test activities may be the time-controlling activities. A quick release linkage device will greatly reduce turnaround time for such a technique. While wave amplitude consistency of such a device has been questioned, experience to date in this program shows that consistency is not a problem.

Droplet streams or sprays will be injected transversely to the bore of the pulse tube, Fig. 3 (conceptually). A number of drop generator types will be used, some of which are being designed and fabricated by the investigating organizations, others of which will be procured from outside suppliers. One prototype drop generator for high pressure applications, for use at UCI, built by John Dressler of Fluid Jet Associates has been assembled, and the required power amplifier and filter have been acquired. Other generator concepts include: 1) a speaker-actuated drop-on-demand type, and 2) a Peterson-type drop generator.

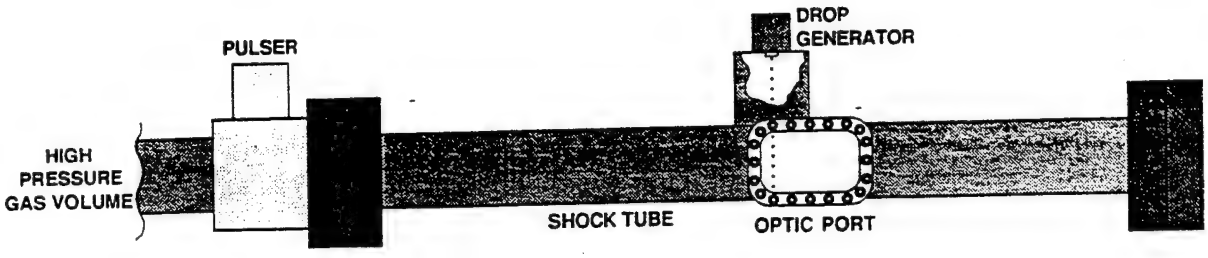

Fig. 3. Pulse Tube Concept

The questions to be answered during the experimental investigations are primarily:

- What effect does a perturbation have on secondary atomization and vaporization?
- Is the magnitude of the effect sufficient to produce instability?
- Can this effect be detected directly in the experimental environment?
- What will the output be and how will it be related to instability?

UTRC is conducting its study according to the following main steps:

- Design and development of shock tube facility
- Development testing at sub- and supercritical conditions
- Single drop testing at sub- and supercritical conditions
- Droplet array testing at sub- and supercritical conditions

The first two steps includes the evaluation of system components for high pressure application and integrated system testing. The components to be evaluated include the pulse-generation method and the drop/array generator. Development testing of the entire system centers around the hardware and diagnostic idiosyncrasies as well as verification of the measurement techniques and simulant fluids at both sub- and supercritical pressures. Event timing, leak testing, spatial and temporal resolution, and sensitivity are all important. Also of importance is the effect that the pulse has on the measurement of droplet vaporization, i.e., deformation and subsequent breakup may occur before the vaporization rate can be quantified.

Once development testing is accomplished, data can be acquired for a specified test matrix using single drops and arrays of drops. A range of conditions and proper simulants will be tested at both sub- and supercritical conditions. The relative effect of the pulse on the vaporization response must be obtained by testing under identical situations both with and without the pulse.

UCI's secondary atomization test plan can be divided into similar steps. The initial work focused on the design and fabrication of the shock tube, drop generator, and support equipment; testing of the fabricated components and the integrated system; and development and verification of the diagnostic techniques. Selection of the pulse method is also important. Miscellaneous requirements include, but are not limited to, leak testing, safety and cleanup evaluation, and control system integration.

After the developmental design, fabrication and testing, the demonstration and production testing of the single drop/stream/array relative to a pulse can be accomplished. The characterization of the secondary atomization mechanism will occur at subcritical and supercritical pressures using a realistic range of conditions and fluids.

DROPLET DEFORMATION

After mutual consultation between P&W, UCI, and UTRC, it has been decided that a common definition of the droplet breakup time needs to be established. A review of past work on droplet breakup has produced a wide array of trends, Fig. 4, and it is highly likely that this is a result of differing definitions of the time it takes for the droplet to begin its breakup. Therefore the breakup time will be defined for this program as the time when the drop begins to lose its symmetry in the plane perpendicular to the relative velocity vector of the pulse, Fig. 5. As shown by Fig. 5, the breakup time is referenced to the instant the shock wave passes the drop (i.e., $t=0$ is when the wave passes the droplet, and the breakup time is when the droplet begins to distort). Evidence has shown that whenever the drop begins to distort as shown in Fig. 5, breakup usually follows. This definition is based on the development testing described in the following sections; however, it may be reconsidered based on subsequent results.

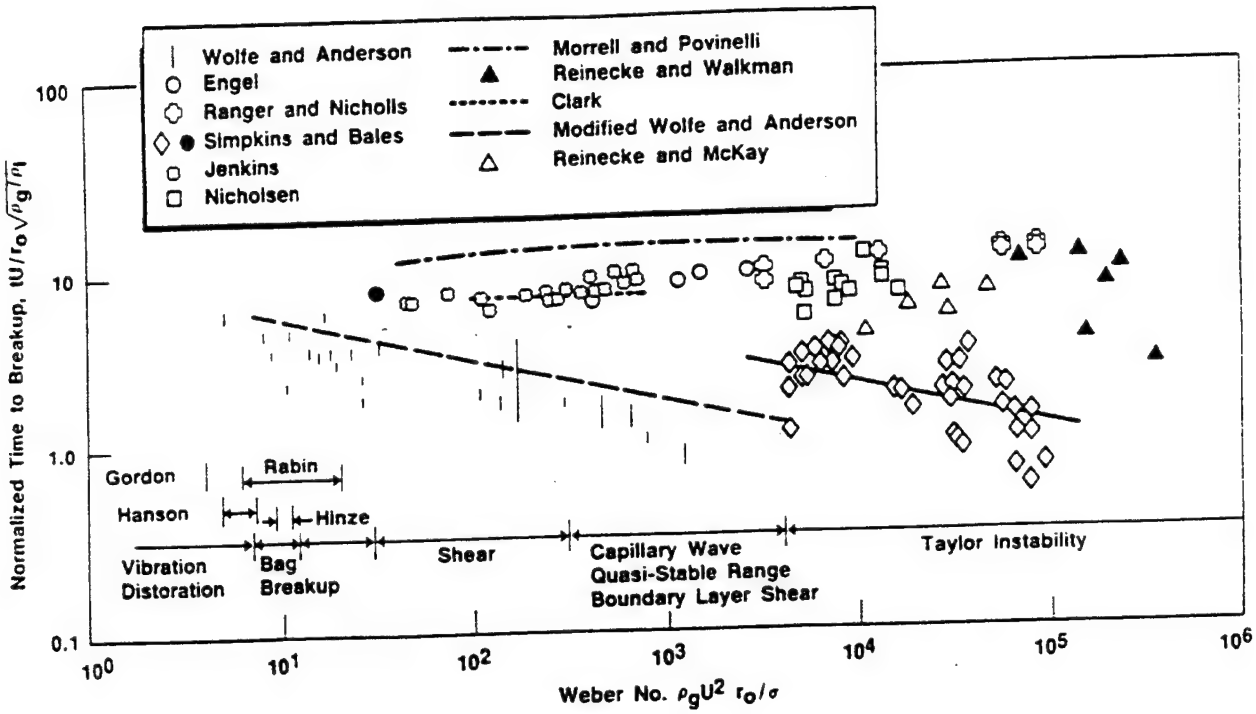

Fig. 4. Breakup Data

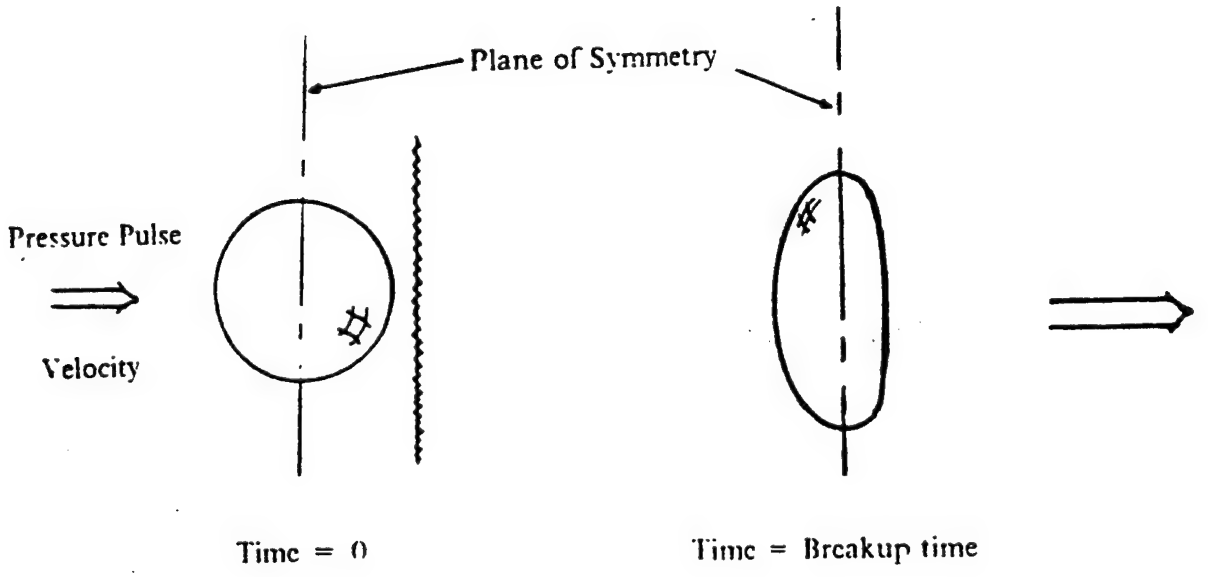

Fig. 5. Droplet Distortion Asymmetry

VAPORIZATION (UTRC)

Accurate measurement of the vaporization rate of a single droplet under conditions which model acoustic wave/drop interactions requires techniques which have only recently been developed. The methods to be used at both sub- and supercritical conditions require at least a 10 percent envelope in the measurement of dr/dt. To obtain this accuracy, advanced laser and optical techniques are being applied by UTRC. Relative to the test plan and schedule, a large portion of the development and verification testing of the subcritical-condition techniques has been accomplished to date.

To achieve the needed accuracy in vaporization rate measurement, two different experiments are planned, one for subcritical pressures and one for supercritical pressures. The majority of the work to date has been with the subcritical pressure method: Morphology-Dependent Resonance (MDR).

The MDR technique turns each fluid droplet into a miniature laser using a laser dye as a dopant in the simulation fluid (Ref. 9-11). When excited by another laser, the droplet will lase in the near-surface region where total internal reflection provides the necessary effective laser cavity. The laser output wavelength then becomes proportional to the droplet circumference. Spectral analysis of the laser light wavelength allows measurement of droplet diameter to within one part in 100,000; repetitive observations allow measurement of droplet diameter changes. In addition, changes in droplet shape from droplet oscillations can also be monitored through corresponding changes in output light wavelength.

At supercritical conditions, changes in fluid refractive index near the simulant fluid critical temperature invalidate the MDR technique. Two approaches which exploit properties of oxygen molecules and can be used under supercritical conditions are 1) the imaging of Raman-shifted light from oxygen molecules, and 2) the application of laser-induced-fluorescence, where the ambient gas is seeded with a gas phase fluorescent compound.

As part of the development and verification testing, UTRC has allocated the required equipment and has begun to obtain initial MDR results. These are described by Winter and Anderson in Ref. 1.

SECONDARY ATOMIZATION (UCI)

Secondary atomization is an indirect instability mechanism which couples with vaporization by generating many small droplets from the original drop. These smaller droplets not only increase the liquid surface area available for combustion, they also tend to follow the path of a pulse-induced flow, thus redistributing the reacting component spatially. In UCI's experimental contribution to the Liquid Stability Mechanisms program, new photographic and image processing technology will provide high resolution qualitative and detailed quantitative analyses of secondary atomization. Most of UCI's secondary atomization work to date has concentrated on concept development and verification; diagnostic evaluation and verification; and design and fabrication of the necessary experimental equipment.

To qualitatively capture the phenomena of droplet deformation, breakup mode, and ligament and surface wave formation, stroboscopic photography is believed best suited. Stroboscopic photography combined with digital image processing and symmetry assumptions allows the entire breakup process to be captured on a single frame of film. Illuminating the event of interest at set intervals by a pulsing light source yields multiple images of the secondary atomization event on a single frame of film. If confusion among drops at different times occurs, a high speed framing camera may be used to record the event.

Critical to the selection of a suitable light source is the fact that it must be capable of resolving down to tens of microseconds. Due to its high power (for photographic illumination) and lower pulse width (to reduce image smearing), the copper vapor laser was chosen as the required light source. The other critical component of the necessary diagnostic equipment is the long distance microscope. Various simple experiments were performed with the components using borrowed equipment, and proof-of-concept verification was obtained. The results of the tests showed that the techniques will work, and lighting investigations revealed that back lighting is the best means of recording the breakup process. Stroboscopic Polaroid photos using off-angle lighting are still believed to provide a powerful means of framing the process prior to recording the event on film. Also of note was the appearance of an unexpected diffraction pattern inside the droplets. The cause of this is being explored, and the utility of such a diffraction pattern for providing an independent means of sizing the droplets is being investigated.

SIMULANT FLUID STUDY (P&W)

In support of the experimental investigation, P&W conducted a parallel evaluation of simulant fluid properties and conditions which compare with actual rocket engine operating environments. Contained in the following paragraphs is a description of the actual rocket chamber conditions to be modelled as well as the corresponding range of engine configurations. Next, the parameters to be matched and the method of selecting the proper combinations of the fluids investigated are discussed. The results of the study for the desired range of conditions are also included for consultation by UCI and UTRC when selecting a test matrix.

Engine Conditions. Experimental modelling of the spray/combustion process inside a high pressure rocket combustion chamber is difficult due to the extreme temperature and turbulent conditions which exist. Under non-combustion conditions, the best an experiment can do is match certain fluid properties and non-dimensional parameters that occur in the real process. A majority of the past studies done on liquid propellant injectors were designed such that cold flow densities, velocities, etc. bracketed their hot flow counterparts over a specified range. Correlations derived from such studies are useful tools. However, if the particular parameter combination that matches the real conditions has not been tested, extrapolation of the results may be invalid. Therefore the investigation presented herein attempts to cover a range of possible engine parameters while matching as closely as possible the combinations which are expected. Included in the following discussion is a summary of the engines selected to be modelled and the corresponding chamber conditions.

Engine Selection. A number of possible rocket engine configurations can be selected to cover a range of chamber conditions, propellants, and injector types, Table I. The range covers possible chamber pressures from sub- to supercritical as well as different injector types. Coaxial injectors represent the gas/liquid category, while impinging-type injectors cover liquid/liquid configurations.

Table I. Engine Configurations Chosen to Model

Engine	P_c-MPa (psia)	O/F Mixture Ratio	Thrust-kN (lb_f)	Injector
STE - LOX/H_2	15.8 (2300)	6.94	2580 (580k)	Coaxial
STE - LOX/CH_4	13.8 (2000)	3.50	2580 (580k)	Coaxial or Impinging
LOX/H_2 Preburner	37.9 (5500)	1.03	---	Coaxial
RL10 – LOX/H_2	4.25 (616)	5.80	98 (22k)	Coaxial
F-1 - RP-1/LOX	6.76 (980)	2.27	6670 (1500k)	Impinging
Monopropellant-Hydrazine	3.45 (500)	---	(Low)	---

The first four engines, with coaxial injection elements, listed in Table I are the ones of greatest interest to the current program. Both booster and upper stage engines are represented along with a sample SSME fuel rich preburner: and in each case, the droplets are of liquid oxygen. The most current applications are those related to the Space Transportation Engine (STE) and the entire National Launch System effort in general. The LOX/CH_4 STE is of particular interest because the conditions best represent the instability testing of other subscale chambers (Ref. 12-14). Due to the need for simplification and associated time constraints, the LOX/liquid methane, LOX/kerosene, and storable propellant combinations, which primarily use impinging injection elements, will not be modelled in the current program. Nonetheless, follow-on studies can easily be done using these and other possible rocket injector/combustion chambers as a target.

Chamber Properties. Once the desired engines to be modelled are established, the expected chamber properties can be defined so that proper cold flow studies can be conceived. However, when considering the modelling of an entire spray, the propellant conditions and chamber properties are relatively simple to define; the cold flow properties can be set up such that the injected conditions are matched, and the chamber conditions can be chosen to match the density and pressure of the combustion products. However, when studying a single droplet, the surrounding medium can be that of the co-flowing gas, the combustion species, or a combination of the two. Hence certain compromises and assumptions are built into the simulant fluid investigation to comply with the conflicting extremes.

In the current study, each extreme is represented in the selection of the droplet ambient conditions. Each engine configuration will thus have two sets of conditions for the droplet ambient gas: one set essentially conforms to the injected gaseous propellant; the other corresponds to the predicted combustion gas properties in the chamber.

Two different assumptions can be made in the prediction of the combusting atmosphere of the injected drop. One is that the ambient species are at the average temperature between the cold propellant and the flame temperature of the mixture. Others have defined the surrounding temperature as such (Ref. 15). For an inlet T_g of 110 K (200°R) and a typical LOX/H_2 flame temperature of 3720 K (6700°R), the average temperature would be 1920 K (3450°R). The results are supported by the data acquired by Boylan and O'Hara, (Ref. 16). Their experimental findings lead to the conclusion that the temperature near the injector of a liquid propellant rocket engine averages around 1940 K (3500°R). Therefore, a combustion gas temperature of 1940 K (3500°R) will be used for a droplet in a combusting atmosphere near the point of injection since either set of assumptions leads to essentially the same result.

When combusting and supercritical conditions are combined, a possible third combination of drop/ambient gas arises. This additional point of interest is when the LOX droplet is near its saturation point. The density, viscosity, and surface tension of a LOX drop varies quite radically with temperature. Table II lists the conditions representative of LOX as well as other possible rocket chamber fluids. The differences in the two LOX extremes are evident in the table. Therefore two liquid oxygen conditions will be specified, one having essentially the injected properties, the other having near-saturated properties. On a similar note, the recent work at the University of Colorado's Center for Combustion Research also considers the variability in LOX conditions (Ref. 17).

The possible combinations of chamber gas and LOX properties to be investigated are summarized in Table III. As a result of high ambient gas densities, the possible combination of cold LOX and injected CH_4 is not included in Table III; the available simulant pressures and fluids can not adequately model this alliance. Note also that only the engine combinations of greatest interest to the program are considered.

Table II. Physical Properties of Liquid Rocket Propellants

Chamber Liquid	ρ_ℓ-kg/m³ (lbm/ft³)	σ (dyne/cm)	μx10⁴-kg/m-s (lbm/ft-s)	P_σ-MPa (psia)	T_σ-K (°R)
LOX	1153 (72)	12.1	2.20 (1.48)	5.07 (736)	155 (279)
Saturated LOX	850 (53)	≃1.0	0.67 (0.45)	5.07 (736)	155 (279)
CH_4	320 (20)	14.2	0.42 (0.28)	4.60 (667)	191 (344)
RP-1	800 (50)	23.0	16.1 (10.88)	2.17 (315)	677 (1218)
Hydrazine	1010 (63)	91.5	9.08 (6.10)	14.72 (2135)	653 (1176)

Table III. Physical Properties of Gas Ambient to Droplet

Engine	Fluids	ρ_g-kg/m³ (lbm/ft³)	γ	μx10⁵-kg/m-s (lbm/ft-s)	T_g-K (°R)	$\overline{M}_g$	ρ_ℓ/ρ_g
STE LOX/H_2	Inj LOX-Inj H_2	31.7 (1.98)	1.4	0.67 (0.45)	1.3 (204)	2.0	36.4
	Inj LOX-Comb	14.7 (0.92)	1.2	6.40 (4.3)	1940 (3500)	15.0	78.3
	Sat LOX-Comb	14.7 (0.92)	1.2	6.40 (4.3)	1940 (3500)	15.0	57.6
STE LOX/CH_4	Inj LOX-Comb	18.6 (1.16)	1.2	5.95 (4.00)	1940 (3500)	21.7	58.4
	Sat LOX-Comb	18.6 (1.16)	1.2	5.95 (4.00)	1940 (3500)	21.7	45.7
LOX/H_2 Preburner	Inj LOX-Comb	16.3 (1.02)	1.3	2.98 (2.00)	1160 (2085)	4.1	70.6
RL10 LOX/H_2	Inj LOX-Inj H_2	5.12 (0.32)	1.4	5.95 (4.00)	216 (388)	2.0	212.4
	Inj LOX-Comb	14.7 (0.92)	1.2	6.40 (4.30)	1940 (3500)	15.0	78.3

Simulation of Engine Conditions. As summarized previously (Ref. 3), the cold flow testing is to be divided into a subcritical and a supercritical phase. A comparison between the chamber liquid critical properties listed in Table II and the engine chamber pressures given in Table I leads to the conclusion that three of the four principle configurations operate in the supercritical regime. To allow a wide range of parameters to be tested in both test phases, the following scheme is suggested. The subcritical, cold flow phase will test the entire range of important parameters for each engine but at pressures which are below the simulant liquids' critical pressures. Thus the effect of everything except critical pressure can be determined. The subsequent supercritical phase will involve the potential relaxation of one matching parameter and the substitution of the engine critical pressure ratio.

The sub- and supercritical simulant fluids will be tested in a pulse tube designed for operation at chamber pressures up to 6.9 MPa (1000 psia). The necessary nomenclature along with a view of a typical pulse tube are shown, Fig. 6. As shown, the usual pulse tube subscripts are employed in this report to represent the test section, 1; upstream of the pulse, 2; and driver section, 4.

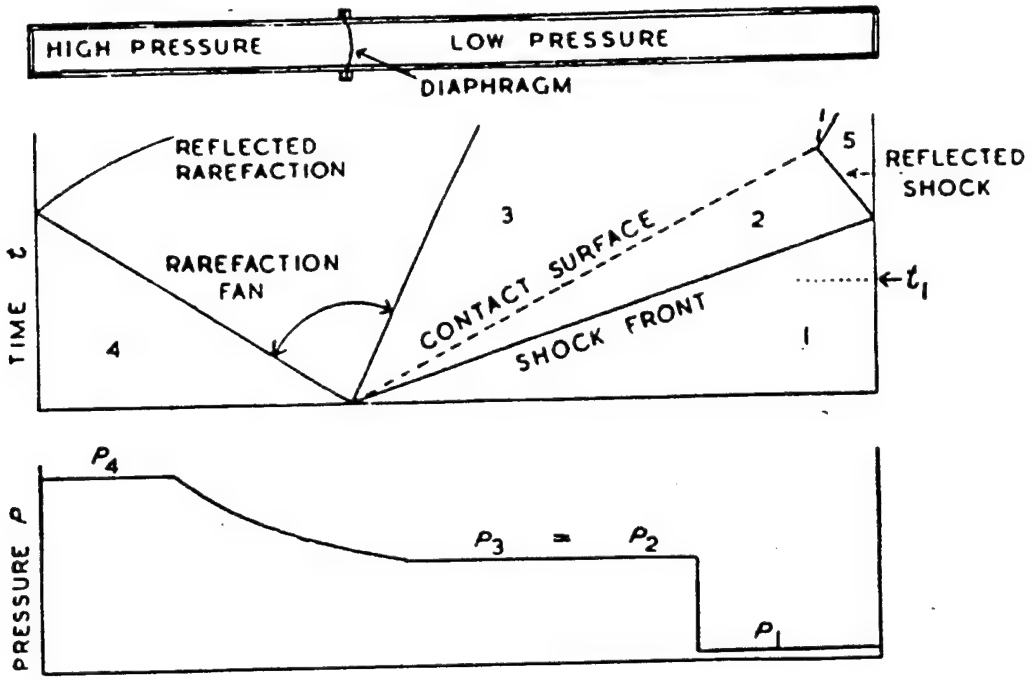

Fig. 6. Pulse Tube Schematic and Nomenclature

For simplicity, cost effectiveness, availability, and the designed test section lengths, the chamber and driver simulant gases will be either helium, nitrogen, or a mixture of the two. Likewise, the relatively high N_2 molecular weight of 28 allows for a cost-effective gas as a simulant in the high density conditions within the test section; hence nitrogen is chosen as the station 1 fluid as often as possible to conserve gas and operate at lower pressures. The selection of the proper pressures and/or mixtures is presented in the following sections, as are the significant parameters and simulant fluid combinations.

Parameter Matching. Non-combusting, cold flow experiments can be used to model rocket combustion conditions by matching the parameters deemed important to the processes under investigation. For the LSM simulant liquid study, the following parameters are chosen based on their importance and their ability to match hot-fire conditions (Ref. 18-21):

1. Liquid droplet Diameter (D)
2. Liquid surface tension (σ)
3. Liquid viscosity (μ_ℓ)
4. Liquid to gas density ratio (ρ_ℓ/ρ_g)
5. Critical pressure ratio, or reduced pressure (P_c/P_{cr})
6. Droplet Reynolds number (Re)
7. Droplet Weber number (We)

In the above list, the gas density in ρ_ℓ/ρ_g is the density of the chamber gas; in terms of the experiments, it represents the density ambient to the droplet in the test section, or ρ_1. Important to the testing but not included in the parameter list is the constraint that the pressure wave should have the characteristics of a steep-fronted pulse. Fig. 7 shows a sample transient plot of a steep-fronted wave in a rocket combustion chamber. These types of waves can be produced by placing suitably-shaped conical inserts into the driver section, as in Ref. 31.

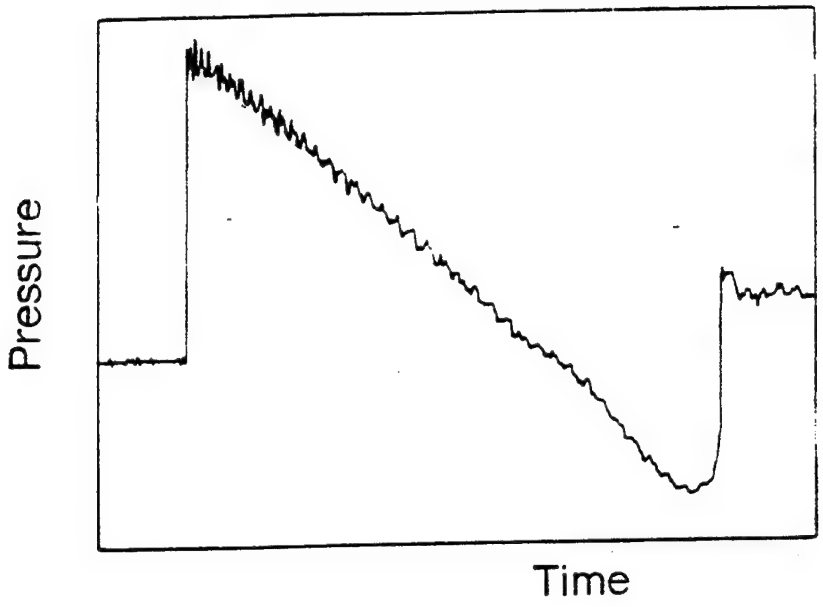

Fig. 7. Typical Steep-Fronted Wave (Ref. 31)

Of the seven chosen parameters, certain combinations are more important depending on which stability mechanism is being investigated. The secondary atomization mechanism requires accurate simulation of droplet viscosity, surface tension, and density ratio because each is crucial to droplet breakup. On the other hand, vaporization experiments depend more on the evaporative nature of the cold flow liquid than on σ and μ_ℓ. Matching the droplet Weber number is again more important for breakup, while Re is very important to both stability mechanisms.

The Reynolds and Weber number are based on the drop/pulse interaction and are defined as:

$$Re = \frac{\rho_2 V_2 D}{\mu_2} \tag{1}$$

$$We = \frac{\rho_2 V_2^2 D}{\sigma} \tag{2}$$

The gas density term in the Weber number relation is the density of the gas behind the pulse (but before the contact surface or, ρ_2) travelling at the velocity V_2. Although some authors view the definition of the density term in the Weber number as arbitrary (Ref. 17), it is herein based on the density of the shearing gas as in atomizer (Ref. 23,24) and pulse wave (Ref. 25) studies. It is likewise assumed that the axial velocity of the droplet is negligible.

In addition to the parameters listed, the strength of the pulse wave is also important. Direct matching of the actual and experimental pulse strengths will lead to an overspecification of the simulant conditions. However, the relative effect of pulse strength shows up as the velocity term in Re. A range in pressure pulse strength from 5-50% of the chamber pressure can be chosen for each engine given in Table I, and the resulting wave velocity can be calculated from the usual 1-D momentum and continuity relations for a pressure pulse (Ref. 26).

With the attainment of realistic pulse strengths, the range in Re/D to be matched can be calculated. The $\Delta P/P$ range chosen is in line with the usual stability criteria. Note that Re/D is solved for instead of Re so that a 1:1 correspondence in drop size between cold and real-flows can be maintained. For the STE configurations, the Re/D range is from 0.34×10^7 to 55.7×10^7 ft^{-1}, and We/D ranges from 6.4×10^5 to 9.9×10^8 ft^{-1}. The We/D and Re/D bounds for the other configurations in Table III fall within the STE limits.

Provided below in Table IV is a sample range of actual Re and We for a typical droplet (100 μm) and the conditions defined under the STE LOX/H_2 configuration in Tables I-III. Typically the Reynolds numbers are lower for the droplet in a combustion atmosphere, and the Weber numbers for a near-saturated-LOX case are much higher than for the colder, oxygen cases due to the low σ of a near-saturated LOX droplet.

Table IV. Sample Range of Re and We for a 100 Micron Droplet

Configuration	We	Re$\times 10^{-4}$
LOX/Inj. H_2	210 - 2.1×10^4	1.5 - 18.0
LOX/Comb.	273 - 2.7×10^4	0.1 - 1.3
Sat.LOX/Comb.	3300 - 3.3×10^5	0.1 - 1.3

Once the Re and We are specified, the various combinations of simulant fluids and necessary pulse tube pressures (P_1, P_2, P_4) can be defined for both the sub- and supercritical phases.

Subcritical Fluids. The subcritical test phase will be set up to investigate the effects of each parameter presented previously except the reduced pressure. Most important to the establishment of the subcritical test conditions is the selection of the proper liquid simulants. Since viscosity and surface tension need to be matched with the LOX conditions given in Table II, these are the variables which require the most scrutiny. However, it should again be stressed that the restrictions on μ_ℓ and σ apply principally to the UCI secondary atomization tests because they are dominant factors in droplet breakup. The UTRC vaporization study requires less emphasis on the breakup mechanism because the need for simulant liquids which are compatible with the laser diagnostics and which are also relatively volatile at room temperature add additional constraints. The level of diagnostic compatibility rests on the ability of the simulant liquid to dissolve the laser dye (dopant for MDR technique). Table V contains the resulting array of subcritical liquids for both UCI and UTRC hardware.

Table V. Subcritical Simulant Liquids

Liquid	ρ-kg/m^3 (lbm/ft^3)	σ (dync/cm)	$\mu\times10^4$-kg/m-s (lbm/ft-s)	P_{vap}-MPa (psia)
Water	1000 (62.4)	73.10	9.67 (6.50)	0.003 (0.5)
Freon 113	1650 (103.0)	17.00	6.84 (4.60)	0.04 (6.0)
n-Pentane	631 (39.4)	16.50	2.26 (1.52)	0.11 (16.0)
Freon 22	1230 (76.8)	9.00	1.98 (1.33)	0.99 (144.0)
N_2O	1225 (76.5)	1.75	0.21 (0.14)	5.31 (770.0)
MIL-C-7024	769 (48.0)	23.00	8.63 (5.80)	---
Freon 12	1304 (81.4)	9.00	2.07 (1.39)	0.69 (100.0)
Ethanol *	791 (49.4)	22.00	11.1 (7.49)	$\simeq$0.0 (0.1)
Methanol *	791 (49.4)	22.60	5.62 (3.78)	0.01 (2.0)
n-Decane *	730 (45.6)	23.80	9.02 (6.06)	$\simeq$0
LOX	1153 (72.0)	12.10	2.20 (1.48)	0.69 (100.0)

* Volatile liquids for vaporization

A wide range of liquid simulants are available to study the secondary atomization mechanism, each having various merits. For example, water does not closely match the viscosity and surface tension of LOX, but it is inexpensive and readily available. Therefore, water is ideal for chamber checkout tests. MIL-C-7024 is another common injector simulant, but it also does not compare well with LOX (although it is closer than water is).

Another hydrocarbon to consider is n-pentane. The low surface tension and viscosity of n-pentane make it an excellent simulant for liquid oxygen. However, the rather low pentane critical pressure of 3.4 MPa (490 psia) must be accounted for when establishing the simulation chamber pressure (P_1) for subcritical tests.

If environmental impacts can be accommodated, the various chlorofluorocarbons listed in Table V also make excellent simulants due to their low values for σ and μ_ℓ. The advantage of Freon 113 is that it is a liquid at STP. On the other hand, Freon 12 and Freon 22 have viscosities nearer to that of LOX but require pressures above 0.69 and 0.99 MPa (100 and 144 psia), respectively, to be in liquid form. Another advantage of Freon 12 and Freon 22 is that they are common household and automotive refrigerants.

Nitrous oxide (N_2O) is another excellent simulant because it is the only simulant in Table V which is close to near-saturated LOX in both σ and μ_ℓ. A disadvantage is that N_2O has a vapor pressure of 5.3 MPa (770 psia) at room temperature. Nonetheless, liquid N_2O is readily available.

The simulants specifically designated for use in the vaporization mechanism tests are given in Table V because of their known volatility and current employment by UTRC. The chlorofluorocarbons listed, as well as other possible fluids not listed, may require investigation in the future in order to accommodate the diagnostic techniques. For simulation of a near-saturated LOX drop, N_2O should again be used. If nitrous oxide is incompatible with the diagnostic techniques, the near-saturated oxygen configuration need not be studied. Ideally, liquid oxygen should be used as the simulant liquid. LOX is included in the list since UTRC's laboratory has been approved to handle cryogenic oxygen.

Supercritical Fluids. Presented in Table VI are the possible choices for the simulation of LOX under supercritical conditions. The limitations in selecting such a list include the restriction that the test section of the pulse tube(s) was designed for 6.9 MPa (1000 psia). This chamber pressure restriction is coupled with the result found by Norton et al. (Ref. 27) that droplet vaporization is not affected by supercritical conditions for reduced pressures below approximately 1.5. Therefore the simulant liquid should not have P_{cr} greater than 4.6 MPa (667 psia).

Table VI. Supercritical Simulant Liquids

Liquid	P_{cr}-MPa (psia)	T_{cr}-K (°R)	ρ-kg/m³ (lbm/ft³)	σ dync/cm	μx10⁴-kg/m-s (lbm/ft-s)	P_{vap}-MPa (psia)
n-Decane	2.1 (306)	618 (1112)	730 (45.6)	23.8	9.08 (6.10)	≃0
Freon 22	5.0 (722)	369 (665)	1230 (76.8)	9.0	1.98 (1.33)	0.99 (144)
Freon 12	4.1 (597)	386 (694)	1304 (81.4)	9.0	2.07 (1.39)	0.69 (100)
n-Octane	2.5 (360)	569 (1024)	703 (43.9)	21.6	5.25 (3.53)	0.003 (0.5)
n-Pentadecane	1.5 (220)	710 (1278)	767 (47.9)	27.1	27.7 (18.60)	---

Application of the reduced pressure criterion of 1.5 to the fluids in Table VI results in the elimination of Freon 22 and even oxygen. The heavy hydrocarbons and Freon 12 however meet the $P_1/P_{cr} = 1.5$ limitation. If the actual engine reduced pressures of 2.7 and 3.1 (neglecting the preburner reduced pressure of 7) are to be met, only the heavy hydrocarbons are adequate. Of these hydrocarbons, octane and decane have been widely used in past supercritical combustion applications (Ref. 15,28,29). Pentadecane has the lowest value of P_{cr} but is expected to be more expensive and less readily available than the others. An exception to the minimum reduced pressure criterion of 1.5 may surface if liquid O_2 must be used to accomodate UTRC's droplet imaging techniques which may require the presence of oxygen molecules (ref. 3).

Other low-P_{cr} liquids such as eicosane and Freon 13 were also considered at one time. The problem with these and other exotic hydrocarbons and fluorine-based compounds is that they are either solids at room temperature or are liquids only at low temperatures.

Test Conditions. After the selection of the simulant liquids, the possible combinations of fluids, parameters, and physical limitations require analysis to arrive at the actual test conditions. Certain fluid/test conditions do not comply with the parameters set up for the chosen real engine configurations. Hence some fluid combinations eliminate themselves. Among the constraints which exist in addition to the drop parameters are the following:

1. P_1 limited to 6.9 MPa (1000 psia)
2. Test section pressure must be greater than the liquid vapor pressure
3. Required mixture of N_2/He must be within possible limits, i.e., molecular weight between 4 and 28 and γ between 1.4 and 1.67
4. Shock tube driver pressure must be realistic (< 20.7 MPa)

Throughout the presentation of the results, the nomenclature developed for Table III is used to define which engine and chamber gas is being modelled. For example, "Coaxial LOX/H_2 (Inj. H_2)" represents the first row of Table III. The selection procedure itself was designed such that more than one liquid can be used to simulate the rocket engine under consideration, leading to greater flexibility. Not included in the study is the selection of the appropriate driver gas, which can be most any readily-available gas such as N_2, helium, argon, etc. Because the driver gas properties do not define the shock velocity (other than indirectly via P_4/P_1), the choice of the driver gas can be left to the capabilities of the particular test facility, the desired test time, and the diagnostics. The procedure and results for selecting the other shock tube fluids and test conditions are given below.

Subcritical Conditions--Secondary Atomization. In the calculation of the test conditions for the subcritical, secondary atomization phase, the parameters and physical properties matching the actual values are $\{Re/D, We/D, \rho_\ell/\rho_1, \sigma, \mu_\ell\}$. The solution for the pulse tube variables is also based on the assumption that the test section gas is some mixture of nitrogen and helium. The test variables which are unknown include: the test section and pulse-upstream pressures; the composition of the chamber fluid (M_1, γ_1); and the static temperature upstream of the pulse (T_2).

The solution procedure for the unknown variables employs the known engine parameters, real gas equations, and the standard shock tube gas dynamic relations (Ref. 30). However, when solving these equations for the pressures and chamber compositions which match the specified rocket conditions, i.e., Re/D, We/D, ρ_ℓ/ρ_1, σ, μ_ℓ, it is found that no realistic solutions exist if the entire set is to be matched. Therefore at least one parameter must be relaxed in lieu of the parameters deemed more important to the secondary atomization process. Following the reasoning given in Section 3.3.3 of reference 22, wave-induced droplet breakup in rocket combustion chambers is due to aerodynamic stripping, where $We/\sqrt{Re} > 0.5$; droplet breakup with this parameter less than 0.5 tends to occur in a "bag"-type fashion. A check on the range of $We/\sqrt{Re}$ for the engine conditions specified in Table III indicates that breakup will occur in the stripping mode over a realistic range of drop sizes. In the stripping regime, We is found to be unimportant. Hence We/D need not be matched between the engine conditions and the cold flow tests, and the chamber composition is no longer an unknown.

Table VII shows the results of the selection procedure over a range of possible subcritical simulant fluids. The ranges in P_2/P_1 and T_2/T_1 match the specified engine Re/D (or, essentially V_2), while P_1 chiefly matches the required ρ_ℓ/ρ_1 for each liquid simulant. In most cases, either Ar or N_2 is specified as the chamber gas because their high molecular weights lead to lower, more economical values of P_1 than if He is used. Exceptions include the RL10 cases which have high liquid/gas density ratios (200-300) leading to relatively low simulant chamber pressures. Liquids with high vapor pressures ($\sim$ 0.7 MPa) such as LOX and Freon12 require He in shock tube section 1 to match the high density ratios while ensuring $P_1 > P_{vap}$. Likewise, the STE conditions modelling a near-saturated LOX drop in a combustion environment lead to the use of N_2O as the simulant. Nitrous Oxide's high P_{vap} of 5.31 Mpa (770 psia) requires a 30/70 percent volume mixture of N_2/He to maintain the needed pressure margin.

Should the possibility arise that We/D cannot be neglected, as assumed above, a revised shock tube condition selection procedure must then be employed. A preliminary test series should be conducted to verify which of the parameters Re/D, We/D, etc. is most important to secondary atomization and which, if any, can be neglected.

Subcritical Conditions--Vaporization. The test conditions and fluids for the subcritical vaporization studies are chosen using the same methodology and assumptions used to select the conditions for the secondary atomization tests. That is, Re/D, ρ_ℓ/ρ_1, σ and μ_ℓ are the parameters to be matched with engine conditions, assuming again that We/D effects are secondary. Therefore the contents of Table VII can also apply to the vaporization mechanism studies. Nonetheless, the investigation of the vaporization mechanism requires volatile liquids as seen in Table V. The shock tube conditions associated with these more-applicable liquids is provided in Table VIII. Other liquids may also require investigation if those provided in Table VIII prove incompatible with the MDR technique over the specified range of test conditions.

Supercritical Conditions. Investigation of the secondary atomization and vaporization mechanisms using single-drop, cold flow tests requires the reduced pressure for the simulant liquid within the test section to be greater than one. The intent of the supercritical testing is to determine what effect a reduced pressure ratio greater than 1 has on the breakup and vaporization of a drop exposed to a pressure disturbance. As previously indicated, the range of engine parameters will be essentially identical to the ones investigated in the subcritical phase, but with the inclusion of an additional parameter, the critical pressure ratio. Of course only the configurations corresponding to rocket engines which operate in the supercritical regime will be matched.

The procedure for matching the conditions is defined using the following parameters: droplet Re/D; reduced pressure ratio (P_1/P_{cr}); density ratio (ρ_ℓ/ρ_1); liquid viscosity; and liquid surface tension. Shock tube station pressures and temperatures are again the unknowns. If the test section gas is fixed, the solution for chamber pressure will be redundant because both ρ_ℓ/ρ_1 and P_1/P_{cr} are specified. Hence the composition of the station 1 gas also requires solution. The composition of the driver gas is assumed known.

Table VII. Possible Subcritical Secondary Atomization Test Conditions

	Liquid	Chamber Gas	P_1 (MPa)	$\frac{P_2}{P_1}$	$\frac{T_2}{T_1}$
Coaxial LOX/H_2 (Inj.H_2)	H_2O	Ar	1.72	1.6 – 3.1	1.2 – 1.6
	Freon22	Ar	2.10	1.5 – 2.8	1.2 – 1.5
	n – Pentane	Ar	1.07	1.8 – 4.0	1.2 – 1.8
	LOX	Ar	2.00	1.5 – 2.8	1.2 – 1.5
	Freon12	Ar	2.24	1.5 – 2.7	1.2 – 1.5
	Freon113	Ar	2.83	1.4 – 2.4	1.1 – 1.4
Coaxial LOX/H_2 (Comb.)	H_2O	N_2	1.14	1.1 – 1.6	1.0 – 1.1
	Freon22	N_2	1.38	1.1 – 1.5	1.0 – 1.1
	n – Pentane	N_2	0.72	1.1 – 1.9	1.0 – 1.2
	LOX	N_2	1.31	1.1 – 1.5	1.0 – 1.1
	Freon12	N_2	1.48	1.1 – 1.5	1.0 – 1.1
	Freon113	N_2	1.86	1.1 – 1.4	1.0 – 1.1
Coaxial LOX/H_2 (Sat.LOX)	N_2O	30/70 (N_2/He)	1.90	1.1 – 1.4	1.0 – 1.1
Coaxial LOX/CH_4 (Comb.)	H_2O	N_2	1.52	1.1 – 1.5	1.0 – 1.1
	Freon22	N_2	1.86	1.1 – 1.4	1.0 – 1.1
	n – Pentane	N_2	0.96	1.1 – 1.7	1.0 – 1.1
	LOX	N_2	1.76	1.1 – 1.4	1.0 – 1.1
	Freon12	N_2	2.00	1.1 – 1.4	1.0 – 1.1
	Freon113	N_2	2.52	1.1 – 1.3	1.0 – 1.1
RL10 (Inj. H_2)	H_2O	N_2	0.41	1.4 – 2.5	1.1 – 1.3
	Freon22	He	2.38	1.1 – 1.4	1.0 – 1.1
	n – Pentane	N_2	0.28	1.7 – 3.2	1.1 – 1.4
	LOX	He	2.22	1.1 – 1.4	1.0 – 1.1
	Freon12	He	2.52	1.1 – 1.4	1.0 – 1.1
	Freon113	N_2	0.69	1.3 – 2.0	1.1 – 1.2
RL10 (Comb.)	H_2O	N_2	0.28	1.1 – 1.9	1.0 – 1.2
	Freon22	He	3.63	1.2 – 1.7	1.1 – 1.2
	n – Pentane	N_2	0.17	1.2 – 2.4	1.0 – 1.3
	LOX	He	3.40	1.2 – 1.7	1.1
	Freon12	He	3.85	1.2 – 1.6	1.1 – 1.2
	Freon113	N_2	0.45	1.1 – 1.6	1.0 – 1.1
Preburner (Comb.)	H_2O	N_2	1.24	1.2 – 2.6	1.0 – 1.3
	Freon22	N_2	1.55	1.1 – 2.3	1.0 – 1.3
	n – Pentane	N_2	0.79	1.3 – 3.3	1.1 – 1.4
	LOX	N_2	1.45	1.2 – 2.4	1.0 – 1.3
	Freon12	N_2	1.65	1.1 – 2.3	1.0 – 1.3
	Freon113	N_2	2.07	1.1 – 2.1	1.0 – 1.2

Table VIII. Possible Subcritical Vaporization Test Conditions

	Liquid	Chamber Gas	P_1 (MPa)	$\frac{P_2}{P_1}$	$\frac{T_2}{T_1}$
Coaxial LOX/H_2 (Inj.H_2)	Ethanol / Methanol	N_2	1.93	1.4 – 2.6	1.1 – 1.4
	n – Decane	N_2	1.79	1.5 – 2.7	1.1 – 1.4
Coaxial LOX/H_2 (Comb.)	Ethanol / Methanol	N_2	0.90	1.1 – 1.8	1.0 – 1.2
	n – Decane	N_2	0.83	1.1 – 1.8	1.0 – 1.2
Coaxial LOX/CH_4 (Comb.)	Ethanol / Methanol	N_2	1.21	1.1 – 1.6	1.0 – 1.1
	n – Decane	N_2	1.10	1.1 – 1.6	1.0 – 1.2
RL10 (Inj. H_2)	Ethanol / Methanol	N_2	0.34	1.6 – 2.9	1.1 – 1.4
	n – Decane	N_2	0.31	1.6 – 3.0	1.1 – 1.4
RL10 (Comb.)	Ethanol / Methanol	N_2	0.21	1.1 – 2.1	1.0 – 1.2
	n – Decane	N_2	0.21	1.1 – 2.2	1.0 – 1.2
Preburner (Comb.)	Ethanol / Methanol	N_2	1.00	1.2 – 2.9	1.1 – 1.4
	n – Decane	N_2	0.90	1.2 – 3.0	1.1 – 1.4

Table IX. Possible Supercritical Test Conditions

	Liquid	Chamber Gas (N_2/He)	$\frac{P_1}{P_{cr}}$	$\frac{P_2}{P_1}$	$\frac{T_2}{T_1}$
Coaxial LOX/H_2 (Inj.H_2)	n – Octane	40/60	1.5	1.72	1.19
	n – Pentadecane	80/20	1.5	1.8 – 2.5	1.2 – 1.4
	n – Decane	50/50	1.5	1.75	1.20
Coaxial LOX/H_2 (Comb.)	n – Octane	10/90	1.5	1.1 – 1.4	1.0 – 1.1
	n – Pentadecane	30/70	1.5	1.1 – 2.0	1.0 – 1.3
	n – Pentadecane	10/90	3.0	1.1 – 1.3	1.0 – 1.1
	Freon12	10/90	1.5	1.05 – 1.11	1.02
	n – Decane	10/90	1.5	1.1 – 1.9	1.0 – 1.2
	n – Decane	0/100	3.0	1.07	1.02
	LOX	10/90	1.1	1.1 – 1.2	1.0 – 1.1
Coaxial LOX/CH_4 (Comb.)	n – Octane	20/80	1.5	1.1 – 1.8	1.0 – 1.2
	n – Pentadecane	40/60	1.5	1.1 – 1.9	1.0 – 1.2
	n – Pentadecane	10/90	3.0	1.1 – 1.3	1.0 – 1.1
	Freon12	20/80	1.5	1.05 – 1.10	1.02
	n – Decane	20/80	1.5	1.1 – 1.8	1.0 – 1.2
	n – Decane	0/100	3.0	1.06	1.02
	LOX	20/80	1.1	1.1 – 1.2	1.0 – 1.1
Preburner (Comb.)	n – Octane	10/90	1.5	1.3 – 2.0	1.1 – 1.3
	n – Pentadecane	30/70	1.5	1.3 – 2.2	1.1 – 1.3
	n – Pentadecane	10/90	3.0	1.2 – 1.5	1.1
	n – Decane	20/80	1.5	1.3 – 2.0	1.1 – 1.3
	LOX	10/90	1.1	1.18	1.06

Solution over the range of liquids provided in Table VI leads to the conclusion that a mixture of helium and nitrogen will serve as the ideal chamber gas simulant. The STE engine values for reduced pressure ($\simeq 3$) and the cut-off level of 1.5 can be investigated with the general result that the higher critical pressure ratio cases are limited to the lower Re conditions due to supply pressure bounds. As mentioned previously, the diagnostic techniques used to study the vaporization mechanism at supercritical pressures may require the presence of O_2 molecules. Hence reduced pressures less than 1.5 may need to be employed to accommodate the LOX P_{cr} of 5.07 Mpa (736 psia) and the maximum chamber pressure of 6.9 Mpa (1000 psia). Table IX provides the results for the supercritical, secondary atomization and vaporization simulant fluids and test conditions. For all cases given in Table IX, the chamber gas mixture is represented as (% volume N_2)/(% volume He).

VERIFICATION OF APPLICABILITY OF MECHANISMS (TASK 3)

There are numerous analytical models and/or stability correlations that can be used to verify the applicability of the mechanisms investigated to the combustion instability of a rocket. The approach which will be followed in this program is to relate the response of the secondary atomization and vaporization processes to the time-dependent spray combustion energy release rate.

This effort will parallel the experimental portion of the effort and will be performed primarily by the research group at UCI under Professor Sirignano's guidance. It will involve a theoretical/computational effort to place existing spray combustion theoretical models in a useful form to treat situations where oxygen vaporization is the rate-controlling factor. Current models have been developed for hydrocarbon fuel droplets vaporizing under subcritical conditions. Initial effort will concentrate on adjusting these transient droplet heating and vaporization models so that liquid-propellant rocket combustion can be studied. The intention here is to have the models in a form for ready use in comparison with experimental results while the experiments are operating.

This effort will not be a fully independent research program because of the funding constraints of the program. Advantage will be taken of other research programs at UCI addressing theoretical models of spray combustion. Existing computer codes from these other programs will be employed as a base for this new study, with suitable modifications for the rocket combustion process and environment.

Effort at UCI over the past decade has been directed toward simplified transient vaporization models which are physically accurate but sufficiently computationally efficient so that hundreds or thousands of droplets in a spray combustor can be tracked. In parallel with the development of simplified vaporization modeling, UCI has pursued "exact" solutions (via finite-difference calculations) of the flow and thermal fields surrounding and within vaporizing droplets. These Navier-Stokes solutions serve two major purposes: 1) correlations for quantities such as droplet drag coefficients are obtained that can be used in spray combustion analyses with the simplified models (which do not independently predict drag coefficients) and 2) the exact solutions can be used as a standard for comparison of the simplified models.

Similar types of improvement and movement towards readiness will be made with atomization models, with emphasis on secondary atomization. The intent here is to obtain a model that predicts droplet size distribution as a function of local, instantaneous conditions in the rocket combustion chamber.

The models selected will be studied using sensitivity analyses. The available and new analytical results will be systematically compared to the experimental data. The goal will be to verify the controlling mechanisms by showing that the responses of the processes, when modeled analytically, result in predicted instabilities.

In the final year of the program, the developed spray combustion computer programs will be used to simulate the experimental runs. The parameter surveys in the calculations will extend beyond the experimental range. This extension will aid in the prediction of trends and in the suggestion of parameter modifications for the experiments. Based upon comparisons with the experimental results, some adjustment in the theoretical models might occur.

PRIORITIZED PLAN FOR FUTURE EFFORT (TASK 4)

INCLUSION INTO STABILITY MODELS

Effort under this element addresses methods to apply the information and insight gained during the analytical and experimental phases of the Liquid Stability Mechanisms program, to models for analyzing and eventually suppressing the initiation of combustion instability. For example, characteristic times for combustion processes can, in principle, be modified to cause out-of-phase feedback to acoustical oscillations. Modifications to the combustion process can cause a responsive phenomenon to become less sensitive to fluctuating conditions. The location in the chamber of a particular combustion process can be modified to minimize the magnitude of the feedback to the oscillation.

FURTHER INVESTIGATION OF MECHANISMS

Effort under this part will concentrate on plans for investigation of additional mechanisms of three kinds. The first, and by far the most likely, would be mechanisms that had been identified during the current program but which time or staffing constraints prohibited testing despite the desirability of doing so. The second would involve investigation of additional mechanisms which have come to the attention of the investigators during the planned testing. The third type would be required if all selected mechanisms had been investigated during the present program and all were conclusively shown to be instability nonparticipants. In this case the effort under Task 1 of the current program would have to be repeated, followed by a repeat of Task 2 and subsequent efforts.

ADDRESS OF UNRESOLVED TECHNICAL ISSUES

Effort under this portion of Task 4 would identify plans to address any technical issues which have not been resolved. It is likely that these will primarily revolve around difficulties in obtaining desired measurements due to the extreme conditions anticipated for these tests. One foreseeable difficulty involves obtaining valid spray droplet size measurements in the dense spray environments expectable at elevated-pressure tests with low surface tension fluids. Other difficulties might involve uncertainties over whether a repeatable perturbation causes a repeatable response.

NOMENCLATURE

VARIABLES

D	Droplet diameter
F	Fuel
$\overline{M}$	Molecular weight
O	Oxidizer
P	Static pressure
P_{vap}	Saturation pressure at 535°R
r	Droplet radius
Re	Reynolds number
T	Temperature
V	Velocity
We	Weber number
γ	Specific heat ratio
ρ	Density
σ	Surface tension
μ	Viscosity

SUBSCRIPTS

1	Test section of pulse tube
2	Region directly upstream of pulse
4	Pulse tube driver section
ℓ	Liquid
g	Gas
c	Chamber
cr	Critical property

ABBREVIATIONS

Comb.	Combustion gas
Inj.	Injected
Sat.	Near-saturated

ACKNOWLEDGEMENTS

The authors gratefully acknowledge the contributions of Professors W. A. Sirignano, G. S. Samuelsen, and R. H. Rangel of the University of California, Irvine; T. W. Eastes of the University of California, Irvine; and L. J. Spadaccini and M. Winter of United Technologies Research Center in the preparation of this paper.

REFERENCES

1. Winter, M. and Anderson, T. J., "Measurements of the Effect of Acoustic Disturbances of Droplet Vaporization Rates," 28th JANNAF Combustion Meeting, San Antonio, Oct. 28 - Nov. 1, 1991.
2. Sirignano, W. A., Delplanque, J. P., and Chiang, C. H., "Numerical Simulation and Modeling of LOX Droplet Vaporization at Supercritical Conditions," 28th JANNAF Combustion Meeting, San Antonio, Oct. 28 - Nov. 1, 1991.
3. Cox, G. B. Jr., "The Liquid Stability Mechanisms Program," 27th JANNAF Combustion Meeting, Cheyenne, Nov. 1990.
4. Heidmann, M. F., and Groeneweg, J. F., "Analysis of the Dynamic Response of Liquid Jet Atomization to Acoustic Oscillations," NASA TN D-5339, 1969.
5. Heidmann, M. F., "Effect of Steady Velocities on the Dynamic Response of Liquid Jet Atomization," NASA TN D-5565, 1969.
6. Ingebo, R. D., "Atomization of Ethanol Jets in a Combustor with Oscillatory Combustor-Gas Flow," NASA TN D-3513, 1966.

7. Tong, A. Y. and Sirignano, W. A., "Vaporization Response of Fuel Droplet in Oscillatory Field," Paper No. 87-HT-58, National Heat Transfer Conference, Aug. 9-12, 1987.

8. Sirignano, W. A., Riva, G., Tong, A., Abramzon, B., and Molavi, K., "Spray Combustion: A Driving Mechanism For Ramjet Combustion Instability," 23rd JANNAF Combustion Meeting, Vol. 1, Oct. 1986.

9. S-X Qian, Snow, Judith B., H-M Tzeng, and Chang, Richard K., "Lasing Droplets: Highlighting the Liquid-Air Interface by Laser Emission", American Association for the Advancement of Science, Vol. 231 pp 485-488, Jan. 31, 1986.

10. H-M. Tzeng, Wall, K. F., Long, M. B., and Chang, R. K., "Evaporation and Condensation Rates of Liquid Droplets Deduced From Structure Resonances in the Fluorescent Spectra", *Optics Letters*, Vol. 9, p 273, July 1984.

11. H-M. Tzeng, Long, M. B., Chang, R. K., and Barber, P. W., "Laser-Induced Shape Distortions of Flowing Droplets Deduced From Morphology-Dependent Resonances in Fluorescent Spectra," *Optics Letters*, Vol. 10 P. 210, May 1985.

12. Jensen, R. J., Dodson, H. and Trueblood, B., "Oxygen/Methane Combustion Stability Investigation," paper presented at the 1988 Advanced Earth-to-Orbit Technology Conference, Huntsville, AL, May 1988.

13. Philippart, K. D. and Moser, M. D., "Stability Analyses of Liquid Oxygen/Methane Injectors Using Currently Available Analytical Tools," AIAA-88-2851, 24th Joint Propulsion Conference, Boston, July 11-13, 1988.

14. Jensen, R. J., Dodson, H. C. and Claflin, S. E., "LOX/Hydrocarbon Combustion Stability Investigation," NASA Contractor Report 182249, July 1989.

15. Sato, J., Tsue, M., Niwa, M. and Kono, M., "Effects of Natural Convection on High-Pressure Droplet Combustion," *Combustion and Flame*, 82, pp. 142-150, 1990.

16. Boylan, D. M. and O'Hara, J., "Gas Velocity and Temperature Near a Liquid Rocket Injector Face," NASA CR-121100, Jan. 1973.

17. Ghafourian, A., Huynh, C., Johnson, P., Dindi, H., Mahalingam, S., and Daly, J. W., "Combustor Design for Study of Combustion Instabilities in Liquid Rocket Engines," University of Colorado at Boulder, WSS/CI 91-54, CCR Report No. 91-07, March 1991.

18. Ferrenberg, A. J. and Varma, M. S., "Atomization Data Requirements for Rocket Combustor Modeling," presented at the 21st JANNAF Combustion Meeting, John Hopkins Univ., 1-4 Oct., 1984.

19. Gross, Klaus, "Liquid Engine Jet Atomization Workshop Report," 24th JANNAF Combustion Meeting, Monterey, CA, CPIA 476, Oct. 5-9, 1987.

20. Krulle, G., Mayer, W., and Schley, C.-A., "Recent Advances in H_2/O_2 High Pressure Coaxial Injector Performance Analysis," AIAA 90-1959, 26th Joint Propulsion Conference, Orlando, July 16-18, 1990.

21. Ghafourian, A., Mahalingam, S., Dindi, H., and Daily, J. W., "A Review of Atomization in Liquid Rocket Engines," AIAA 91-0283, 29th Aerospace Sciences Meeting, Reno, Jan. 7-10, 1991.

22. Harrje, David T. and Reardon, Frederick H., editors, "Liquid Propellant Rocket Combustion Instability," NASA SP-194, 1972.

23. Kennedy, J. B., "High Weber Number SMD Correlations for Pressure Atomizers," *J. Engineering for Gas Turbines and Power*, Vol. 108, Jan. 1986, pp. 191-195.

24. Lefebvre, A. H., "Airblast Atomization," *Progress in Energy and Combustion Science*, Vol. 6, 1980, pp. 233-261.

25. Yoshida, T. and Takayama, K., "Interaction of Liquid Droplets With Planar Shock Waves," *J. of Fluids Engineering*, Vol. 112, Dec. 1990, pp. 481-486.

26. Shapiro, A. H., *The Dynamics and Thermodynamics of Compressible Fluid Flow*, Volume I, John Wiley, New York, 1953.

27. Norton, C. M., Litchford, R. J., and Jeng, S., "An Experimental Study of High-Pressure Droplet Combustion," AIAA 90-2441, 26th Joint Propulsion Conference, Orlando, July 16-18, 1990.

28. Faeth, G. M., Dominicis, D. P., Tulpinsky, J. F., and Olson, D. R., "Supercritical Bipropellant Droplet Combustion," Twelfth (International) Symposium on Combustion, Poitiers, France, July 14 to 20, 1968.

29. Hsieh, K. C. and Shuen, J. S., "Analysis of Multi-Component Droplet Vaporization at Near Critical Conditions," AIAA 88-0637, AIAA 26th Aerospace Sciences Meeting, Reno, Jan. 11-14, 1988.

30. Bradley, John M., *Elementary Shock Wave Theory*, John Wiley and Sons, New York, 1962.

31. Temkin, S. and Mehta, H. K., "Droplet Drag in Accelerating and Decelerating Flow," *JFM*, Vol. 116, pp. 297-313.

APPENDIX G - SECONDARY ATOMIZATION BY CONVECTIVE FLOWS

Secondary atomization or drop breakup is typically defined as the breakup of a liquid droplet into two or more daughter droplets by a convective gas or liquid flow. The convective flow must have relative velocity sufficient to overcome the droplet's surface tension restoring force. Secondary atomization is distinguished from primary atomization in which some volume of liquid is initially atomized from a liquid stream or sheet. So-called microexplosions of droplets and droplet collisions with other droplets or other surfaces can also result in breakup of an existing drop but will not be addressed in this review. Additionally breakup by shear flows will not be addressed here due to the presence of a recent review (Rallison, 1984).

Applications

Because of the significant number of applications and the wide variation thereof, secondary atomization has been studied over a long period of time by many different investigators. The bulk of the research has been performed in the following areas:

1. atomization of liquid fuels in preparation for and during combustion in all types of combustors (i.e., Lefebvre, 1989; Lefebvre, 1983)

2. atomization of liquids for application of paint, insecticides, drugs, and other coatings (i.e., Kwok and Liu, 1991).

3. meteorology with associated breakup of rain drops.

4. chemical industry dispersion methods such as spray drying, emulsification in liquid-liquid systems, and production of froths, foams, and aerosols (i.e., Masters, 1985; Rallison, 1984; Kay, 1974).

5. shock or detonation waves in gas/liquid systems with applications to combustion instability (i.e., Culick, 1989; Harrje and Reardon, eds., 1972; Dabora, Ragland, and Nicholls, 1969) or in liquid/liquid systems with applications to nuclear reactor safety (i.e., Tan and Bankoff, 1985; Patel and Theofanous, 1981).

6. erosion and other associated interactions between high speed aircraft and rain or steam turbines and prematurely condensing water drops (i.e., Bowden, ed. 1966).

In combustion systems, primary and secondary atomization processes prepare the liquid phase for vaporization into and mixing with the gas phase. The degree of secondary atomization determines vaporization and mixing rates of the droplet phase in the surrounding gas. In dilute sprays, vaporization is typically found to control the mixing rate. In some dense sprays, however, secondary atomization can be found to control the mixing rate (Hsiang and Faeth, 1992). Secondary atomization typically occurs in the near

injector region where ligaments of liquid break off from a jet or sheet and then further breakup as they are sheared by co-flowing gas. Another source of drop breakup is the reaction induced expansion of the combustion gases which rapidly accelerate any unburned droplets of fuel. As a liquid droplet breaks apart more of the surface area per unit volume of that phase is available for the vaporization process and the liquid is distributed about a larger volume. Thus in addition to primary atomization, secondary atomization can directly effect the distribution of the liquid phase and therefore the local gas properties such as mixture ratio of the flow field. The resulting drop size and spatial distribution affects how rapidly the mixture can be expected to burn, where it will burn relative to the injection point and what length of combustor is required to contain the reaction.

In coating applications, primary issues related to secondary atomization are concerned with how to deliver the liquid to a surface 1) before it dries, 2) without significant vaporization of the carrier liquid (usually an organic thinner or water) so that spreading can occur on impact, and 3) with the desired coverage and/or finish quality. Thus control of the degree to which droplets undergo secondary atomization can be quite important as drop size influences all three of these items. Recently, environmental issues in air assisted spray painting have made reduction of overspray and volatile organic compounds and enhancement of transfer efficiencies important considerations which require finer control of drop size distribution and thus secondary atomization effects.

In meteorology, secondary atomization influences the size, velocity, and distribution of rain drops, hail, sleet, and snow. Researchers are interested in how raindrop size and velocity impact soil, animals, foliage, structures, and vehicles. Prediction and prevention of destructive effects of precipitation is a major goal. Erosion associated with raindrop impact is the primary concern, and literally causes billions of dollars of damage each year.

In the chemical industry, dispersion methods whereby a particulate phase is distributed in a continuous phase are important in the manufacturing of many products. Spray drying is used to create powders like soap and milk. In spray drying, the degree of secondary atomization can determine the final particle size. Liquid-liquid emulsifications are used to produce products like mayonnaise and shampoo. Emulsions are mixtures of components that are otherwise immiscible. Secondary atomization by both convective flow and shear can play a role in agitators designed to break the dispersed phase into droplets of colloidal dimensions where emulsifying agents can act to decrease surface tension and prevent coalescence and eventual separation of the components.

For detonations in gas/liquid systems, secondary atomization may play a role in sustaining the detonation. In high frequency combustion instability in liquid rocket engines, a spontaneously generated shock wave can cause propellant droplets to shatter with a consequence of more rapid vaporization and combustion. When the associated heat release is sufficiently in phase with the pressure wave, such an instability can develop. Here secondary atomization may play an indirect role in providing a vaporized liquid propellant to the gas phase for combustion in phase with the passing wave.

In liquid metal fast breeder reactors, a hot liquid (fuel) is sometimes brought in contact with a cold vaporizable liquid (coolant) with a resulting explosive interaction termed a vapor explosion or fuel coolant interaction. The secondary atomization in this case occurs when a vapor explosion generated pressure wave fragments molten uranium oxide (fuel) droplets present in liquid sodium (coolant) resulting in production of new interfacial area of the molten fuel, thus enabling rapid heat transfer necessary to sustain the propagation of the pressure wave.

In supersonic aircraft, leading edge erosion by raindrops is a concern. The aircraft skin, windows and internal engine parts are all subject to impact by raindrops. While typical sized raindrops (1-5 mm) could cause damage to a supersonic aircraft due to the high relative speed, the aircraft is preceded by a shock which acts to break apart such a drop into droplets on the order of a few microns in size. Droplets of this size are probably incapable of causing erosion of the intercepted object, and thus the secondary atomization process protects the supersonic aircraft. Nonetheless, the time and distance traveled prior breakup and impingement on surfaces is of concern in situations where the shock is close to the structure. Thus reduction in damage can be achieved by designing a body whose detached shock is sufficiently far removed so as to allow drop fragmentation to be completed. Additionally, the initial diameter plays a role in the size of the daughter droplets. Consequently, there is an initial diameter below which the daughter droplets will impinge on the vehicle with insignificant mass.

In steam turbines, a fine mist droplets arising in spontaneous condensation indirectly causes erosion of internal surfaces. These droplets collect on structural components and are detached in large drops which undergo secondary atomization and impinge on turbine blades causing erosion.

While the applications are varied, many aspects of the same basic phenomena are observed from application to application. Questions and issues of common interest in the study of this phenomena are as follows

1. How does breakup occur?
2. Under what flow conditions does it occur?
3. How is the drop deformed and what is its drag coefficient history prior to breakup?
4. How long does the process take?
5. At what rates does it occur?
6. What drop sizes are produced and what influences these drop sizes?
7. How are the daughter droplets distributed in the flow field and what are their velocities?

Literature Review

Previous Reviews. While there is a substantial portion of the literature devoted to atomization in general, secondary atomization is usually considered a subset thereof. Thus reviews of atomization usually include sections on secondary atomization. Ferrenberg, Hunt, and Duesberg (1985) contains the most recent such review. Lapple, Henry, and Blake (1967), while dated, is comprehensive and also contains a section on secondary atomization. Hinze (1955) has reviewed early work specific to drop breakup, while more recent, yet still relatively dated reviews, include those of Harvey (1973), Forsnes and Ulrich (1968), and Luna and Klikoff (1967). Forsnes and Ulrich (1968) in particular, has annotated reviews of hard-to-find early work.

Diagnostic Techniques. Diagnostic techniques for study of this phenomena have typically employed use of high speed cameras to obtain images for qualitative analysis of the process. Shock tubes or tubes through which a gas stream is passed are the test articles of choice. Techniques for introducing the drop to these flows include suspension of pendant droplets from capillary tubes and wires, acoustic levitation, solenoidal retraction of a wire with a pendant drop on its tip, and injection into the gas stream by a drop generator.

More recently, holography has been employed to observe the product droplets of the secondary atomization process and computer aided image analysis applied to size the product droplets (Hsiang and Faeth, 1992). High speed holographic cinematography is under consideration, but has yet to be developed for this application.

Characterizing Parameters. As in many other areas of fluid mechanics the dimensionless parameters which are used to characterize drop breakup behavior are ratios of forces and times. For the sake of discussion, the ensuing descriptions shall be written from a standpoint of a liquid droplet with relative velocity to a surrounding gas, as this is the most commonly researched situation.

The relative convective flow over the drop surface exposes it to inertial forces of the convective gas flow which impose normal pressure and shear forces on its surface. The ratio of these forces is roughly proportional to the Reynolds number given as

$$\mathrm{Re} = \rho U_{rel} D_o / \mu \qquad \text{(G-1)}$$

The drop also experiences surface tension forces which act tangential to the droplet surface and act to maintain its spherical shape. The normal pressure forces induced by the convective flow act to deform the droplet from this spherical shape. The ratio of these dynamic pressure forces to surface tension forces is proportional to the Weber number given as

$$\mathrm{We} = \rho U_{rel}^2 D_o / \sigma \qquad \text{(G-2)}$$

The drop also experiences body forces, analogous to gravity, due to acceleration or deceleration of the surrounding convective flow. Such forces are uniform on every fluid particle in an undeformed droplet and are opposite to the direction of the acceleration. The surface becomes unstable when this force points in a direction from the less dense to the more dense fluid. For liquid drops accelerating in gas flows this occurs on the windward face of the droplet. For an open container of liquid this occurs when the container is inverted from its otherwise stable state and the liquid begins to pour out under the influence of gravity. The force opposing this instability in the liquid surface is surface tension. The ratio of acceleration forces to surface tension forces is proportional to the Bond number given as

$$Bo = \rho_o a D_o^2 / \sigma \qquad \text{(G-3)}$$

If the acceleration is caused by relative motion of the surrounding gas and the droplet, then the acceleration can be related to the drag force and the bond number can be given in terms of the Weber number as

$$Bo = 3C_D We/4 \qquad \text{(G-4)}$$

A related dimensionless parameter used to describe bubbles rising under the influence of bouyancy has recently been applied in the discussion of drop breakup by Faeth (1992) and is very similar to the Bond number. The Eotvas number is given as

$$Eo = (\rho_o - \rho) a D_o^2 / \sigma \qquad \text{(G-5)}$$

This number is virtually equivalent to the Bond number for most atmospheric situations but can change substantially for low liquid/gas density ratios.

The deformation of a drop from its stable spherical shape tends also to be prevented by liquid viscous forces in the droplet interior. The deformation process is longer for drops with high liquid viscosities and shorter for low liquid viscosities. In transient convective gas flows, the viscosity can be considered as a rate limiting parameter. If a droplet of relatively high liquid viscosity is unable to achieve an unstable shape during the passing of a shock for instance, breakup may be prevented. Oscillation periods of the droplet surface could also be expected to be directly proportional to the drop liquid viscosity. The ratio of liquid viscous forces to surface tension forces is proportional to the Ohnesorge number given as

$$Oh = \mu_o / (\rho_o D_o \sigma)^{1/2} \qquad \text{(G-6)}$$

In a proliferation of dimensionless parameters, the Laplace number is given as

$$La = 1/Oh^2 \qquad \text{(G-7)}$$

A number of researchers have by dimensional analysis found a dimensionless time to breakup of the form,

$$\tau_b = K(\rho / \rho_o)^{1/2} U_{rel} t_b / D_o \qquad \text{(G-8)}$$

where the reference time is that time required to traverse one drop diameter in the gas fixed coordinate system and is given by

$$t_{ref} = D_O / U_{rel} \qquad \text{(G-9)}$$

Whether the drop breaks apart or oscillates the natural oscillation period of the droplet given by Rayleigh (1945) as

$$t_v = \pi / 4(\rho_o D_o^3 / \sigma)^{1/2} \qquad \text{(G-10)}$$

is expected to play an important role, especially in transient flow conditions where the aerodynamic forces may initiate such an oscillation.

Types of Breakup. There have been three basic types of droplet breakup observed, "bag", "shear", and "catastrophic". Others described in the literature appear to be transitional or combinations of varying degrees of these three basic types.

The bag type of breakup is characterized by deformation of the droplet into an ellipsoid with its semimajor axis perpendicular to the flow direction. As the droplet flattens, its radius of curvature at the axis of symmetry increases and the stagnation pressure is felt over a larger area. Eventually an unstable situation is achieved whereby the center of the drop is pushed downstream of the outer edge forming a thin membrane in the shape of a bag or parachute with the outer edge forming an annular ring of fluid with the bulk of the liquid mass. The bag bursts creating a fine mist of droplets followed by failure of the annular ring breaking into larger droplets. Bag type breakup typically occurs at Weber numbers just above critical values and requires that the flow duration be applied significantly longer than required in shear or catastrophic breakup. Photographic evidence of this mode of breakup is widely available (Krzeckowski, 1980; Reichman and Temkin, 1974; Simpkins, 1974; Wolfe and Anderson, 1964; Hanson, Domich, and Adams, 1963; Rabin, Schallenmuller, Lawhead, 1960). See Figure G-1 for a typical example.

A commonly observed transitional mode observed between bag and shear regimes is the "parasol" or "bag-stamen" type in which a re-entrant spike of fluid emanates back into the oncoming flow from the stagnation point and remains as the rim and the remaining portion of the bag disintegrate and blow downstream. Photographic evidence of this mode of breakup is also widely available (Krzeckowski, 1980; Simpkins, 1974; Wolfe and Anderson, 1964; Hanson, Domich, and Adams, 1963). See Figure G-2 for a typical example.

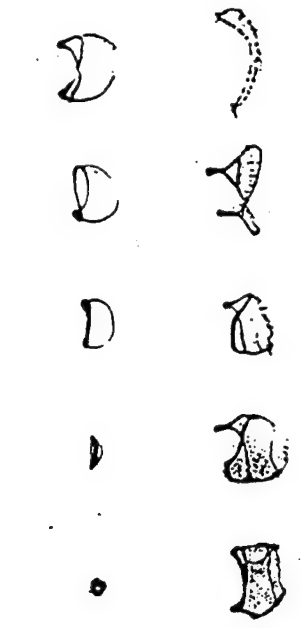

We = 11 (FROM LANE & GREEN)

Figure G-1
Typical Bag Mode Droplet Breakup

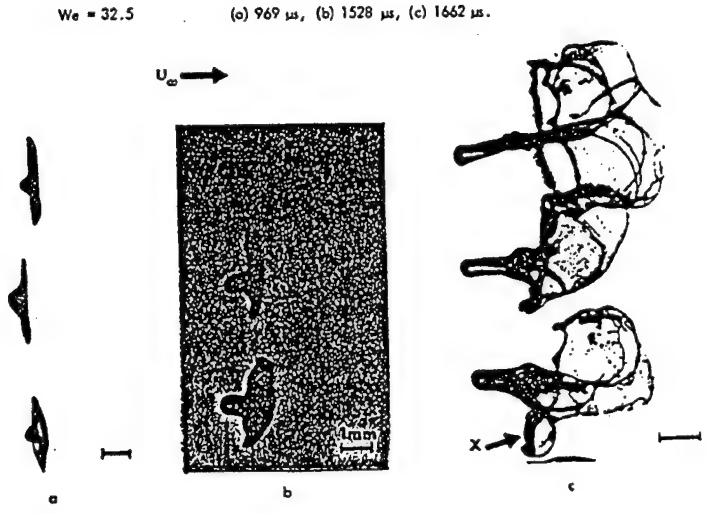

Figure G-2
Typical Parasol Mode Droplet Breakup

The shear type of breakup is characterized by deformation of the droplet into a lenticular shape with small waves forming on the windward side and liquid from the crests of these waves being eroded off by aerodynamic shear and capillary wave breakup and is typically attributed to Kelvin-Helmholtz instability. The droplets which compose the mist are so small that they tend to follow the streamlines in the wake of the original drop. This type of breakup occurs at $O(10^2) < Bo < O(10^5)$. Photographic evidence of this mode of breakup is also available (Krzeckowski, 1980; Simpkins, 1974; Ranger and Nichols, 1972; Simpkins and Bales, 1972; Ranger and Nichols, 1969; Dickerson and Schuman, 1965; Wolfe and Anderson, 1964; Hanson, Domich, and Adams, 1963; Rojec, 1963; Rabin, Schallenmuller, Lawhead, 1960; Rabin and Lawhead, 1959; Gordon, 1959; Engel, 1958; Lane, 1951). Of these, Rojec (1963) shows the most detail in photographs of a suspended droplet. See Figure G-3 for a typical example.

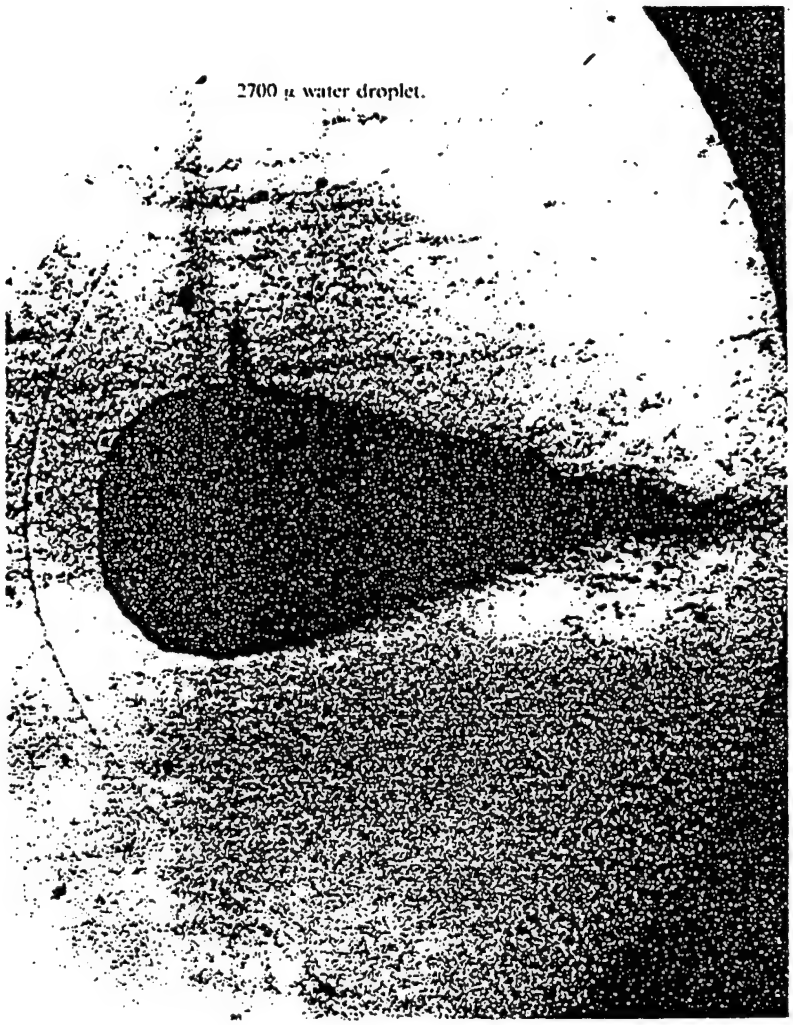

Figure G-3
Typical Shear Mode Droplet Breakup

The catastrophic type is characterized by rapid growth of surface waves on the windward face of the droplet with abrupt disintegration of drop before significant distortion or stripping. This is attributed to growth of acceleration waves induced by the rapid convective flow about the drop and is also known as the Rayleigh-Taylor instability regime. This behavior is observed at $Bo > O(10^5)$. Reinecke and Waldman (1970) and Reinecke and McKay (1969) used an X-ray absorption technique which yielded microdensitometry traces on X-ray plates to determine rate parameters associated with the droplet mass.

Borisov et al. (1981) has suggested criteria for breakup by these different mechanisms as follows:

"bag" breakup:

$$8 < We < 40$$
$$0.2 < WeRe^{-0.5} < 1.6 \qquad \text{(G-11)}$$

"shear" breakup:

$$20 < We < 2 \times 10^4$$
$$1 < WeRe^{-0.5} < 20 \qquad \text{(G-12)}$$

"explosive" or "catastrophic" breakup:

$$2 \times 10^3 < We < 2 \times 10^5$$
$$20 < WeRe^{-0.5} < 2 \times 10^2 \qquad \text{(G-13)}$$

Effect of Flow Transients. A number of researchers (Rabin and Lawhead, 1959; Lane, 1951; Hinze, 1948b) have distinguished between the breakup behavior of a droplet in a steady stream of gas as opposed to a transient stream of gas such as that experienced in the passing of a shock. Shock tube tests by Gordon (1959) indicate that the type of breakup and critical Weber number were strongly influenced by the duration and velocity of flow behind the shock wave. The gas flow history about the drop and the motion and deformation histories of the drop are transient in nature unless the droplet is introduced stably to the gas stream at its terminal velocity. This is obviously not a common occurrence in nature and a drop is either accelerating or decelerating depending on the velocity at which it is introduced to the gas flow. The time varying external forces of pressure, frictional drag, and body forces applied to the droplet as it deforms determine how the breakup process occurs. Characteristic times associated with deformation, oscillation, flow duration, surface wave period, and others ultimately control this process.

The "steady" case is actually quasi-steady since the droplet is actually accelerating or decelerating due to the drag force. In this case the acceleration is gradual and any initial disturbance associated with it is small. Falling raindrops or a drop detaching from an

accelerating mass of liquid exemplify this case. For this type of flow the existence of a critical Weber number or speed above which breakup occurs is typically found for a given liquid.

In transient flow conditions, the droplet is typically suddenly exposed to a convective gas stream following a shock. Shock tubes are most commonly used to investigate this phenomena (Hsiang and Faeth, 1992; Temkin and Ecker, 1989; Weirzba and Takayama, 1988; Yoshida, Weirzba and Takayama, 1988; Temkin and Mehta, 1982; Borizov et al., 1981; Krzeckowski, 1980; Reichman and Temkin, 1980; Temkin and Kim, 1980; Simpkins, 1974; Ranger and Nichols, 1972; Reinecke and Waldman, 1970; Simpkins and Bales, 1972; Reinecke and McKay, 1969; Ranger and Nichols, 1969; Dickerson and Schuman, 1965; Haas, 1964; Wolfe and Anderson, 1964; Hanson, Domich, and Adams, 1963; Rojec, 1963; Rabin, Schallenmuller, Lawhead, 1960; Rabin and Lawhead, 1959; Gordon, 1959; Engel, 1958; and Lane, 1951). Rabin, Schallenmuller, and Lawhead (1960) have suggested that the acceleration applied to the droplet as well as the duration of the flow have the greatest bearing on the breakup phenomena. To this end, the Bond number has been found to characterize the time over which the droplet deforms and breaks up for low Ohnesorge number droplets. A droplet subject to such a flow field is susceptible to both catastrophic and shear breakup. However bag mode breakup, while requiring longer duration flow fields, has also been observed in shock tubes (Eastes and Samuelsen, 1993; Hanson, Domich, and Adams, 1963).

Taylor (1949) found that the value of the critical Weber number for a droplet in a steady gas stream to be a factor of $2^{1/2}$ greater than that for the same droplet in a transient gas stream if the oscillation period does not substantially exceed the flow duration.

Deformation. The shape of a droplet falling under the influence of gravity in a steady is influenced by surface tension forces, hydrostatic forces within the droplet, shape dependent aerodynamic forces, internal circulation of the droplet fluid, oscillations whether natural or excited, viscosities of the droplet liquid and the convective gas flow, boundary layer separation at some point on the drop surface, vortex shedding, and the drop diameter itself.

As previously inferred, deformation is a critical stage in both bag and shear type breakup. In each case the pressure distribution about the drop, itself a function of the drop shape, creates a pressure difference between the windward and leeward sides of the drop which tends to flatten it. If the deformation is insufficient to break up the droplet it may vibrate or oscillate in any number of modes. The deformation need not be linear as breakup is not always a forgone conclusion in a nonlinear deformation. For bag mode breakup, this process has been observed to flatten the drop so that the lateral spread is on the order of three to four initial drop diameters prior to breakup (Ranger and Nichols, 1969). This severe extent of deformation does not lend itself well to a linearized solutions of low wave number disturbances associated with bag mode breakup, but is adequate for large wave number disturbances associated with shear and catastrophic breakup modes (Harvey, 1973).

Hinze (1948a) linearized the hydrodynamic equations of motion of the drop and considered normal pressure distribution as the deforming forces to obtain closed form solutions for very low and very high liquid viscosities. For low viscosity drops, where $Oh^2 << 1$, he calculated the normalized deformation as

$$\delta/D_0 = -0.0425We_{cr} \qquad \text{(G-14)}$$

and for high viscosity drops, where $Oh^2 >> 1$, he calculated the normalized deformation as

$$\delta/D_0 = -0.02375We_{cr} \qquad \text{(G-15)}$$

Determination of droplet shape has typically been accomplished using regular perturbation techniques at very low We such as that by Frankel and Weihs (1983). Harper, Grube, and Chang (1972) have more recently shed new light on the drop response phenomena in a so-called "unified theory" by employing modern perturbation techniques and obtained solutions in the form of an expansion for small values of gas to liquid density ratio, ε. They have also calculated that the value of Bond number associated with the critical Weber number is O(1) and less than 44.9. Above the lowest critical value of Bond number, 44.9, the drop is unstable to small disturbances of arbitrary form. However up to a Bond number of 4×10^5, the rate of growth of unstable modes is small compared to aerodynamic distortion. In this so-called "quasi-stable" regime, $4 \times 10^2 < Bo < 4 \times 10^5$, deformation is algebraic and breakup is apparently due to boundary layer stripping. For convenience, their plot of these regimes of dynamic response is presented in Figure G-4.

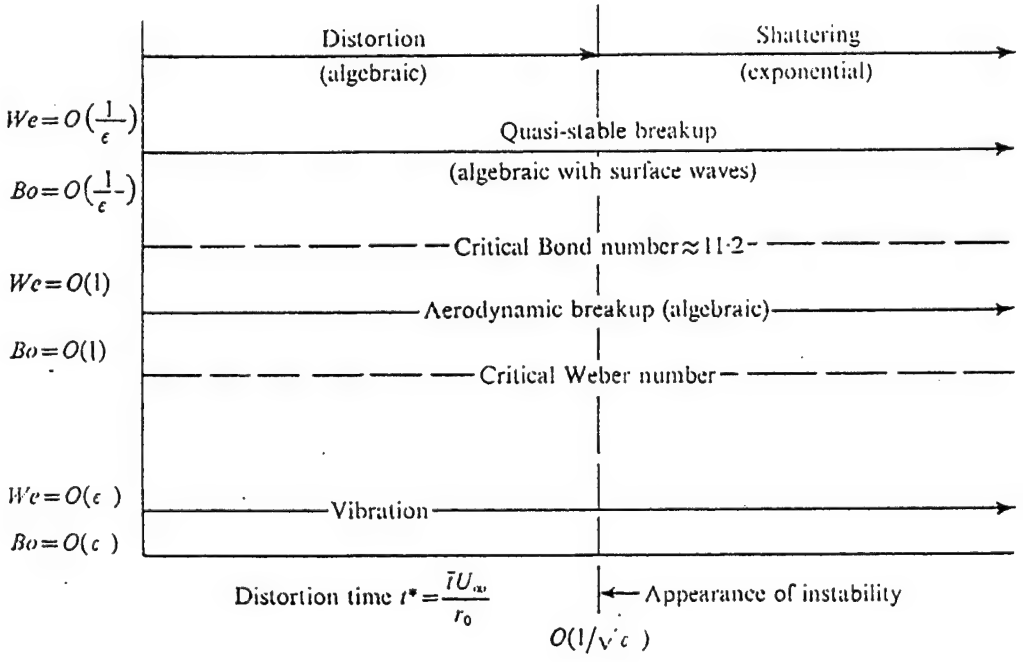

Figure G-4
Regimes of Dynamic Response

The most recent work has brought finite difference techniques to bear in the investigation of both deformation and breakup. Liang, Eastes, and Gharakhani (1988) employed direct numerical simulation with a volume-of-fluid technique to track the free surface to examine both bag and shear mode breakup. Qualitative agreement with breakup times, drag coefficients, and shapes from experimental photos was achieved. Other researchers (Deng and Jeng, 1990; Dwyer and Dandy, 1989; Fritts, Fyfe, and Oran, 1984) have employed Lagrangian grids to track the free surface deformations and obtained similar results.

Critical Weber Number. While deformation and breakup phenomena are experimentally well established, attempts to predict the critical conditions associated with breakup are for the most part limited to semi-empirical approaches. Advances in perturbation analysis and direct numerical simulation offer renewed hope.

Hinze (1984a) postulated the existence of a critical Weber number above which breakup would occur. While a critical quantity should be unique by definition, values over one and a half orders of magnitude (from 1 to about 50) are routinely given in the literature. Hinze (1955) modified his original Weber criteria to include the effect of viscosity and found the equivalent of

$$We_{cr} = C(1 + \alpha\varepsilon^{1/2}Oh). \tag{G-16}$$

The coefficient of Oh was found to decrease to zero as Oh approaches zero. Correspondingly in a review, Luna and Klikoff (1967) suggested that a Weber number corrected for liquid viscosity and the variation in flow duration with time is the best criterion for evaluating drop breakup. Recently, Kreczkowski (1980) has proposed that the breakup mode is controlled by Weber number, Laplace number, and liquid gas viscosity ratio, which is also consistent with Equation G-16. Hsiang and Faeth (1992) have found that progressively higher We are required for breakup as Oh increases which is consistent with the findings of Hinze (1955) and Kreczkowski (1980).

Rabin, Schallenmuller, and Lawhead (1960) proposed a criterion for breakup by shear type breakup as

$$We_{cr} = Re^{1/2} \tag{G-17}$$

which was confirmed by others (Borizov et al., 1981; Borizov, Gel'fand, and Kograko, 1974; Dickerson and Coultas, 1966) in subsequent investigations.

Drag Coefficient. Simpkins and Bales (1972) have summarized most of the existing data on drag coefficient data from deforming drops in Figure G-5. Most of the data is 2 to 3 times greater than the compressible flow solid sphere value of C_D= 1.0. They refer to rigid disk data which ranges between 1.8 and 2.8 for disks in compressible flow which is reasonably close to the deformed drop data shown.

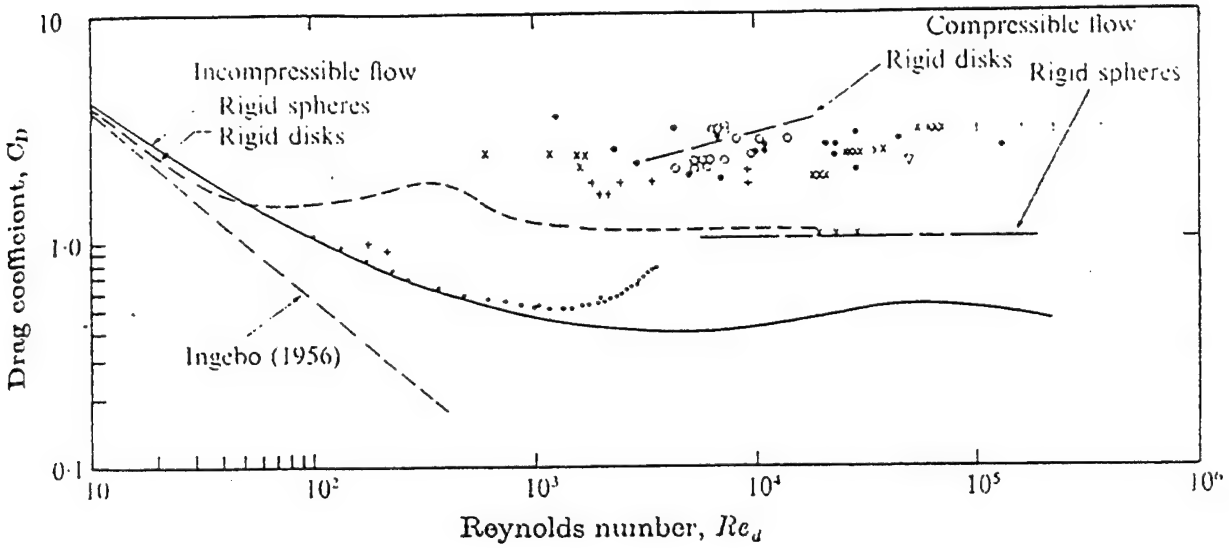

Present results: O, air; ×, argon. +, Rabin *et al.* (1960); ●, Jaarsma & Dorkson (1967); †, Ranger & Nicholls (1969); ▽, Reinecke & Waldman (1970); •, Gunn & Kinzor (1949).

Figure G-5
Drag Coefficient as a Function of Re for Deformed Droplets

Rabin, Scallenmuller, and Lawhead (1960) measured drag coefficients in their shock tube experiments and have suggested that for $10^2 < Re < 10^4$ the following expression is valid:

$$C_D = 0.386 Re^{0.177} \qquad \text{(G-18)}$$

The drag coefficients for droplets in shear mode and thus at very high Re were found to range between 2 and 3 (Ranger and Nichols, 1969; Rabin, Scallenmuller, and Lawhead, 1960).

Temkin and Kim (1980) show that for a rigid sphere moving unsteadily in a fluid, the drag coefficient may be expressed as

$$C_D = C_{Ds} - (\rho_o / \rho - 1)\frac{D_o}{U_{rel}^2}\frac{dU_{rel}}{dt} \qquad \text{(G-19)}$$

They along with Temkin and Mehta (1982), seeking to avoid droplet deformation, have obtained drag coefficients which correlate reasonably well with this expression for We < 0.15 and Re < 100.

While most drag coefficients have been derived using the crosssectional area of a sphere of liquid Hsiang and Faeth (1982) found that their data was consistent with solid sphere drag coefficients for low deformation but as the semimajor axis approached twice the original drop diameter, the drag coefficient approached results for a thin disk.

Breakup Times and Distances. While most researchers are interested in breakup times and distances, Ferrenberg, Hunt, and Duesberg (1985) point out that the definition of breakup time and thus the breakup distance is ambiguous and sometimes not even mentioned in the literature. Typically it is defined as the time elapsed from the point of exposure to the beginning of disintegration, the time required for disintegration, or the sum of these. Liang, Eastes, and Gharakhani (1988) summarize most existing data and correlations of dimensionless breakup times, τ_b (with K=1 in Equation G-7) as a function of We over all the known breakup regimes in Figure G-6. The breakup times range over an order of magnitude, O(1) to O(10), in the shear and catastrophic breakup regimes and are not much better in other regimes. Table G-1 summarizes values of K found by other researchers.

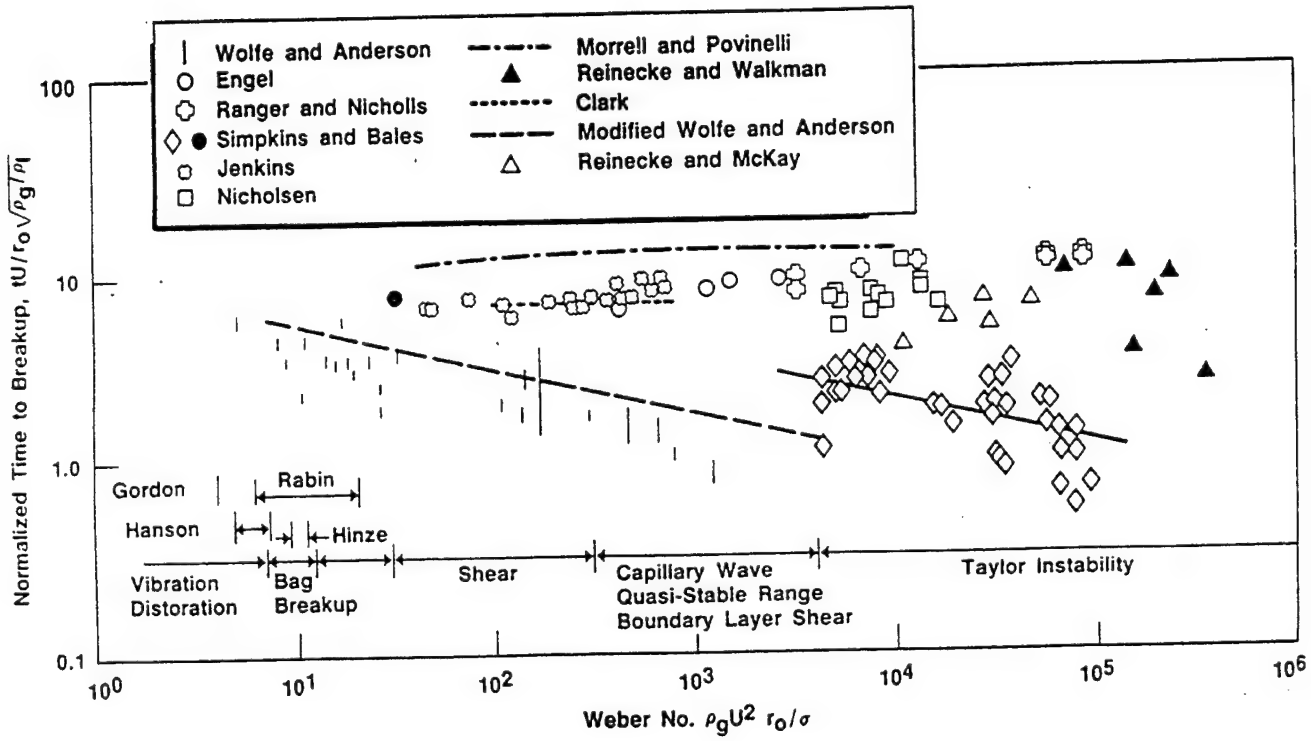

Figure G-6
Breakup Time as a Function of We

Table G-1. Breakup Time Constant for Equation G-8

K	Investigator
5	Ranger and Nicholls (1969)
1	Wolfe and Anderson (1964)
2.0	Gordon (1959)
0.57	Hinze (1948b)

Luna and Klikoff (1967) indicate in their review that drop breakup requires sufficient flow duration, and thus We_{cr} is necessary but not sufficient to obtain breakup.

Wolfe and Anderson (1964) theorized that breakup is a rate process and employed rate process theory to derive the following expression relating drop breakup time to gas and liquid parameters:

$$\tau_b = D_O/[(A^2+BP)^{1/2}-A] \qquad \text{(G-20)}$$

where $A = 16\mu_o/(\rho_o D_o)$, $B = 2/\rho_o$, $P = 0.5C_D\rho_o U_{rel}^2 - k\sigma/D_o$, and k is a constant related to the drop curvature and breakup mode. Interestingly enough and possibly by design, for negligible viscosity and surface tension and $C_D = 1$, this expression is found to be the equivalent of Equation G-8.

Ranger and Nicholls (1964) found in the initial stages of shear mode breakup that the non dimensional displacement, ξ followed a parabola in the dimensionless time, τ as follows:

$$\xi = 3C_D\tau^2/8 \qquad \text{(G-21)}$$

They found that their data fit this equation quite well for $C_D = 3$, although other data tends to fit better if C_D is about 2. As breakup proceeded the displacements were substantially greater due to the decreasing size of the droplet. For their tests they obtained ξ_b on the order of 25.

Hsiang and Faeth (1992) found that all of their data for $10 < We < 10^3$ at $Oh < 0.1$ agreed well with the breakup time correlation of Ranger and Nicholls (1969). For $0.1 < Oh < 3.5$ and $We < 10^3$ they found it necessary to multiply this correlation by a factor of 1 - Oh/7 although they point out that very few data were used to develop this correlation.

Drop Sizes and Stripping Rates. A great deal of work has been done to characterize the atomization process of various atomizers and injectors under varying flow conditions. Size distributions and velocities for the drops which comprise the spray field are commonplace in the literature. These characterizations undoubtedly include the effects of

secondary atomization, yet isolation of secondary atomization effects has only been attempted by a few and are discussed here. Presumably, diagnostic techniques other than imaging are not capable of following a drop through this process.

Dickerson and Schuman (1965) found, through painstaking analysis of streak and framing camera movies of shock tube experiments, a correlation of volume loss history for drops undergoing shear breakup equivalent to the following:

$$\frac{dV_o/dt}{V_o} = 6.74x10^{-5}\frac{S_o\mu_o}{\rho_o D_o^4}(D_o U_{rel}\sqrt{\rho\rho_o}/\mu_o)^{2.8}We^{-0.42} \qquad \text{(G-22)}$$

This equation is stated to be valid for a quasi-steady process and liquids with similar properties to RP-1, a rocket propellant similar to kerosene.

Wolfe and Anderson (1964) developed from capillary theory the following expression for mass mean diameter.

$$(MMD/D_o)^3 = \frac{136\mu_o\sigma^{3/2}D_o^{5/2}}{\rho^2\rho_o^{1/2}U_{rel}^4} \qquad \text{(G-23)}$$

This equation is said to be valid for cases in which the dynamic pressure forces are much greater than either viscous or surface tension forces (high Re and We) and actually fits their data rather well. Unfortunately their drop diameters were relatively large (> 1000μm) for practical combustion systems.

Hsiang and Faeth (1992) present a droplet size correlation for bag, transition (parasol, bag-stamen), and shear for Oh < 0.1 and We < 10^3 as follows:

$$\frac{SMD}{D_o} = 6.2(\rho_o/\rho)^{1/4}\sqrt{\mu_o/(\rho_o U_{rel} D_o)} \qquad \text{(G-24)}$$

They achieved a 0.91 correlation coefficient fitting their data.

Collins and Charwat (1971) analytically derive a model for mass loss for catastrophic breakup which requires numerical integration of the governing equations as a function of time. They obtained excellent agreement with data from Reinecke and McKay (1969). Ranger and Nicholls (1969) have developed a similar technique which trends correctly but does not fit their data that well.

Critique and Recommendations

Ferrenberg, Hunt, and Duesberg (1985) have suggested that atomization data available to date was "largely empirical and ad hoc, only qualitatively understood, and of little general utility." They attribute this to the great complexity of the atomization process and the inaccuracies, errors, and limitations associated with drop size measurements. The "black box" approach applied to atomization, in general, by the bulk of researchers has yielded practical information such as drop size distribution as a function of spatial coordinates in the spray field for a specific atomizer operating under specific conditions with specific fluids. Unfortunately, extrapolation of the correlations developed by these researchers to different atomizers operating under different conditions with different fluids has proven unsatisfactory in most cases.

Diagnostic advances in the few short years since 1985 have done much to improve this seemingly sorry state of affairs. Phase Doppler interferometry has been applied by a number of researchers to quantitatively characterize spray fields in many practical situations (i.e., McDonnel and Samuelsen, 1988). Optical patternation techniques are now being developed as well (i.e., Iguchi, McDonnel, and Samuelsen, 1993). Such diagnostic improvements have led researchers to now consider seemingly obvious parameters such as surface finish in the atomizer hardware, upstream geometry prior to injection, and the shape of volume into which the spray is introduced. In general, the physics of the atomization process is now being examined under closer scrutiny.

Secondary atomization appears to be qualitatively understood as well, yet physical parameter dependencies have been developed beyond those in primary atomization. Fortunately, researchers examining secondary atomization, although fewer in number, have used simple, reasonably well defined experiments in attempts to understand the physical processes involved. Based on these experimental observations, models have been developed which permit better understanding of the associated physics.

While the types of breakup are reasonably well characterized, the conditions under which they occur are not well defined. Characterizing parameters sometimes vary by orders of magnitude in the transition between regimes. Certainly those dimensionless parameters outlined previously have been shown to be useful in characterizing the breakup phenomena in specific regimes, but a well defined theory has yet to be developed.

The transient nature and history dependence of the drop breakup process makes characterization with a few dimensionless parameters difficult and has not been investigated adequately since it was discovered in the early 50's. Coupling of the droplet internal flow field with its associated deformation and the convective external flow is realized only in the most comprehensive direct numerical simulations of full Navier-Stokes finite difference models.

Imaging techniques employing high speed cinematography and painstaking human analysis of the resulting frames have provided early glimpses of the drop breakup process, but the

human link in the analysis process has substantially limited progress. Because of recent advances in laser diagnostics, a great deal of literature on spatial drop size/velocity distributions on various atomizers under various flow conditions is available for continuous atomization processes. However, because of the small time scales associated with drop breakup and temporal resolution available from most current diagnostic techniques, an equivalent level of characterization for secondary atomization is only now being developed.

Recently applied holography (Hsiang and Faeth, 1992) and high speed cinematography (Eastes and Samuelsen, 1993) with microscopic lenses are able to temporally and spatially resolve the drop breakup process. Advances in computer image analysis have recently been developed to provide quantitative image analysis for these techniques.

The parametric mapping of regimes of breakup, dynamic response characterization, and temporally and spatially resolved examination of the breakup process are all now possible. Initially experimental efforts will lead this effort, but as data is made available to modelers, physical understanding of the observations can be achieved. Systematic experimental examination of the basic processes holds the key to understanding the global processes in secondary atomization and ultimately atomization in general. The aforementioned advents in imaging diagnostic techniques should go a long way to effect this investigation. Similarly, direct numerical simulation of the fully coupled drop/free stream system should aid in understanding effects that cannot be easily inferred from the experiments.

Appendix G Bibliography

Anderson, T.J. and Winter, M., (1992) "Measurements of Droplet Vaporization Rate Enhancement Caused by Acoutic Disturbances," 29th JANNAF Combustion Meeting, NASA Langley Research Center, Hampton, VA, Oct. 1992.

Ateshkhadi, A., Eastes, T.W. and Samuelsen, G.S. (1993) "Primary Breakup of a Liquid Jet in a Transverse Shock-Induced Flow," AIAA Paper 93-2335, 29th Joint Propulsion Meeting, Monterey, CA, July, 1993.

Bachelo, W.D. (1980) "Phase/Doppler Spray Analyzer for Simultaneous Measurements of Drop Size and Velocity Distributions," Appl. Opt., vol. 19, pp. 363-370.

Belousov, A.B., Grushin, V.A., Kirsanov, V.P., and Loktev, V.G. (1988) "High-speed Pneumatic Valve," Instruments and Experimental Techniques, vol. 31, no. 6, p. 1596, Nov-Dec 1988.

Borisov, A., Gel'fand, B., Natanzon, M., and Kossov, O. (1981) "Droplet breakup Regimes and Criteria for their Existence," J. Engng. Phys., vol. 40, no. 1, pp. 44-49.

Borisov, A., Gubin, M., and Kogarko, S.M. (1974) "The Varieties of Droplet breakup Behind Shock Waves and Their Characteristics," J. Engng. Phys., vol. 27, no. 1, pp. 119-126.

Bowden, F.P., ed. (1966) "A Discussion on Deformation of Solids by Impact of Liquids, and its relation to Rain Damage in Aircraft and Missles, to Blade Erosion in Steam Turbines, and to Cavitation Erosion," Phil. Trans. Royal Soc., Series A, Math. and Phys. Sci., vol. 260, no. 1110, pp. 73-315.

Box, G.E.P., Hunter, W.G., and Hunter, J.S. (1978) Statistics for Experimenters, John Wiley and Sons, New York, NY, 1978.

Bradley, J. N. (1962) Shock Waves in Chemistry and Physics, John Wiley and Sons, New York, NY, 1962.

Brown, R.S. (1985) "Blowdown Pulser Design Criteria for Solid-propellant Rockets," J. Propulsion and Power, vol. 2, no. 2, pp. 110-116, Mar-Apr. 1985.

Collins, R. and Charwat, A.F. (1971) "The Deformation and Mass Loss of Liquid Drops in High-Speed Flow of Gas," Israel J. Tech., vol. 9, no. 5, pp. 453-465.

Connon, C.H. (1993) Private Communication, 1993.

Corat, E.J. and Trava-Airoldi, V.J. (1990) An Efficient High-repetition-rate Fast-pulsed Gas Valve," Rev. Sci. Instrum., 61(3), pp. 1068-1071, Mar. 1990.

Cox, G.B. (1990) "The Liquid Stability Mechanisms Program," Proceedings of the 27th JANNAF Combustion Meeting, Warren Air Force Base, Cheyenne, Wyoming, November 1990.

Cramer F.B., Webber, W.T., and Lawhead, R.B., (1958) "Research on the Basic Fluid Dynamic Phenomena Related to Rocket Combustion Instability Summary Technical Note," Wright Air Development Center Tech. Note, WADC-TN-57-426.

Culick, F.E.C. (1989) "Combustion Instabilities in Liquid-Fuelled Propulsion Systems," AGARD Conference Paper No. 450, Neuilly sur Seine, France, Nov. 1989.

Deng, Z.-T. and Jeng, S.-M. (1990) "Numerical Simulation of Droplet Deformation in Convective Flows," AIAA Paper 90-2309, AIAA/SAE/ASME/ASEE 26th Joint Propulsion Conference, Orlando, FL, Jul. 1990.

Dickerson R.A. and Coultas, T.A. (1966) "Breakup of Droplets in an Accelerating Gas Flow," AIAA Paper 66-611, 1966.

Dickerson R.A. and Schuman, M.D. (1965) "Rate of Atomization of Droplets," J. Spacecraft and Rockets, vol. 2, no. 1, pp 99-100.

Dodd, F.E. (1992) Private Communication, 1992.

Dressler, J.L. and Kraemer, G.O. (1990) "A Multiple Drop-Size Drop Generator for Calibration of a Phase-Doppler Particle Analyzer", in Liquid Particle Size Measurement Techniques: 2nd Volume, ASTM STP 1083, Hirleman, E.D., Bachelo, W.D., and Felton, P.G., Eds., American Society for Testing and Materials, Philadelphia, pp. 30-44.

Dwyer, H.A. and Dandy, D.S., (1989) "Three-Dimensional Deformation, of Liquid Drops," WSS/CI Paper 89-66, Western States Section, Combustion Institute, Livermore, CA, Oct. 1989.

Eastes, T.W. (1989) "Response of a 'Tuned' Helmholtz Resonator to a Steep-fronted, High Amplitude Wave," Proceedings of the 26th JANNAF Combustion Meeting, Jet Propulsion Laboratory, Pasadena, California, October 1989.

Eastes, T.W. and Samuelsen, G.S. (1992) "Secondary Atomization by High Amplitude Pressure Waves", AIAA Paper 92-3120, 28th Joint Propulsion Meeting, Nashville, TN, July, 1992.

Engel, O.G., (1958) "Fragmentation of Waterdrops in the Zone Behind an Air Shock," Journal of Research of the National Bureau of Standards, vol. 60, no. 3, Mar. 1958, pp. 245-280.

Faeth, G.M., (1992) "Drop/Gas Interactions in Dense Sprays," AFOSR Contractor's Meeting in Propulsion Proceedings, University of California, San Diego, LaJolla, CA, June 1992.

Faeth, G.M., (1990) "Structure and Atomization Properties of Dense Turbulent Sprays," Proceedings of the 23rd Symposium (International) on Combustion, The Combustion Institute, Pittsburgh, PA, 1990, pp. 1345-1352.

Ferrenberg, A., Hunt, K., and Duesberg, J., (1985) "Atomization and Mixing Study," Rockwell International, Rocketdyne Division Report RI/RD85-312, 1985.

Forsnes, V.G. and Ulrich, R.D. (1968) "A Literature Review and Discussion of Liquid Particle Breakup in Gas Streams," Naval Weapons Center Report, NWC-TP-4589, China Lake, CA, July 1968.

Frankel, I. and Weihs, D. (1983) "Shape and Stability of a Liquid Drop Moving at Low Weber Numbers," Appl. Sci. Res., vol 40, pp. 279-294.

Fritts, M.J., Fyfe, D.E., and Oran, E.S., (1984) "Simulations of Fuel Droplet Flows," in Dynamics of Flames and Reactive Systems, Prog. Aero. and Astro., vol. 95, 1985.

Gaydon, A. G. and Hurle, I. R. (1963) The Shock Tube in High-temperature Chemical Physics, Reinhold Publishing Corporation, New York, NY.

Gentry, W.R. and Geise, C.F. (1978) "Ten-microsecond Pulsed Molecular Beam Source and a Fast Ionization Detector," Rev. Sci. Instrum., 49(5), pp. 595-600, May 1978.

Gordon, G.D. (1959) "Mechanism and Speed of Breakup of Drops," J. Appl. Phys., vol. 30, no. 11, Nov. 1959, pp. 1759-1761.

Haas, F.C., (1964) "Stability of Droplets Suddenly Exposed to a High Velocity Gas Stream," AIChE J., vol. 10, no. 6, Nov. 1964, pp. 920-924.

Hammer, S.S. and Agosta, V.D. (1966) "Wave Slope - Gas Dynamics Interactions in Liquid Rockets," AIAA J., vol. 4, no. 4, April 1966.

Hanson, A.R., Domich, E.G., and Adams, H.S, (1963) "Shock-Tube Investigation of the Breakup of Drops by Air Blasts," Phys. Fluids, vol. 6, No. 8, Aug. 1963, pp. 1070-1080.

Harper, E.Y., Grube, G.W., and Chang, I.-D., (1972) "On the Breakup of Accelerating Liquid Drops," JFM, vol. 52, part 3, pp. 565-591.

Harrje, D.T. and Reardon, eds. (1972) "Liquid Propellant Rocket Combustion Instability," NASA SP-194, US Government Printing Office, Washington, DC, 1972.

Harvey, D.W. (1973) "Liquid Drop Breakup", McDonnel Douglas Astronautics Co. Internal Report, Huntington Beach, CA, August 1973.

Henins, I. and Marshall, J. (1969) "A Pulsed Gas Valve for Fast Timeable High Pressure Operation," Rev. Sci. Instrum., 40(7), pp. 875-878, July 1969.

Hinze, J.O. (1955) "Fundamentals of the Hydrodynamic Mechanism of Splitting in Dispersion Processes," Forced Deformations of Viscous Liquid Globules," AIChE J., vol. 1, no. 3, pp. 289-295.

Hinze, J.O. (1948a) "Forced Deformations of Viscous Liquid Globules," Appl. Sci. Res., series A, vol 1, no.9, pp. 263-272.

Hinze, J.O. (1948b) "Critical Speeds and Sizes of Liquid Globules," Appl. Sci. Res., series A, vol 1, no. 9, pp. 273-288.

Hsiang, L.-P. and Faeth, G.M., (1992) "Secondary Drop Breakup in the Deformation Regime," AIAA 92-0110, 30th Aerospace Sciences Meeting, Reno, NV., Jan. 1992.

Jensen, R.J. (1989) "A summary of the JANNAF Workshop on Liquid Rocket Engine Combustion Driven Instability Mechanisms," Proceedings of the 26th JANNAF Combustion Meeting, Jet Propulsion Laboratory, Pasadena, CA, Oct. 1989.

Kay, J.M. (1974) An Introduction to Fluid Mechanics and Heat Transfer, with Applications in Chemical and Mechanical Process Engineering, 4th ed., University Press, Cambridge, England, 1974.

Komar, J.J. (1978) "Rapid Response Gas Injection Technique," Rev. Sci. Instrum., 49(10), pp. 1474-1476, Oct. 1978.

Krzeczkowski, S.A. (1980) "Measurement of Liquid Droplet Disintegration Mechanisms," Intl. J. Multiphase Flow, vol. 6, no. 3, pp. 227-239.

Kuswa, G., Stallings, C. and Stamm, A. (1970) "Improved Fast Opening Gas Puff Valve," Rev. Sci. Instrum., 41(10), pp. 1362-1363, Oct 1970.

Kwok, K.-C. and Liu, B.Y.H. (1991) "New Research Approach to Air Spray Painting," Proceedings of the 5th ICLASS, Gaithersburg, MD, pp. 105-112.

Lane, W.R. (1951) "Shatter of Drops in Streams of Air," Ind. Eng. Chem., vol. 43, June 1951, pp. 1312-1317.

Lapple, C.E., Henry J.P., and Blake, D.E., "Atomization - A Survey and Critique of the Literature," Stanford Research Institute Report No. 6, Menlo Park, CA, (also ASTIA AD-81-314), 1967.

Lecourt, R. and Foucaud, R. (1987) "Experiments on Stability of Liquid Propellant Rocket Motors," AIAA Paper 87-1772, AIAA/SAE/ASME/ASEE 23rd Joint Propulsion Conference, San Diego, California, June-July 1987.

Lefebvre, A.H. (1989) Atomization and Sprays, Hemisphere Publishing, New York, NY, 1989.

Lefebvre, A.H. (1983) Gas Turbine Combustion, Chap. 10, Hemisphere Publishing, New York, NY, 1983.

Liang, P.Y., Eastes, T.W., and Gharakhani, A., (1988) "Computer Simulations of Drop Deformation and Drop Breakup," AIAA Paper 88-3142, AIAA/ASME/SAE/ASEE 24th Joint Propulsion Conference, Boston, MA, Jul. 1988.

Lovejoy, C.M. and Nesbitt, D.J. (1987) "Slit Pulsed Valve for Generation of Long-path-length Supersonic Expansions," Rev. Sci. Instrum., 58(5), pp. 807-811, May 1987.

Luna, N. and Klikoff, W. (1967) "On Aerodynamic Breakup of Liquid Drops," Sandia National Laboratory Report SC-RR-66-2716, Albuquerque, NM, 1967.

Masters, K. (1985) Spray Drying Handbook, 4th Edition, George Godwin Publishing, London, England, 1985.

McDonnel, V.G. and Samuelsen, G.S. (1988) "Application of Two-Component Phase-Doppler Interferometry to the Measurement of Particle Size, Mass Flux, and Velocities in Two-Phase Flow," Proceedings of 21st Symposium (International) on Combustion, The Combustion Institute, Pittsburgh, PA, 1988, pp. 1961-1971.

Mehta, H.K. (1980) "Droplet Drag and Breakup in Shock-Wave Induced Unsteady Flows," Ph.D. Dissertation, Rutgers University, New Brunswick, NJ, 1980.

Milora, S.L., Combs, S.K. and Foust, C.R. (1986) "Fast-opening Magnetic Valve for High-pressure Gas Injection and Applications to Hydrogen Pellet Fueling Systems," Rev. Sci. Instrum., 57(9), pp. 2356-2358, Sept. 1986.

Otis, C.E. and Johnson, P.M. (1980) "A Simple Pulsed Valve for Use in Supersonic Nozzle Experiments," Rev. Sci. Instrum 51(8), pp.1128-1129, Aug. 1980.

Patel, P.D. and Theofanous, T.G. (1981) "Hydrodynamic Fragmentation of Drops," JFM, vol. 103, pp. 207-223.

Peterson, R.B. (1988) "Characterization of a Simple, High Reynolds Number Droplet Generator, for Combustion Studies," Rev. Sci. Instrum. vol. 59, no. 6, June 1988. pp. 960-966.

Rabin, E., Schallenmuller, A.R., and Lawhead, R.B. (1960) "Displacement and Shattering of Propellant Droplets, Rocketdyne Report R-2431, AFOSR TR-60-75, Mar. 1960.

Rabin, E., and Lawhead, R.B. (1959) "The Motion and Shattering of Burning and Non-burning Propellant Droplets," North American Aviation, Rocketdyne Report R-1503, AFOSR TN-59-129, (also ASTIA AD-210-768), Mar. 1959.

Rallison, J.M. (1984) "The Deformation of Small Viscous Drops and Bubbles in Shear Flows," Ann. Rev Fluid Mech., vol. 16, pp. 45-66.

Ranger, A.A., and Nicholls, J.A., (1969) "Aerodynamic Shattering of Liquid Drops," AIAA J., vol. 7, no. 2, Feb. 1969, pp. 285-290.

Ranger, A.A. and Nicholls, J.A., (1972) "Atomization of Liquid Droplets in a Convective Stream," Int. J. Heat Mass Transfer, vol. 15, pp. 1203-1211.

Rayleigh, Lord (1945) Theory of Sound, Volume II, Second Edition, Dover Press, New York, NY, 1945.

Reichman, J.M., and Temkin, S. (1980) "A Study of the Deformation and Breakup of Accelerating Water Droplets," Proc. Int. Coll. on Drops and Bubbles, 28-30 Aug. 1974, Pasadena, CA, pp.446-464.

Reinecke, W.G. and McKay, W.L., (1969) "Experiments on Waterdrop Breakup Behind Mach 3 to 12 Shocks," Sandia Corp. Report SC-CR-70-6063, 1969.

Reinecke, W.G. and Waldman, G.D., (1970) "Experiments on Waterdrop Breakup Behind Strong Shocks with Applications to Flight," Avco Report AVSD-0110-70-77, May 1970.

Rojec E.A. (1963) " Photographic Presentation of Shear-Type Droplet Breakup," North American Aviation, Rocketdyne Division Research Report No. 63-39, Nov. 1963.

Sharma, S.P. and Park, C. (1990) "Operating Characteristics of a 60- and 10-cm Electric Arc-driven Shock Tube-Part I: The Driver," J. Thermophysics, vol. 4, no. 3, pp. 259-265, July 1990

Simpkins, P.G., and Bales, E.L., (1972) "Water-Drop Response to Sudden Accelerations," JFM, vol. 55, part 4, pp. 629-639.

Simpkins, P.G. (1974) "Non-Linear Effects on Droplet Deformation," Proc. Int. Coll. on Drops and Bubbles, 28-30 Aug. 1974, Pasadena, CA, pp. 372-389.

Sirignano, W.A. (1990) "Liquid Stability Mechanisms Program, Interim Report, Task I" United Technologies Corp., Pratt & Whitney Government Engines and Space Propulsion, FR-XXXX, Apr. 1990.

Switzer, G.L. (1991) "A Versatile System for Stable Generation of Uniform Droplets," Rev. Sci. Instrum. vol. 62, no. 11, Nov. 1991. pp. 2765-2771.

Tan, M.J. and Bankoff, S.G. (1985) "On Fragmentation of Drops," Paper 85-WA/FE-1, Trans. ASME, J. Fluids Engr., ASME Winter Annual Meeting, Miami Beach, FL, Nov. 1985.

Taylor, G.I. (1949) " The Shape and Acceleration of a Drop in a High Speed Air Stream," in Scientific Papers of G.I. Taylor, G.K. Batchelor, ed. University Press, Cambridge, UK pp. 457-464, 1963.

Temkin, S. and Ecker, G.Z. (1989) "Droplet Pair Interactions in a Shock-Wave Flow Field," JFM, vol. 202, pp. 467-497.

Temkin, S. and Kim, S.S.(1980) "Droplet Motion Induced by Weak Shock Waves," JFM , vol. 96, part 1, pp. 133-157.

Temkin, S. and Mehta, H.K. (1982) "Droplet Drag in Accelerating and Decelerating Flow," JFM, vol. 116, pp. 297-313.

Warren, W.R. and Harris, C.J. (1970) "A Critique of High Performance Shock Tube Driving Techniques," in Shock Tubes Proceedings of the Seventh International Shock Tube Symposium, University of Toronto, Toronto, Cananda, I.I. Glass, editor, pp. 143-176.

Watters, R.L. and Walters, J.P. (1977) "Device for Stroboscopic Extraction of Atmospheric Pressure Species into Regions of High Vacuum," Rev. Sci. Instrum., 48(6), pp. 643-646, June 1970.

Webber, W.T. (1959) "Effects of Gas Motion on Heterogeneous Combustion: Natural Convection, Standing Acoustic Waves, and Shock Waves - Final Summary Report," WADC TR-59-50 (ASTIA AD-228500), contract AF 33(616)-3556, April 1959.

Webber, W.T. (1959) "Effects of Gas Motion on Heterogeneous Combustion; Natural Convection, Steady Forced Convection, Standing Acóustic Waves, and Shock Waves Final Summary Report," Rocketdyne Report R-1421, WADC-TR-59-50, ASTIA AD-228500, April 1959.

Wierzba, A., and Takayama, K., (1988) "Experimental Investigation of the Aerodynamic Breakup of Liquid Droplets," AIAA J., vol. 26, No. 11, Nov. 1988, pp. 1329-1335.

Williams, F.A. (1961) "Structure of Detonations in Dilute Sprays," Phys. Fluids, vol. 4, no. 11, 1961.

Wolfe, H.E. and Anderson, W.H. (1964) "Kinetics, Mechanism, and Resultant Droplet Sizes of Aerodynamic Breakup of Liquid Drops," Aerojet-General Corp. Report No. 0395-04(18) SP, (also ASTIA AD-437340), Downey, CA, April, 1964.

Yoshida, Y., Wierzba, A., and Takayama, K., (1988) "Breakup and Interaction of Two Droplet Columns in a Shock Wave Induced High-Speed Air Flow," Proc. 4th ICLASS, Sendai, Japan, Aug. 1988, pp. 101-108.

APPENDIX H - REVIEW OF PULSE TECHNIQUES

Over the past 30 years, a number of shock tube driving techniques have been developed to extend the ranges of operation of shock tubes. These techniques can be somewhat arbitrarily classified into the following categories; 1) conventional diaphragm, 2) electric and magnetic field interaction, 3) detonation, and 4) unconventional energy addition/wave process coupled drivers. The objectives of these techniques are varied and include maximizing shock velocity, driven gas temperature, pressure, density, driven gas kinetic to static energy ratio, uniformity of flow field, and duration of test. Many of these techniques are so-characterized and described by Warren and Harris (1970).

The primary objective of the current investigation requires that the pulse simulate the waveform typically associated with transverse oscillations in a liquid rocket combustion instability. Secondary objectives include variability of wave strength from a few percent up to 50 or 100 percent, a characteristic N-wave shape, repeatable amplitude and shape, good definition of the shock induced flowfield, fast turn-around, low-risk development, simplicity, safety, and ease of implementation and fabrication. The various techniques are evaluated based on these criteria. Specific techniques considered are briefly described and evaluated as follows.

A detonation technique employing electrically initiated squibs was considered and has been used by this author in past work (Eastes, 1989). While attractive due to its simplicity and ease of implementation and fabrication, repeatability is not acceptable for this application. Other disadvantages are shrapnel and contact surface interference should the initial reflection be required in future activities. The excessive safety procedures required to utilize such devices, while prudent, are also quite cumbersome. Additionally, the ability to vary the output to consistently low amplitudes is questionable. Pulse guns and piston pulsers, as commonly used for stability rating of liquid rocket engines (Harrje and Reardon, eds., 1972) are conceptually similar and suffer from many of the same problems although diaphragms are often employed with the explosive device to improve amplitude repeatability. A similar concept was employed recently (Sharma and Park, 1990) where an exploding wire was used to burst a diaphragm in an arc-driven shock tube.

Fast-acting valves have been successfully employed by a number of researchers (Corat and Trava-Airoldi, 1990; Belousov et al., 1988; Lovejoy and Nesbitt, 1987; Milora, Combs, and Foust, 1986; Otis and Johnson, 1980; Komar, 1978; Gentry and Geise, 1978; Watters and Walters, 1977; Kuswa, Stallings, and Stamm, 1970; Henins and Marshall, 1969). All of these valves appear to be specially fabricated for the particular application however. Lovejoy and Nesbitt (1987) were the only researchers to modify the operation of off-the-shelf hardware. Gentry and Giese (1978) employ a novel, yet simple, design which relies on electrical charge repulsion to flex a beam whose face is initially sealed against an orifice, however the mass flow is insufficient for the present application. Henins and Marshall (1969) compressed a nylon rod against an orifice with a hydraulic jack and released it to produce a pulse. Many of the valve techniques sited are limited to

very small mass flowrates (~ 1 gram/sec.). While valve techniques are believed to provide consistent pulse amplitudes and quick turn-around time during testing, they are relatively untested and posed a development risk. In addition to the difficulty in obtaining fast reaction times with off-the-shelf hardware, excessively high pressure volumes are required to be maintained prior to pulsing. This requires larger valves to handle the high pressure, which slows the reaction time due to the increased mass of the valve's gate, and requires source tanks and facility hardware to contain these pressures, which greatly reduces overall facility safety. Additionally, the spool valve technique described by Webber (1959) and conceptually similar to that of Watters and Walters (1977) suffers from lack of a vendor willing to fabricate such a device in low volumes, even though it requires less machining and is simpler than existing designs. Internal fabrication of this device posed unnecessary development risk.

Techniques requiring a flowing system such as those described in Harrje and Reardon, eds. (1972), Webber (1959), and Lecourt and Foucaud (1987), as opposed to a shock tube are believed to add unnecessary complication to the problem at hand and are more appropriate to actual hot-fire rocket engine instability investigations. These devices produce repeated pulses and include the siren, like the Ling transducer, and the spinning cogged-wheel techniques.

A burst diaphragm technique was found to have associated with it the least development risk due to its wide use (Warren and Harris, 1970; Hammer and Agosta, 1966; Temkin and Ecker, 1989; Brown, 1985; Temkin and Mehta, 1982; Temin and Kim, 1980). Although turn-around time may be substantially more than that associated with valve-based techniques, other activities between tests associated with cleaning windows, depressurization of the shock tube, and changing film in the drum camera, tend to be the test rate controlling activities. Wave amplitude repeatability of the device in the present tests is consistent with that reported by other investigators.

Appendix H Bibliography

Belousov, A. B., Grushin, V. A., Kirsanov, V. P., and Loktev, V. G. (1988) "High-speed Pneumatic Valve," *Instruments and Experimental Techniques*, Vol. 31, No. 6, P. 1596, Nov.-Dec. 1988.

Brown, R. S. (1985) "Blowdown Pulser Design Criteria for Solid-Propellant Rockets," *J. Propulsion and Power*, Vol. 2, No. 2, pp. 110-116, Mar.-Apr. 1985.

Corat, E. J. and Trava-Airoldi, V. J. (1990) "An Efficient High-repitition-rate Fast-pulsed Gas Valve," *Rev. Sci. Instrumn.*, 61(3), pp. 1068-1071, Mar. 1990.

Eastes, T. W. (1989) "Response of a 'Tuned' Helmholtz Resonator to a Steep-fronted, High Amplitude Wave," *Proceedings of the 26th JANNAF Combustion Meeting*, Jet Propulsion Laboratory, Pasadena, CA, Oct. 1989.

Gentry, W. R. and Geise, C. F. (1978) "Ten-microsecond Pulsed Molecular Beam Source and a Fast Ionization Detector," *Rev. Sci. Intrumn.*, 49(5), pp. 595-600, May 1978.

Hammer, S. S. and Agosta, V. D. (1966) "Wave Slope - Gas Dynamics Investigation of the Breakup of Drops by Air Blasts," *Phys. Fluids*, Vol. 6, No. 8, pp. 1070-1080, Aug. 1963.

Harrje, D. T. and Reardon, eds. (1972) "Liquid Propellant Rocket Combustion Instability," NASA SP-194, US Government Printing Office, Washington, DC, 1972.

Henins, I. and Marshall, J. (1969) "A Pulsed Gas Valve for Fast Timetable High Pressure Operation," *Rev. Sci. Instrumn.*, 40(7), pp. 875-878, July 1969.

Komar, J. J. (1978) "Rapid Response Gas Injection Technique," *Rev. Sci. Instrumn.*, 49(10), pp. 1474-1476, Oct. 1978.

Kuswa, G., Stallings, C., and Stamm, A. (1970) "Improved Fast Opening Gas Puff Valve," *Rev. Sci. Instrumn.*, 41(10), pp. 1362-1363, Oct. 1970.

Lecourt, R. and Foucaud, R. (1987) "Experiments on Stability of Liquid Propellant Rocket Moters," AIAA Paper 87-1772, 23rd Joint Propulsion Conference, San Diego, CA, June-July 1987.

Lovejoy, C. M. and Nesbitt, D. J. (1987) "Slit Pulsed Valve for Generation of Long-Path-Length Supersonic Expansions," *Rev. Sci. Intrumn.*, 58(5), pp. 807-811, May 1987.

Milora, S. L., Combs, S. K., and Foust, C. R. (1986) "Fast-Opening Magnetic Valve for High-Pressure Gas Injection and Applications to Hydrogen Pellet Fueling Aystems," *Rev. Sci. Intrumn.*, 57(9), pp. 2356-2358, Sept. 1986.

Otis, C. E. and Johnson, P. M. (1980) "A Simple Pulsed Valve for Use in Supersonic Nozzle Experiments," *Rev. Sci. Intrumn.*, (51(8), pp. 1128-1129, Aug. 1980.

Sharma, S. P. and Park, C. (1990) "Operating Characteristics of a 60- and 10-cm Electric Arc-driven Shock Tube - Part I: The Driver," *J. Thermophysics*, Vol. 4, No. 3, pp. 259-265, July 1990.

Temkin, S. and Ecker, G. Z. (1989) "Droplet Pair Interactions in a Shock-Wave Flow Field," *JFM*, Vol. 202, pp. 467-497.

Temkin, S. and Kim, S. S. (1980) "Droplet Motion Induced by Weak Shock Waves," *JFM*, Vol. 96, Part 1, pp. 133-157.

Temkin, S. and Mehta, H. K. (1982) "Droplet Drag in Accelerating and Decelerating Flow," *JFM*, Vol. 116, pp. 297-313.

Warren, W. R. aand Harris, C. J. (1970) "A Critique of High Performance Shock Tube Driving Techniques," in *Shock Tubes Proceedings of the Seventh International Shock Tube Symposium*, University of Toronto, Toronto, Canada, I. I. Glass, editor, pp. 143-176.

Watters, R. L. and Walters, J. P. (1977) "Device for Stroboscopic Extraction of Atmospheric Pressure Species into Regions of High Vacuum," Rev. Sci. Instrumn., 48(6), pp. 643-646, June 1970.

Webber, W. T. (1959) "Effects of Gas Motion on Heterogeneous Combustion: Natural Convection, Standing Acoustic Waves, and Shock Waves - Final Summary Report," WADC Tr-59-50 (ASTIA AD-228500), contract AF 33(616)-3556, April 1959.

APPENDIX I - HARDWARE DESIGN DRAWINGS

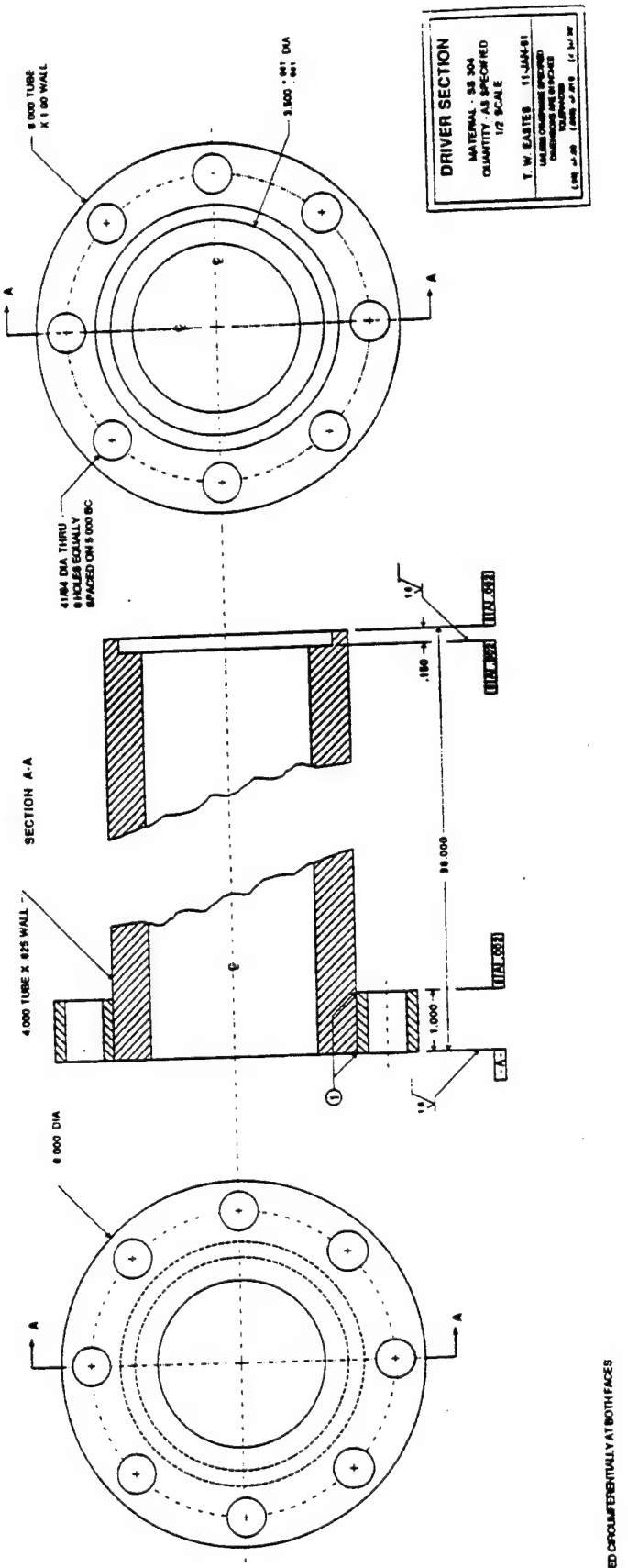

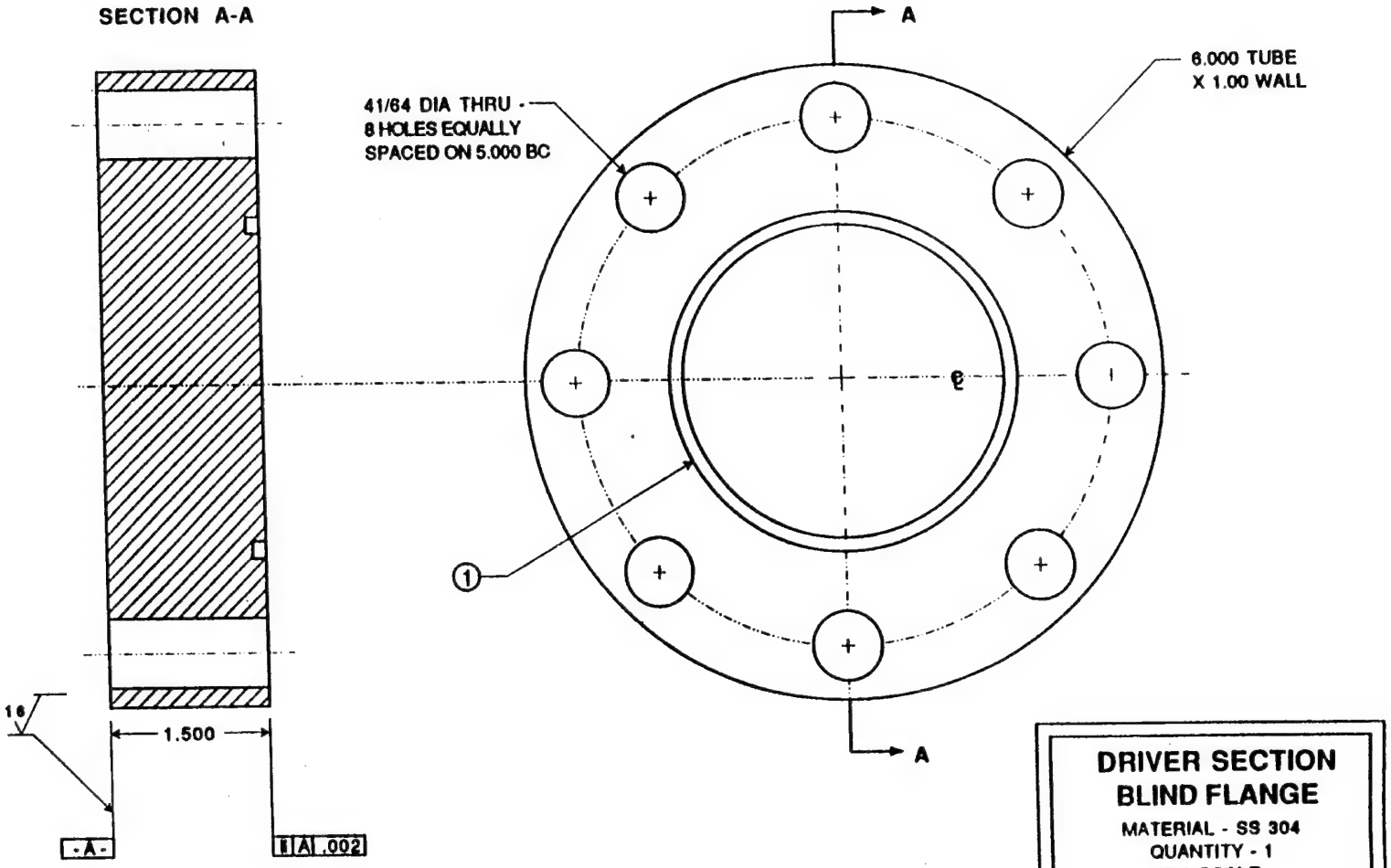

NOTES:
1. O-RING FACE SEAL GLAND DIMENSIONS PER PARKER SPECS FOR O-RING 2-234 FOR INTERNAL PRESSURE BY GASES.

DRIVER SECTION
BLIND FLANGE

MATERIAL - SS 304
QUANTITY - 1
3/4 SCALE

T. W. EASTES 11-JAN-91

UNLESS OTHERWISE SPECIFIED
DIMENSIONS ARE IN INCHES
TOLERANCES
(.00) +/-.03 (.000) +/-.010 (∠)+/-30'

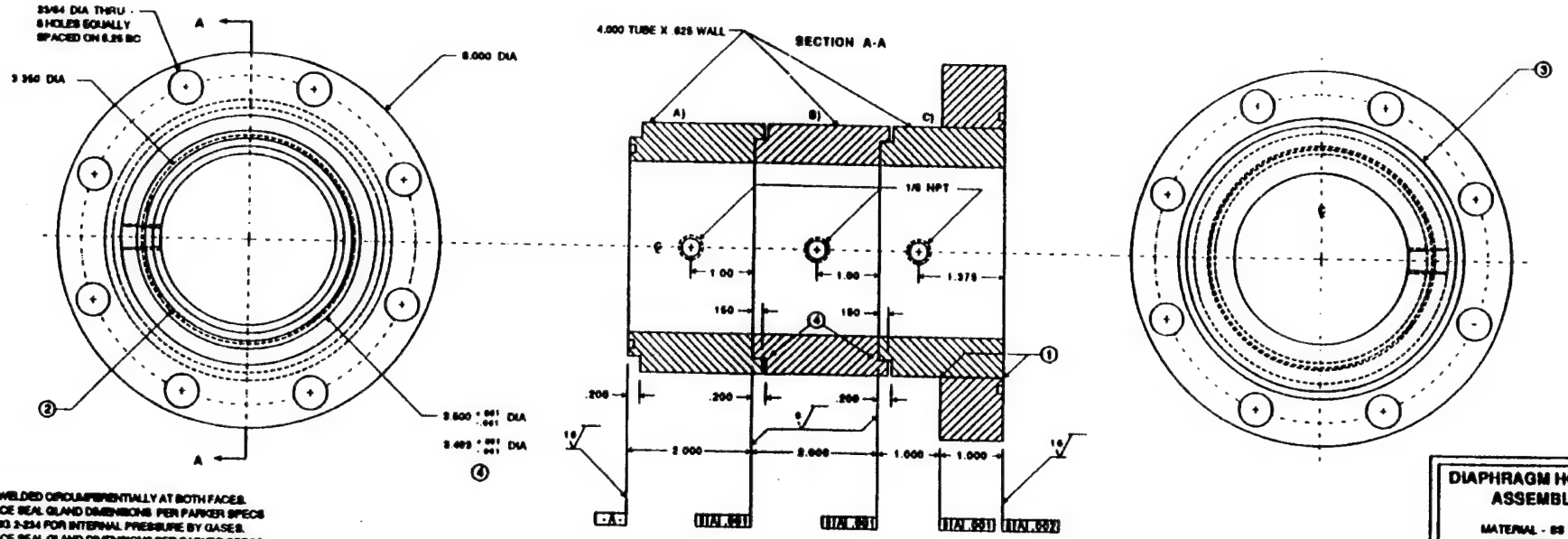

NOTES:
1. FLANGES WELDED CIRCUMFERENTIALLY AT BOTH FACES.
2. O-RING FACE SEAL GLAND DIMENSIONS PER PARKER SPECS FOR O-RING 2-234 FOR INTERNAL PRESSURE BY GASES.
3. O-RING FACE SEAL GLAND DIMENSIONS PER PARKER SPECS FOR O-RING 2-344 FOR INTERNAL PRESSURE BY GASES.
4. FIRST DIMENSION APPLIES TO OUTER RACE OF FIT AND SECOND DIMENSION APPLIES TO INNER RACE OF FIT BETWEEN MATING PARTS. SEE DETAIL DRAWINGS A) FORE, B) MID, AND C) AFT DIAPHRAGM HOLDERS.

DIAPHRAGM HOLDER ASSEMBLY

MATERIAL - SS 304
QUANTITY - 1
1/2 SCALE

T. W. EASTES 29-APR-01

VALVES DIAPHRAGM SPECIFIED
DIMENSIONS ARE IN INCHES
TOLERANCES
(.XXX) ±.005 (.XXX) ±.010 ( ) per SP

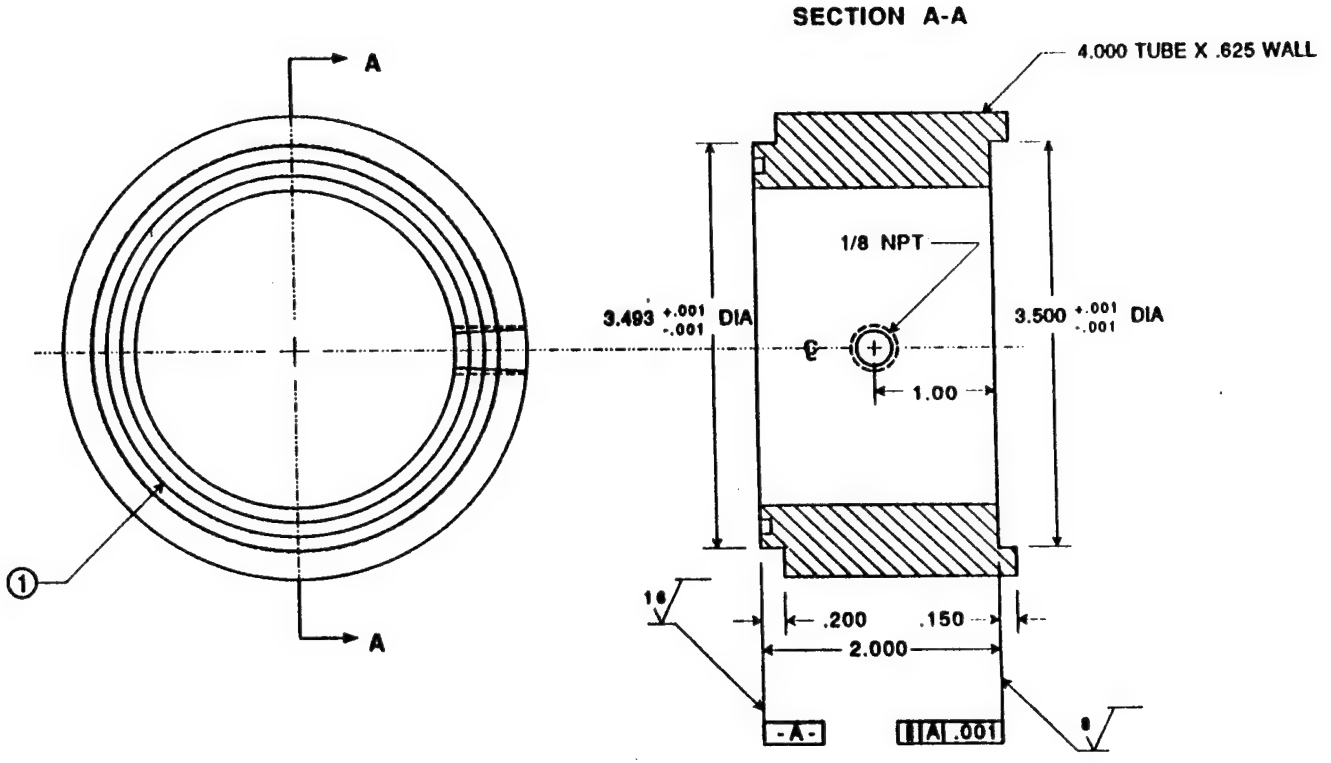

FORE DIAPHRAGM HOLDER
MATERIAL - SS 304 QUANTITY - 1 3/4 SCALE
T. W. EASTES 29-APR-91
UNLESS OTHERWISE SPECIFIED DIMENSIONS ARE IN INCHES TOLERANCES (.00) +/-.03 (.000) +/-.010 (∠) +/-30'

NOTES:
1. O-RING FACE SEAL GLAND DIMENSIONS PER PARKER SPECS FOR O-RING 2-234 FOR INTERNAL PRESSURE BY GASES.

SECTION A-A

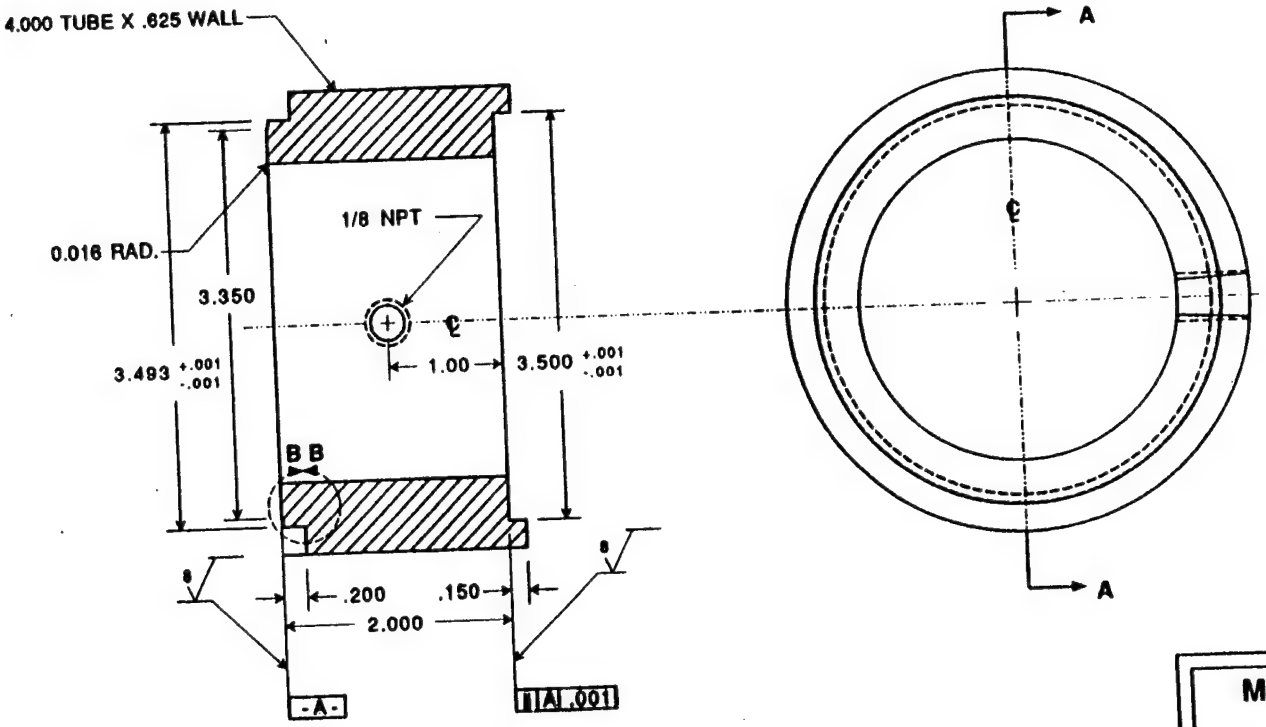

VIEW B-B

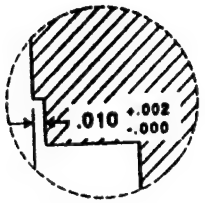

MID DIAPHRAGM HOLDER

MATERIAL - SS 304
QUANTITY - 1
3/4 SCALE

T. W. EASTES 29-APR-91

UNLESS OTHERWISE SPECIFIED
DIMENSIONS ARE IN INCHES
TOLERANCES
(.00) +/-.03 (.000) +/-.010 (∠)+/-30'

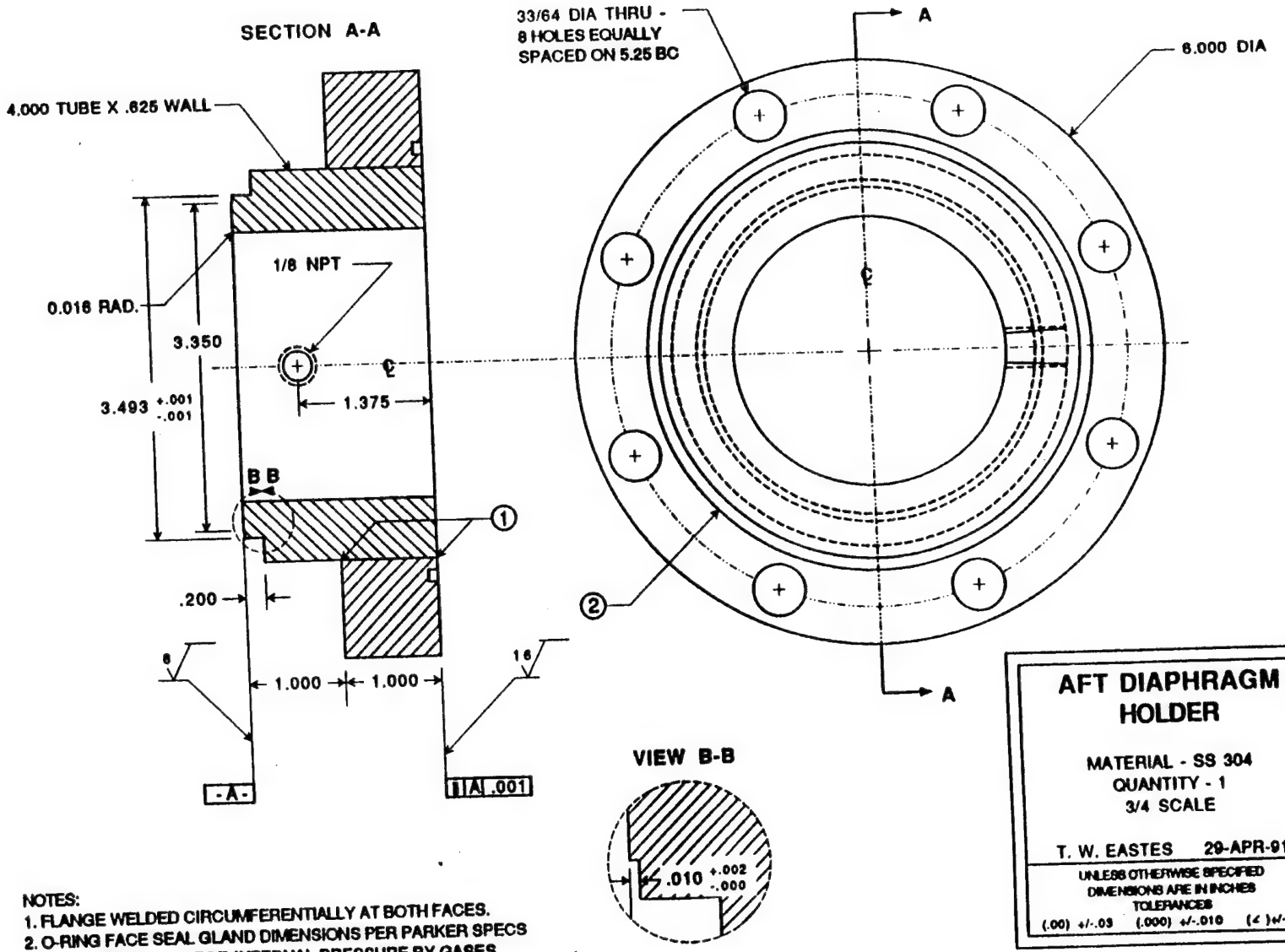

NOTES:
1. FLANGE WELDED CIRCUMFERENTIALLY AT BOTH FACES.
2. O-RING FACE SEAL GLAND DIMENSIONS PER PARKER SPECS FOR O-RING 2-244 FOR INTERNAL PRESSURE BY GASES.

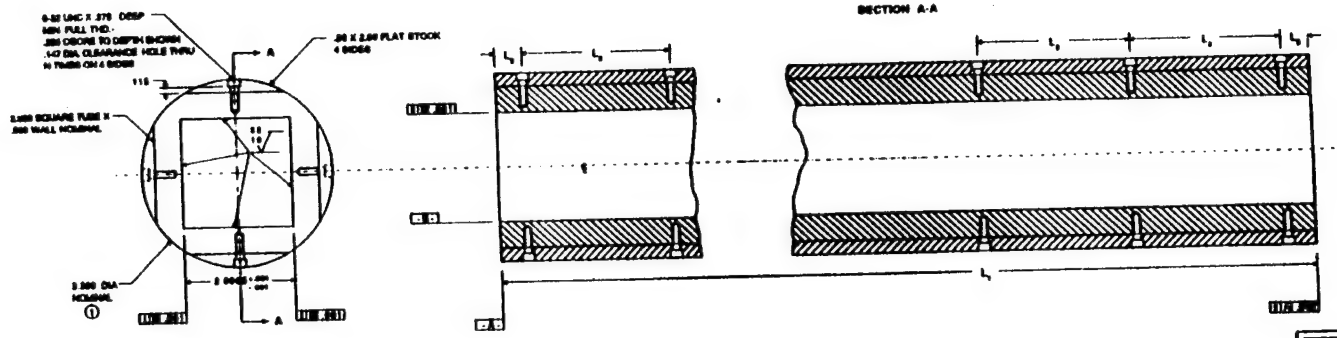

DASH #	QUANTITY	HOLE LOCATIONS L_1	L_2	L_3	N. # HOLES
-1	1	6.00	6.00	5.000	8
-2	1	11.00	6.00	5.000	16
-3	1	16.00	6.00	5.000	16
-4	1	21.00	6.00	5.000	16
-5	1	26.00	6.00	5.000	16

NOTES:
1. SQUARE SECTION MACHINED TO FIT TELESCOPICALLY INTO SHOCK TUBE ENCASEMENT SECTIONS.
2. SECTION COMPOSED OF 5.00 SQUARE TUBE X .500 WALL WITH FOUR .50 X 2.00 FLAT STOCK PIECES BORINED TO THIS PIECES AND THEN TURNED TO 3.000 DIA.

BORE SECTION

MATERIAL - AL 6061
QUANTITY - AS SHOWN
1/2 SCALE

T. W. EASTES 11-JAN-01

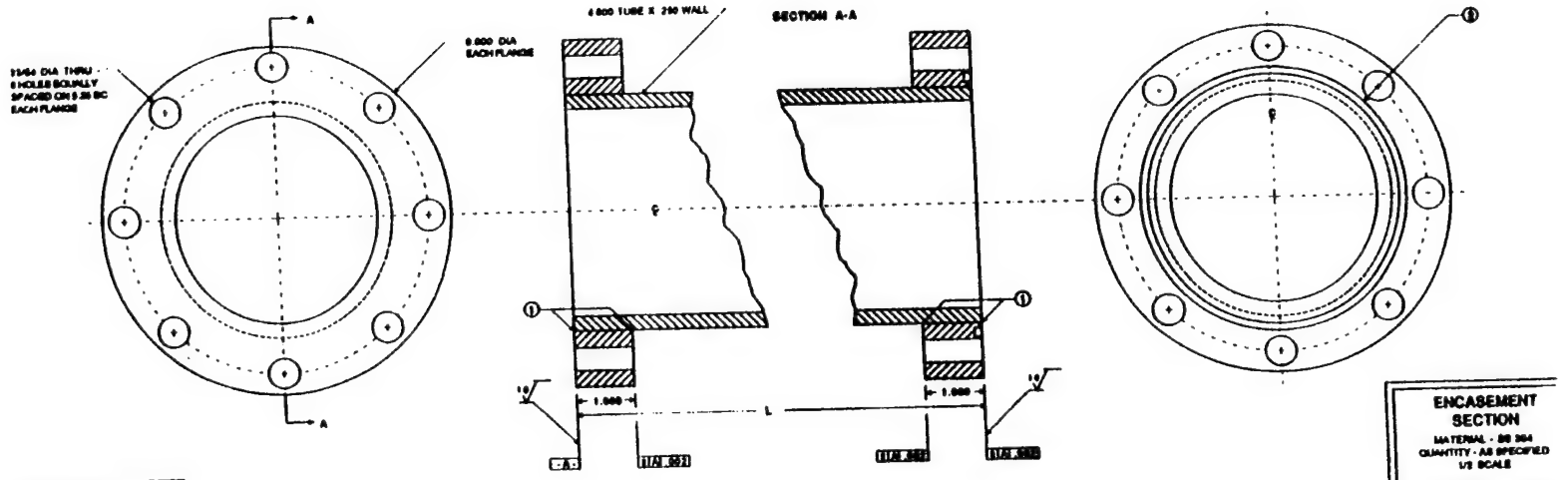

DASH #	QUANTITY	L_1
-1	1	6.00
-2	1	12.00
-3	2	24.00
-4	2	36.00

NOTES:
1. FLANGES WELDED CIRCUMFERENTIALLY AT BOTH FACES.
2. O-RING FACE SEAL GLAND DIMENSIONS PER PARKER SPECS FOR O-RING S-944 FOR 6M MINIMAL PRESSURE BY GAMES.

ENCASEMENT SECTION

MATERIAL - SS 304
QUANTITY - AS SPECIFIED
1/2 SCALE

T. W. EASTES 11-JAN-91

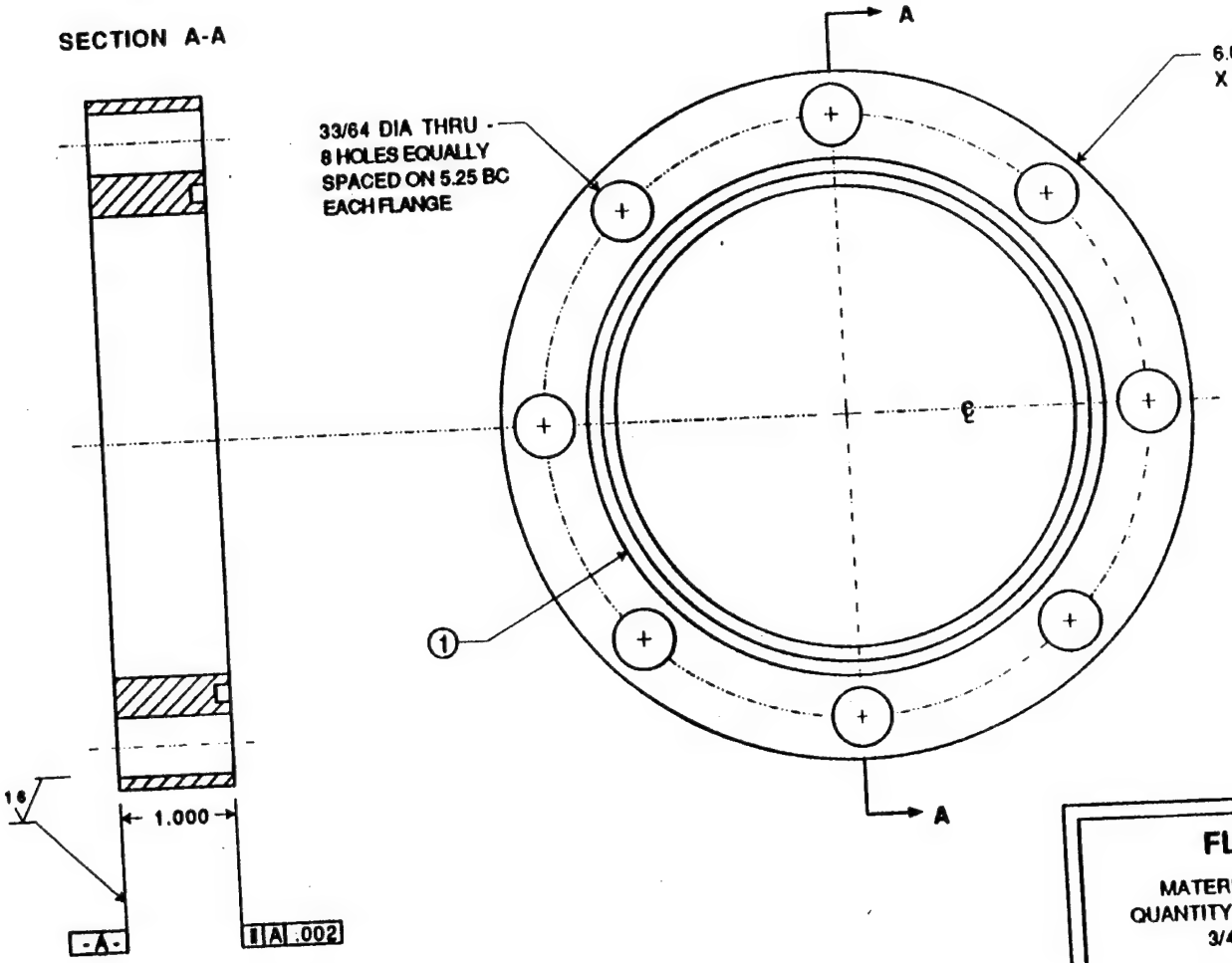

FLANGE

MATERIAL - SS 304
QUANTITY - AS SPECIFIED
3/4 SCALE

T. W. EASTES 11-JAN-91

UNLESS OTHERWISE SPECIFIED
DIMENSIONS ARE IN INCHES
TOLERANCES
(.00) +/-.03 (.000) +/-.010 (∠)+/-30'

NOTES:
1. O-RING FACE SEAL GLAND DIMENSIONS PER PARKER SPECS FOR O-RING 2-244 FOR INTERNAL PRESSURE BY GASES. MACHINE WHEN CALLED FOR ONLY.

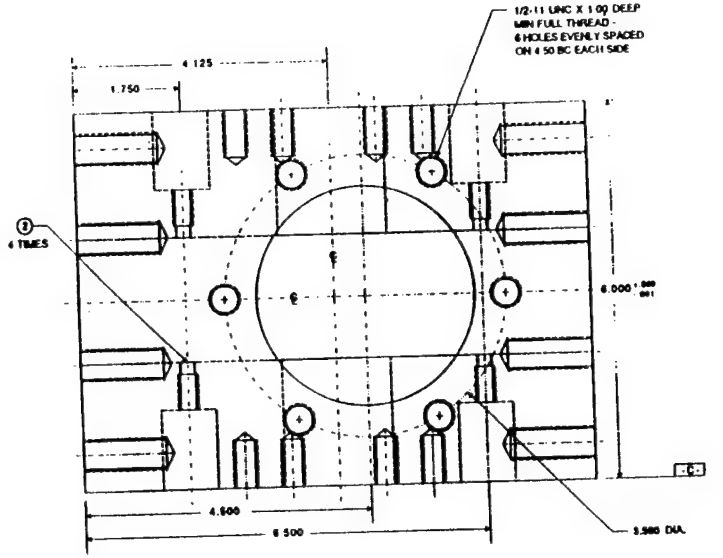

SECTION A-A

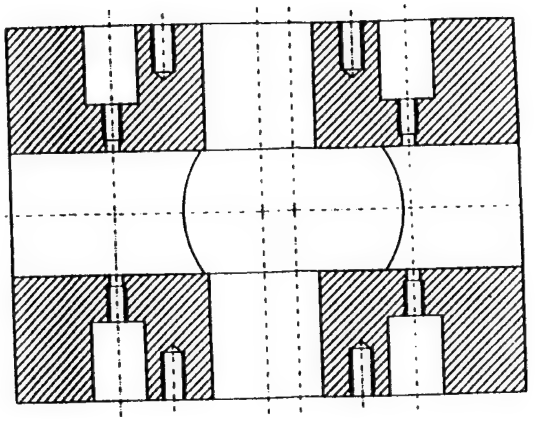

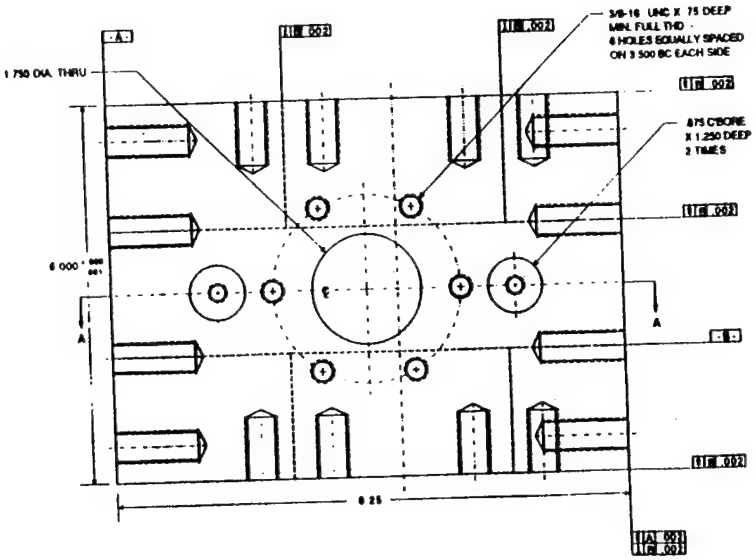

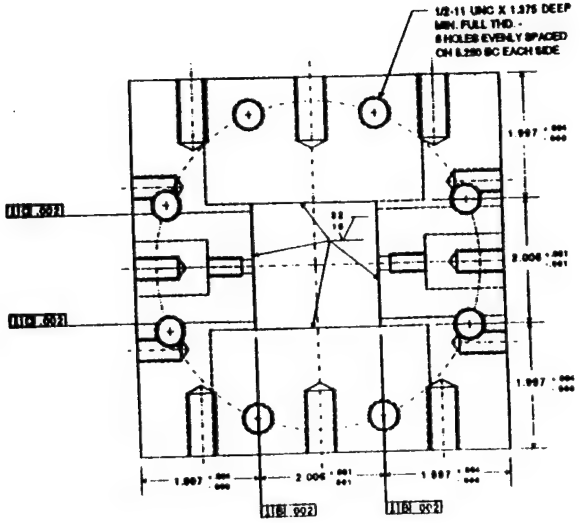

NOTES:
1. ALL SURFACES WITH BOLT CIRCLES MILLED TO 32 FINISH
2. SEE DETAIL DRAWING FOR POB PORT.

TEST SECTION
MATERIAL - SS 304
QUANTITY - 1
1/2 SCALE
T. W. EASTES 29-NOV-90
UNLESS OTHERWISE SPECIFIED DIMENSIONS ARE IN INCHES TOLERANCES

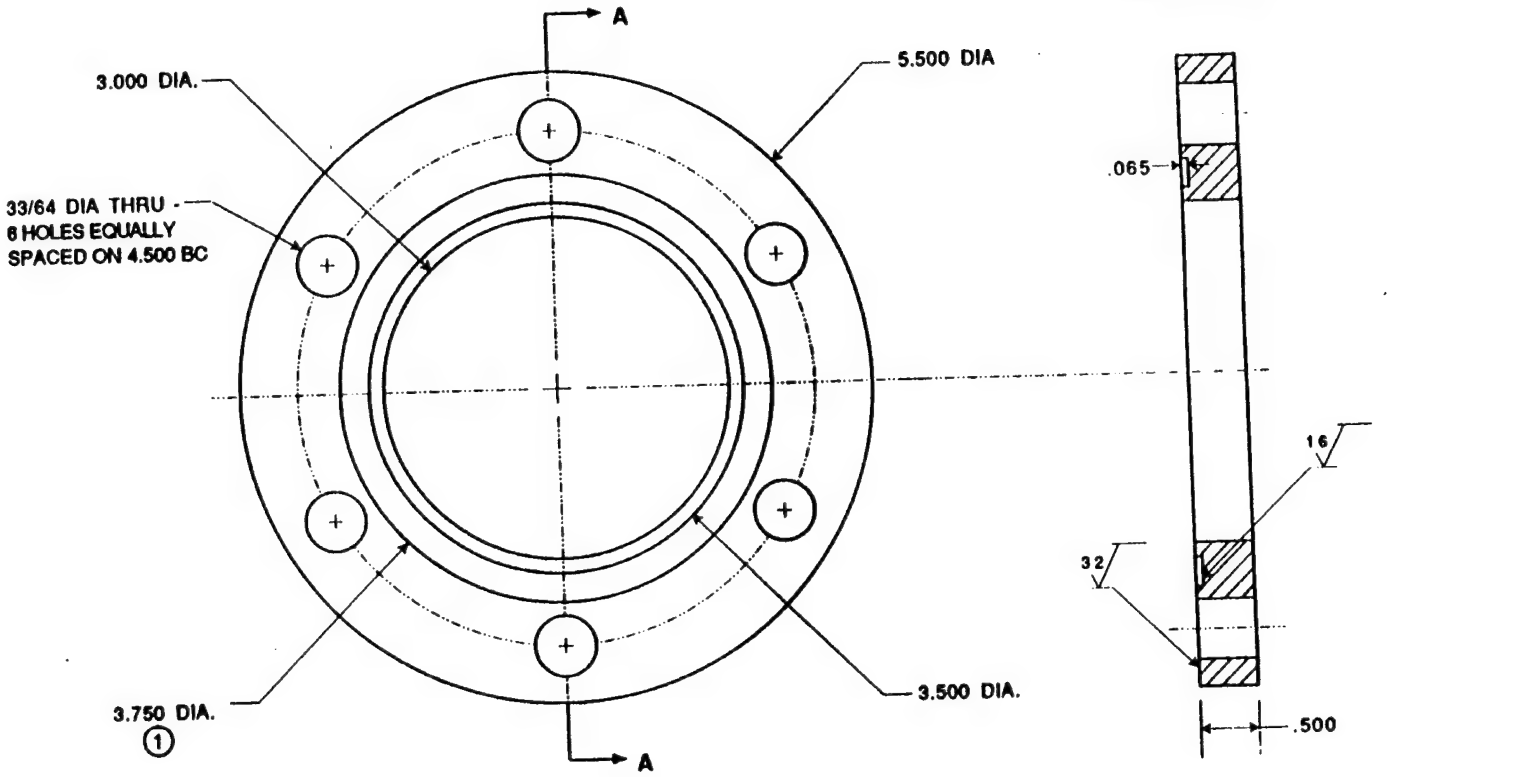

WINDOW RETAINER
MATERIAL - SS 304
QUANTITY - 2
3/4 SCALE

T. W. EASTES 29-NOV-90

UNLESS OTHERWISE SPECIFIED
DIMENSIONS ARE IN INCHES
TOLERANCES
(.00) +/-.03 (.000) +/-.010 (∠)+/-30'

NOTES:
1. RUBBER SEALING GASKET 3.75 OD. X .25 WIDE X .125 THICK WITH CRUSH INSTALLATION.

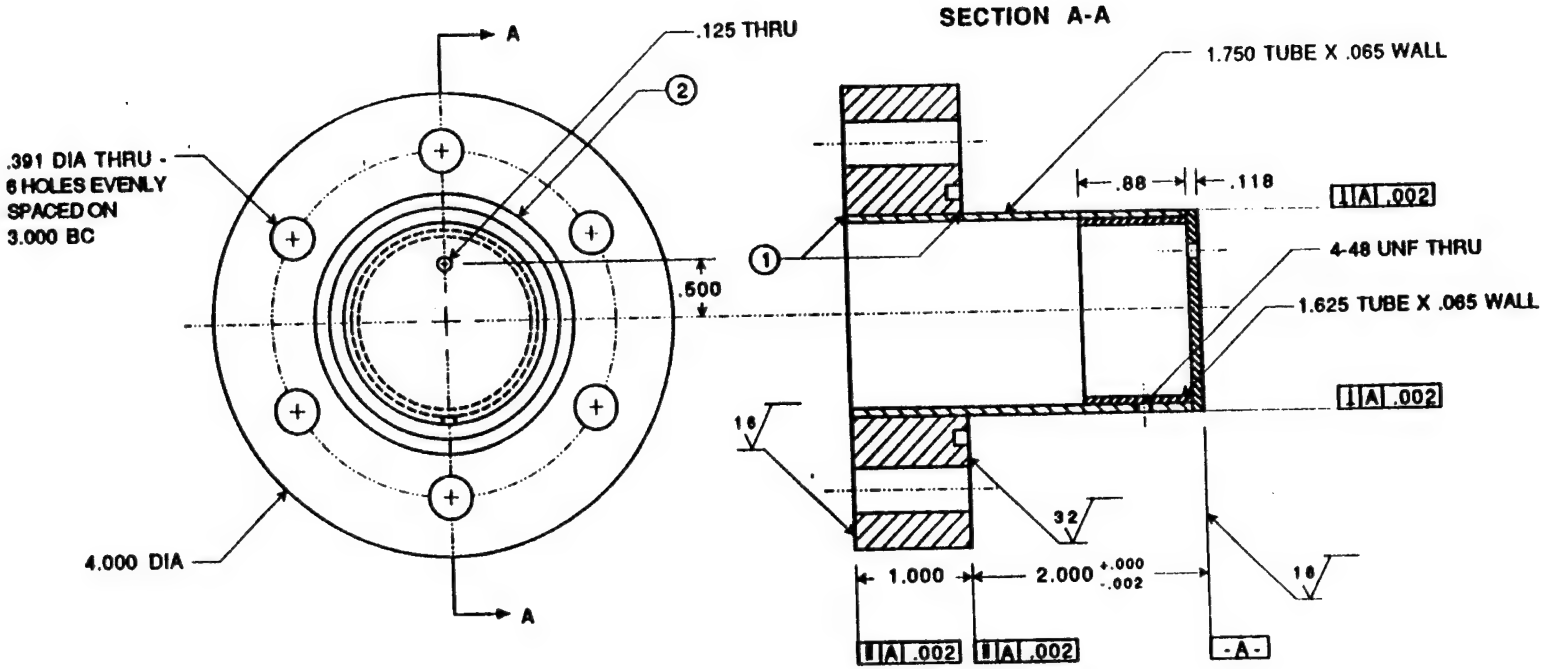

TOPHAT ASSEMBLY
MATERIAL - SS 304
QUANTITY - 2
3/4 SCALE
T. W. EASTES 29-NOV-90
UNLESS OTHERWISE SPECIFIED DIMENSIONS ARE IN INCHES TOLERANCES (.00) +/-.03 (.000) +/-.010 (∠) +/-30'

NOTES:
1. FLANGE WELDED CIRCUMFERENTIALLY AT BOTH FACES.
2. O-RING FACE SEAL GLAND DIMENSIONS PER PARKER SPECS FOR O-RING 2-226 FOR INTERNAL PRESSURE BY GASES.

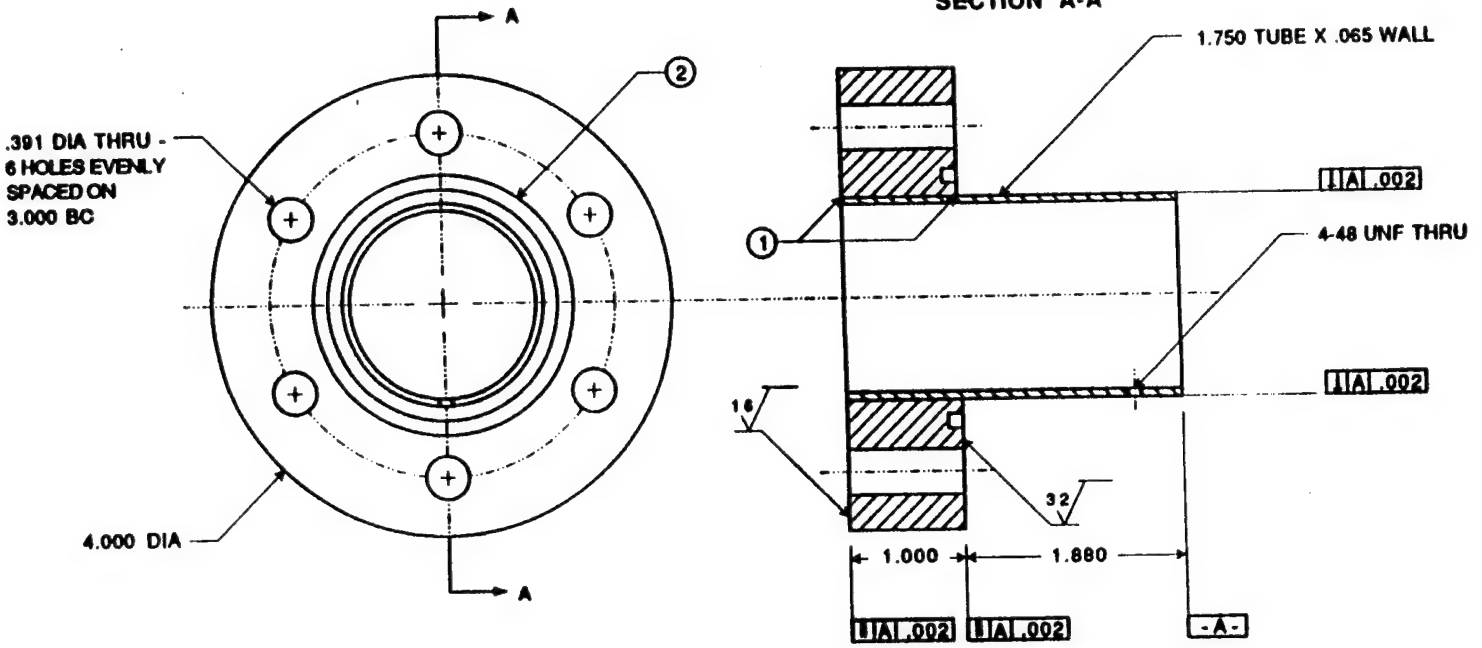

NOTES:
1. FLANGE WELDED CIRCUMFERENTIALLY AT BOTH FACES.
2. O-RING FACE SEAL GLAND DIMENSIONS PER PARKER SPECS FOR O-RING 2-226 FOR INTERNAL PRESSURE BY GASES.

TOPHAT BRIM
MATERIAL - SS 304
QUANTITY - 2
3/4 SCALE

T. W. EASTES 29-NOV-90

UNLESS OTHERWISE SPECIFIED
DIMENSIONS ARE IN INCHES
TOLERANCES
(.00) +/-.03 (.000) +/-.010 (∠)+/-30'

SECTION A-A

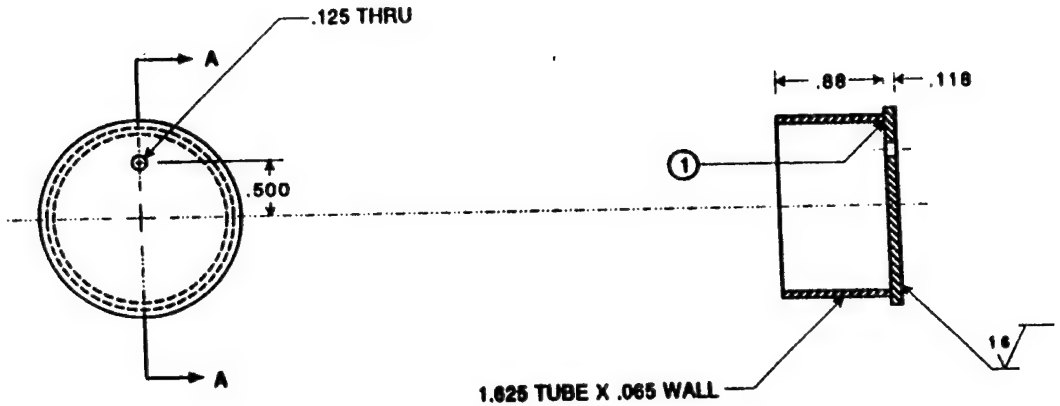

TOPHAT CROWN
MATERIAL - SS 304
QUANTITY - 2
3/4 SCALE
T. W. EASTES 29-NOV-90
UNLESS OTHERWISE SPECIFIED DIMENSIONS ARE IN INCHES TOLERANCES (.00) +/-.03 (.000) +/-.010 (∠)+/-30'

NOTES:
1. PLATE WELDED CIRCUMFERENTIALLY AT INNER DIAMETER.

APPENDIX J

"Secondary Atomization by High Amplitude Pressure Waves"**

** Republished with AIAA permission (Bonnie Midnica).

AIAA 92-3120
Secondary Atomization by High Amplitude Pressure Waves

T.W. Eastes and G.S. Samuelsen
UCI Combustion Laboratory
University of California
Irvine, CA

AIAA/SAE/ASME/ASEE
28th Joint Propulsion Conference and Exhibit
July 6-8, 1992 / Nashville, TN

SECONDARY ATOMIZATION BY HIGH AMPLITUDE PRESSURE WAVES

T.W. Eastes* and G.S. Samuelsen+

UCI Combustion Lab
Department of Mechanical and Aerospace Engineering
University of California
Irvine, California 92717-3550

List of Symbols

a = acceleration
Bo = Bond number, $\rho_o a R^2/\sigma_o$
D = drop diameter
Oh = Ohnesorge number, $\mu_o/(\rho_o D\sigma_o)^{1/2}$
R = drop radius
Re = Reynolds number, $\rho U_{rel} D/\mu$
t = time
U_{rel} = relative velocity between convective flow and drop
We = Weber number, $\rho U_{rel}^2 D/\sigma_o$
α = empirical function of viscosity
μ = molecular viscosity
ρ = density
σ = surface tension
τ = dimensionless time

Subscripts
b = breakup
cr = critical value
max = maximum value
o = drop property
∞ = gas property

Abstract

Secondary atomization or (drop breakup) can occur in at least three different manners in liquid rocket engine combustion chambers: 1) in the high velocity shearing flow field in the near injector region of a shear coaxial injector, 2) as gases expand and accelerate in the reaction zone, and 3) during combustion instability. In all of these situations the convective flow relative to the droplet can be quite high and easily simulated in the laboratory by a shock tube. This paper presents preliminary activity in the undertaking of a set of experiments designed to investigate drop breakup by the convective flow field associated with the passing of a shock. Topics to be covered include the background, previous work, the apparatus, the diagnostic technique, scaling to actual rocket engine conditions, and preliminary results.

I. Introduction

Motivation

In liquid rocket engines, primary and secondary atomization processes prepare the liquid phase for vaporization into and mixing with the gas phase. The degree of secondary atomization determines vaporization and mixing rates of the droplet phase in the surrounding gas. In dilute sprays, vaporization is typically found to control the mixing rate. In some dense sprays, however, secondary atomization can be found to control the mixing rate.[1]

Secondary atomization typically occurs in the near injector region where ligaments of liquid break off from a jet or sheet and then further breakup as they are sheared by co-flowing gas. Another source of drop breakup is the reaction induced expansion of the combustion gases which rapidly accelerate relative to any unburned propellant droplets. As a liquid droplet breaks apart more of the surface area per unit volume of that phase is available for the vaporization process and the liquid is distributed about a larger volume. Thus in addition to primary atomization, secondary atomization can directly effect the distribution of the liquid phase and therefore the local gas properties such as mixture ratio of the flow field. The resulting drop size and spatial distribution affects how rapidly the mixture can be expected to react, where it will react relative to the injection point and what length of combustor is required to contain the reaction.

In combustion instability in liquid rocket engines, secondary atomization may play a role in sustaining the instability. In high frequency combustion instability for such systems, a spontaneously generated shock wave can cause propellant droplets to shatter with a consequence of more rapid vaporization and combustion. When the associated heat release is sufficiently in phase with the pressure wave, such an instability can develop. Here, secondary atomization may play an indirect role in providing a vaporized liquid propellant to the gas phase for combustion in phase with the passing wave. If the fluctuation of energy release responding to a pressure disturbance causes a further change of pressure in phase with the initial disturbance, then the result may be an instability.[2] High frequency acoustic combustion instabilities can result in severe hardware damage due to the high pressure amplitudes and accelerated heat transfer rates. High amplitude pressure waves can cause structural failure, and the high heat transfer rates can cause excessive erosion of the combustion chamber walls; both of which may result in catastrophic failure of the rocket engine as well as the vehicle. Additionally, design provisions for combustion instability tend to reduce performance and increase costs.

A further complication in liquid rocket engines is that in most engines the liquid of which the droplets are composed is injected at pressures above the critical pressure. The critical pressure of oxygen, for example, is about 730 psia and typical chamber pressures range between 500 and 6000 psia. While the critical pressure for the hydrogen/oxygen system typically present in rocket engine combustion chambers can be substantially more than critical pressure, it is important to note that the convective flow field may act prior to the liquid propellant achieving thermodynamic equilibrium.

In the environment of a liquid rocket engine secondary atomization occurs when a convective field acts to break up already formed droplets which have been created in the primary

---

* Graduate Researcher
\+ Professor, Director, Associate Fellow, AIAA

atomization process. This interaction can cause one or more of the following to occur.

1. Transverse motion.
2. Reorientation of the internal Hill's spherical vortex.
3. Aerodynamic deformation.
4. Oscillation.
5. Surface wave formation.
6. Ligament formation and breakup into smaller droplets.
7. Stripping of small drops from the original droplet.
8. Total disintegration of the original droplet.
9. Greatly enhanced evaporation from both the original droplet and smaller drops which are stripped from it.
10. Collision with neighboring droplets with associated motion, dynamics, breakup, and/or coalescence.

Ultimately each of these processes enhances the vaporization rate by providing additional liquid surface area so that gas phase combustion can occur.

Questions and issues of primary interest in attempts to understand and model breakup phenomena include:

1. How does breakup occur?
2. Under what flow conditions does it occur?
3. How is the drop deformed and what is its drag coefficient history prior to breakup?
4. How long does the process take?
5. At what rates does breakup or stripping occur?
6. What drop sizes are produced and what influences these drop sizes?
7. How are the daughter droplets distributed in the flow field and what are their velocities?

II. Background

Previous Reviews

While there is a substantial portion of the literature devoted to atomization in general, secondary atomization is usually considered a subset thereof. Thus reviews of atomization usually include sections on secondary atomization. Ferrenberg et al.[3] contains the most recent such review. Lapple et al.,[4] while dated, is comprehensive and also contains a section on secondary atomization. Hinze[5] has reviewed early work specific to drop breakup, while more recent, yet still relatively dated reviews, include those of Forsnes and Ulrich,[6] and Luna and Klikoff.[7]

Characterizing Parameters

In addition to classical dimensionless parameters used to characterize secondary atomization such as Re, We, Bo, and Oh, dimensional analysis also yields a dimensionless time to breakup of the form,

$$\tau_b = (\rho/\rho_o)^{1/2} U_{rel} t_b / D. \qquad 1)$$

Although the definition of breakup time is somewhat ambiguous or at times ignored in the literature,[3] it is typically defined as the time elapsed from the point of exposure to the beginning of disintegration, the time required for disintegration, or the sum of these. In this discussion, the sum is considered. Liang et al.[8] summarize most existing data and correlations of dimensionless breakup times, τ_b as a function of We over all the known breakup regimes. The dimensionless breakup times range over an order of magnitude with values varying from 0.5[9] to 5.0.[10]

Hinze[11] postulated the existence of a critical Weber number above which breakup would occur. While a critical quantity should be unique by definition, values over one and a half orders of magnitude (from 1 to about 50) are routinely given in the literature. Hinze[5] modified his original Weber criteria to include the effect of viscosity and found the equivalent of

$$We_{cr} = C(1 + \alpha Oh). \qquad 2)$$

Correspondingly in a review, Luna and Klikoff[7] suggested that a Weber number corrected for liquid viscosity and the variation in flow duration with time is the best criterion for evaluating drop breakup. Recently, Kreczkowski[12] has proposed that the breakup mode is controlled by We, Oh and liquid/gas viscosity ratio, which is also consistent with Equation 2. Hsiang and Faeth[13] have recently observed that higher We_{cr} are found as Oh increases which is consistent with the findings of Hinze and Kreczkowski.

Rabin et al.[14] have suggested that the acceleration applied to the droplet as well as the duration of the flow have the greatest bearing on the breakup phenomena. Luna and Klikoff[7] indicate in their review that drop breakup requires sufficient flow duration, and thus We_{cr} is necessary, but not sufficient to obtain breakup. To account for this apparent transient dependence, Bo has been found to characterize the time over which the droplet deforms and breaks up for low Oh droplets and the type of breakup and critical Weber number were found to be strongly influenced by the duration and velocity of flow behind the shock wave.[10]

The time varying external forces of pressure, frictional drag, and body forces applied to the droplet as it deforms apparently determine how the breakup process occurs. Characteristic times associated with deformation, oscillation, flow duration, surface wave period, and others ultimately control this process.

Types of Breakup

There have been three basic types of droplet breakup observed, "bag", "shear", and "catastrophic". Others described in the literature appear to be transitional or combinations of varying degrees of these three basic types.

Borisov et al.[15] has suggested criteria for breakup by these different mechanisms as follows:

"bag" breakup: $8 < We < 40$, $0.2 < WeRe^{-0.5} < 1.6$ 3)

"shear" breakup: $20 < We < 2 \times 10^4$, $1 < WeRe^{-0.5} < 20$ 4)

"catastrophic" breakup: $2 \times 10^3 < We < 2 \times 10^5$, $20 < WeRe^{-0.5} < 2 \times 10^2$ 5)

The bag type of breakup is characterized by deformation of the droplet into an ellipsoid with its semimajor axis perpendicular to the flow direction. As the droplet flattens, its radius of curvature increases and the stagnation pressure is felt over a larger area. Eventually an unstable situation is achieved whereby the center of the drop is pushed downstream of the outer edge forming a thin membrane in the shape of a bag or parachute with the outer edge forming an annular ring of fluid with the bulk of the

liquid mass. The bag bursts creating a fine mist of droplets followed by failure of the annular ring breaking into larger droplets. Bag type breakup typically occurs at Weber numbers just above critical values and requires that the flow duration be applied significantly longer than required in shear or catastrophic breakup. Photographic evidence of this mode of breakup is widely available. (i.e., Krzeczkowski[12] and Rabin et al.[14])

The shear type of breakup is believed to be most important in liquid rocket engine flow regimes. It is characterized by deformation of the droplet into a lenticular shape due to the pressure difference between the windward and leeward sides with small waves forming on the windward side and liquid from the crests of these waves being eroded off by aerodynamic shear and capillary wave breakup and is typically attributed to Kelvin-Helmholtz instability. The droplets which compose the mist are so small that they tend to follow the streamlines in the wake of the original drop. This type of breakup occurs for $O(10^2) < Bo < O(10^5)$. Photographic evidence of this mode of breakup is also widely available. (i.e., Ranger and Nicholls,[9] Gordon,[10] Krzeczkowski,[12] and Rabin et al.[14])

The catastrophic type is characterized by rapid growth of surface waves on the windward face of the droplet with abrupt disintegration of drop before significant distortion or stripping. This is attributed to growth of acceleration waves induced by the rapid convective flow about the drop and is also known as the Rayleigh-Taylor instability regime. This behavior is observed at $Bo > O(10^5)$. Reinecke and Waldman[16] used an X-ray absorption technique which yielded microdensitometry traces on X-ray plates to determine rate parameters associated with the droplet mass.

Diagnostic Techniques

Diagnostic techniques for study of secondary atomization phenomena have typically employed use of high speed framing cameras to obtain images for qualitative analysis of the process. Shock tubes[9,10,12-17] or tubes through which a gas stream is passed[11] are the test articles of choice. Techniques for introducing the drop to these flows include suspension of pendant droplets from capillary tubes and wires, acoustic levitation, solenoidal retraction of a wire with a pendant drop on its tip, and injection into the gas stream by a drop generator.

More recently, holography has been employed to observe the product droplets of the secondary atomization process[13,17] and computer aided image analysis applied to size the product droplets.[13]

III. Experiment

Description

In this effort, the secondary atomization process is observed by injecting drops with a drop generator transversely to the bore of a shock tube and creating a shock which propagates through the drop path. The shock tube is operated at atmospheric conditions, although provisions exist for operating at up to 60 atmospheres. For a single set of test conditions, a sequence of still shadowgraphs of the breakup event are taken at progressively longer delay periods after the shock passing.

Scaling

Appropriate scaling is extremely important in this effort. Due to the nature of the liquid rocket engine combustion chamber environment, relatively little is known about the behavior of fluids at these conditions.

The shock tube experiments proposed for study of secondary atomization are designed to observe how drops of varying sizes breakup when subjected to convective fields of very high velocity. In order to extend these observations to what might be typical in an actual liquid propellant rocket engine, experimental parameters and conditions are specified as follows:

1. Drop sizes will be varied over a range believed to be characteristic of a typical rocket engine (50-500 microns).
2. Pressure wave amplitudes will be varied to obtain convective flow velocities to hundreds of meters per second.
3. The fluids for the droplet and the ambient gas will be selected to be similar in relationship to each other as those of a typical rocket engine.

A typical rocket engine for purposes of the above specifications is considered to be akin to the Space Shuttle Main Engine (SSME) or engine designs being considered for the National Launch System (NLS) program. These engines typically employ coaxial injector elements with liquid hydrogen and liquid oxygen as the propellants and operate at chamber pressures approaching 3000 psia. While some engines operate at conditions in which the droplet fluid is at subcritical conditions, for the newer high chamber pressure rocket engines, liquid oxygen is typically introduced at supercritical conditions.

Prudent experimental practice indicates that the relative effects of selected study parameters should be studied independently so that their relative sensitivity to the phenomena can be assessed. Due to the limited nature of the proposed experiments, a number of judgements regarding the relative importance of such parameters is required "a priori". A factorial-style[18] test matrix can then be developed based on these parameter relevance estimates. In the initial experiments, efforts to simplify the experiment and the flow field are necessary, as deconvolution of these effects is essential to any successful modeling effort undertaken.

Drop Generation

Several drop generation techniques will be applied for this effort due to the various drop configurations anticipated. The classic Berglund-Liu (used in tests presented here) and more recently developed Dressler[20] type drop generators will be employed where interdrop spacing effects are deemed insignificant with the drop-on-demand (DOD) drop generator by Switzer[20] reserved for conditions where interdrop spacing effects are believed significant. At high pressures, a capillary tube with annular coflowing gas due to Peterson[21] is believed necessary to avoid breakup upon injection where the higher density gas into which the droplet is injected significantly increases We. Compressibility effects on piezoelectric crystals are suspect as well at these higher pressures.

Shock Tube

The double diaphragm shock tube to be used for this effort is square in crossection (2" x 2") and capable of holding pressures to 1000 psia in the driven section and 3000 psia in the driver section (see Figure 1 for a system schematic with diagnostic orientation). This will permit, for instance, breakup phenomena to be observed

with an ambient pressure of 650 psia with the droplet subjected to a 50% wave. The driven section is 36" in length and provides a test time of approximately 3 ms in the uniform flow region behind the shock. The test section provides a station where droplets are introduced into the bore of the shock tube, collected liquid is removed, and viewports are placed to fully view the secondary atomization process. The design of the test section also maintains constancy of the 2" by 2" crossection to minimize reflections from test section internal surfaces which could adversely affect the tractability of the flow field. Provisions for location of pressure transducers before and after the drop injection station are also made. The modularity of the test section provides for easy modification for any future efforts.

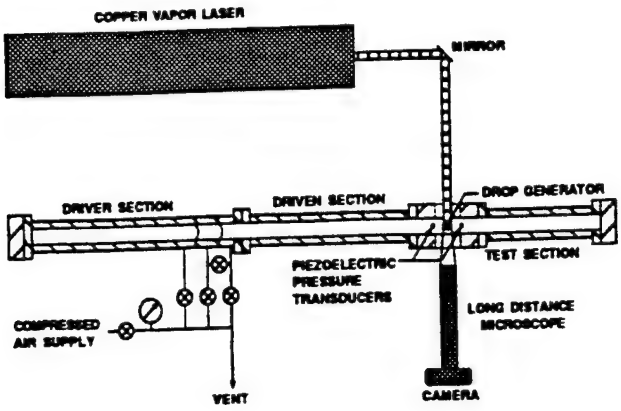

Figure 1. Shock tube experiment schematic.

Diagnostics

For these experiments, still 35 mm photography (Pentax, 35mm ME Super) with a copper vapor laser (Oxford Model CU-10A) light source and a 6X F/2.8 long distance microscopic lens (Infinity Model K-2 with CF-3 objective) will provide detailed images of the event. Piezoelectric pressure transducers (PCB Model 113A21) will measure the pressure history and help characterize the flow field experienced by a drop during the event.

The copper vapor laser provides sufficient pulse energy (0.1-1 mJ) for photographic illumination and short pulse duration (20-30 nanoseconds) to minimize image smearing. For example, a 10 micron droplet traveling at 100 m/s moves one forth of its diameter during a 25 nanosecond pulse.

A schematic showing the diagnostic strategy is shown in Figure 2. For the still shadowgraphs, the laser is turned off, the camera shutter opened, and the shock initiated. Based on detection of the shock by the pressure transducer a preset delay elapses at which time the laser pulse is fired and the shutter on the camera is then closed.

Measurements

Quantitative measurements which can be made are wave pressure history, drop character, and product or stripped drop character. Qualitative measurements which can be made include observations of breakup mode, drop deformation, ligament formation, and surface wave formation. Photographic analysis will be used to make topological quantitative and qualitative measurements. The pressure history of the wave is to be measured by high frequency response piezoelectric pressure transducers and the associated velocity, temperature, and density field deduced from simple 1-D compressible flow relations.

Adaptability of Data to Modeling Effort

Development of a suitable model for study of secondary atomization in liquid rocket engines requires descriptions at both sub- and supercritical conditions, examination of the atomization physics, quantization of the breakup process, highly resolved temporal and spatial measurements, and response characterization over a large range of flow conditions.

The systematic approach to this effort provides for concurrent experimentation and model development. Because current modeling and previous experimental work has only been done at subcritical droplet fluid conditions, the bulk of the experimental effort will be done at these conditions. The facility described here will permit detailed experimental observation of the secondary breakup process. This will permit the model to be developed from a more physical and, therefore, fundamental basis. With this basis firmly established, extension to supercritical conditions can then be undertaken. The experimental effort seeks to provide some limited data at supercritical conditions to provide a physical basis for the model at these conditions.

The experiments presented here are designed to support model development and help verify model accuracy. Together, the experiment and theory will help us to understand the physics associated with secondary atomization. Future experimental effort may be suggested by theory, thus permitting further refinement of the model.

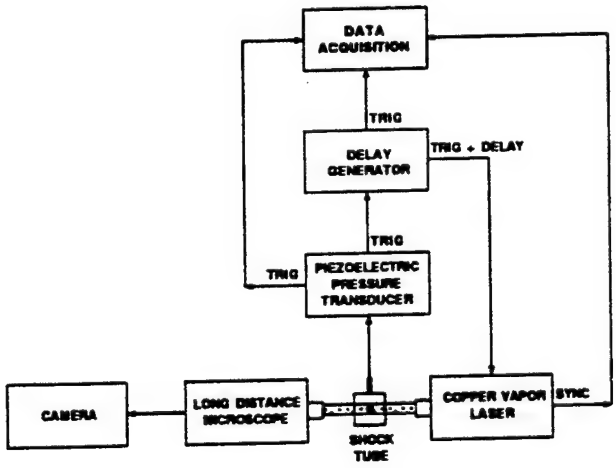

Figure 2. Shadowgraph diagnostic strategy.

IV. Results and Discussion

Preliminary still shadowgraphs of the breakup process were taken during shock tube characterization tests. A sequence of these at a magnification of approximately 8 is shown in Figure 3. The times are measured from the time at which the shock impinges on the drop stream. Characterizing data for this sequence is as follows:

Drop liquid - methanol
Drop diameter, D= 180 μm
Ambient fluid - air
Ambient pressure= 1 atm

Ambient temperature= 70 F
Shock strength= 1.35
Re_{max}= 1150
We_{max}= 70
Bo_{max}= 30
Oh= 0.01
τ_b= 6

Based on these values, the mode of breakup is found to be in the shear mode according to Equation 4, but is characterized as an intermediate between "bag" and "shear" or "multimode" breakup by Hsiang and Faeth.[13] Analysis of the photos indicates the stripped droplet sizes decrease from approximately 30 μm at 120 μs to 12 μm after 210 μs. The breakup time, τ_b seems to be a very subjective quantity and arguments could be made for values of t_b from 270 μs up. Another interesting calculation revealed that the volume of the apparent chord of a sphere at 60 μs is just that. Interdrop spacing is initially about 1.4 diameters which appears to be insufficient to eliminate interaction between adjacent droplets.

Conclusions

The preliminary photographic data presented here represents the type of images available through recent advances in imaging using a copper vapor laser light source. The facility described has been developed to continue the task of mapping regimes of secondary breakup, dynamic response characterization, and temporally and spatially resolved examination of the secondary breakup process for liquid rocket engine applications. Initially experimental efforts will lead this effort, but as data is made available to modelers, physical understanding of the observations can be achieved. Systematic experimental examination of the basic processes holds the key to understanding the global processes in secondary atomization and ultimately atomization in general.

Acknowledgements

This work is being sponsored by the Phillips Laboratory at Edwards Air Force Base through a contract to Pratt and Whitney Government Engines and Space Propulsion. Jay Levine of Phillips Laboratory is the program monitor and George Cox and Eric Petersen of Pratt and Whitney are the program managers. Arash Ateshkadi assisted in obtaining the photos and preparation of the paper.

References

1. Faeth, G.M., (1990) "Structure and Atomization Properties of Dense Turbulent Sprays," 23rd Symposium (International) on Combustion, The Combustion Institute, Pittsburgh, PA, 1990, pp. 1345-1352.
2. Culick, F.E.C. (1989) "Combustion Instabilities in Liquid-Fuelled Propulsion Systems," AGARD Conference Paper No. 450, Neuilly sur Seine, France, Nov. 1989.
3. Ferrenberg, A., Hunt, K., and Duesberg, J., (1985) "Atomization and Mixing Study," Rockwell International, Rocketdyne Division Report RI/RD85-312, 1985.
4. Lapple, C.E., Henry J.P., and Blake, D.E., "Atomization - A Survey and Critique of the Literature," Stanford Research Institute Report No. 6, Menlo Park, CA, (also ASTIA AD-81-314), 1967.
5. Hinze, J.O. (1955) "Fundamentals of the Hydrodynamic Mechanism of Splitting in Dispersion Processes," Forced Deformations of Viscous Liquid Globules," AIChE J., vol. 1, no. 3, pp. 289-295.
6. Forsnes, V.G. and Ulrich, R.D. (1968) "A Literature Review and Discussion of Liquid Particle Breakup in Gas Streams," Naval Weapons Center Report, NWC-TP-4589, China Lake, CA, July 1968.
7. Luna, N. and Klikoff, W. (1967) "On Aerodynamic Breakup of Liquid Drops," Sandia National Laboratory Report SC-RR-66-2716, Albuquerque, NM, 1967.
8. Liang, P.Y., Eastes, T.W., and Gharakhani, A., (1988) "Computer Simulations of Drop Deformation and Drop Breakup," AIAA Paper 88-3142, AIAA/ASME/SAE/ASEE 24th Joint Propulsion Conference, Boston, MA, Jul. 1988.
9. Ranger, A.A., and Nicholls, J.A., (1969) "Aerodynamic Shattering of Liquid Drops," AIAA J., vol. 7, no. 2, Feb. 1969, pp. 285-290.
10. Gordon, G.D. (1959) "Mechanism and Speed of Breakup of Drops," J. Appl. Phys., vol. 30, no. 11, Nov. 1959, pp. 1759-1761.
11. Hinze, J.O. (1948) "Forced Deformations of Viscous Liquid Globules," Appl. Sci. Res., series A, vol 1, no. 9, pp. 263-272.
12. Krzeczkowski, S.A. (1980) "Measurement of Liquid Droplet Disintegration Mechanisms," Intl. J. Multiphase Flow, vol. 6, no. 3, pp. 227-239.
13. Hsiang, L.-P. and Faeth, G.M., (1992) "Secondary Drop Breakup in the Deformation Regime," AIAA 92-0110, 30th Aerospace Sciences Meeting, Reno, NV., Jan. 1992.
14. Rabin, E., Schallenmuller, A.R., and Lawhead, R.B. (1960) "Displacement and Shattering of Propellant Droplets, Rocketdyne Report R-2431, AFOSR TR-60-75, Mar. 1960.
15. Borisov, A., Gel'fand, B., Natanzon, M., and Kossov, O. (1981) "Droplet breakup Regimes and Criteria for their Existence," J. Engng. Phys., vol. 40, no. 1, pp. 44-49.
16. Reinecke, W.G. and Waldman, G.D., (1970) "Experiments on Waterdrop Breakup Behind Strong Shocks with Applications to Flight," Avco Report AVSD-0110-70-77, May 1970.
17. Wierzba, A., and Takayama, K., (1988) "Experimental Investigation of the Aerodynamic Breakup of Liquid Droplets," AIAA J., vol. 26, No. 11, Nov. 1988, pp. 1329-1335.
18. Box, G.E.P., Hunter, W.G., and Hunter, J.S. (1978) Statistics for Experimenters, John Wiley and Sons, New York.
19. Dressler, J.L. and Kraemer, G.O. (1990) "A Multiple Drop-Size Drop Generator for Calibration of a Phase-Doppler Particle Analyzer", in Liquid Particle Size Measurement Techniques: 2nd Volume, ASTM STP 1083, Hirleman, E.D., Bachelo, W.D., and Felton, P.G., Eds., American Society for Testing and Materials, Philadelphia, pp. 30-44.
20. Switzer, G.L. (1991) "A Versatile System for Stable Generation of Uniform Droplets," Rev. Sci. Instrum. vol. 62, no. 11, Nov. 1991. pp. 2765-2771.
21. Peterson, R.B. (1988) "Characterization of a Simple, High Reynolds Number Droplet Generator, for Combustion Studies," Rev. Sci. Instrum. vol. 59, no. 6, June 1988. pp. 960-966.

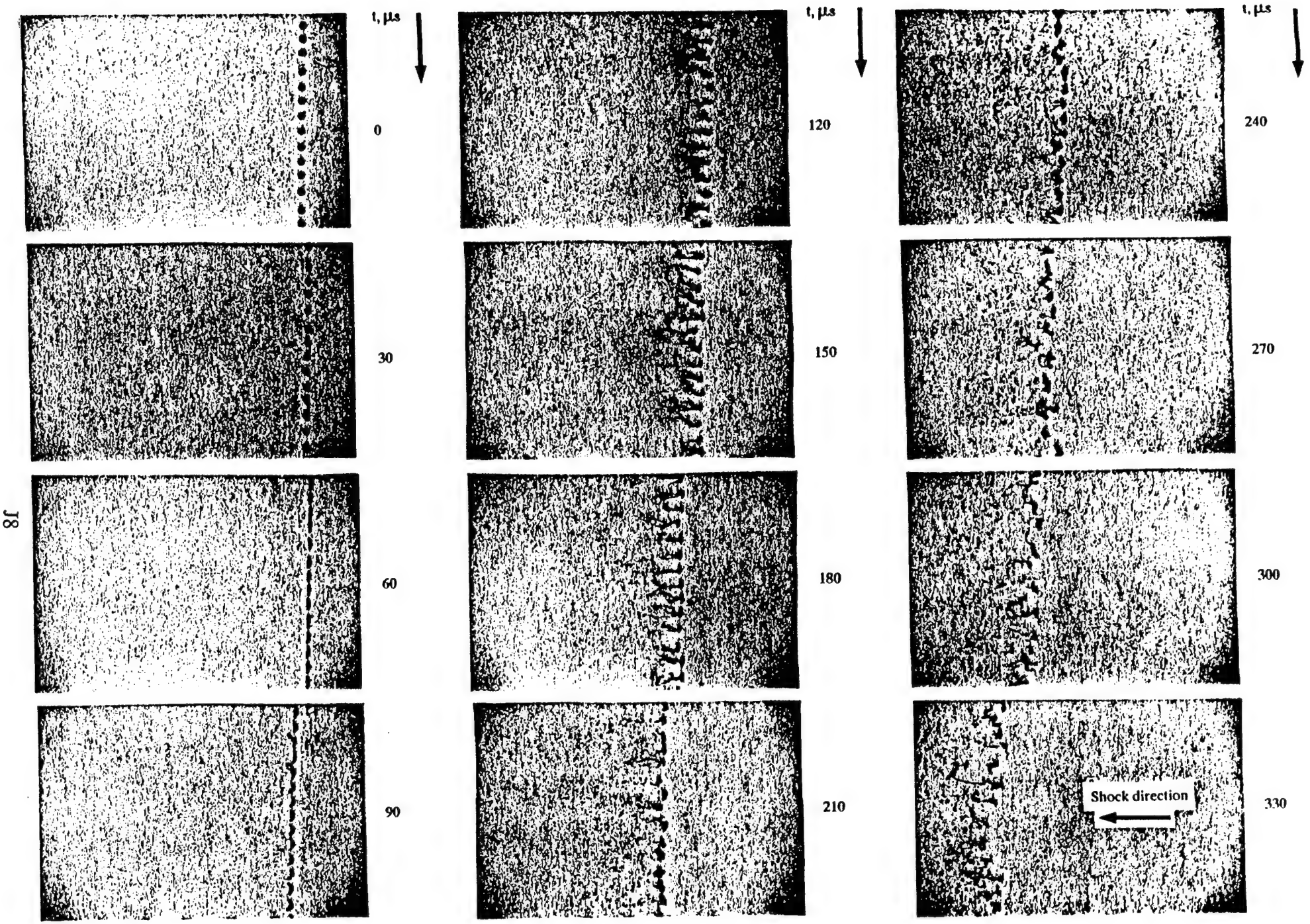

Figure 3. Shadowgraphs of 180 μm methanol drop stream subjected to 35% shock with 30 μs interframe spacing.

APPENDIX K

"Oscillatory Fuel Droplet Vaporization: Driving Mechanism for Combustion Instability"

Oscillatory Fuel Droplet Vaporization:

Driving Mechanism for Combustion Instability

A. Duvvur*, C. H. Chiang† and W. A. Sirignano‡

Department of Mechanical and Aerospace Engineering

University of California, Irvine

Abstract

Liquid fuels are commonly used in the propulsion of ramjets and rockets. They offer great flexibility in terms of controlling the rate of energy release. However, combustion instability has historically been a major problem in the development of liquid fuelled ramjets and rockets. Previous investigations which employed a simplified droplet vaporization model indicated that droplet vaporization is indeed capable of driving an instability. In this study, an established droplet vaporization model has been used to make an exact evaluation of the effects of pressure and velocity oscillations on the vaporization process and then to

*Research Assistant

†Postdoctoral Associate

‡Professor of Mechanical and Aerospace Engineering, Fellow AIAA.

determine whether droplet vaporization is capable of driving combustion instability. In addition, a parametric study has been conducted by using various frequencies of oscillation and amplitudes of fluctuation for the longitudinal mode. Depending on the local relative velocity between the gas and the droplet it is possible that the wake may be ahead of the droplet or behind the droplet, with reference to the chamber. This phenomenon has also been included in the parametric study. It has been found that droplet vaporization is indeed capable of driving instability in some frequency domains and preliminary results show that the amplitude of the oscillation does not have very significant effects on the response factor of the system.

Nomenclature

a	a'/a'_0, instantaneous radius
c'	speed of sound
G	response factor
p	$(p' - p'_\infty)/(\rho'_{g,\infty} {U'_{\infty,0}}^2)$, pressure
T	T'/T'_∞, temperature
U	$U'/U'_{\infty,0}$, horizontal component of velocity
V	$V'/U'_{\infty,0}$, vertical component of velocity
Y_i	mass fraction
z'	axial location
t'	time

P	$P'/(\rho'_{g,\infty}{U'_{\infty,0}}^2)$, pressure fluctuation
m	$m'/(\rho'_{g,\infty}U'_{\infty,0}{a'_0}^2)$, vaporization rate fluctuation

Greek Symbols

ϵ'	amplitude of oscillation
λ'	wavelength
γ	specific heat ratio
ϕ	starting phase
μ'_g	viscosity of gas phase
τ_{Hg}	$t'\mu'_{g,\infty}/({a'_0}^2\rho'_{g,\infty})$, gas-hydrodynamic-diffusion time

Subscripts

∞	conditions at the free stream
f	fuel
h	droplet heating
p	pressure
po	position
r	radial direction
t	time

u	velocity
z	axial direction

Superscripts

$'$	dimensional quantity
$-$	Steady value

Introduction

Combustion instability has plagued liquid rocket development programs since the early fifties. Indeed, instabilities have been observed in almost all devices that involve combustion in a chamber and subsequent energy release because any enclosed chamber has an infinite number of resonant modes of oscillation. Depending on the frequency and mode, varying levels of damage may be sustained. The spontaneous onset of instability in the combustion chamber usually augments heat transfer rates in the combustion chamber and can sometimes cause vibration levels in excess of 1000 g.[1]

In recent times, there has been a renewed interest in the study of combustion instability mechanisms in an effort to find a reliable method to predict the occurrence of this phenomenon in a particular liquid rocket combustor. There is reason to believe that instability may be understood by studying the vaporization process.[2–5] Droplet vaporization research

has also made notable headway in the last decade and is now a highly developed science.[6-9] A large amount of time and resources have been invested in accurate modelling of droplet vaporization. Experimental results have been used to validate the new theories and as a result, substantial insight has been gained in droplet vaporization theory. It is now possible to use more accurate vaporization models to study the effect of an unstable atmosphere on a vaporizing droplet.

Experimental evidence shows that the combustion in a liquid propellant rocket combustion chamber is never perfectly smooth. The liquid rocket engine is susceptible to instabilities because it only takes a small fraction of the total energy released to sustain an unstable mode of operation and the nearly closed nature of the system prevents it from resisting the oscillations. For this reason, the supply of energy from the transient combustion process, which is in phase with the wave motion, sustains the oscillations in this closed loop.[10]

Design of a combustion chamber that would minimize the coupling between the combustion and the fluid mechanics would require a thorough understanding of the mechanism of combustion instability. Such an understanding would permit lowering of rocket engine development costs and would allow the design of intrinsically stable, high performance liquid rocket engines.[3,11]

It is known that the driving force behind combustion instability is the energy input from the combustion process. The Rayleigh criterion is the most commonly used criterion to determine if a particular mechanism is capable of driving the combustor into an unstable mode or not. The Rayleigh criterion may be stated as: a mechanism can drive the instability

if the associated burning rate oscillates with the proper combination of a large enough amplitude and a small enough phase lag with the pressure oscillation.

The time lag theory was first applied to combustion instability problems by Crocco and his colleagues at Princeton. Time lag models have been used with some success in the study of combustion instability.[12-16] These models are based on the fact that there is a finite time delay between the introduction of the fuel into the combustion chamber and the actual combustion process resulting in energy release and if a small pressure pulse is applied to a steadily burning propellant, the regression rate will take a certain amount of time to reach its new steady value.[17] However, time-lag approaches are useful for a first look at instability but more detailed analyses of the flow are better.[17]

Efforts to understand liquid rocket instability have typically been based either on an acoustic analysis or an analysis of the vaporization process. Crocco and his researchers developed the time lag theory which is based on the time delay in the combustion process.[12,13,16] The n-τ model accommodates both transverse and longitudinal mode waves and uses both linear (small perturbation) and non-linear analysis for finite amplitudes.[1] This theory has its limitations in that it treats mainly one-dimensional mean flow cases. The time lag theory was first applied to nonlinear behavior by Sirignano.[16] There has been extensive work on the time lag theory and it has been modified to include other physical phenomenon like shock waves. Acoustics played a crucial role in the instability phenomenon as was indicated by the resemblance between the frequency of the oscillations and the acoustic modes of the combustor. There was thus an interest in the problem of acoustic resonance.

Classical droplet vaporization theory is founded in the well known d^2 law. However, this analysis assumes that the droplet is travelling at the velocity of the gas and that there is spherical symmetry. It is known that this theory, though well formulated, has rather limited applications. The relative motion between the droplet and the ambient gas (which is non zero in most cases) leads to an increase in the heat and mass transfer rates. It is known that for droplets with initial radius of twenty five microns and greater, the time for velocity relaxation due to drag is comparable or greater than the droplet lifetime.[7] These and other effects like internal circulation, neglected by the classical droplet vaporization theory, lead to considerably smaller characteristic lengths and times for liquid-phase heat and mass transfer. The strong coupling between the drag, heat transfer, mass transfer, relative droplet velocity and internal circulation necessitates a numerical solution.

Strahle[18] studied unsteady droplet combustion in 1960 using a linear model. He used an infinite conductivity model and hence neglected the thermal wave within the droplet. The assumption of infinite liquid conductivity meant zero liquid thermal inertia and this prevented the droplet from responding to the ambient oscillations.[18] This yielded results that did not suggest that vaporization was a candidate driving mechanism for instability. The assumption of infinite thermal inertia was relaxed by Priem and Heidman by the use of a uniform temperature assumption.[19] This resulted in an overestimation of the liquid thermal inertia. However, they successfully demonstrated that vaporization did affect stability and that it could be controlled by varying the vaporization process parameters.[20,21] However, the amplitude of the response was not sufficient to drive the instability. Tong and Sirignano

used a more exact one-dimensional droplet model and examined the response of a vaporizing droplet to oscillating ambient pressure and velocity conditions.[4] They examined the effect of both standing and travelling waves. The use of more reasonable assumptions demonstrated that droplet vaporization under oscillatory conditions was capable of driving instability. The component of the vaporization rate in phase with the pressure was found to be larger for a travelling wave than for the stationary wave. The model assumed that vaporization was rate controlling and that mixing and chemical reactions were very rapid. In addition, a quasi-steady gas-phase behavior was assumed. Internal circulation in the liquid was accounted for by a vortex model. In the model, the gas phase heat and mass transfer rates were modelled by using the average of the rates between the two. Bhatia and Sirignano[5] employed a one-dimensional vaporization model developed by Abramzon and Sirignano[6] to study ramjet instability. Their results indicated that vaporization was rate controlling and they were also successful in identifying a ratio of oscillation period to droplet heating time.

Chiang *et al*[9] and Chiang[8] developed an advanced exact droplet vaporization model with fewer assumptions that was formulated with the intention of being a reference model against which simpler models could be measured. This axisymmetric, single droplet model included effects of surface blowing, transient heating and internal circulation. Variable properties of the gas phase were taken into account, and viscosity variations in the liquid phase were also calculated.

There is adequate reason to believe that the liquid phase may prove to be a driving mechanism for instability. For this reason, the transient heating and vaporization of the fuel

droplets under oscillating conditions must be examined. This is based on the knowledge that transient and liquid thermal inertia are very important under steady operating conditions and therefore it is expected that they should also be important under unsteady conditions. Previous work by Tong and Sirignano[4] does indeed support this theory and it has been shown that unsteady droplet vaporization is a likely candidate mechanism for driving instability. Their model also assumes constant properties and is a one-dimensional analysis. The Tong and Sirignano model is limited to the liquid phase and therefore vital information like drag coefficient can not be obtained from their study.

It should be noted that not all the droplets injected into the chamber of a liquid rocket combustor, which is under an oscillatory mode of operation, experience the same ambient conditions. As combustion is a continuous process and fuel droplets are injected constantly, droplets injected at different times need not necessarily be going through the same cycle.

This study examines the role of droplet vaporization under oscillating atmospheric conditions and is an extension of previous work by Tong and Sirignano.[4] Details of this work may be found in Reference 24. The model used here is an advanced model with fewer assumptions and the emphasis is on studying the effects of an oscillating gas phase on the heat and mass transfer processes in the liquid phase. The present study employs an advanced variable-property droplet model which calculates both the gas and liquid phase. The axisymmetric model has a regressing surface and includes convective effects. A stream function-vorticity approach is used in the liquid phase. The oscillations of temperature, pressure and velocity in the gas phase will show significant changes in the heat and mass transfer rates and also in

drag coefficients. Droplets are introduced at various times in order to evaluate the combined effect and this should provide a comprehensive picture of droplet vaporization under all injection conditions. The response factor of the system is calculated in order to determine if the vaporization process is capable of driving instability.

Description of the Problem and Model

Fuel injection in liquid propellant rockets is performed with an atomization device. Upon injection, the droplet experiences an acceleration and the gas quickly adjusts to the presence of the droplet and a boundary layer is formed. Internal circulation within the droplet and a recirculation zone in the wake are soon established. The continuous transfer of momentum, results in a reduction of the relative velocity between the gas and the droplet, causing a drop in the relative droplet Reynolds number. The surrounding gas heats the droplet interior and also supplies energy for the vaporization of the fuel at the surface. The vaporization process is initially slow but accelerates later. This heat transfer process results in nonuniform droplet temperatures for the entire droplet lifetime. Thermal heating of the droplet continues throughout the lifetime of the droplet and is therefore a source of unsteadiness in the liquid phase. The primary heat transfer mechanism is initially diffusion but switches to convection with the establishment of internal circulation and then reverts back to diffusion as the droplet decelerates relative to the gas. The vaporizing fuel vapor has significant effects on the properties of the surrounding gas. In the case of an unstable combustor, the ambient conditions fluctuate in time and space, as these complex processes are taking place. The value of the phase in the cycle at the instance of injection identifies the time history of the

ambient condition variations seen by the droplet.

Numerical computation of a detailed spray model is not feasible with the facilities available today. The problem considered in this study is that of a single n-octane droplet, injected into the hot gases of a combustor. The model employed in this study is shown in Figure 1. This axisymmetric model with variable properties has been employed in order to be able to make a detailed calculation of the heat and mass transfer process. In the numerical model employed, the effects of decreasing relative velocity, varying thermophysical properties, transient heating, internal circulation of liquid, boundary layer blowing and moving interface have been incorporated into the calculations.

The steady part of the relative velocity is taken to be 25 m/s, upon introduction of the droplet into the combustor. Note that the actual value can vary between 15.7 m/s and 34.2 m/s depending on the time of injection and the spatial location. A mean pressure of 10 atm is used. The operating pressure again varies with time and the actual value depends not only on the magnitude of the velocity oscillation but also the initial phase of injection. Gas-phase perturbations are introduced on the velocity, pressure and temperature. The velocity and pressure oscillations are dictated by the classical standing wave pattern and the corresponding temperature oscillation is calculated by assuming an isentropic flow. This study examines the effects of variation of critical parameters such as the initial phase of injection, frequency and amplitude of oscillation on the vaporization history of the droplet.

The exact solution of this problem requires the simultaneous solution of the hydrodynamic, energy and transport equations in the gas phase. This would necessitate the inversion

of large matrices and impose great demands on the computing resources available. In order to solve the equations in a more efficient manner, an iterative technique is utilized. The gas-phase temperature, momentum and species equations are solved using the alternate direction predictor corrector method.[8] The pressure equation is indirectly satisfied by using a pressure correction to update the pressure and velocity fields in a manner that ensures the satisfaction of the continuity equation. An underrelaxation is used to ensure that the pressure correction does not diverge.

A stream function-vorticity formulation is used in the liquid phase to simplify the calculations. This allows for all the important flow characteristics to be captured while preserving a good degree of accuracy. The elliptic stream function equation is solved by using the successive-over-relaxation technique. The vorticity and liquid temperature equations are parabolic and are solved by the alternate direction predictor corrector method.[8]

Governing Equations

For the governing equations in the liquid and gas phase one may refer to work by Chiang[8] and Chiang *et al.*[9] The initial conditions corresponding to the injection of a droplet into an unstable combustor would depend on the particular time and location of injection. T, p and V_z are therefore dependent on ϕ_t and ϕ_{po}. V_r and Y_f are set to zero on the inflow side and the gradients set to zero on the downstream side. The flow may reverse at lower Reynolds numbers, but the boundary conditions remain the same. In such a situation, the boundary conditions are, in effect, specified downstream with the gradient set to zero on the upstream side.

Inlet Conditions (Gas Phase):

Velocity Condition:

$$U'_\infty(z',t') = \overline{U}'_\infty + \epsilon'_u \sin\frac{2\pi z'}{\lambda'} \sin\frac{2\pi c' t'}{\lambda'}$$

Pressure Condition:

$$p'_\infty(z',t') = \overline{p}'_\infty + \epsilon'_p \cos\frac{2\pi z'}{\lambda'} \cos\frac{2\pi c' t'}{\lambda'}$$

where

$$\epsilon'_u = \frac{a'}{\gamma}\frac{\epsilon'_p}{\overline{p}'_\infty}$$

Temperature Condition:

$$\frac{T'_\infty}{\overline{T}'_\infty} = \left(\frac{p'_\infty}{\overline{p}'_\infty}\right)^{\frac{\gamma-1}{\gamma}} \approx 1 + \frac{\gamma-1}{\gamma}\frac{\epsilon'_p}{\overline{p}'_\infty}\cos\frac{2\pi z'}{\lambda'}\cos\frac{2\pi c' t'}{\lambda'}$$

On the outlet side, the pressure is specified in a similar manner but the gradients of the temperature and velocity are set to zero.

Evaluation of Rayleigh Criterion

In order to determine whether vaporization is capable of driving instability, it is necessary to consider the contributions of every droplet present in the combustor at a particular instant of time. For the vaporization to be able to drive instability, it is necessary to evaluate the component of the vaporization rate that is in phase with the pressure. This is done by evaluating the response factor, G as suggested by the Rayleigh criterion:[4]

$$G = \frac{\oint\int mP\,d\tau_{H_g}\,d\zeta}{\oint\int P^2\,d\tau_{H_g}\,d\zeta}$$

where ζ is a constant for each droplet during its lifetime. The ζ value represents the phase at the time of injection.

The definition of G given above involves integration in an Eulerian frame of reference. In order to apply this to the present model, it is adapted to a Lagrangian frame of reference. Figure 2 shows the droplets born at various phases. In an Eulerian time frame (represented by solid lines), droplets injected at different phases are present at different axial locations at a given time. By the above definition, G is calculated by integrating in horizontal sweeps, over axial location and then over the Eulerian time. Lagrangian time varies along the dotted lines of constant initial phase value (constant ζ) in the figure. G can therefore be evaluated by integrating in diagonal sweeps, over Lagrangian time and then by integrating over the phase value at the time of injection.

Figure 3 shows the vaporization rate histories (schematic) of all the droplets present in a combustor at a particular instant of time. The area of interest is that between a phase of zero and 2π. It is seen that droplets injected at phases of -2π, $-3\pi/2$, $-\pi$ and $-\pi/2$ have contributions to the area of interest (marked as A, B, C and D respectively). However, it may be seen that this area corresponds to the area marked A, B, C and D on the vaporization curves of droplets injected at zero, $\pi/2$, π and $3\pi/2$ respectively. Thus, integrating over the vaporization curves of all droplets born between zero and 2π would in effect give the contributions of all droplets present in the combustor. The integral is evaluated over time, at intervals of $\pi/2$ to obtain the elementary response factor, G_e which is defined as:

$$G_e = \frac{\int mP d\tau_{Hg}}{\int P^2 d\tau_{Hg}}$$

The elementary response factor is fitted with a cubic spline. The spline was fit from both directions and the difference was evaluated to be less than 0.5%. The elementary response factor is then integrated over the phase to evaluate the total response factor. It may be noted that the denominator is independent of phase but the integral was left to maintain consistency. The sophisticated droplet vaporization model used in this study is highly computationally intensive. The solution of each phase point requires over two hundred minutes of Cray time. In order to remain within the time available only four phase values were computed and then a spline was fit to the results in order to integrate over period.

In order to be able to overcome the losses and drive combustion instability, G should have a minimum positive value. For the case of distributed combustion, this value corresponds to 3.72 for longitudinal mode instability.[12]

Results and Discussion

Numerical codes exhibit varying degrees of grid and time-step dependence. In order to evaluate the accuracy of the results, it is important to estimate the degree of dependence on the grid chosen and the time step used. All results are relatively insensitive to the time-step size. A time step of 0.001 has been used throughout this investigation. Four different parametric studies have been conducted. These involved 1) frequency comparison, 2) amplitude comparison, 3) droplet configuration comparison and, 4) variation in the liquid fuel.

The variations of pressure and velocity for each of the four phases are shown in Figure 4. Each droplet undergoes a unique cycle of ambient conditions. A variety of frequencies

has been known to occur in liquid propellant rockets and in ramjets. For this reason, the frequency of the instability is a key parameter in the study of combustion instability and it is necessary to identify the frequencies that may be sustained by droplet vaporization. For the purposes of this study, the frequency may be better described by the time period of the oscillation in terms of the droplet heating time. Three different time periods, corresponding to 0.3, 0.6 and 0.9 droplet heating time have been examined. In all the cases, the spatial phase of injection corresponds to an eighth of a wavelength and the amplitude of the pressure oscillation is 0.2% of the steady value (10 atm). The response factor, G, was calculated for each case in a manner described in the previous chapter. Figure 5 shows the pressure history of droplets exposed to the three frequencies. The imposed 2% pressure oscillation has a significant effect on the variation of the vaporization rate. The distribution of the elementary response factor for the three cases is shown in Figure 6. The elementary response factor distribution varies substantially for the three time periods studied, though it is periodic in nature. The total response factor for each of the frequencies is shown in Table 1.

A response factor greater than 3.72 is required for the vaporization process to be able to drive instability. The oscillation with a time period of 0.3 droplet heating time is not capable of driving instability. A negative value of G implies that the system damps any oscillations. The oscillation with a time period of 0.6 droplet heating time has a high response factor and is therefore capable of driving longitudinal mode instability. This means that the component of the vaporization rate in phase with the pressure is large enough to supply enough energy to the system so as to drive it into an unstable mode of operation. With a time period of 0.9

Vaporization Rate Response	
$\frac{\tau}{\tau_h}$	G
0.3	-0.52
0.6	5.81
0.9	2.98

Table 1: Comparison of response factor for varying frequencies.

droplet heating time, the system is not capable of driving instability. The response factor is positive, but it is not strong enough to overcome the losses in the combustor. The time period of 0.6 gas hydrodynamic diffusion times corresponds to the frequency domain found to be most unstable by Bhatia and Sirignano.[5]

Figure 7 shows the two different droplet configurations studied. In the first case, the droplet is moving faster than the ambient gas and, the wake of the droplet is therefore behind the droplet. In the second configuration, the droplet is moving slower than the gas and in this configuration, the wake is ahead of the droplet. The velocity fluctuation is in phase with the steady component of the velocity. Thus, a positive velocity fluctuation means an increase in the Lagrangian velocity. This augments the vaporization rate and other surface properties. In the first case, however, a velocity increase in the gas phase means a decrease in the Lagrangian velocity of the droplet. Note that, in actual rockets, both these situations

exist since the droplet is initially faster than the gas but as the combustion process proceeds the gases accelerate and eventually move faster than the droplet. Thus, in practical rockets, the wake is initially behind the droplet but moves ahead of the droplet with the passage of time. In the case of ramjet combustors, the gases are initially at high velocity and the fuel is injected at nearly zero velocity. In this situation, the wake remains ahead of the droplet for the entire lifetime. The two droplet geometries described earlier have been studied with a 2% pressure oscillation. The spatial phase of injection corresponds with an eighth of a wavelength and the time phase of injection corresponds to a quarter time period. The time period of the oscillation for the two configurations is 0.6 droplet heating time. A comparison of the ambient pressures and velocities for the two cases is shown in Figure 8. The pressure variation remains the same for both cases but there is a substantial difference in the absolute magnitude of the relative velocity history of the two droplets due to the difference in the effect of the velocity fluctuation. The distribution of the elementary response factor for the two cases over the entire time period is shown in Figure 9. The elementary response factor for the droplet faster case is negative over the entire time domain, indicating a heavy damping. The case with the gas moving faster than the droplet has both negative and positive elementary response factor values. The integrated response factor values for these two situations have been evaluated and the results are given in Table 2.

For the case with the gas travelling faster than the droplet, the response factor is high and capable of driving instability; but, in the case of the droplet traveling faster than the gas, the response factor is negative and actually damps the oscillations.

Vaporization Rate Response	
Configuration	G
Gas Faster	5.81
Droplet Faster	-76.47

Table 2: Comparison of response factor with droplet faster and gas faster geometries.

Depending on the nature of a particular combustor and the operating conditions, the magnitude of the amplitude of the oscillation may vary. In order to get a better understanding of the effects of varying amplitudes, two cases with pressure oscillations of one and two percent have been studied. The cases shown here correspond to a time period of 0.6 droplet heating time and the time phase injection corresponds to a quarter time period. The spatial phase of injection corresponds to an eighth of a wavelength. The responses for the two cases with different amplitudes of oscillation have been computed to understand the effects of amplitude variation on the response factor of the combustor. Figure 10 shows the velocity and pressure variation for the two cases. The pressure is seen to vary in the same manner in both cases, though the amplitude is different. The velocity cycle for the droplets is however, entirely different. The initial velocity of the 2% oscillation case is higher than that of the 1% oscillation case. However, a more rapid decrease in the Lagrangian velocity causes it to intersect the velocity curve of the 1% pressure oscillation case. The distribution of the

response factor is shown in Figure 11. It may be seen that the distribution of the response factor is different for the two cases. The total response factor for the two cases examined is shown in Table 3.

Vaporization Rate Response	
Pressure Oscillation	G
1%	5.02
2%	5.81

Table 3: Comparison of response factor with varying amplitudes.

There is a decrease in the response factor with a decrease in the amplitude of the oscillation. However, a 50 % decrease in the amplitude of the pressure oscillation only causes a 13 % decrease in the response factor which is still capable of driving the instability. Though the distribution of the response factor is very different for the two cases, its effect on the response factor is not so marked.

The effects of varying the volatility of the fuel were studied. The base fuel that has been employed in the calculations is normal octane. A second fuel has the latent heat of decane but otherwise has the properties of octane. We refer to this less volatile fuel as pseudo-decane. The distribution of the elementary response factor is shown in Figure 12. The integrated response factor values for the two cases have been evaluated and the results

are given in Table 4. Clearly, the more volatile fuel has a larger response factor.

Vaporization Rate Response	
Configuration	G
Octane	5.81
Pseudo-decane	4.97

Table 4: Comparison of fuels with varying volatility.

Conclusions

An advanced, axisymmetric convective droplet vaporization code has been successfully employed in the study of combustion instability. The imposed oscillations have significant effects on the heat and mass transfer process and on the liquid properties. Droplet vaporization produces enough energy in phase with the pressure to drive longitudinal mode combustion instability. An investigation of the frequency domain showed that droplet vaporization was only capable of driving combustion instability in certain frequency domains. This is in good agreement with previous work done by Tong and Sirignano and Bhatia and Sirignano. The frequency of the oscillation is a key parameter in determining the fraction of the total energy that is in phase with the pressure oscillation. An evaluation of the effect of the disturbance amplitude on the response factor indicates that the effects of amplitude variation are not very significant. It is important to identify whether the wake is ahead of the droplet or behind it as there is a significant change in the response factor for the two

situations.

A variation of the volatility of the fuel has a fairly significant effect on the response factor, though it is not as significant as identifying the orientation of the wake. This is due to a comparable decrease in the contributions from droplets that have a positive contribution as well as those that make a negative contribution. Droplet vaporization studies related to combustion instability have neglected to emphasize whether the wake of the droplet is ahead of the droplet or behind it. It is necessary to identify the particular configuration as the response factor for the two is vastly different. When the droplet is faster than the gas, the system has a high damping whereas when the gas is faster than the droplet, the response factor is high enough to drive the instability. This is primarily due to the diverse effect the velocity oscillation has on the relative velocity. Our results are consistent with previous findings that the convective vaporization mechanism is much more strongly coupled to velocity oscillations than to pressure oscillations.

Acknowledgements

This work was supported by funds from the U S Air Force Phillips Laboratory monitored by Mr. J. Levine. The funds came to UC Irvine via a subcontract from Pratt and Whitney administered by Mr. George Cox.

References

[1] D. T. Harrje and F. H. Reardon, eds., *Liquid Propellant Rocket Combustion Instability.*

Washington, D. C.: NASA SP-194, 1972.

[2] W. A. Sirignano, "Task one report: Liquid stability mechnanism, Submitted to Pratt and Whitney," tech. rep., UCI, 1990.

[3] R. J. Jensen, "A summary of the JANNAF workshop on liquid rocket engine combustion driven instability mechanisms," in *Proceedings of the 26th JANNAF Combustion Meeting*, (Pasadena, California), October 1989.

[4] A. Y. Tong and W. A. Sirignano, "Oscillatory vaporization of fuel droplets in an unstable combustor," *J. of Propulsion and Power*, vol. 5, no. 3, pp. 257–261, 1989.

[5] R. Bhatia and W. A. Sirignano, "One-dimensional analysis of liquid-fueled combustion instability," *J. of Propulsion and Power*, vol. 7, pp. 953–961, November 1991.

[6] B. Abramzon and W. A. Sirignano, "Droplet vaporization model for spray combustion calculations," *International Journal of Heat and Mass Transfer*, vol. 32, pp. 1605–1618, November 1989.

[7] W. A. Sirignano, "Fuel droplet vaporization and spray combustion theory," *Prog. Energy. Combust. Sci.*, vol. 9, pp. 291–322, 1983.

[8] C. H. Chiang, *Isolated and Interacting, Vaporizing Fuel Droplets: Field Calculation With Variable Properties.* PhD thesis, University of California, Irvine, Department of Mechanical Engineering, 1990.

[9] C. H. Chiang, M. S. Raju, and W. A. Sirignano, "Numerical analysis of convecting, vaporizing fuel droplet with variable properties," *Int. J. Heat and Mass Transfer*, vol. 35, no. 5, pp. 1307–1324, 1992.

[10] F. E. C. Culick, "Combustion instabilities in propulsion systems," in *Proceedings of the Propulsion and Energetics Panel 72nd B specialists' meeting*, (Bath, England), 1989.

[11] G. B. Cox and P. L. Petersen, "Liquid stability mechanisms program summary," in *Proceedings of the 28th JANNAF Combustion Meeting*, (San Antonio, Texas), October 1991.

[12] L. Crocco and S. I. Cheng, *Theory of Combustion Instability in Liquid Propellant Rocket Motors*, vol. 8. London, England: Butterworths Scientific Publications, 1956.

[13] L. Crocco, "Theoretical studies on liquid-propellant rocket instability," in *Proceedings of the Tenth Symposium (International) on Combustion*, pp. 1101–1128, 1965.

[14] F. H. Reardon and R. J. Clifford, "Calculation of the combustion distribution in a liquid-fuel ramjet," in *Proceedings of the 26th JANNAF Combustion Meeting*, (Pasadena, California), 1989.

[15] F. H. Reardon and A. Duvvur, "Calculations of the combustion time lag in coaxial-dump ramjet combustors," in *Proceedings of the 32nd Heat Transfer and Fluid Mechanics Institute*, (Sacramento, California), 1991.

[16] W. A. Sirignano, *A Theoretical Study of Nonlinear Combustion Instability: Longitudinal Mode.* PhD thesis, Princeton University, Department of Aerospace and Mechanical Sciences, 1964. Report No. 677.

[17] F. A. Williams, *Combustion Theory.* Menlo, California: Benjamin-Cummings, 1985.

[18] W. C. Strahle, "Unsteady reacting boundary layer on a vaporizing flat plate," *AIAA J.*, vol. 3, pp. 1195–1198, June 1965.

[19] R. J. Priem and M. F. Heidmann, "Propellant vaporization as a design criterion for rocket engine combustion chambers," Report TR-R67, NASA, 1960.

[20] R. J. Priem and D. C. Guentert, "Combustion instability limits determined by a non-linear theory and a one-dimensional model," Report TN D-1409, NASA, 1962.

[21] R. J. Priem, "Theoretical and experimental models of unstable rocket combustors," in *Proceedings of the Ninth Symposium (International) on Combustion, The Combustion Institute*, (Pittsburgh, PA), pp. 982–992, 1963.

List of Figures

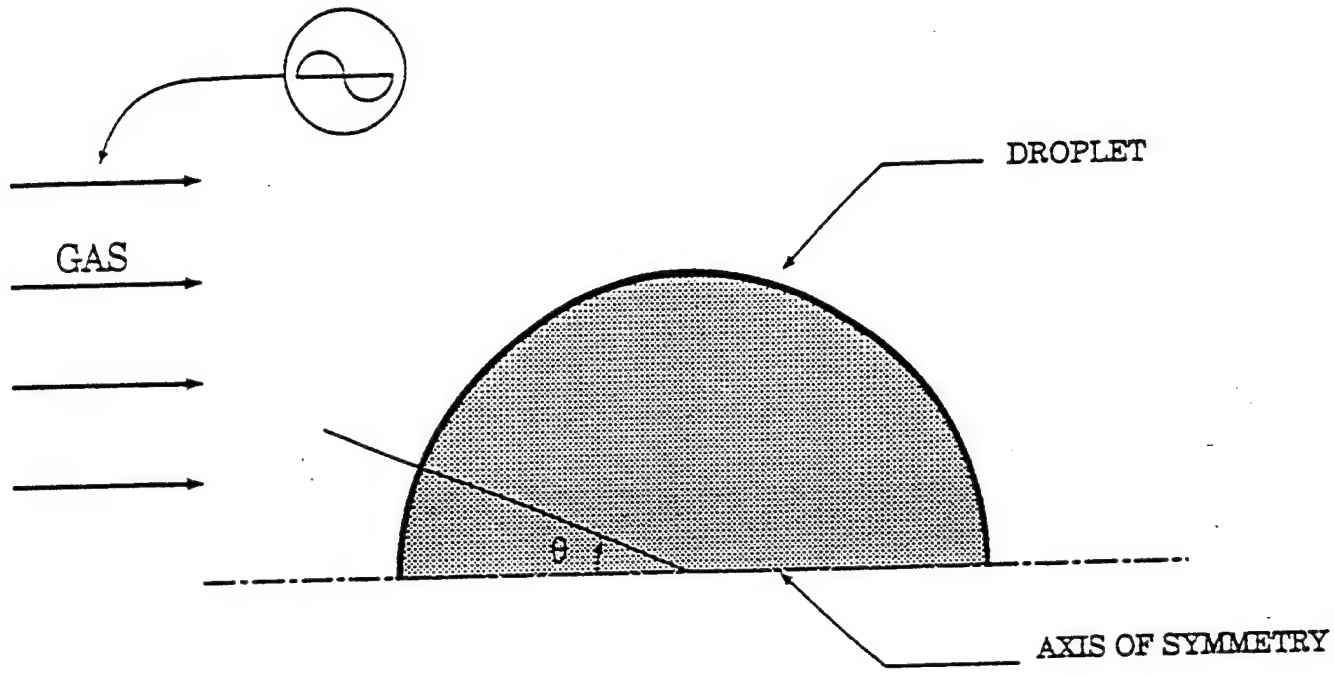

Figure 1: Droplet model employed in the present study.

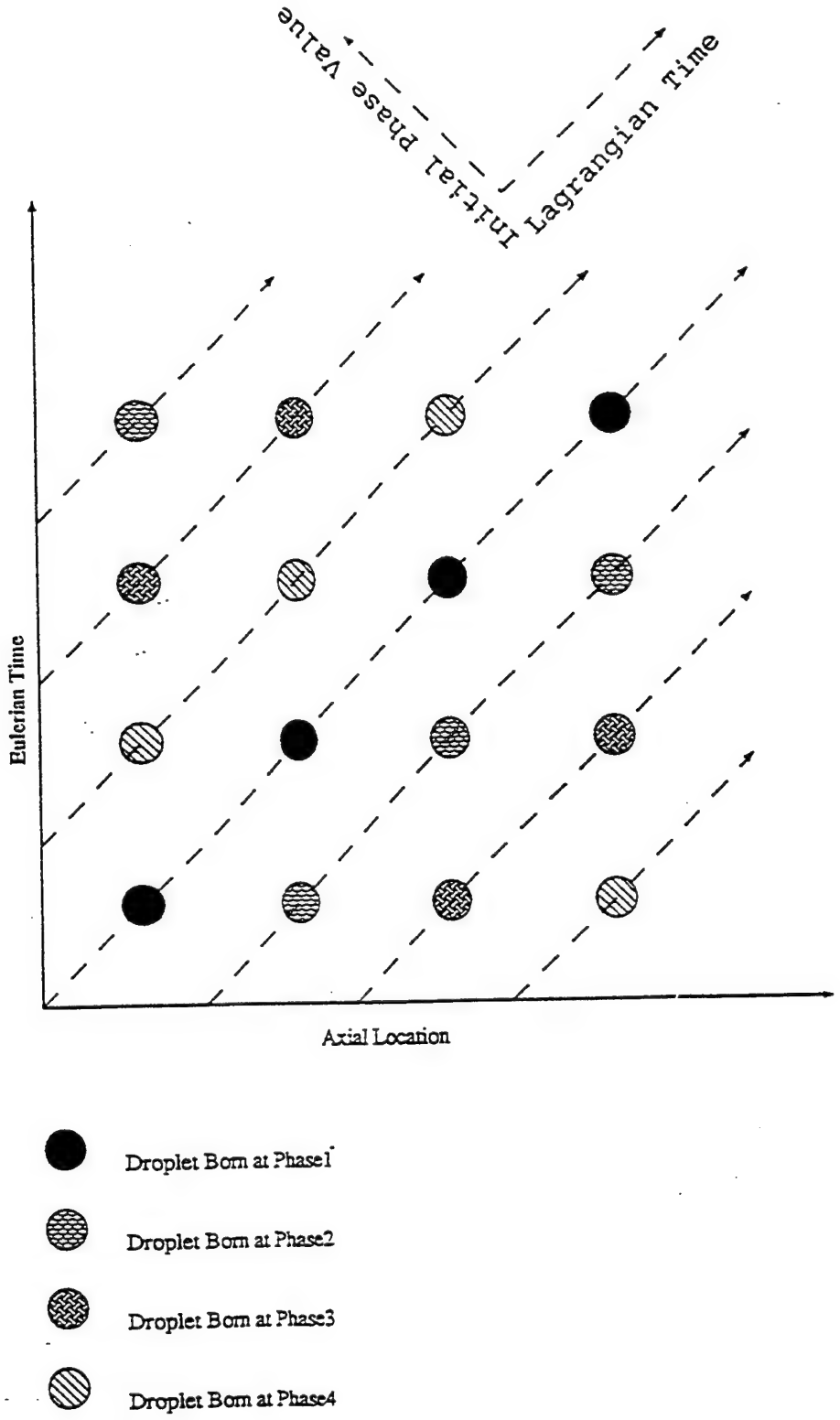

Figure 2: Evaluation of G in a Lagrangian frame of reference.

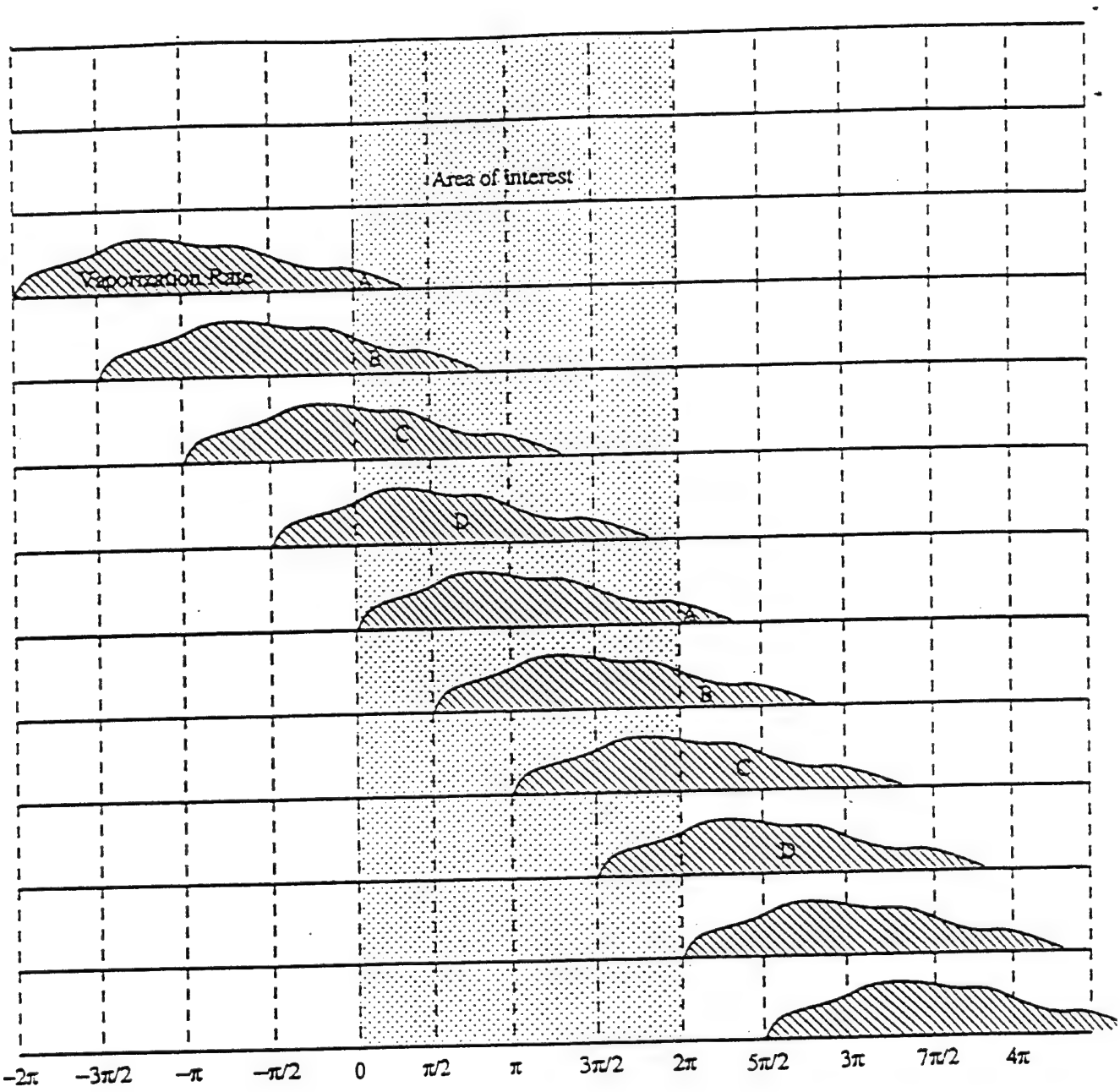

Figure 3: Vaporization rate (schematic) distribution for various droplets present in the combustor .

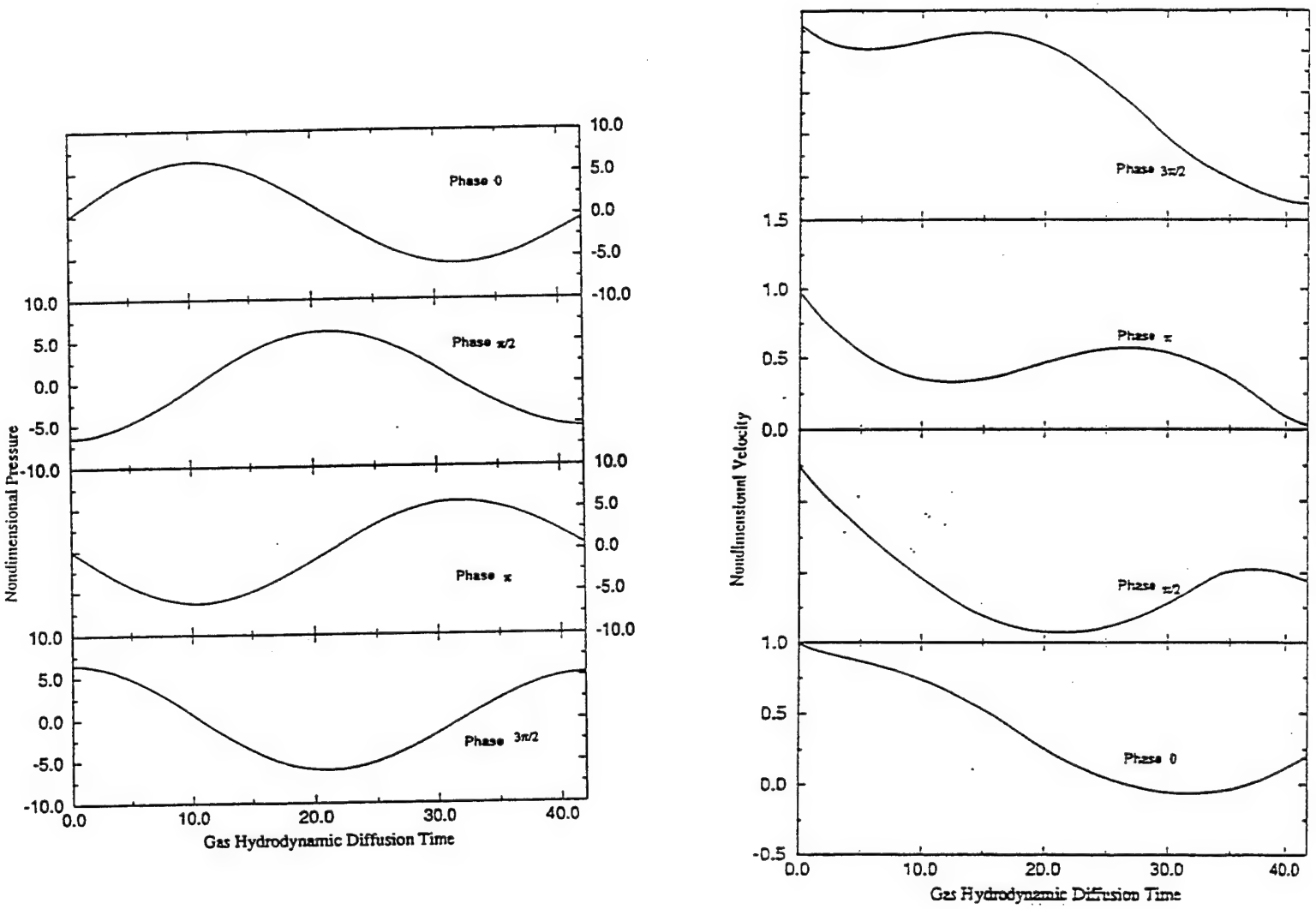

Figure 4: Ambient pressure and velocity history with varying injection times.

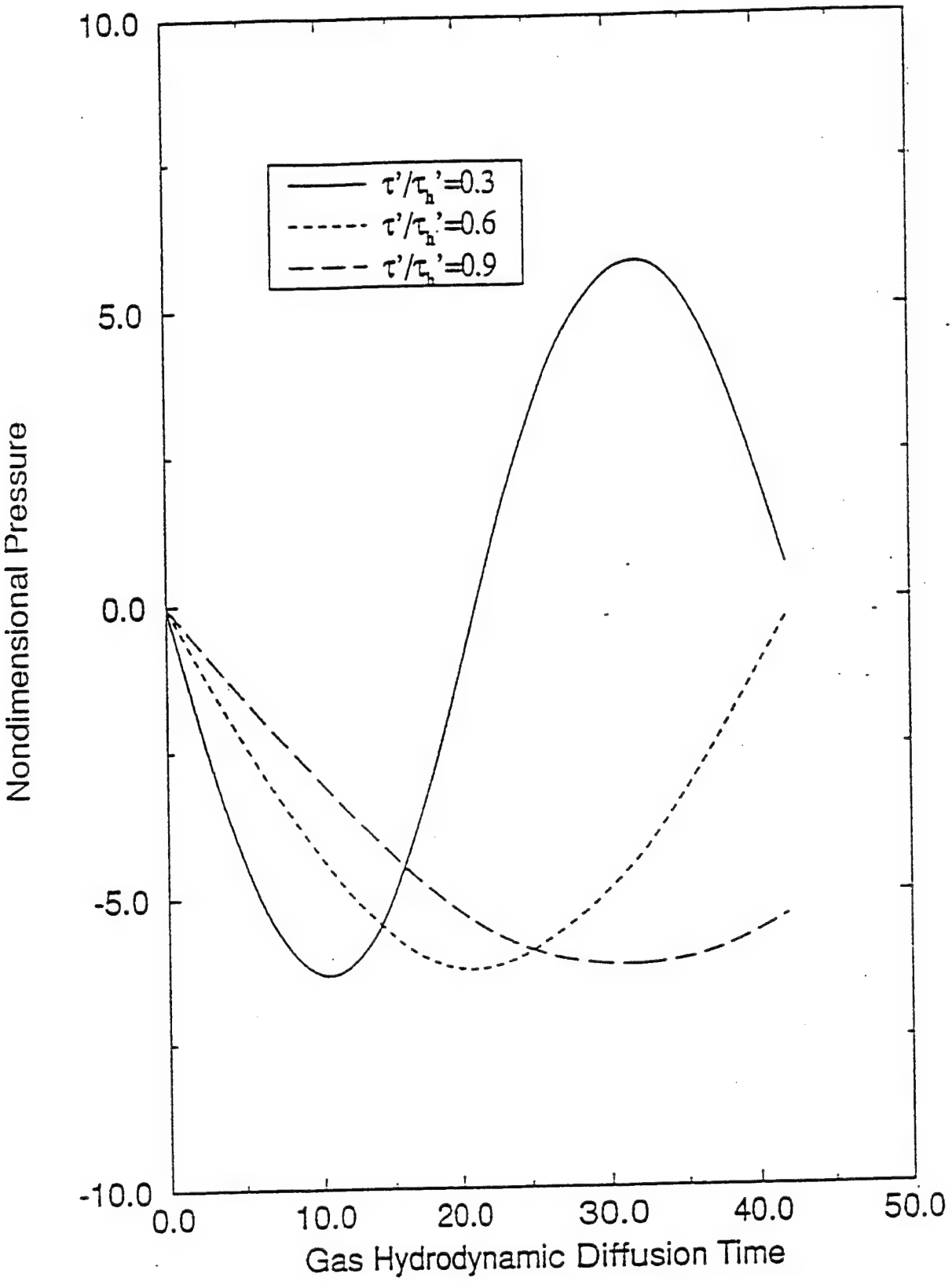

Figure 5: Ambient pressure history with varying frequencies.

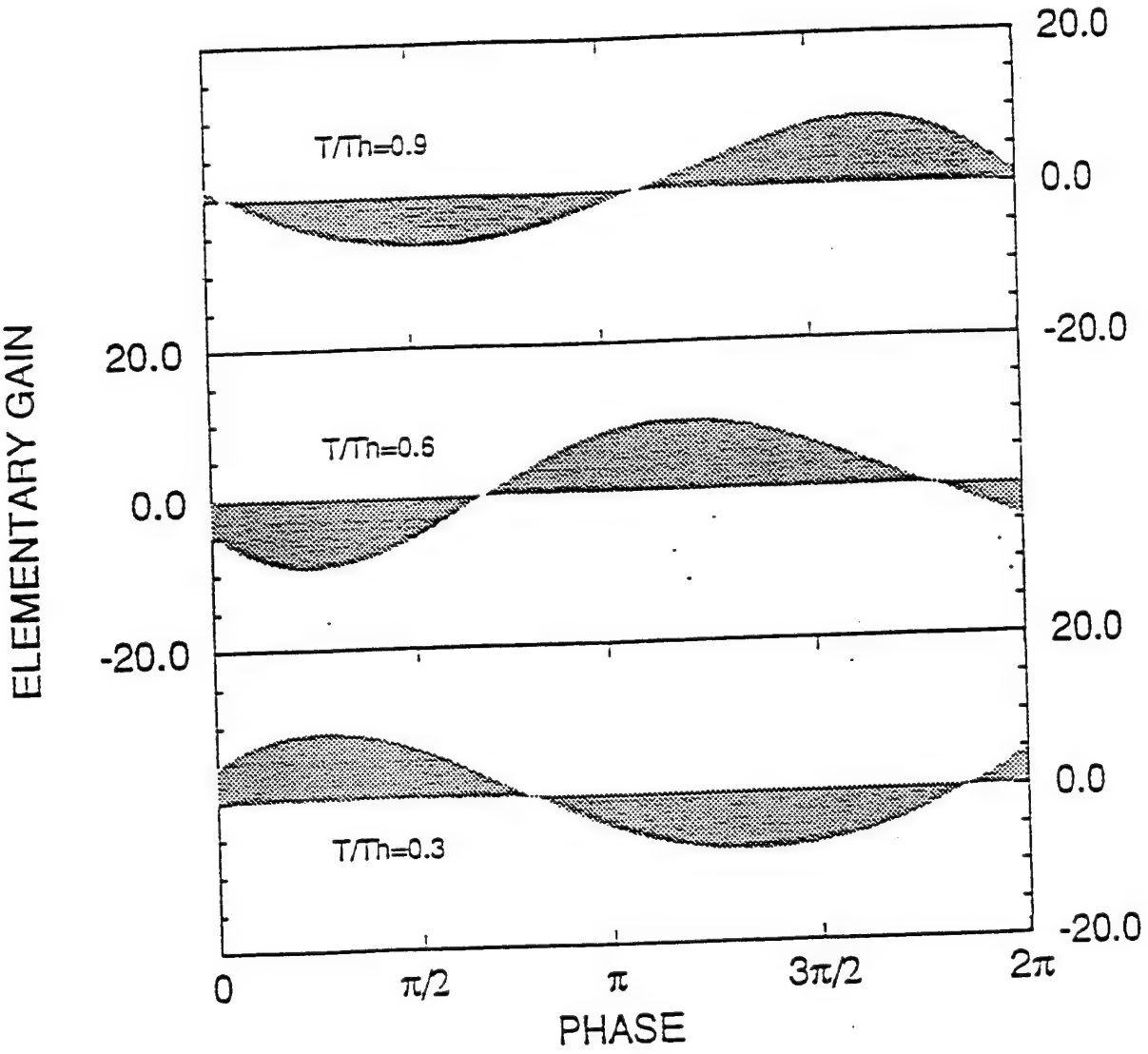

Figure 6: Distribution of elementary gain for varying time periods.

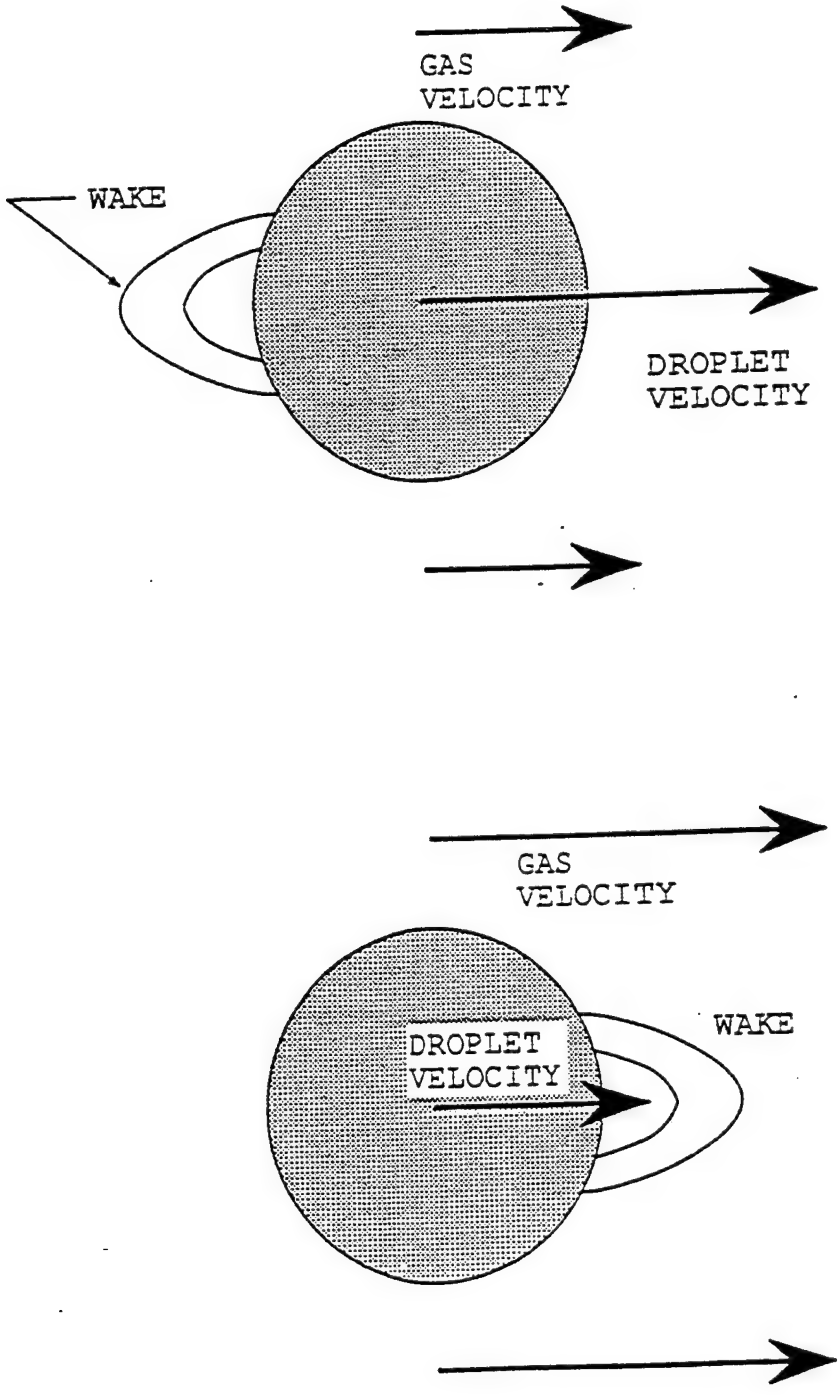

Figure 7: Schematic of droplet faster and gas faster configurations.

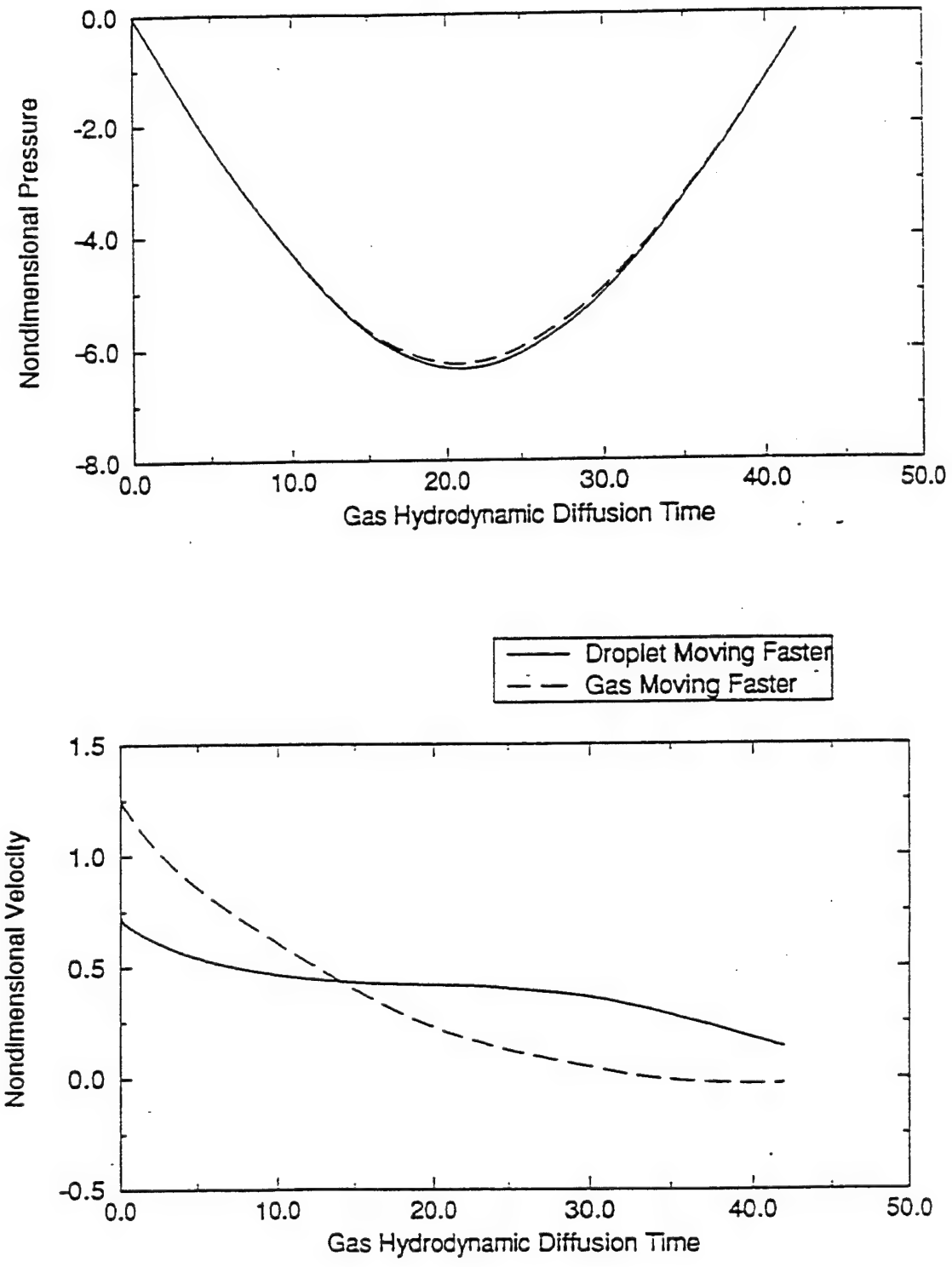

Figure 8: Pressure and velocity variation for droplet faster and gas faster configurations.

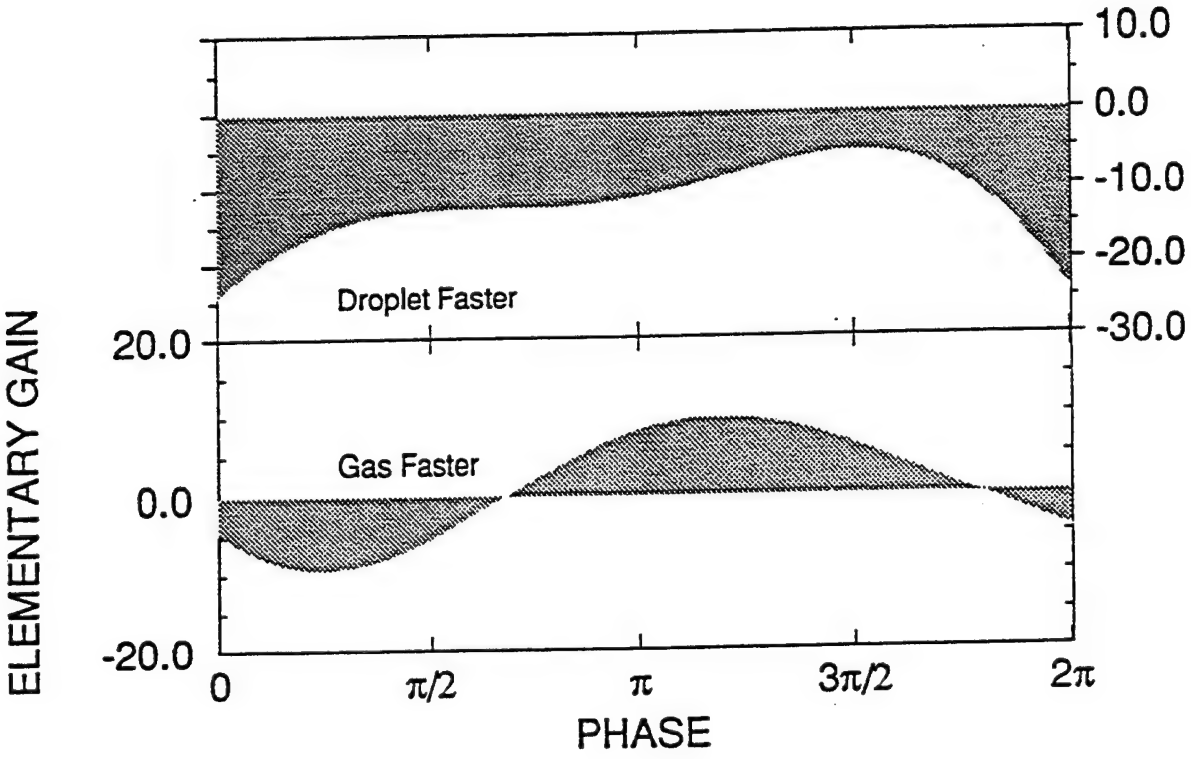

Figure 9: Distribution of elementary gain for varying configurations.

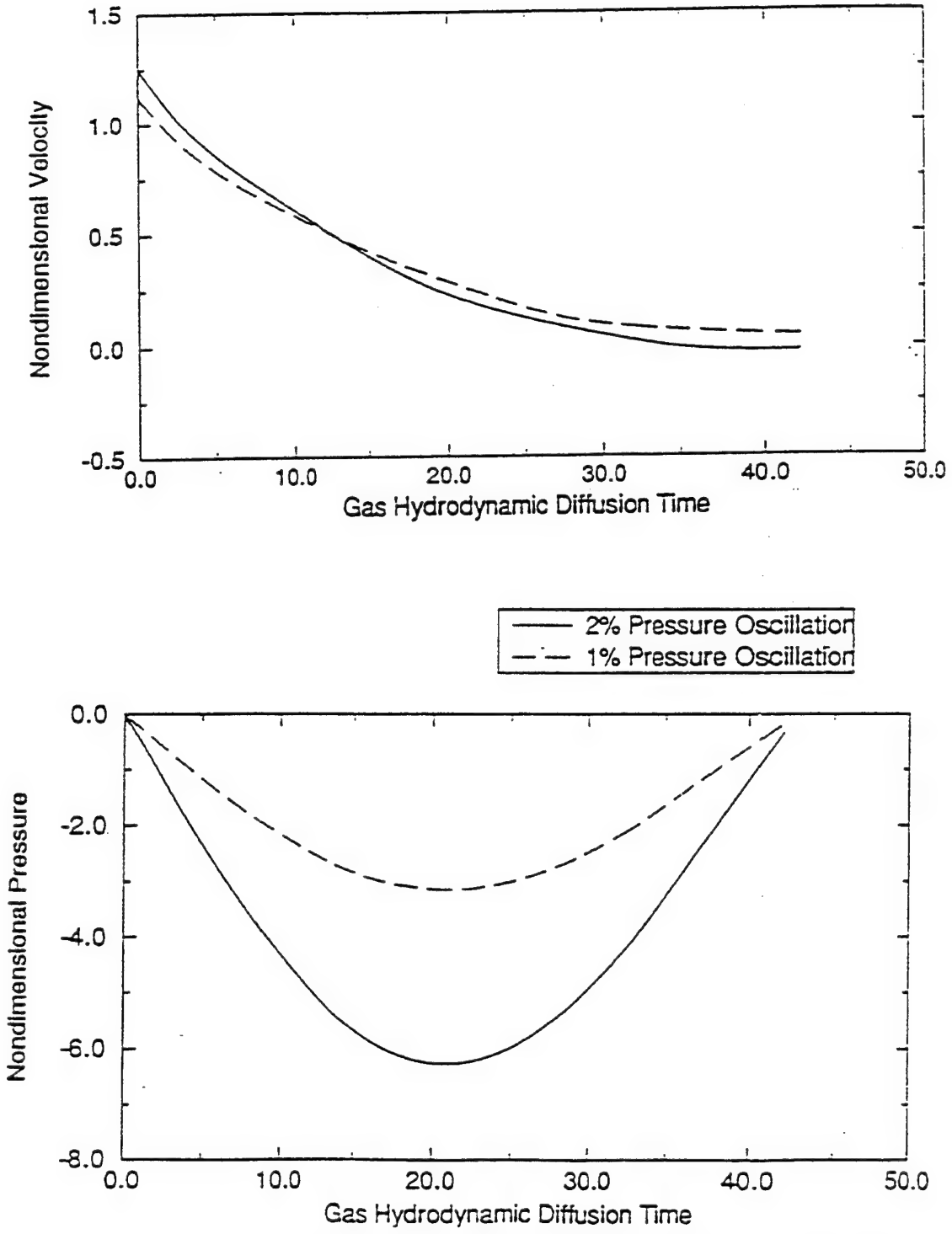

Figure 10: Velocity and pressure variation for varying amplitudes.

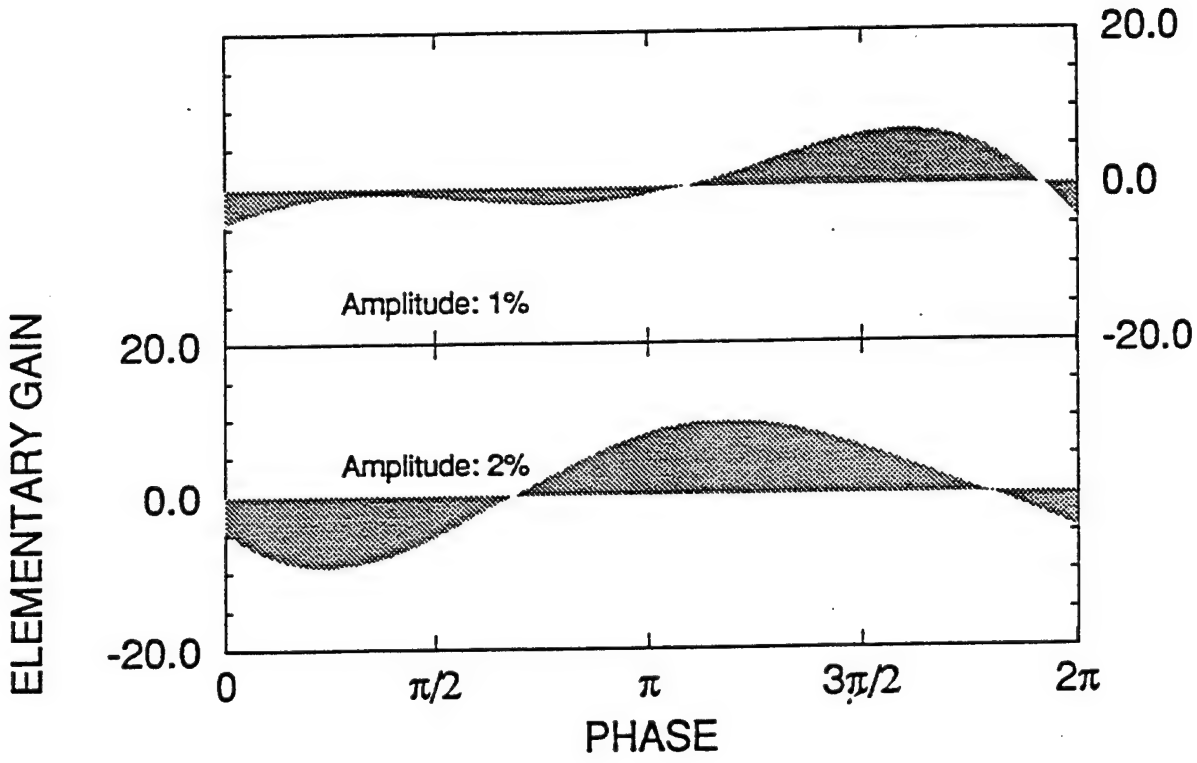

Figure 11: Distribution of elementary gain for varying amplitudes.

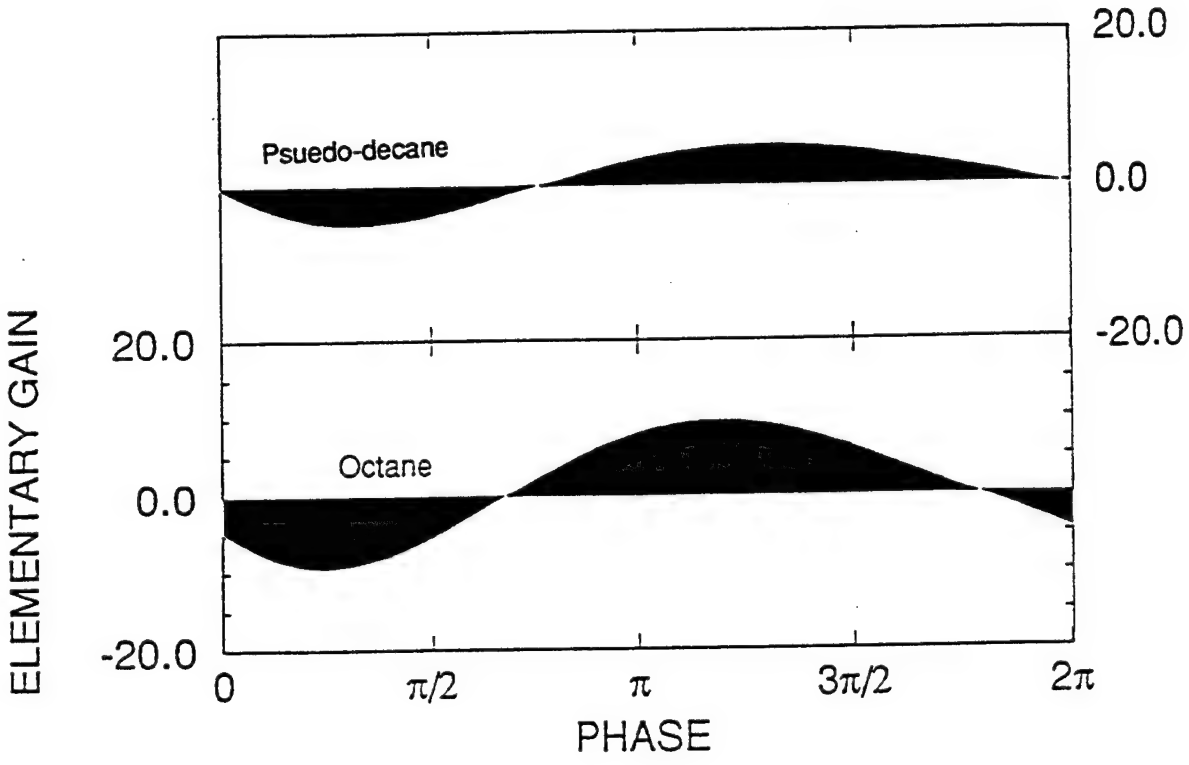

Figure 12: Distribution of elementary gain for varying fuel volatilities.

APPENDIX L

"Liquid Instability Technology - Diagnostics and Measurements"

Liquid Instability Technology - Diagnostics and Measurements

by

Michael Winter
&
Torger J. Anderson

United Technologies Research Center
East Hartford, CT 06108

June 8, 1993

Liquid Instability Technology - Diagnostics and Measurements

by

Michael Winter
&
Torger J. Anderson

United Technologies Research Center
East Hartford, CT 06108

Executive Summary

Understanding of the mechanisms leading to instabilities in liquid-fueled rocket engines has been limited by an inability to measure the processes that occur in the severe environment within a rocket engine combustor. This measurement limitation extends even to relatively mild but complicated environments such as liquid sprays or droplet interactions with acoustic pulses. Laser-based diagnostics offer potential for making precise and non-intrusive measurements in such environments. They require no physical probe which would otherwise interfere with the process being measured or would be unable to survive the severe environment. In addition, laser-based techniques are available with could, potentially, make measurements not previously attainable. With further development, these methods offer the potential to advance the understanding of mechanisms leading to liquid rocket engine instabilities.

Under a previous program, UTRC has demonstrated how application of advanced diagnostics such as Morphology-Dependent Resonances (MDR's) with outstanding accuracy and resolution led to better fundamental understanding. Through that program UTRC also brought on-line a capability to make routine measurements on supercritical LOX droplets showing the first look at dispersal of supercritical O_2 droplet fluid. This suggested program describes a number of potential diagnostic techniques, explaining their current status, the obstacles to be overcome in developing them and their potential for furthering the understanding of liquid rocket instabilities. These techniques would be brought to bear on rocket stability

problems by measuring the transition of LOX droplets to a supercritical fluid in high pressure environments in both static and dynamic (after a shock wave or in an acoustically-driven environment) conditions.

Background

Acoustic instabilities within the combustors of liquid-fueled rocket engines have been a concern since their development. The mechanisms leading to these instabilities are not well understood and measurements of the processes are extremely limited due to the harsh environment in which the processes occur. Since these mechanisms are not well understood, engine performance is sacrificed in order to avoid conditions which generate these instabilities. The cause is believed to be a reaction rate enhancement produced by and in phase with acoustic waves within the combustor. The enhancement may result from atomization of the fuel and oxidizer droplets or increased evaporation[1] caused by the surrounding gas flow which amplifies pressure waves leading to the instability. Complicating the difficulty in understanding the process is the fact that liquid sprays are injected into a combustor in which conditions are supercritical. The resulting fuel/oxidizer supercritical mixing processes are not well understood.

Our focus for studying the instability mechanisms has been on understanding evaporation enhancement in single droplets and expanding to sprays and their surrounding flow fields. Theoretical models have been generated which describe the evaporation process for a droplet in a flow field[1-2] but, even for these simple processes, experimental validation has been limited because of the inability to make well-resolved measurements on such small length and short time scales. Recent results have demonstrated the value of laser-based diagnostics, capable of non-intrusive temporally-resolved measurements which can be used to acquire results with significant spatial resolution by taking advantage of the spectral character of the medium.[3]

While these measurements have limited application due to the measurement environment, a number of alternative

techniques offer potential capabilities for gaining further understanding of liquid/gas mixing processes in the subcritical, supercritical and transcritical regimes. A discussion of each of these techniques is provided below, followed by a description of a potential measurement program and the expected pay-off.

UTRC has considerable experience in developing droplet diagnostics using laser-based techniques. Techniques have been developed and used to study internal circulation inside of single droplets on the order of several hundred μm in diameter using fluorescence and oxygen-quenching processes.[4] The spectral structure of fluorescence emissions from smaller droplets (on the order of 100 μm in diameter) have been used to evaluate droplet size and evaporation rates.[3,5] Additional experience in a wide range of other laser-based diagnostics can be readily called upon in the evaluation of the diagnostic strategies described below. These include processes such as laser-induced fluorescence, degenerate four-wave mixing, and both visible and u.v. Raman measurements.

UTRC has built a high pressure pulse facility in which to study potential mechanisms driving the instability processes. This facility has been used to provide a supercritical environment for observing the droplet break-up process and has optical access for the development and employment of laser-based diagnostics. The pulse tube has a 50 x 50 mm square cross section and a windowed test section capable of withstanding up to 1000 psi. A driver section separated by a dual burst disk system provides a capability to generate shock waves of repeatable strength so that prescribed conditions can be studied. In experiments for a previous program, waves with pressure ratios on the order of 1.1 were repeatably produced. A cryogenic droplet generator has been developed and used in this program to produce liquid oxygen (LOX) droplets of several hundred micron diameters at high pressures. These were then subjected to the weak shock waves. Helium was used for the high pressure fluid in the pulse tube to simulate the low molecular weight of H_2 and minimize heat transfer and density gradient problems associated with the location of the cryogenic droplet generator in the pulse tube.

Measurement Technology

Each of the measurement techniques described is potentially capable of providing results from droplets or sprays. The emphasis is on employment of these techniques in laboratory facilities simulating the high pressure and flow environments of rocket combustors, but, the techniques could ultimately be employed in small scale rocket engines.

A number of strategies are available and consideration should be given to those tabulated below. Each of these techniques will be discussed in more detail.

	Diagnostic Technique	Measurement Capabilities
I	Spontaneous Raman	temperature, density, imaging
II	Stimulated Raman	temperature, density, phase
III	Stimulated Brillouin (SBS)	droplet size, liquid-phase concentration
IV	SBS w/ degenerate four-wave mixing (DFWM) or DPCFWM	temperature, density, imaging
V	Morphology-Dependent Resonances (MDR's)	droplet size, shape, evaporation rates, critical transition
VI	Second Harmonic Generation	droplet critical phase surface

I. Spontaneous Raman

Raman scattering is the inelastic scattering of light from molecules resulting from rotational, vibrational or electronic energy exchange between an incident photon and an illuminated molecule. It occurs virtually instantaneously within 10^{-12} seconds or less after the molecule is excited. Spontaneous Raman scattering is well suited to diagnostics of clean systems (i.e. lacking particulates and droplets). No specific laser wavelength is required, but since the scattering intensity varies inversely with the fourth power of the laser wavelength, a u.v. illumination source is desired. Due to the quantization of the molecular energy states, the Raman spectrum occupies

fixed frequency separations from the laser frequency, and the spectral shape is characteristic of the species and temperature of the molecule from which it scattered. As a result, temperature can be determined from the acquired spectrum.

Unfortunately, Raman signal intensities are typically very weak with cross sections on the order of 10^{-31} cm^2/sr. However, since the scattering is proportional to the number of molecules in the sample volume, signal intensity increases proportionally with pressure. This is particularly important for supercritical transport studies for conditions typical of rocket engine combustors where higher pressures are required. In fact, recent studies have shown[6] that, at such elevated pressures, the signal can become non-linear with number density and care must be taken to avoid stimulated Raman scattering.

Raman imaging is usually performed by recording the spectrally-integrated signal corresponding to a single vibrational quantum level.[6] This is accomplished by positioning the appropriate optical filter in front of a two-dimensional camera and only passing a narrow spectral band of light. The light scattering at any pixel will depend on the number of molecules within the measurement volume and, hence, provides a measure of the density.

In experiments containing two species, for example liquid oxygen injected into nitrogen gas, the density and distribution of O_2 and N_2 can be imaged using two cameras, each filtered to acquire the Raman signals generated only from one of the species of interest. In this way an instantaneous image of the mixing process can be acquired.

II. Stimulated Raman

Stimulated Raman employs the same molecular transitions as the spontaneous process except that the emissions are also stimulated by the incident laser beam. While the resulting signal intensity is lower than its spontaneous counterpart, requiring a greater medium density to be detectable, the signal is generated as a forward propagating beam and, therefore, can be collected in its entirety. This has the additional advantage

of allowing other incoherent emissions from the measurement volume to be easily separated from the signal.

The low signal level resulting from stimulated Raman requires that the incident laser be focused to obtain sufficient energy density and, consequently, it is not possible to acquire an image. However, signal strength will be enhanced when the technique is employed in a high pressure environment simulating that of a rocket combustor. It may be possible to use the technique to probe the environment surrounding a droplet in the sub- and supercritical regimes to measure gas density of the droplet medium. Furthermore, it has been suggested that the droplets themselves could form laser cavities, enhancing the signal levels on the order of 300 times due to lowering of non-linear thresholds within the cavity.[7] The spectral structure can identify characteristics such as droplet size.

III. Techniques Incorporating Stimulated Brillouin Scattering (SBS)

While generally considered more of a nuisance in most previous laser applications, stimulated Brillouin scattering (SBS) has potential as a diagnostic for droplet and spray measurements. This process results from the interaction of a coherent beam with the molecules of the medium through which it is transported. While it is prominent only in long beam paths or through high density media, it results in a nearly-phase conjugate beam back scattered along the incident beam path at a slightly shifted wavelength.[8] Its application as a diagnostic can be directly through analysis of the SBS signal or as a tool in applying degenerate four-wave mixing (DFWM) as a diagnostic.

SBS is a relatively weak process which generally requires a dense medium such as a liquid and a high field intensity resulting from a focused laser beam. The phase conjugate beam which is produced exactly follows the incident laser beam path in reverse and, as a result, can be easily acquired and separated from any incoherent scattering. Its application as a droplet diagnostic would result from SBS signals generated when a coherent beam, incident on the spherical surface of

liquid droplets in a gaseous medium, focuses in the droplet interior. A measure of SBS intensity from a single droplet or droplets in a spray provides a means of evaluating the number and sizes of SBS sources and thus the size distribution of the droplets.

SBS may be of further value in analyzing spray systems where it could be employed directly as a diagnostic for highly dense sprays. While a laser beam may not penetrate though such sprays, SBS, generated from within the droplets, would propagate counter to the laser beam path. Simultaneous measurements of the transmitted laser intensity and SBS strength could identify features such as liquid volume fraction and droplet size and spatial distributions. Combinations of this technique may be useful as a coherent diagnostic with phase specificity. In this way, measurements may be possible from the dense core of a spray.

IV. Degenerate Four-Wave Mixing

Degenerate four-wave mixing (DFWM) may be useful for performing measurements in the dense core region of an optically-thin (low absorption) spray, particularly when employing the SBS process. With optical phase conjugation, laser beams that pass through a phase-randomizing medium such as droplets and ligaments can return to the detector undisturbed after propagating a round trip. Diagnostics with this property hold the potential for successfully obtaining information from thicker sprays than has been possible in the past with more conventional approaches.

DFWM requires the phase-matching of three laser beams, two of which are pump beams precisely opposed, to generate a signal beam at the same wavelength.[9,10] This signal is counter-propagating to the third, or probe, laser beam, also at the same wavelength. The wavelength of the beams is tuned to an absorption of a species of interest in the medium and the signal is a stimulated emission subsequent to that absorption. The technique has been used to make temperature measurements in steady-state laminar flames by scanning the laser frequency across an OH absorption spectrum and recording the resulting DFWM spectrum.[11,12] It has also been used in an imaging

configuration where, when the wavelength is tuned to a single absorption, the location of OH in the flame can be measured.[13,14] One difficulty in employing the process in systems with large and fluctuating density gradients (e.g., turbulent flames or liquid sprays) is that the alignment of the opposing counter-propagating beams is continuously fluctuating and the resulting misalignment causes a reduction in signal intensity. This can be interpreted as variations due to temperature or density fluctuations. The problem must be overcome in order to employ what otherwise might be a successful technique in liquid spray studies for measuring evaporation and mixing.

One method of overcoming this problem is the application of SBS to DFWM, developed at UTRC and offering a means of continuous self-alignment of the counter-propagating pump beam.[15] This is accomplished by focusing one pump beam into a medium such as hexane, a strong SBS reflector, after the beam exits the measurement medium. The SBS beam which is generated will precisely return along the path of the incident beam, maintaining the alignment of what is now called a double phase conjugate four wave mixing (DPCFWM) system. This alignment continues to maintain itself, even while density fluctuations are occurring in the beam path medium.[16] This technique may be extremely valuable for applications in small scale rocket facilities such as the UTRC 2500 pound thrust model rocket, and, hence, its development for these applications is warranted.

V. MDR Measurements at Critical Point Transition

Morphology-dependent resonances, or MDR's, have been used at UTRC as a diagnostic tool to accurately measure droplet circumference and, ultimately, evaporation rates.[5] MDR's are spectral modal signal enhancements (in the previous case, fluorescence signals) caused by containment of low-angle-of-incidence emissions within a droplet cavity due to total internal reflection near the droplet surface.

While the fluorescence MDR technique has been used to determine evaporation rates of subcritical droplets, it's application to critical condition measurements is limited. The

high temperatures and pressures at the critical points of most suitable dye solvents, as well as the durability of the dyes under these conditions, greatly complicate the experiment. On the other hand, suitable dyes do not exist which can be dissolved in cryogenic liquids with low temperature critical points. However, MDR's could be produced using stimulated Raman processes and could provide similar information about droplet size. It is even feasible that with planar illumination of individual droplets, specific planar MDR modes could be excited and shapes of slightly aspherical droplets could be evaluated.

MDR theory being developed by Professor Steven Hill will facilitate analyzing these data.[17,18] It may extend the application of these diagnostics to the study of aspherical droplets and critical and supercritical conditions where the density is no longer a discontinuity at the droplet surface and refractive index becomes a function of radius.

VI. Critical Point Detection Using Second Harmonic Generation

The nonlinear optical phenomenon which an undoped fluid should show most prominently in the vicinity of its critical point is second harmonic generation. In gases and liquids the second-order non-linear susceptibility is always zero due to molecular inversion symmetry. At an interface, however, there is a layer of molecules which lack an inverse symmetric partner, allowing the second order nonlinear susceptibility to be greater than zero. This allows the medium to convert incident light, to the second optical harmonic (frequency-doubling). An example of this approach for detecting critical point transition would be to consider a single component liquid which is sealed in a vessel at its critical pressure but below its critical temperature and heated from one side. As the heat diffuses across the test cell, the fluid undergoes a thermodynamic transition corresponding to when the fluid achieves the critical temperature, and it changes from the bulk "supercluster" state to smaller clusters whose diameters are approximately the wavelength of light. In this region, second harmonic generation will result. Recording the frequency-converted light from a laser sheet onto a two-dimensional camera one should observe a point of origin for this light

which would propagate with the thermal wave. While previously untested, this second harmonic generation is ready for experimental evaluation as a means of tracking the critical temperature or isotherm as a function of time.

Suggested Tasks

UTRC will conduct a research program to advance the state-of-the-art in spectroscopic measurement of droplets and sprays undergoing critical-point phase transitions and provide data which may include densities, concentrations, temperatures and critical-surface tracking. The goal of this program is to produce diagnostic techniques to identify processes relating to liquid stability issues and which can acquire information about phenomena occurring in critical or supercritical conditions. As they develop, these techniques will be evaluated in the UTRC high pressure pulse facility under dynamic conditions corresponding to those of rocket combustors. These tasks reflect a three year effort; the scope of the program can be tailored to meet the needs of the Air Force.

Task I

UTRC will use its high pressure pulse tube facility to acquire data describing droplet breakup and distribution in critical and supercritical environments as the result of acoustic disturbances. Initial measurements will include back-lit images of droplets following an initial period after the disturbance. Disturbances will be generated as weak shock waves through the rupture of a diaphragm separating the test section from a higher pressure driver and will have pressure ratios on the order of 1.1 or lower. Considerations will also be made to generate continuously varying and repetitive conditions, rather than step change disturbances, through the use of an acoustic driver. If employed, such a device will provide considerable information describing the effect of the disturbance wave form on the droplet break up and distribution process.

Task II

Optical diagnostic techniques, such as those described in the **Measurement Technology** section, will be studied with a focus toward employing one or more technique to acquire

quantitative data describing droplet breakup in a supercritical environment. Of particular interest is a time-dependent measure of the spatially-distributed concentration of droplet fluid following a flow field disturbance. Techniques which provide a means of acquiring an instantaneous image of concentration will be the focus of this investigation.

Task III

UTRC will attempt to provide quantitative measurements of the droplet fluid distribution process resulting from the influence of an acoustic pulse on droplets in a supercritical environment. This task will be an integration of the use of the facility as in Task I with measurements using the techniques developed in Task II. The measurements will be of limited scope in terms of droplet conditions, but will provide a demonstration of the measurement techniques and a set of results which will describe the droplet breakup process.

Payoff

The completion of this program should provide two basic results. It will define diagnostic techniques applicable to the evaluation of supercritical droplet and spray systems. The intent is to develop techniques applicable to understanding the problems associated with instabilities in liquid-fueled rocket engines. However, these diagnostics will have further applicability for developing an understanding of other droplet and spray processes.

The second result of this program will be the application of techniques for the measurement of fluid mixing properties, in critical and supercritical conditions; an important step for understanding instabilities associated with liquid-fueled rocket engine operation. The measurements should be capable of describing mixing of supercritical droplet injectants or progression of the critical surface within a subcritical droplet in a supercritical environment. These results should be valuable in understanding the stability processes occurring in combustors operating at or above the critical conditions.

References

1. A. Y. Tong and W. A. Sirignano, "Oscillatory Vaporization of Fuel Droplets in an Unstable Combustor," AIAA Journal of Propulsion and Power, Vol. 5, pp. 257-261, May-Jun 1989.

2. A. Y. Tong and W. A. Sirignano, "Multicomponent Transient Droplet Vaporization with Internal Circulation and Approximate Solution," Numerical Heat Transfer, Vol. 10, pp. 253-278, 1986.

3. Tzeng, H.-M., K. F. Wall, M. B. Long and R. K. Chang, "Evaporation and Condensation Rates of Liquid Droplets Deduced from Structure Resonances in the Fluorescene Spectra," Optics Letters, Vol. 9, pp. 273275, Jul 1984.

4. Quian, S.-X., J. B. Snow, H.-M. Tzeng and R. K. Chang, "Lasing Droplets: Highlighting the Liquid-Air Interface by Laser Emission," Science, Vol. 231, pp. 486-488, Jan 1986.

5. T. J. Anderson and M. Winter, "Measurements of the Effect of Acoustic Disturbances on Droplet Vaporization Rates," presented at the AIAA Aerospace Sciences Meeting, Jan. 6-9, Reno, NV, paper no. AIAA-92-0108.

6. M. Golombok and D. B. Pye, "Coherence Restriction on Phase Conjugation in Droplets," Journal of Physics D, Vol. 24, pp. 835-838, 1991.

7. W. P. Acker, A. Sepenguzel, R. K. Chang, and S. Hill, "Stimulated Raman Scattering of Fuel Droplets," Applied Physics B, Vol. 51, pp. 9-16, 1990.

8. R. L. Abrams, J. F. Lam, R. C. Lind, D. G. Steel and P. F. Liao, in Optical Phase Conjugation, R. A. Fisher, ed., (Academic Press, London, 1983), pp. 211-284; D. G. Steel and R. C. Lind, Optics Letters, Vol. 6, pp. 587-589, Jul 1981.

9. P. Ewart and S. V. O'Leary, "Comparisons of Sodium: Rare-Gas Potentials by Measurement of Excited-State Degenerate

Four-Wave Mixing," Journal of Physics B, Vol. 15, pp. 3669-3677, Sep-Oct 1982.

10. J. Pender and L. Hesselink, "Phase Conjugation in a Flame," Optics Letters, Vol. 10, pp. 264-266, Jun 1985.

11. P. Ewart and S. V. O'Leary, "Detection of OH in a Flame by Degenerate Four-Wave Mixing," Optics Letters, Vol. 11, pp. 279-281, May 1986.

12. T. Dreier and D. J. Rakestraw, "Degenerate Four-Wave Mixing Diagnostics on OH and NH Radicals in Flames," Applied Physics B, Vol. 50, pp. 479-485, Jun 1990.

13. P. Ewart, P. Snowdown and I. Magnusson, "Two-Dimensional Phase-Conjugate Imaging of Atomic Distributions in Flames by Degenerate Four-Wave Mixing," Optics Letters, Vol. 14, pp. 563-565, Jun 1989.

14. D. J. Rakestraw and R. L. Farrow, "Two-Dimensional Imaging of OH in Flames by Degenerate Four-Wave Mixing," Optics Letters, Vol. 15, pp. 709-711, Jun 1990.

15. M. Winter and P. Radi, "Nearly Degenerate Four-Wave Mixing Using Phase Conjugate Pump Beams," Optics Letters, Vol. 17, pp. 320, Mar 1992.

16. M. Winter and P. Radi, "Double Phase Conjugate Four-Wave Mixing of OH in Flames," presented at the 24th International Symposium on Combustion, Sydney, Australia, Jul 5-10, 1992.

17. Chouwdhury, D. Q., S. C. Hill and P. W. Barber, "Morphology-Dependent Resonances in Radially Inhomogeneous Spheres," Journal of the Optical Society of America, Vol. 8, pp. 1702-1705, Nov. 1991.

18. Mazumder, M. M., S. C. Hill and P. W. Barber, "Morphology-Dependent Resonances in Inhomogeneous Spheres: Comparison of the Layered T-matrix Method and Time-Independent Perturbation Method," accepted for publication in the Journal of the Optical Society of America, 1992.